Selective Oxidation of Biomass-Derived Chemicals

Modvig, Amalie Elise

Publication date:
2017

Document Version
Publisher's PDF, also known as Version of record

Selective Oxidation of Biomass-Derived Chemicals

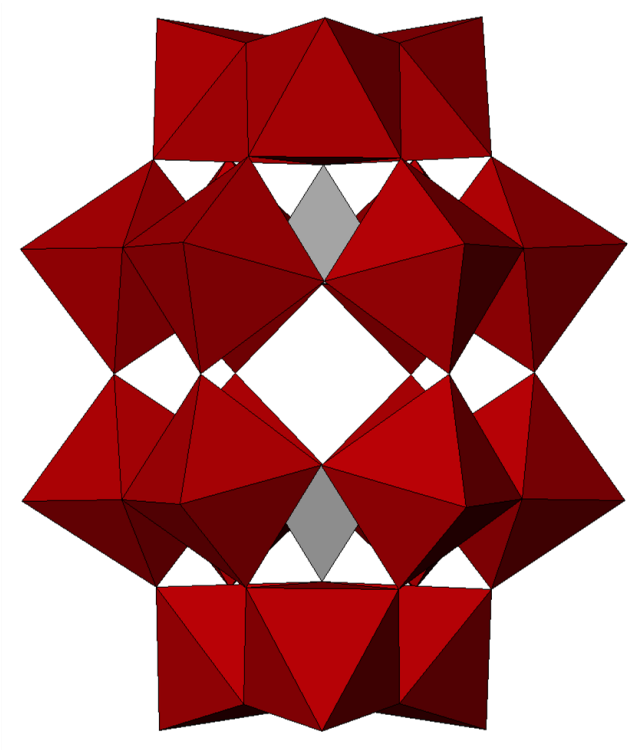

Ph.D. dissertation by Amalie Elise Modvig, M.Sc.

May 2017

DTU Chemistry

Amalie Elise Modvig
Selective Oxidation of Biomass-Derived Chemicals
Ph.D. dissertation, May 2017
Technical University of Denmark
E-mail address: ammod@kemi.dtu.dk

Cover photo:
X-ray diffraction data of $K_6P_2W_{18}O_{62}$, illustrated in Atoms.

Preface

The work presented in this dissertation was carried out at the Centre for Catalysis and Sustainable Chemistry (CSC), Department of Chemistry at the Technical University of Denmark (DTU). The work was performed under supervision of Prof. Anders Riisager during the period May 1st 2014 to May 31st 2017. The project was initially co-supervised by Assoc. Prof. Peter Fristrup (DTU) until July 1st 2016. The project was funded by the SPIR initiative as part of the Bio-Value platform, by the Danish Council for Strategic Research and the Danish Council for Technology and Innovation, and was carried out in collaboration with Haldor Topsøe A/S (HTAS).

Furthermore, this dissertation include research performed during an external research stay at Friedrich-Alexander University (FAU), Erlangen, Germany, from February 28th 2016 to May 31st 2016, under supervision of Prof. Dr. Peter Wasserscheid and Dr. Ing. Jakob Albert. The results are presented in Chapter 5.

This dissertation is divided into seven chapters, opening with a general introduction to the areas of research and importance hereof in Chapter 1. Chapter 2 describes the applied instruments for catalysts characterization and the design of equipment for fast reaction optimization. A project on selective oxidation of glycolaldehyde into glycolic acid is presented in Chapter 3, followed by Chapter 4 where oxidations over ceria-supported ruthenium hydroxide were performed on glycolaldehyde and selected alcohols. Chapter 5 includes the research performed at FAU concerning synthesis of Wells-Dawson structured heteropolyoxometalates and application as catalysts for oxidation of selected alcohols and sugars. The projects are summarized in Chapter 6 followed by assessment of the project aims stated in Chapter 1.

The tables, schemes and figures were prepared by me, unless otherwise noted.

Amalie E. Modvig

Kgs. Lyngby, Denmark, May 2017

Acknowledgements

First of all, I am grateful to my supervisor Prof. Anders Riisager for giving me the opportunity to spend three years researching at DTU under his guidance. It has been a great experience and pleasure to be part of his research group.

Furthermore, I would like to thank Assoc. Prof. Søren Kegnæs, Assoc. Prof. Susanne Mossin, Prof. Rasmus Fehrmann and past and present members of CSC for creating an open and inspiring research atmosphere at CSC and for helpful advices at group meetings and other gatherings.

I would also like to thank those who have performed specialized instrumental characterization of my samples.

A special thanks to Dr. Saravanamurugan Shunmugavel for helping me through the beginning of my Ph.D. work until leaving for a job in India. I would also like to thank Dr. Ing. Jakob Albert and Prof. Wasserscheid for accepting me into their research group during my external research stay at FAU and supervising me during my stay and for continuing the collaboration after returning to Denmark. Dorothea Voss (FAU) deserves a special thanks for close collaboration and recordings of analytical data during my research stay.

Another special thanks go to Jonas Andersen and Agata Gallas-Hulin for their advice and helpful suggestions.

I'd like to extent my deepest gratitude to my family and friends for supporting me throughout my Ph.D. study, especially for enduring me these last months of my project. I especially want to thank my closest family, particularly my parents, for being there for me during the beginning of my Ph.D. studies.

Abstract

Due to depleting fossil resources, alternative feedstock for obtaining chemicals is of great importance. Biomass provides a promising alternative renewable carbon source; however, new sustainable processes for conversion of biomass are required to sufficient implementation into the industry. These processes should be able to compete with the established processes based on fossil resources.

Glycolaldehyde is an often-observed by-product formed from degradation of larger sugars. Due to competing ecological and economical aspects of the well-established processes for extraction and conversion to chemicals from fossil resources, limited amounts of waste chemicals *i.e.* by-products are allowed in the processes of conversion of biomass and biomass-derived compounds. It is therefore important to develop methods for conversion of these simple by-products that are environmentally benign and of low cost.

The objective of this dissertation was to develop new, alternative and sustainable methods for oxidative catalytic upgrading of biomass-derived compounds, with focus on oxidation of glycolaldehyde and simple alcohols as model substrates for larger sugars.

Supported gold nanoparticle were studied for the selective oxidation of glycolaldehyde to glycolic acid, which has found applications in various industries. Limitations by competing reactions and catalyst deactivation was observed, affording up to 68% of glycolic acid at mild and aqueous conditions. The green oxidant, molecular oxygen, was applied for these oxidations and the reaction took place under base-free conditions.

Oxidation of glycolaldehyde was further studied in the formation of formic acid. Efficient release of hydrogen from formic acid has proven formic acid a viable precursor for hydrogen, facilitating safe transportation and storage. Hydrogen has found application in various industries including energy conversion by fuel cells. High yields of formic acid was obtained from oxidation of glycolaldehyde over a supported ruthenium catalyst. The effect of the size of the support was studied, however, minor differences was observed. A slightly better yield of formic acid was obtained from nanoparticulate ceria.

Vanadium-substituted Keggin polyoxometalates have proven efficient catalysts for conversion of various biomass compounds into formic acid. The Wells-Dawson-type heteropolyoxometalates are less thoroughly studied for biomass

conversion. Tungsten-based Wells-Dawson heteropolyoxometalates were synthesized and examined for the oxidation of alcohols and sucrose. However, successful oxidations of the alcohols and sucrose were not observed. The search for application of the synthesized Wells-Dawson heteropolyoxometalate is ongoing in collaboration with the group of Prof. Wasserscheid at FAU in Germany.

It was shown, that glycolaldehyde can be selectively converted into glycolic acid or formic acid, depending on the catalyst applied, under mild, aqueous and base-free conditions. High product stability in the ceria-supported ruthenium hydroxide catalyzed oxidation to formic acid, together with the good catalyst activity observed when reusing the catalysts, rendered the developed procedure for formic acid production highly applicable for industrial use. Furthermore, the synthesized Wells-Dawson polyoxometalate catalysts afforded low catalytic oxidative activity.

Resumé

Vore fossile ressourcer er ved at være opbrugt og derfor er alternative råmaterialer, til at producere kemikalier fra, meget vigtige for samfundet. Biomasse er en lovende alternativ vedvarende karbonkilde, men der er behov for nye bæredygtige løsninger for industriel omdannelse af biomasse, som kan konkurrere med de etablerede processer baseret på fossile ressourcer.

Glykolaldehyd er et biprodukt der ofte ses i forbindelse med nedbrydelse af større sukkermolekyler. Grundet konkurrerende miljø- og økonomiske aspekter i forhold til de veletablerede processer for ekstraktion og omdannelse af fossile ressourcer, er kun begrænsede mængder af spild, som sukker-biprodukter, tilladt for bæredygtige omdannelser af biomasse og biomasse-afledte forbindelser. Det er derfor vigtigt at udvikle metoder for omdannelse af disse simple biprodukter, som er miljøvenlige og har lave omkostninger.

Formålet med denne afhandling var at udvikle nye, alternative og bæredygtige metoder for oxidative katalytiske opgraderinger af biomasse-afledte forbindelser med fokus på oxidation af glykolaldehyd og simple alkoholer som modelsubstrater for større sukkermolekyler.

I forbindelse med den selektive oxidation af glykolaldehyd til glykolsyre, som har fundet anvendelse i forskellige industrier, blev guld nanopartikler på et bæremateriale studeret. Begrænsninger fra konkurrerende reaktioner og deaktivering af katalysatoren blev observeret, og op til 68% omdannelse af glykolaldehyd til glykolsyre blev opnået ved milde og vandige betingelser. Den grønne oxidant, molekylær oxygen, blev brugt til disse oxidationer og reaktion skete uden tilstedeværelse af base.

Oxidation af glykolaldehyd blev yderligere studeret i dannelsen af myresyre. Effektiv frigivelse af hydrogen fra myresyre har vist, at myresyre er et funktionsdygtigt udgangsstof for hydrogendannelse, som er mulig at transportere og opbevare under sikre forhold. Hydrogen har fundet anvendelse i forskellige industrier inklusiv energikonvertering i brændselsceller. Højt udbytte af myresyre blevet opnået fra oxidation af glykolaldehyd over en katalysator baseret på ruthenium på et bæremateriale. Effekten af størrelsen på bærematerialet blev studeret, men kun mindre forskelle blev observeret. En smule øget udbytte blev opnået ved brug af nanopartikler af cerium oxid sammenlignet med cerium oxid mikropartikler.

Vanadium-substituerede Keggin heteropolyoxometallater har vist sig at være effektive katalysatorer for omdannelse af biomasse-forbindelser til myresyre. Denne omdannelse er ikke grundigt studeret for brug af Wells-Dawson heteropolyoxometallater som katalysatorer. Wolfram-baserede Wells-Dawson heteropolyoxometallater blev syntetiserede og testet for oxidation af alkoholer og sukrose, dog uden nævneværdig succes. Søgen efter anvendelser for disse syntetiserede Wells-Dawson heteropolyoxometallater er stadig i gang i samarbejde med Prof. Wasserscheids gruppe på FAU i Tyskland.

Det blev vist, at glykolaldehyd kan omdannes selektivt til glykolsyre eller myresyre, afhængig af den anvendte katalysator under milde, vandige og base frie betingelser. Høj produktstabilitet samt god katalysator aktivitet ved genbrug af katalysatoren gør den udviklede procedure for oxidation af glykolaldehyd til myresyre med en ruthenium hydroxid katalysator, til en højst anvendelig metode for industriel produktion. Lav katalytisk oxidations aktivitet blev observeret for de syntetiserede Wells-Dawson polyoxometallat katalysatorer.

Table of Contents

Chapter 1. Introduction

Today, the most industrial processes are catalytic. Catalytic processes often provide more environmental benign solutions of converting raw materials into feasible chemicals. Many of the industrial chemical-processes are based on fossil feedstock, however, depleting fossil resources has increased the demand for processes for chemical production from renewable feedstocks. High carbon-content of biomass (42-54%) render biomass a promising renewable source for production of carbon-containing chemicals.[1] Development of new and efficient sustainable methods for synthesis of bulk and fine chemicals from a renewable feedstock is of great importance. Catalysis provide an environmental benign solution for obtaining bulk and fine chemicals from biomass.

In this introductory chapter, a brief overview of the concepts of catalysis and sustainable chemistry, followed by a more specific literature review on relevant biomass chemistry is presented. The last section outlines of the aims and content of this dissertation.

1.1 Catalysis

Catalysis is of great importance for industrial chemistry owing to the ability of catalysts to increase efficiency of reactions without being consumed in the process.[2] More than 90% of produced chemicals contain at least one catalyzed step in the manufacturing process.[3,4] Increased efficiency of reactions can be obtained from applying small amounts, or catalytic amounts, of catalyst due to regain of the unaltered catalyst after the reaction, rendering the catalyst readily available for another reaction cycle. Additionally, the catalysts can often be reused many times, improving the efficiency and economy of industrial processes compared to non-catalytic processes. Non-catalytic industrial processes often require stoichiometric amounts of reagents, generating vast amounts of waste products such as inorganic salts, which can be toxic and hence, costly to dispose. Applying catalysis reduces the waste and cost. Catalysis is therefore very important for sustainable chemistry, enhancing the atom economy.[5,6]

The phenomenon “catalysis” was first recognized by Berzelius in 1835, describing enhanced chemical reactions.[7,8] Today, catalysis is defined as a foreign substance that accelerate a chemical reaction without being consumed in the process. Catalysis enhances the rate of reaction by providing an alternative, lower energy state, thereby lowering the activation energy, however, the position of the thermodynamic equilibrium remains unchanged.[8,9] The lower activation barrier allows for catalyzed reactions to occur at decreased temperatures, often limiting the amount of formed by-products. The lower energy state is achieved by formation of a temporary catalyst-reactants intermediate, followed by regeneration of the catalyst rendering the catalyst ready for recycling.

Catalysts are not consumed in the catalytic process, however, decrease of catalyst activity may occur over time. Reversible or irreversible chemical deactivation by catalyst poisoning of substrates or products, decrease the catalytic activity. However, solid catalysts can often be regenerated by calcination, affording a re-activated catalyst readily available for reuse. This process can be repeated, however, slightly lower activity is often observed after regeneration and eventually, replacement of the catalyst is necessary. The decreased activity after regeneration may be caused by irreversible thermal deactivation of the catalyst through sintering or leaching, aggregation of the active material or loss of active material. Furthermore, steaming or mechanical deactivation by attrition or erosion may cause irreversible deactivation that eventually leads to necessary catalyst replacement.

Catalysis can be divided into two classes: homogeneous and heterogeneous catalysis. Homogeneous catalysis refers to catalytic reactions where the catalyst is in the same phase as the reactants. In contrast, heterogeneous catalysis refers

to reactions where the catalyst is in a different phase from the reactants. Typically, the reactants are gases or liquids, catalyzed by a solid catalyst.

Homogeneous metal-based catalysts are widely studied, and often provide excellent activity and selectivity, due to simple tuning by change of ligands. Highly complex structures of organic molecules has been synthesized in good yields and high selectivity. In general, heterogeneous metal-based catalysts are less selective, and tuning of selectivity is more complicated. However, the great advantage of heterogeneous catalysis lies in the separation of the catalyst for reuse.

1.1.1 Heterogeneous Catalysis

Heterogeneous catalysis is of great importance for chemical industrial processes due to ease of separation and reuse of the catalyst, reducing the cost of the process. Currently, 85-90% of the catalytic processed on industrial scale are catalyzed by heterogeneous catalysts.[10] Solid catalysts are the most widely used for large-scale productions of chemicals and fuels.[11] Solid catalyst are divided into subgroups including unsupported (bulk), supported, confined, hybrid, polymerization and other catalysts. The work presented in this dissertation focuses on supported catalysts.

Supported catalysts are highly important for many industrial processes due to stabilization of the dispersion of the active component on a high surface area. Some supports contribute with additional properties such as acidic or basic sites, generating bifunctional catalysts. Typically, the supports are porous material with high thermal stabilities such as metal oxides *e.g.* Al_2O_3, SiO_2, ZrO_2, TiO_2, CeO_2 and zeolites. Supported transition metals are often highly redox-active catalysts, making them excellent catalysts for oxidation and hydrogenation of organic compounds. Metals with higher surface energy than the support tend to reduce their surface areas by agglomeration into larger particles.[12] For efficient catalysis, small, nanosized, highly dispersed particles have proven highly active. Stabilization of these dispersed nanosized particles is desirable and can be obtained from metal-support interactions of high surface area supports. Experimental and modelling reports, support the dissertation, that low-coordinate surface metal atoms are the active atoms of the metal nanoparticle.[13,14] The low-coordinate atoms resides in the corners, *i.e.* the atoms in contact with the support. Smaller particles increase the number of low-coordinate surface atoms and, hence, increase the activity of the catalyst.

The general mechanism of supported metal nanoparticles includes three overall steps: adsorption of the reactants on the nanoparticle surface by physi- or chemisorption (weak van der Waals or chemical bonds, respectively), catalysis generating adsorbed products and desorption of products completing the catalytic cycle (Figure 1.1). In general, catalytic studies on heterogeneous reactions are challenging. Three generally accepted models have been proposed for adsorption of reactants: Langmuir-Hinshelwood (LH), Elay-Rideal (ER) and Mars-van-Krevelen (MK), illustrated in Figure 1.1 (b), (c) and (d). Most surface catalytic reactions are considered to follow the LH mechanism in which the reactants are adsorbed on the surface independently prior to the reaction. The ER mechanism describes a situation where one reactant is adsorbed on the surface and reacts directly with another reactant from the gas phase. In the MK mechanism, adsorption of one of the reactants (A) on the surface affording a thin layer on the catalyst is first formed. The adsorbed reactant can react with the second reactant B, generating the product. In this scenario it is necessary to regenerate the active catalyst in a subsequent step.

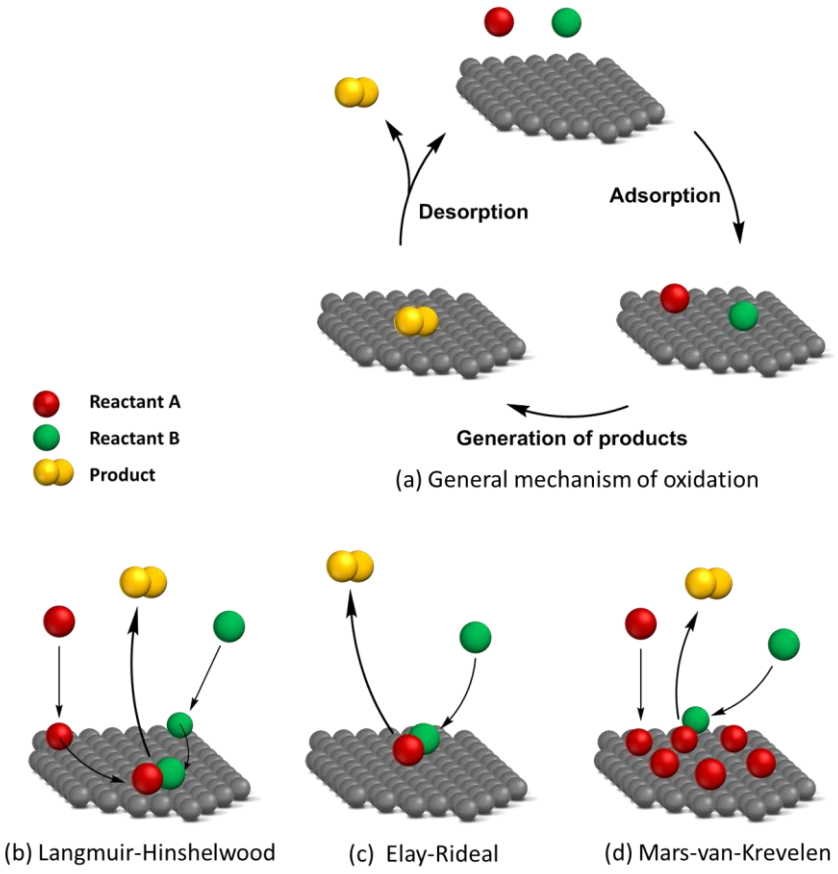

Figure 1.1: (a) general mechanism of heterogeneous supported nanoparticle catalysis, (b), (c) and (d) detailed mechanisms.

1.2 Green (Sustainable) Chemistry

With increasing environmental concerns followed by constricted legislation, the demand for sustainable processes of fine chemical synthesis is increasing. Increasing pollution and depletion of fossil resources are the main concerns considered in green chemistry. The green chemistry concept focuses on development of sustainable chemical processes that are non-toxic to living organisms and the environment, thereby reducing the effect on the environment. Anastas and Warner proposed twelve principles to be considered when developing green processes with the goal of optimizing process efficiency, minimizing the use and generation of hazardous substances, use of renewable feedstocks and production of bio-degradable or reusable products.[15,16]

Evaluation of the "green-ness" of processes is most commonly based on E- and C-factors. The E-factor is a measure of produced by-products or waste (kg) divided by the amount of formed product (kg) and should be minimized for green processes.[17] Similarly, the C-factor is a measure of produced CO_2 (kg) divided by the weight of formed product (kg).[18,19] E-factors for industrial production of chemicals and C-factors for various resources are presented in Table 1.1 and Table 1.2.

Table 1.1: E-factors for industrial chemical productions[20]

Chemical Production	Annual Tonnage	E-factor
Petrochemicals	$10^6 – 10^8$	< 0.1
Bulk Chemicals	$10^4 – 10^6$	1 – 5
Fine Chemicals	$10^2 – 10^4$	5 – 50
Pharmaceuticals	$10 – 10^3$	25 - 100

Table 1.2: C-factors for various resources[19]

Resource Type	Kg(CO_2)/kg(resource)
Crude oil	0.09
Natural gas	0.08
Coal	0.02
Biomass	-1.89

Replacement of stoichiometric reagents with catalysts decreases the energy use and reduce the formation of hazardous side-products. Catalysis is therefore of great importance in green chemistry and development of green catalytic processes has received considered attention the last decades.[21] To achieve successful development of efficient and sustainable chemical processes, combining fundamental research on catalysis with industrial demands is highly important.

1.3 Biomass – A Renewable Feedstock

Use of biomass in green chemistry is of great importance due to dramatic increase of population leading to depletion of fossil resources. Biomass is the most abundant carbon resource available, and provides an excellent alternative and renewable feedstock to fossil fuels.[22] In the context of chemistry, biomass is defined as any biological material derived from living organisms, which include several sources such as forestry, animal, agricultural and urban sources, depicted in Figure 1.2. Living biomass absorbs carbon as it grows, which can be extracted and used for energy or chemical production, generating a carbon-neutral cycle, *i.e.* a renewable carbon source.[23]

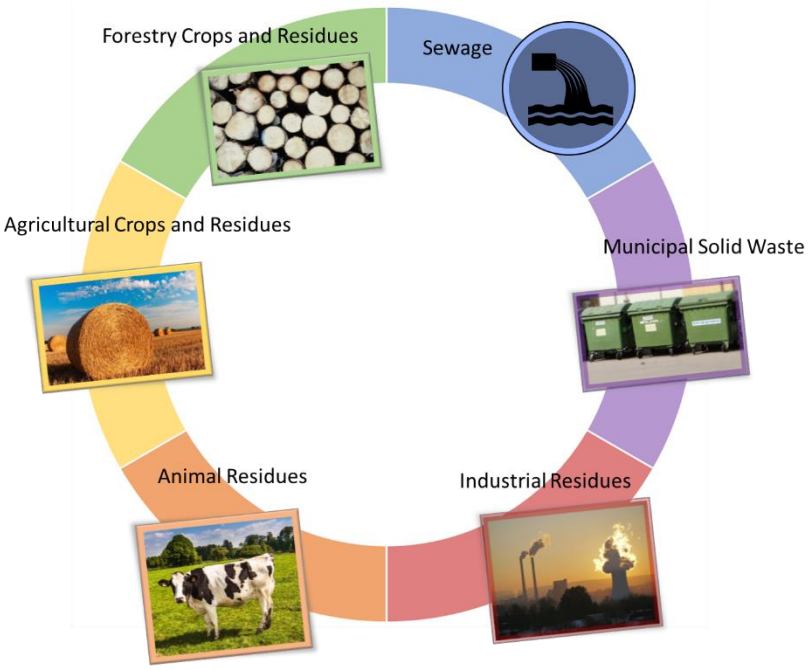

Figure 1.2: Biomass sources

Some of the most promising biomass feedstocks are derived from agricultural and forestry sources, including grains and starch crops, wheat straw, hard and soft wood etc. Biomass-based chemicals and fuels are generally produced from sugar and starch-containing crops *e.g.* beet, corn and grain which are also food-components (first-generation biomass). Preferably, the biomass feedstock should be non-eatable to diminish competition with food sources. Second-generation biomass is generally composed of lignocellulosic biomass, and is obtained from waste-products, decreasing the competition with food sources. Lignocellulose is found in the cell walls of plant tissue, and is composed of three principle components: cellulose (40-50 wt%), lignin (20-30 wt%) and hemicellulose (25-35 wt%) (Figure 1.3). C5 and C6 sugars can be derived from cellulose and hemicellulose, whereas aromatic compounds can be obtained from lignin.

Figure 1.3: Lignocellulosic biomass, cellulose (green), lignin (red) hemicellulose (light green).[24]

With the motivation for green chemistry, sustainable methods for conversion of biomass-derived compounds into feasible chemicals are highly desired. Several hydroxyl groups and carbonyls are often present in biomass-derived compounds (Figure 1.4), and selective catalytic protocols for conversion of these has received, and is still receiving considered attention as a means of developing green protocols for industrial production of bio-fuels and chemicals.[24] This dissertation focus on the development of selective catalytic oxidation of selected biomass-derived compounds.

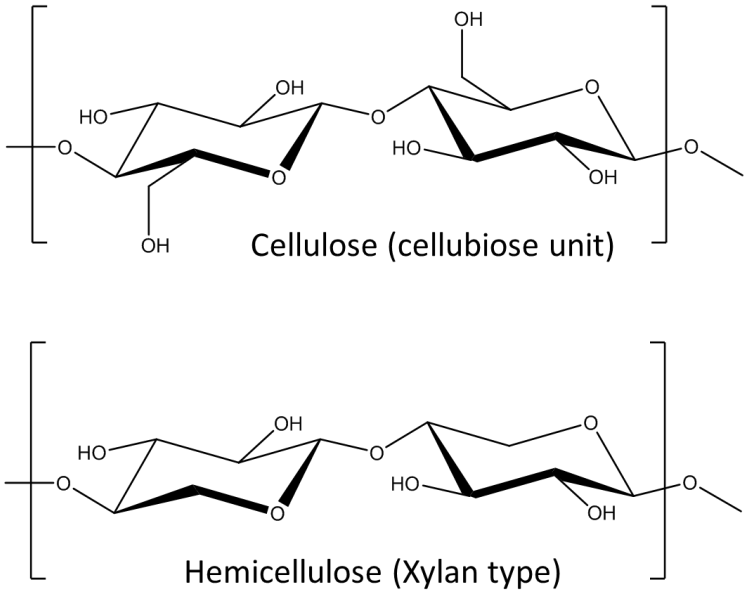

Figure 1.4: Chemical structures of cellulose and hemicellulose

1.3.1 Glycolaldehyde and Alcohols

Glycolaldehyde (GAD) is the smallest sugar, consisting of two carbons containing both an aldehyde and a hydroxyl group. GAD is often observed as a by-product from degradation of larger biomass-derived compounds. Currently GAD has been produced in high yields from glucose in critical water and from bio-oils (Scheme 1.1).[25–27]

Several studies on conversion of GAD into feasible products has been reported, including direct amination into diamine or ethanolamine applicable in the polymer and pharmaceutical industry,[28] aldol condensations affording various C6 and high-value C4 sugars, feasible in food and pharmaceutical industries,[29,30] hydrothermal treatment and hydrogenation giving the polymer building blocks, lactic acid and ethylene glycol,[31–33] oxidation into glyoxal, glycolic acid, or glyoxylic acid[34–36] and various other (Scheme 1.2).[37–40] Great potential of GAD for becoming a valuable biomass-derived platform molecule leads the need for new and sustainable protocols for conversion of GAD into feasible chemicals. Biomass-derived compounds often contain several hydroxyl moieties and development of protocols for selective conversion of these are of great importance in green chemistry.[41–44]

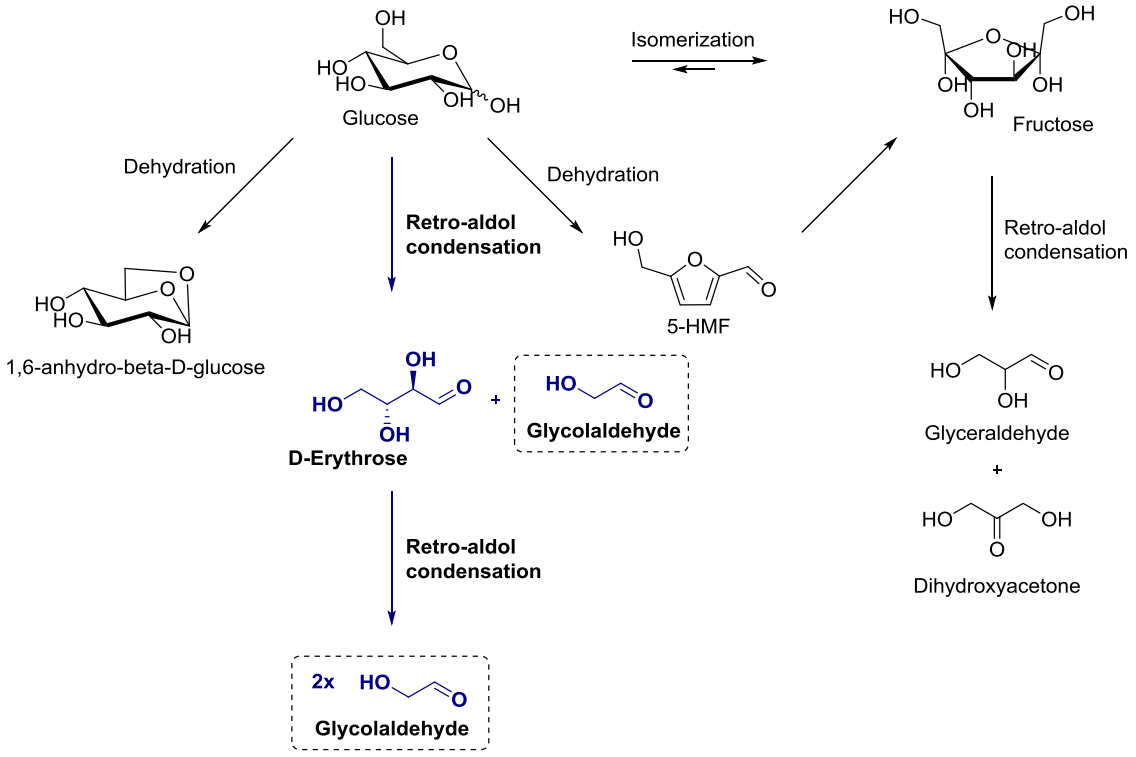

Scheme 1.1: Reaction pathways of glycolaldehyde production from glucose under low water density conditions in supercritical water. Adapted from Sasaki *et al.*[26]

Alcohol moieties are highly abundant in biomass-derived compounds and selective transformations of alcohols is of great importance for industrial production of chemicals. Simple alcohols were applied as model substrates for more complex biomass-derived sugars *e.g.* C5 and C6 sugars and combinations thereof.

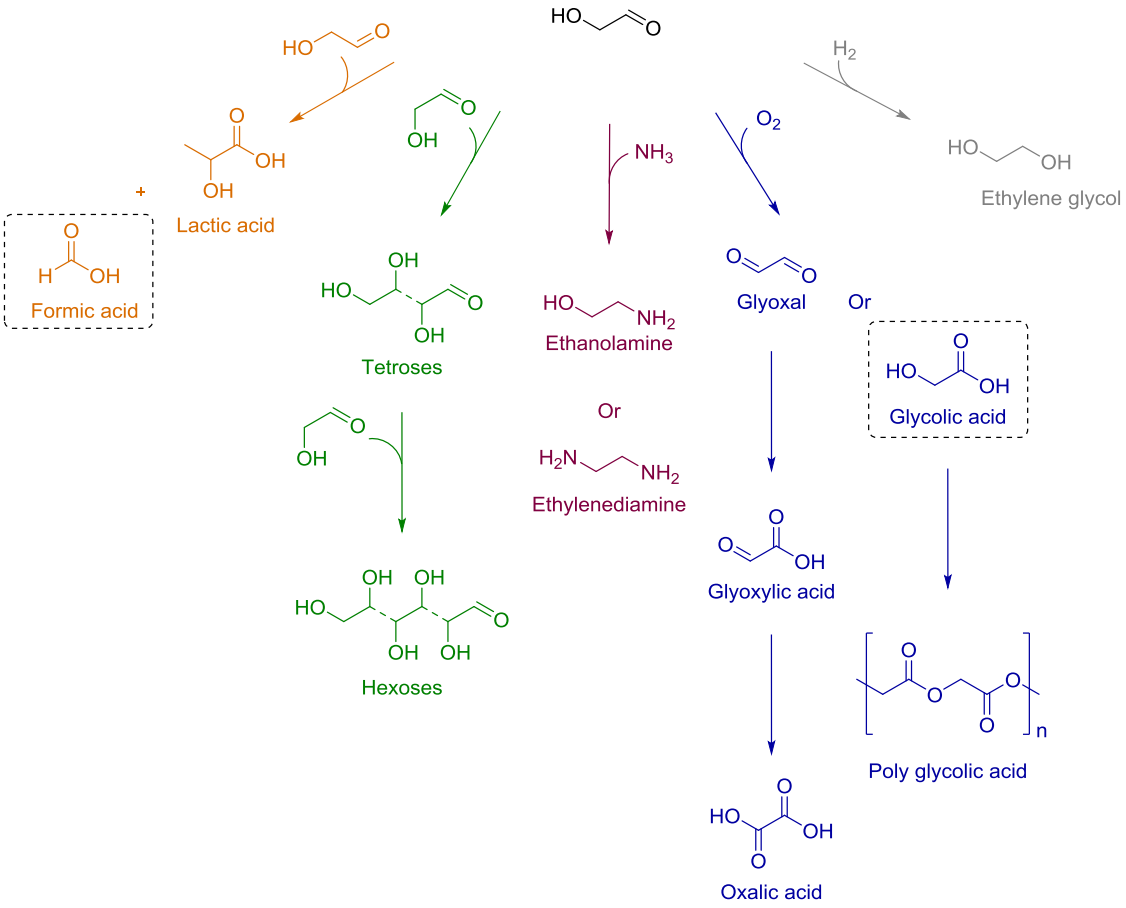

Scheme 1.2: Reported conversions of glycolaldehyde.[28–40]

1.4 Oxidations of Biomass-derived Compounds

Several publications on conversion of biomass and biomass-derived chemicals into chemicals have been published.[22,42,45–54] Oxidations are widely used in production of bulk and fine chemicals, and more than 20% industrial organic compounds are manufactured from catalytic oxidation or ammoxidation of hydrocarbons.[55] However, many manufacturing processes produce large amounts of by-products and waste. Due to strict ecological standards, the demand for new environmentally benign methods for selective oxidation is being stressed. Within the field of homogeneous catalysis, several high yielding methods have been developed, however, for industrial productions limitations of the homogeneous solutions, including corrosion, plating, handling, recovery and reuse have been reported.[56] Heterogeneous catalysis provides a means of easy recovering and handling of the catalysts, and often represents the more environmentally benign solution. The requisite for selective catalytic oxidation

protocols to meet the principles of green chemistry is of growing interest and especially selective heterogeneous-catalyzed oxidations has received considerable attention.[41,42,57–71]

Several challenges has to be met, when developing protocols for the selective oxidations in green chemistry. Low or ambient pressure of a green oxidant, such as air, molecular oxygen or other oxidants generating H_2O as the only by-product, green solvent or neat reaction conditions with low catalyst loadings at mild, preferably, ambient conditions and severely reduced or completely avoided formation of toxic by-products or additives are some of the challenges that has to be considered when developing new green methods for oxidation. Moreover, high efficiency *i.e.* high activity and selectivity of the catalysts is required.

Supported nanoparticles are excellent sustainable alternatives to conventional metal catalysts due to increased surface area of the active metal from high dispersion of the active nanoparticles on a solid support and facile separation of the catalyst.[41,72–75] Oxidation of alcohols to aldehydes or carboxylic acids is a fundamental transformation in the bio-chemical industry.[44] Originally, Pt-group based catalysts (Ru, Rh, Pd and Pt) were studied for the heterogeneous-catalyzed selective oxidations of biomass-derived compounds such as glucose, xylose, 5-HMF and ethanol. Pd and Pt are generally highly active in oxidations, however, moderate selectivities are often reported *e.g.* between aldehyde and alcohol functionalities within the same compound.[52] Combining these active metals with catalytic promoters, such as Bi, Pb, Co, Au and Ru, has in general increased the selectivity of these oxidations. Bi is believed to protect Pd from oxidation, preventing inactivation of the catalyst.[76] The Pt-group based catalysts are typically supported on high surface area alumina or carbon.[56] The past 30 years, supported gold nanoparticles has received considerable attention due to high selectivity and activity in oxidation reactions, see Chapter 3.[77]

Upgrading of bio-ethanol to acetic acid by oxidation has been reported over supported Pd, Pt, Ru and Au catalysts[57,63,66,68,78–81] and over Mo-V-Nb mixed oxides[82] affording good yields and selectivities. The food and beverage additive, gluconic acid, was successfully synthesized in high yield from glucose over supported Au, Pd-Bi and Pt.[64,76,83–88] A general challenge for glucose oxidation is the selectivity. Often several oxidation products is observed.[89,90] The poor selectivity has been attempted overcome by combinations of metals such as supported Pt-Pd-Bi, Pd-Bi Au-Pt and Rh-Pd.[88,91] In general, higher activity is observed in the presence of a base, however, base-free oxidation over supported Au catalysts of biomass-derived compounds, such as 5-HMF, have been reported.[64,86] Considerable attention has been given to the platform molecule 5-HMF. 5-HMF contains both an alcohol and an aldehyde moiety and selective

oxidations has been vastly examined (Scheme 1.3).[22,45,49,92] The group of Corma reported high activity and selectivity for oxidative esterification of 5-HMF into furan dicarboxylate ester over Au/CeO_2 under base-free conditions.[93] Aqueous, base-free oxidation of 5-HMF to furan dicarboxylic acid (FDCA) was reported by our group over spinel-supported Ru affording good yield and selectivity (Scheme 1.3).[94] FDCA is considered a bio-renewable monomer for production of polyesters, polyamides polyurethanes, replacing terephthalic, isophthalic, and adipic acids.[95] Several other catalysts have been reported to catalyze oxidation of 5-HMF and reviews on biomass conversion most often include conversion of 5-HMF.[45,49,51,60,91,93,96–99]

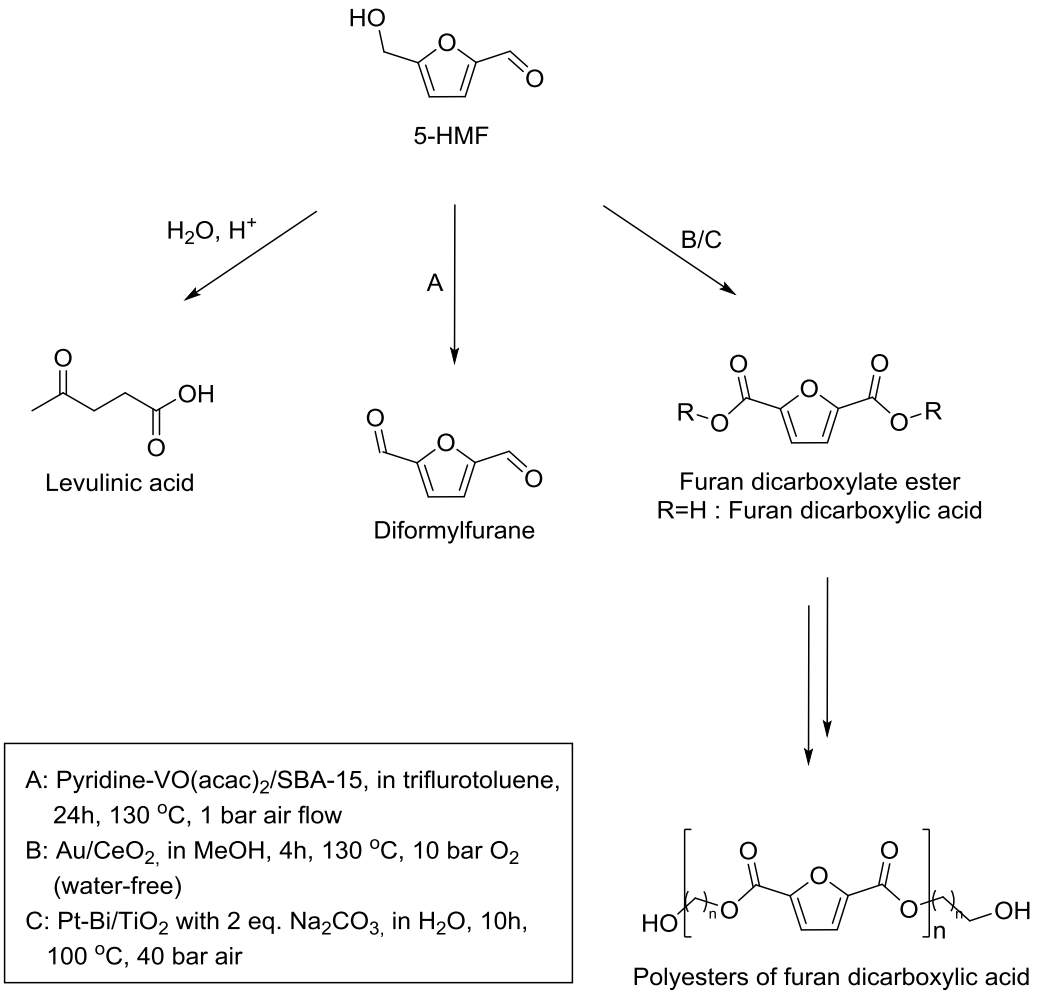

Scheme 1.3: Transformations of 5-HMF.[22,45,92–94]

Selective oxidation of nearly any kind of agricultural or wood biomass to formic acid was successfully achieved, first by the group of Wasserscheid, using a homogeneous phospho-vanadium-based heteropolyoxometalate catalyst.[61,67,100–102] Good yields of formic acid were obtained at relatively mild conditions.

1.5 Aims of Dissertation

This dissertation focuses mainly on heterogeneous catalysis with solid catalysts, however, chapter 5 covers a project on homogeneous catalysis performed in collaboration with the group of Professor Wasserscheid at Friedrich-Alexander University, Erlangen, Germany.

The specified targets were to examine and develop catalytic systems for:

- Selective oxidation of glycolaldehyde to glycolic acid at mild, aqueous and base-free conditions with a heterogeneous catalyst.

- Selective oxidation of glycolaldehyde to formic acid at mild, aqueous and base-free conditions with a heterogeneous catalyst.

- Selective oxidation of various alcohols to acetic acid at mild, aqueous and base-free conditions with a heterogeneous catalyst.

- Heteropolyoxometalate-catalyzed selective oxidation of alcohols and sugars into formic acid at mild, aqueous and base-free conditions (homogeneous catalysis).

Chapter 2. Characterization and Equipment

A short introduction to the most important characterization techniques and analysis methods used in dissertation is presented, followed by a brief overview of the applied equipment including a schematic overview of designed small high-pressure vessels for fast reaction optimization on a small scale.

2.1 Characterization of Catalysts

Adequate characterization of solid catalysts is of great importance for understanding of the physical properties and succeeding optimization of catalyst preparation. This section provides a brief overview of the characterization techniques used in this dissertation.

2.1.1 Elemental Analysis

Appropriate quantitative elemental analysis of catalysts is important for reliable determination of the catalyst metal content, for assessment of preparation methods and studying of the effect metal loading of the catalyst on a reaction. A brief introduction to the methods relevant for this dissertation is presented below.

2.1.1.1 X-Ray Fluorescence Spectroscopy

X-ray Fluorescence Spectroscopy (XRF) is a non-destructive elemental analysis technique based on detection of the characteristic fluorescent X-ray emitted when excited, ionized atoms relaxes, illustrated in Figure 2.1. A primary, high-energy X-ray source irradiates the sample, resulting in ejection of inner shell electrons of the irradiated atoms. Relaxation of the excited atoms results in emitting of unique secondary or fluorescent X-ray for each element, which is detected. Quantitative elemental composition can be determined from the analysis of the intensity of each characteristic emitted fluorescent X-ray.

XRF is directly applicable for analysis of solid catalysts, rendering XRF a particularly useful method of analysis. However, XRF is a surface technique resulting in analysis of the sample surface within a limited area. Furthermore, the range of atoms is typically limited to elements with atomic number greater than 12, due to low quality spectra obtained for lighter atoms.[103,104]

The XRF data presented in this dissertation was obtained from a PANalitical Epsilon3-XL instrument equipped with a high-resolution silicon drift detector and x-ray tube excitation (Rh, Ag, Mo anode materials, 20 kV, 100 µA). The element concentration was determined using the Omniant calibration program of the instrument, based on calibration lines of standards present in the instrument. The powder samples were analyzed directly in the apparatus.

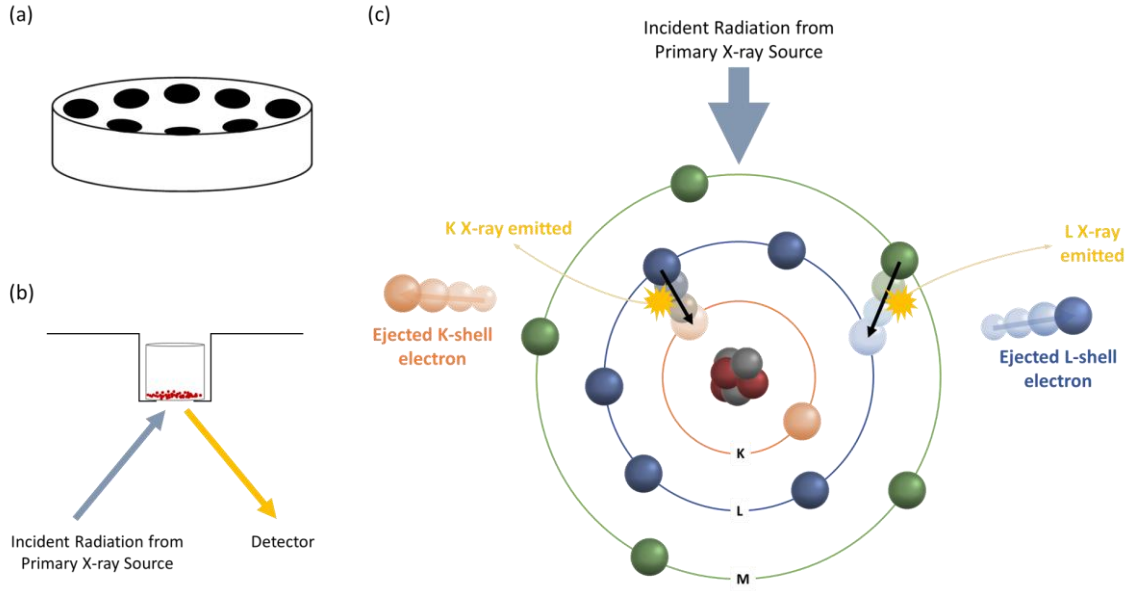

Figure 2.1: (a) Sample holder, (b) irradiation of sample from below the sample holder and (c) schematic diagram of excitation, relaxation followed by fluorescent X-ray emission.

2.1.1.2 Energy Dispersive X-Ray Spectroscopy

Energy dispersive X-ray spectroscopy (EDS) is a useful technique for quantitative elemental analysis of solid catalysts. In EDS, a sample is typically excited by radiation with an electron beam from an electron microscope, emitting X-rays when relaxing to the ground state, similar to XRF (Figure 2.1c). Quantitative measurements of elemental composition can be achieved from analysis of the emitted wavelengths and number of X-rays, based on appropriate standard materials for calibration. Similar to XRF, higher resolution of spectra for heavy atoms is often observed, due to multiple possible excited states resulting in a distinct pattern of emitted X-rays.[105,106]

In this dissertation, EDS was measured in a scanning electron microscope (section 0), providing excellent images of the samples combined with elemental analysis. However, EDS is a surface technique and elemental analysis is based on limited areas of the sample selected from concurrent SEM imaging. Various areas of the samples are typically analyzed to give an averaged value of the elemental composition. EDS was analyzed using an Oxford INCA system.

2.1.1.3 Inductively Coupled Plasma Atomic Emission Spectroscopy

Inductively Coupled Plasma Atomic Emission Spectroscopy (ICP-AES) is a highly accurate elemental analysis technique. Atomization of the sample in a plasma containing free electrons affords excited electronic states. The emitted photons can be detected and quantified, when returning to the lower energy states. The emission intensity is proportional to the element concentration of the sample. The plasma, typically Ar gas that is heated to 6000-10000 K, is sparked from a coil ionizer, affording free electrons, which are carried by the plasma until collision with the sample elements.[107]

However, ICP-AES analysis is generally limited to liquid samples for proper evaporation. Typically, the sample is dissolved in an appropriate solvent, however, dissolving of some solid catalysts can be challenging and possibly result in unreliable element concentrations. The ICP-AES data presented in this dissertation was obtained from a Perkin Elmer Plasma 400, using double distilled water as solvent at FAU, by Dr. Nicola Taccardi.

2.1.2 Electron Microscopy

Electron microscopy is a convenient imaging technique for analysis of solid materials, such as catalysts, and is widely used in morphology examinations and determination of particle sizes.

Two types of electron microscopy was used for analysis in this dissertation: scanning electron microscopy (SEM) and transmission electron spectroscopy (TEM). Irradiation of the sample by a focused high-energy electron beam is similar for both types of electron microscopy, however, the method of image production is different (Figure 2.2a). The shorter wavelengths of electrons compared to visible light, produces much higher magnifications than what can be achieved by traditional optical spectroscopy. The high resolution images provides a means of visualization of very small particles, however, the described electron microscopies are based very small sections of the sample and analysis of various sections is required for an adequate averaged analysis.[11,108]

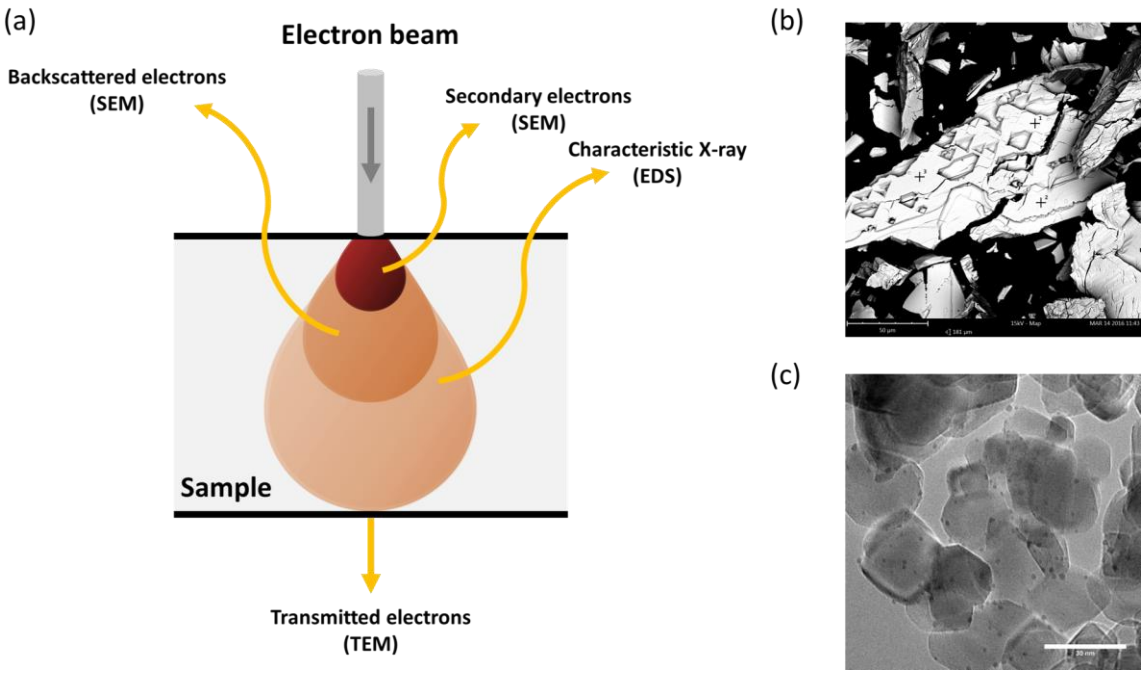

Figure 2.2: (a) schematic illustration of signals emitted from interaction volume of electron and sample, (b) SEM imaging of $K_6P_2W_{18}O_{62}$ (Chapter 5) and (c) TEM of titania-supported gold nanoparticles (Chapter 3).

2.1.2.1 Scanning Electron Microscopy

In SEM, the images are produced from detection of reflected low-energy electrons, either secondary or backscattered electrons, generated from excitation of sample atoms by a high energy electron beam scanning over a selected section of the sample (Figure 2.2a). The electron beam is accelerated to 1-30 keV depending on the nature of the sample. The penetration depth of the electron beam into the sample depends on the sample material and applied acceleration voltage. High penetration depth affords more information of the bulk of the sample section than the surface. Higher acceleration voltage is required for heavier atoms compared to lighter atoms to obtain comparable penetration depths. Radiation is generated in the entire interaction volume, however, only the emitted electrons departing the sample will be detected, and a 3D image of the catalyst topography is produced from these (Figure 2.2b).[108,109]

The data presented in this dissertation, was obtained from SEM coupled with EDS for elemental analysis of sample sections. The emitted characteristic X-rays detected in EDS are illustrated in Figure 2.2a. SEM-EDS was performed on a Quanta 200 ESEM FEG operated at 10 kV and spot size of 2.0. Samples were

placed on a carbon film. The SEM-EDS analysis was performed by laboratory technicians Rolf Jensen and Berit Wenzell.

2.1.2.2 Transmission Electron Microscopy

As suggested by the name, high energy electrons transmitted through the sample is detected in TEM imaging (Figure 2.2). The transmitted electrons provide information of the internal structure of the sample section, rendering TEM particularly efficient in examination of solid catalysts. Determination of catalyst morphology, crystallization, nanoparticle size and dispersion based on TEM is widely applied for catalyst characterization.

TEM is a bright field imaging technique and only the electrons going directly through the sample are detected and produce the high-resolution image. Darker shadings of more dense or simply thicker areas of the sample will appear due to stronger elastic and inelastic scattering of electrons, generating contrasts in the imaging of different elements. Differentiating of elements *e.g.* in supported nanoparticles, allows for determination of nanoparticle size and distribution on support in the analyzed section (Figure 2.2c).[108,109]

The TEM images presented in this dissertation was obtained from a FEI Tecnai T20 G2 microscope, operating at 200 eV. The samples were dispersed directly on holey carbon grids. TEM images was recorded by Jerrik J. Mielby and Ph.D. student Simone L. Zacho.

2.1.3 X-Ray Powder- and Single Crystal X-ray Diffraction

X-ray Powder Diffraction (XRPD) is a fast analysis method providing information on composition, crystal phases and average crystal sizes of a powder sample. The crystal phases can be deduced from the detected peak pattern arising from the different scattering angles. The peak broadening can be used for determination of the average crystallite size using the Scherrer equation (2.1, where τ is the mean size of the crystalline domain, K is the shape factor, λ is the incident X-ray wavelength, β is the line broadening at half the maximum intensity of the peak and θ is the Bragg angle). The information obtained from XRPD is highly useful for characterization of solid catalysts, and XRPD is widely used for determination of active species, structure-activity relationships and optimization of catalyst synthesis procedure.[103,110]

$$\tau = \frac{K\lambda}{\beta \cos\theta} \tag{2.1}$$

In XRPD, X-rays are directed onto a powder sample, resulting in diffraction of the beam according to Bragg's law (2.2, where d is the spacing between the lattice planes, λ is the incident X-ray wavelength and θ is the Bragg angle). A diffractogram can be generated from the detected diffraction angles and intensities, and used for determination of the crystallite phase and averaged size.[111]

$$\lambda = 2d \sin\theta \tag{2.2}$$

Single Crystal X-ray Diffraction (single crystal XRD) is based on a similar principle compared to that of XRPD, however, in single crystal XRD, the X-ray beam is directed onto a single crystal of the sample, affording a diffraction pattern of spots which is detected. It is therefore important to be able to grow stable and sufficient size crystals (typically > 0.1 mm) for proper structure elucidation. From single crystal XRD, the full structure of a crystal can be elucidated from refinement of the detected scattering angles and intensities. The elucidated structure is based on average bond lengths and angles recorded for the crystal. Very small molecules (>100 atoms in the unit cell) and very large molecules (>10000 molecules in the unit cell) often afford insufficient resolutions for structural elucidation.[112]

The diffraction patterns were obtained from a Huber G670 Guinier diffractometer using a Cu-K radiation from a focusing quartz monochromatic beam, with an exposure time of 1 h at an incident wavelength of 1.54060 Å, in the 2θ interval 3-100°. All XRD data was recorded by laboratory technician Lise Lotte Berring and the single crystal data was refined by Assoc. Prof. Kenny Ståhl. The single crystal data was obtained from a SuperNova Dual Atlas using *CrysAlis PRO*, Agilent Technologies.

2.1.4 Gas Physisorption

The surface area of a solid catalyst can have a great influence on reactions. In heterogeneous catalysis, adsorption of the involved components is a crucial step. Higher surface area of the catalyst allow for more components to adsorb on the surface. Therefore, it is of great importance to determine the surface area for efficient catalyst optimization.

In gas physisorption, the ability to physically adsorb molecules is exploited for determination of the catalyst surface area. A gas, typically N_2, is adsorbed onto the surface of the catalyst and the surface area is determined from the volume of the adsorbed gas, based on Brunauer-Emmet-Teller (BET) theory, which is an extension of the Langmuir theory. The physisorption data is described by an adsorption isotherm, depicting the dependence of amount adsorbed gas over partial pressures of the applied gas at a constant temperature in a graph. The dependence was traditionally described by the Langmuir model (2.3, where V is the amount of gas adsorbed, V_m is the amount of gas adsorbed in one monolayer, p is the pressure and b is the adsorption coefficient). However, the simplified Langmuir model, which is based on adsorption on a monolayer of the surface, was extended to apply for multilayer adsorption by Brunauer, Emmet and Teller, see Equation 2.4 (where V is the amount of gas adsorbed, V_m is the amount of gas adsorbed in one monolayer, p is the pressure, p^0 is the saturation pressure and C is the BET constant).

$$\frac{V}{V_m} = \frac{bp}{1+bp} \tag{2.3}$$

$$V = V_m \frac{C\frac{p}{p^0}}{\left[1-\frac{p}{p^0}\right]\left[1+(C-1)\frac{p}{p^0}\right]} \tag{2.4}$$

Applying the BET equations allow for determination of the BET surface area which is used in this dissertation. Furthermore, information of pore volume and size distribution of potential micro-, meso- and macro pores is obtainable from gas physisorption by BET analysis.[11,103,113]

The nitrogen physisorption data presented in this dissertation were obtained from a Micromeritics ASAP 2020 instrument using liquid nitrogen. The samples were outgassed in vacuum at 150 °C for 6 hours prior to measurements. The total surface areas were calculated according to the BET method. The BET surface areas were recorded by head laboratory technician Bodil F. Holten

2.1.5 Infrared Spectroscopy

Infrared (IR) spectroscopy is a widely applied technique used for identification and purity of compounds.[112] IR spectrometers are relatively inexpensive and are therefore often widely available. A sample, which can be solid, liquid gaseous or in solution, is irradiated with IR light, affording absorption of IR energy and vibrational excitation of chemical bonds in the sample. The absorbance intensity, which is determined from detected transmitted or reflected light, is plotted against the frequency, affording a spectrum, which can be interpreted for identification of functional groups of the sample. Absorption occur at resonant frequencies of the vibrational frequencies, which is used for identifying functional groups present in the sample.

In Fourier transform infrared (FTIR) spectroscopy, an IR beam containing a wide range of frequencies is used for irradiation of the sample. Different combinations of frequencies are applied on the sample and the collected data is transformed into a high-resolution spectrum by Fourier transformation calculating the absorbance at each wavelength. FTIR is one of the most widely used IR techniques due to fast accessibility to high resolution spectra.

Attenuated total reflection (ATR) coupled with IR allows for direct analysis of a sample without further preparation. The IR beam is directed onto a crystal with a high refractive index, such as diamonds, reflecting the beam in a way that exceeds beyond the surface of the crystal into the sample. The ATR-FTIR analysis was performed on a Bruker ALPHA-P ATR-IR at DTU and on a JASCO FTIR-4100 at FAU.

2.1.5.1 Nondispersive Infrared Detector

Nondispersive infrared (NDIR) detector is an IR technique often applied on gases for determination of specific gas concentrations. The NDIR used in this dissertation was specific for CO and CO_2 detection. The tuning of the NDIR is obtained by applying an optical filter, elimination all other wavelengths than the specific wavelengths for detection of the selected gas molecules, in this case CO and CO_2.[114] The volumetric concentration of the gas phase CO and CO_2 content was measured for the oxidation reactions presented in Chapter 3 using a Rosemount BINOS 100 coupled to the high pressure reactor, and the volumetric concentration of CO_2 in Chapter 4, using a Quantek Instruments Carbon Dioxide Analyzer, Model 906. Selected experiments from Chapter 4 were analyzed for CO formation on the Rosemount BINOS 100.

2.2 Equipment

All oxidation experiments were performed in high-pressure apparatus, and suitable, small high-pressure reactors were constructed for faster reaction optimization.

2.2.1 Mini High-Pressure Vessels

Small-scale high-pressure vessels are highly useful for fast optimization of reaction conditions, screening of catalysts and studying of substrate scope limitations. Moreover, the cost of chemicals is reduced in small-scale reactions, and the setup capacity was designed to run up to six parallel reactions, reducing the work time significantly. Six mini high-pressure vessels (MV) were designed and constructed. My design is illustrated in Figure 2.3 and images of the finished reactors is presented in Figure 2.4 (see Appendix A for detailed design).

The reactors were constructed from stainless steel with total internal volume of 18.4 mL of the sealed reactors. The joint between the connector and the bottom was fitted with a Teflon ring for complete sealing at elevated pressures. The bottom of the inside of the MVs were rounded for better stirring of the magnets.

A tube reaching from the top of the fittings into the bottom was equipped with a click-connector for gas inlet at the top, leading the gas directly into the liquid-phase of the reaction for better gas-entrainment (middle tube in Figure 2.3). The bottom of the gas-inlet tube was fitted with six small holes for better gas-distribution into the liquid phase. The gas-outlet tube was fixed into the top part of the reactor and fitted with a valve (left tube). This tube was connected directly to the NDIR instrument for analysis of the gas phase of the reaction. The third tube was fitted with a digital thermometer, monitoring the internal reaction temperature of the liquid phase during the reactions. The MVs were fitted with a manometer for monitoring of the pressure. Additionally, the MVs were equipped with a safety valve, bursting at 50 bar. Due to limitations of pressure testing facilities, the MVs were only tested up to 50 bar without any detection of gas leak. A heating block of aluminum, fitting on a standard magnetic stirrer, was produced for heating of the reactors.

The MV reactors were constructed by Ishaq Khaliqdad and Andreas Graff Pedersen (DTU Chemistry, workshop). The schematic overview of the design was illustrated by Ishaq Khaliqdad (Figure 2.3).

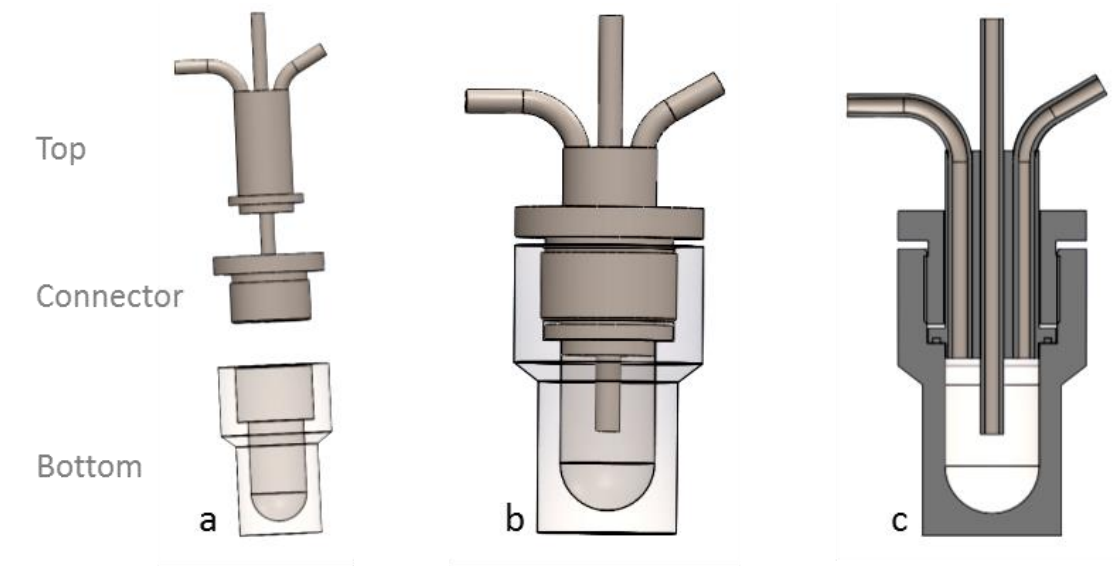

Figure 2.3: Schematic of design of mini high-pressure vessels.

Figure 2.4: Images of mini high-pressure vessels

Chapter 3. Selective, Base-free Oxidation of Glycolaldehyde to Glycolic Acid in Water

Increasing demands for environmentally friendly protocols for selective oxidations of biomass-derived compounds at mild conditions has been observed over the past years. This chapter focuses on the benign oxidation of the smallest α-hydroxy sugar, glycolaldehyde, into glycolic acid at mild conditions.

3.1 Introduction

An essential synthetic transformation in the chemical industry is the oxidation of alcohols and aldehydes.[115] Deprived fossil based feedstock has increased the importance of bio-derived chemicals, and hence, the importance for developing protocols for transformation of biomass-derived molecules into feasible chemicals.[68,116] One method for catalytic upgrading of alcohols and aldehydes is by oxidation into aldehydes, ketones, acids and esters. The demand for

developing benign and efficient methods for the selective oxidations of biomass-derived compounds has increased over the past years.[117–119]

Glycolaldehyde (GAD) is the simplest sugar and is an often-observed by-product from the degradation of larger biomass-derived compounds. Conversion of GAD into fine chemicals is of great interest due to increasing availability from biomass. Currently, GAD is obtainable in high yields from glucose in critical water or from bio-oil, and new methods are currently being developed.[25–27]

3.1.1 Glycolic Acid

Glycolic acid (GA) is the smallest α-hydroxy carboxylic acid. At present, GA has found use in various industries including textile dyeing, food preservative, cleansing agents, leather and fur-processing, cosmetics, medicinal and polymer (Figure 3.1).[120–125] The approximate worldwide annual consumption of GA is 2000 – 3000 ton.[120]

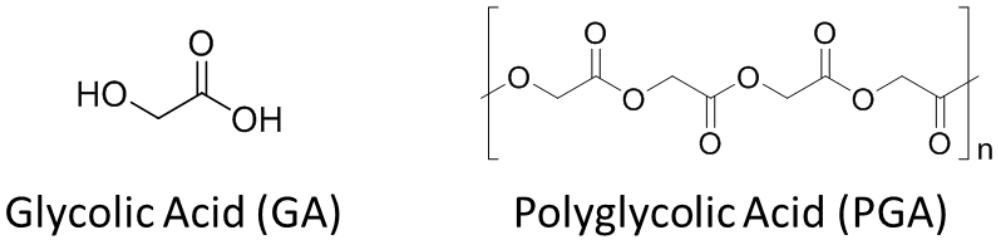

Figure 3.1: Chemical structures of glycolic acid and polyglycolic acid.

Currently, the two main manufacturer of GA are Hoechst and Du Pont producing 57 and 70% aqueous solutions of GA, respectively.[120,126] The low-cost carbonylation of formaldehyde with synthesis gas is the predominant approach to GA synthesis (Du Pont).[126,127] Other approaches include hydrolysis of molten monochloroacetic acid with aqueous sodium hydroxide (Hoechst),[126,128] electrolytic reduction of oxalic acid,[129,130] hydrolysis of the corresponding nitrile or from isolation from natural sources like sugarcane, sugar beets, pineapple, cantaloupe and grapes (Scheme 3.1).[120,131,132]

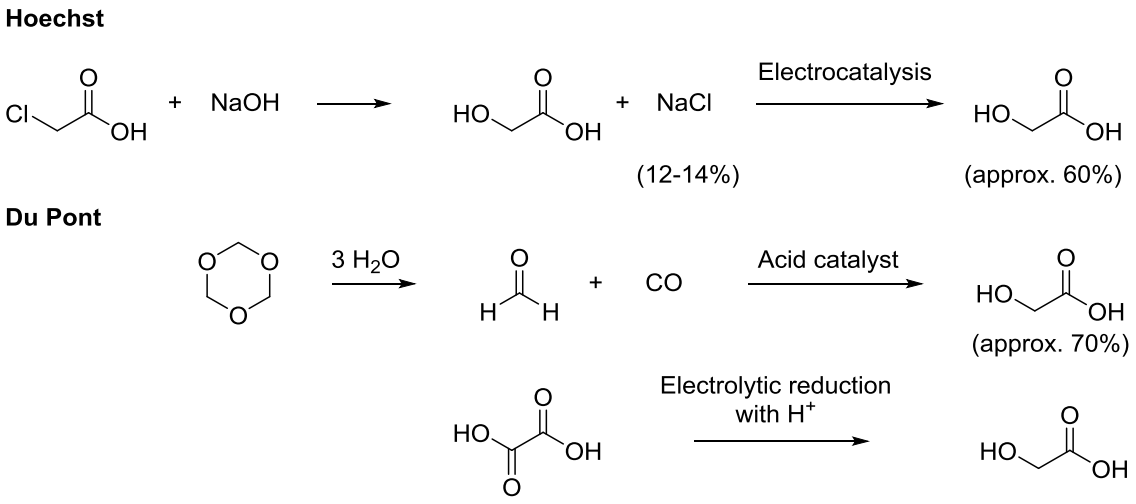

Scheme 3.1: Production of glycolic acid.[120,126]

Moreover, GA has been synthesized from glycerol by zinc-catalyzed oxidation with H_2O_2 reported by Zhen *et al*., and from acid-catalyzed hydroxylcarboxylation of formaldehyde, methylene diacetate and methylene dipropionate as reported by Barnicky *et al.*.[133,134]

3.1.2 Supported Gold Nanoparticles

Until the 1970's, gold was considered a chemically inert material for catalytic processes. In 1973, Bond and Sermon reported on the hydrogenation of olefins catalyzed over a supported gold catalyst, which intrigued a renewed interest for gold catalysis.[135,136] Haruta *et al.* reported the first supported gold-catalyzed oxidation of CO in 1987.[137,138] Since then, supported gold nanoparticles (NPs) have been recognized as highly active, selective and green catalysts in numerous reactions including oxidations, epoxidations, hydrochlorinations, C-C bond formation, hydrogenations, water gas shift, and several reviews has been published over the years.[22,45,91,138–154] Gold based catalyzed reactions are of great potential for industrial production of fine chemicals due to their high activity and selectivity at mild conditions, rendering the gold catalysts feasible for environmentally friendly manufacturing of organic chemicals with green oxidants.[149] However, the catalytic properties of gold NP are highly dependent on the applied preparation method, the support and the size of the NPs.[2,155,156]

Furthermore, sintering of gold particles is very sensitive to the reaction conditions and the conditions of storage.

The first “gold rush” in the 1990’s was initiated by the discovery of CO oxidation, the second wave in the 2000’s by the selective oxidations such as epoxidations and sugars, and recent interest in supported gold NP-catalyzed hydrogenations have been reported.[22,45,52,138–140,142,144,148,157]

Small gold NPs (typically 1-5 nm) are considered highly active catalysts, and the activity has a tendency to decrease with increasing particle size, hence, it is crucial to have efficient protocols for preparation of small supported gold nanoparticles and storage conditions that prevent aggregation and sintering of the NPs (see 0).[77,91,155] Furthermore, the selectivity is also highly influenced by the particle size. For supported gold NP-catalyzed oxidations, a maximum in activity and selectivity is often observed between 1 and 5 nm gold NP, depending on the substrate and the desired selectivity of the reaction. Smaller NP are highly active and C-C cleaved- and fully oxidized products are often the major end-products. Kethchie *et al*. reported, that small highly dispersed gold NP are highly active in the formation of hydrogen peroxide on the gold surface during the oxidation of glycerol, possibly promoting the C-C cleavage.[23,158,159] In contrast, large gold NP are less active and selective, and a fine balance between selectivity and activity can be achieved by optimizing the size of the gold NP.

Various protocols for proper preparation methods of small gold NP on wide variety of supports has been published.[77,151,155,156,160–164] The support is necessary to prevent agglomeration and coalescence of the gold NP.[145] Typically, metal oxides (M_xO_y) are the support of choice due to high stability and high symbiotic reactivity when combined with gold NPs.[165] Particularly, the metal oxides of the first row of transition metals have been reported active for numerous reactions.[2] Furthermore, the structure of the support influence the size and distribution of the gold NP, which in turn affects the activity and selectivity as mentioned above. In general, supports with high surface area result in higher distribution of the gold NPs, and hence, smaller NP more readily available for substrate interaction. Product selectivity is also influenced by the pore size of the support, as shown by Rodrigues *et al*. varying the mesopore sizes of carbon xerogels in the oxidation of glycerol.[166] Narrow pores favored formation of glyceric acid, while higher selectivity for dihydroxyacetone was observed with wide pores. Additionally, the density of defects and the crystallinity of the support affect the adsorption ability. Some supports may exhibit an electronic effect, actively taking part in the reaction mechanism.[145] The influence of the support and the mechanistic role of the support is not fully understood. Elucidation of these could provide a means of fast optimization of the support for highly active and selective supported gold catalysts.[145]

3.1.3 Oxidations with Supported Gold Nanoparticles

Among the various applications in catalysis with supported gold NP, oxidations have received considerable attention. High activity and selectivity of the supported gold NP at mild conditions provide efficient catalysts for a wide variety of selective oxidations. Selected examples of oxidations are presented in Scheme 3.2.

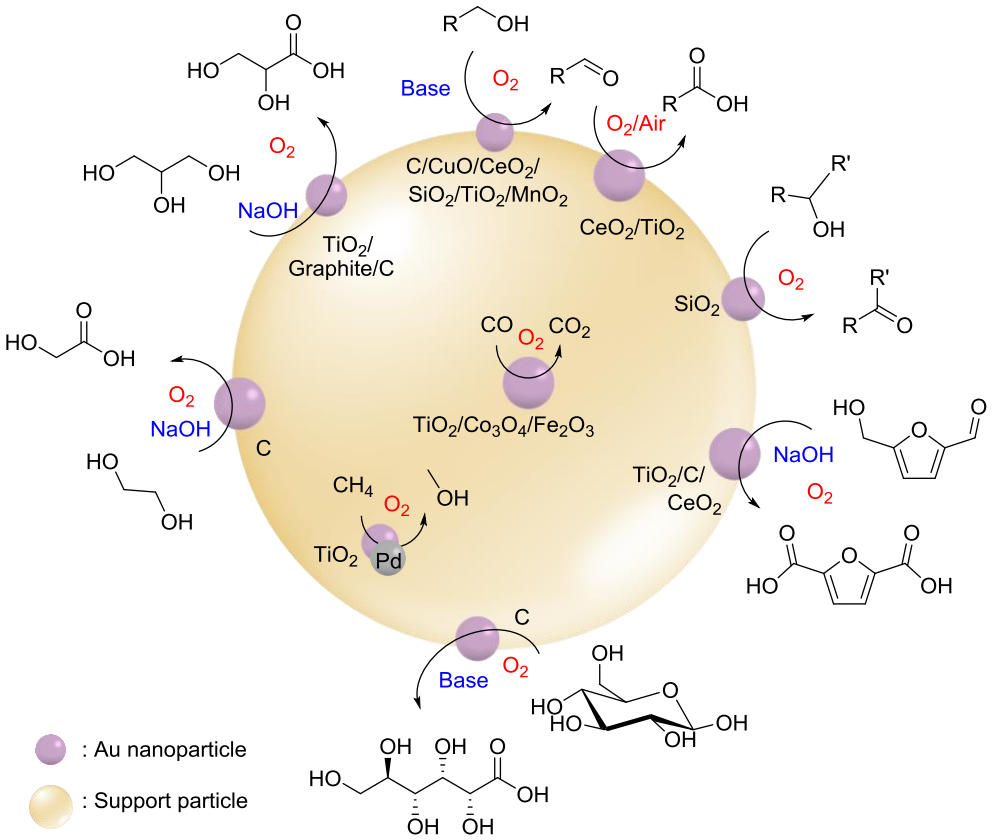

Scheme 3.2: Examples of oxidations with supported gold NP.[57,60,66,85,93,99,137–140,163,167–176]

As previously mentioned, the supported gold catalysts provides a means of environmentally-friendly oxidation procedures satisfying several of the green chemistry principles, making the gold-catalyzed oxidations highly feasible for conversion of biomass and biomass-derived compound. Several biomass-derived molecules have been converted into platform molecules or fine chemicals by gold-catalyzed oxidations.[85,91,93,177] Especially the selective oxidation of alcohols in various biomass-derived substrates has received considerable attention, and optimized procedures for several polyfunctional alcohols has been published.[65,71,85,88,171,178–190]

3.1.3.1 Base-free Oxidation with Supported Gold Nanoparticles

Several studies on base-free oxidation of alcohols and aldehydes have been reported over the years. In general, gold NP supported on metal oxides appears advantages in the base-free oxidation compared to oxidations with carbon- and polymer-supported gold NP.[86,93,173] However, in recent years, base-free oxidations have been reported for several supported gold NP including hydrotalcite-and carbon-supported catalysts on substrates such as 5-HMF, glycerol and glucose.[64,77,191–193]

3.1.3.2 Mechanism of Oxidation

The precise mechanism of gold-catalysis and oxygen activation on the gold NP surface is still a matter of debate. The generally accepted mechanism for the aqueous oxidation of aldehydes with base over gold NP is the oxidative dehydrogenation. Aldehydes are readily hydrated in aqueous media, generating geminal diols, which can be oxidized over the gold NP to the corresponding carboxylic acid by oxidative dehydrogenation, see Scheme 3.3. The oxidant, typically molecular oxygen or air, is necessary to re-oxidize the catalyst by removal of the deposited electrons on the gold NP that forms during the dehydrogenation of the substrate.[180,181,194] The mechanistic details of the substrate oxidation, hydride formation and oxygen activation have been heavily discussed in literature and several propositions have been published based on calculations and experimental studies of the oxidation.[60,87,143,153,156,163,181,194,195]

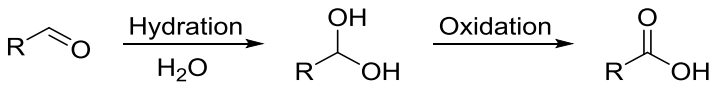

Scheme 3.3: Oxidation of aldehydes.

Typically, supported gold-catalyzed oxidations are executed in the presence of a base. The base promotes geminal diol formation of the aldehyde, by assisted deprotonation of water. Moreover, the added base neutralize formed acidic products. Gold NPs have been reported to be acid-sensitive promoting agglomeration of the NP, and hence, decreasing the activity and selectivity of the catalyst.[87] In addition, free carboxylic acids adsorb strongly on gold surface blocking active sites, deactivating the catalyst.[196] Increased base concentrations was reported to accelerate the oxidation rate. [143,147,153,197]

A similar reaction mechanism has been proposed for the base-free oxidation catalyzed by gold NP (Scheme 3.4).[64,80,163] The geminal diol, formed from hydration of the aldehyde, forms a gold-alkoxide specie, releasing two protons (step 1). The gold-alkoxide specie undergoes oxidative dehydrogenation generating a highly reactive gold-hydride specie, which is the rate determining step of the reaction (step 2).[145] The metal-oxide bond-breaking and the metal-hydride formation were suggested to be concerted, however, asynchronous.[145] The formed hydride is oxidized by activated oxygen, generating hydrogen peroxide by reaction with the released proton (step 3 and 4). The activation of oxygen is a crucial step of the oxidation. Molecular oxygen is associatively adsorbed on the gold cluster surface, forming a superoxide ($O_2^{\bullet}$) which is the active oxygen specie.[64,80,163] Hydrogen peroxide is readily decomposed to water and oxygen in aqueous media. Regeneration of the catalytic sites by release of hydrogen peroxide affords the overall reaction equation presented in Scheme 3.5.

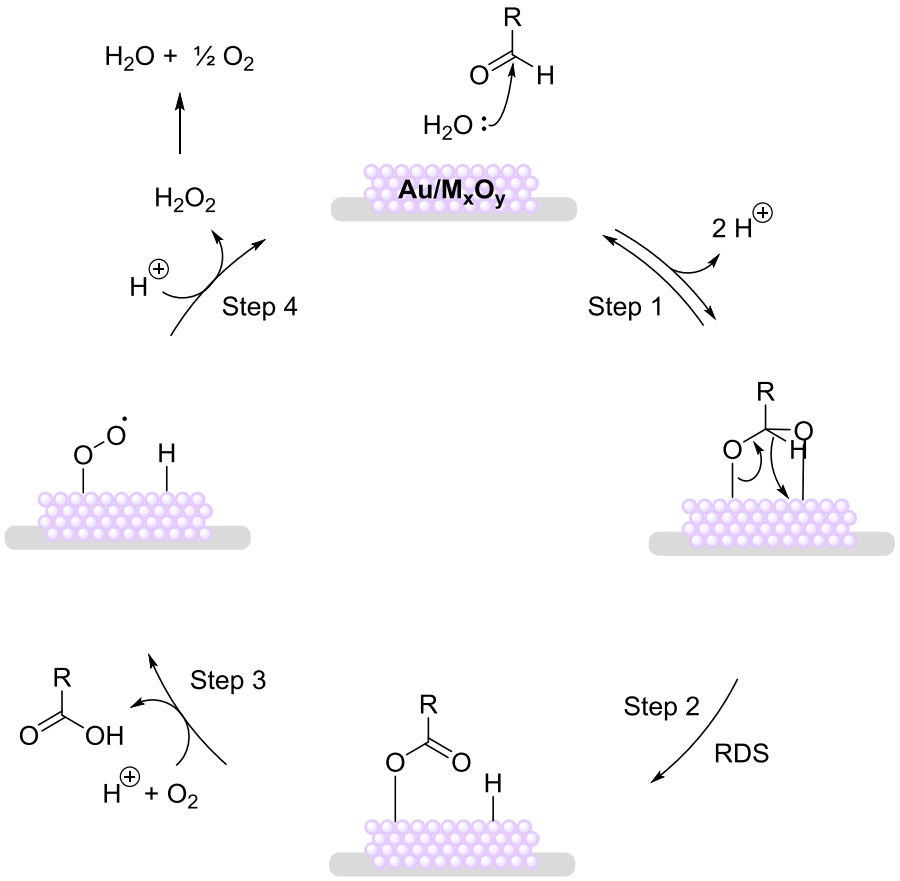

Scheme 3.4: Proposed mechanism for base-free oxidation of aldehydes over gold NP. [64,80,145,163]

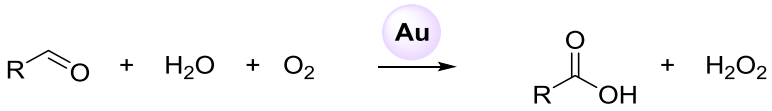

Scheme 3.5: Overall oxidation of aldehydes over gold NP.

From ^{18}O labelling experiments it was shown, that the incorporated oxygen of the carboxylic acid originates from the water,[60,194] agreeing with general observations of hydration of aldehydes in water, forming a germinal diol which adsorbs on the gold surface. Furthermore, based on experimental evidence, it was shown, that hydrogen peroxide was formed as the reduction product, in agreement with the proposed mechanism presented in Scheme 3.4.[180,181] For CO oxidation it was reported, that adsorbed oxygen on the gold surface enhances the adsorption of CO, suggesting that O_2 adsorption is a central step of the reaction mechanism.[156,198]

As previously mentioned, the catalytic activity of gold NP is strongly dependent on the gold particle size.[160] Low coordinate-gold atoms are present at the edges and corners of the NP. The abundance of these low-coordinated atoms has been attributed the largest effect on the catalytic activity. The large surface area of gold and the largest number of low-coordinate gold atoms can be obtained by synthesizing small and highly dispersed gold NP, which elucidates the higher activity of smaller gold NP.[13,14] The low-coordinate gold atoms facilitate the adsorption of oxygen and substrate and possibly, the full oxidation reaction takes place at the edges and corners of the gold NP. Furthermore, this site of reaction is adjacent to the support, and several effects of the support has been proposed to effect the activity and/or the selectivity of the catalyst.[199,200] Previously, a radical mechanism was proposed for the oxidation, however, this theory was eliminated by adding a radical scavenger to the reaction.[191,201]

Several forms of GAD are present in aqueous solution at room temperature, including dimeric and monomeric species (Scheme 3.6).[202,203] The dimeric specie A represents the form of the solid state, and the hydrated aldehyde D constitute the major form in aqueous solution. As previously mentioned, the hydrated aldehydes are readily available for gold-alkoxide formation, the first step of the oxidative dehydrogenation of GAD (Scheme 3.4).

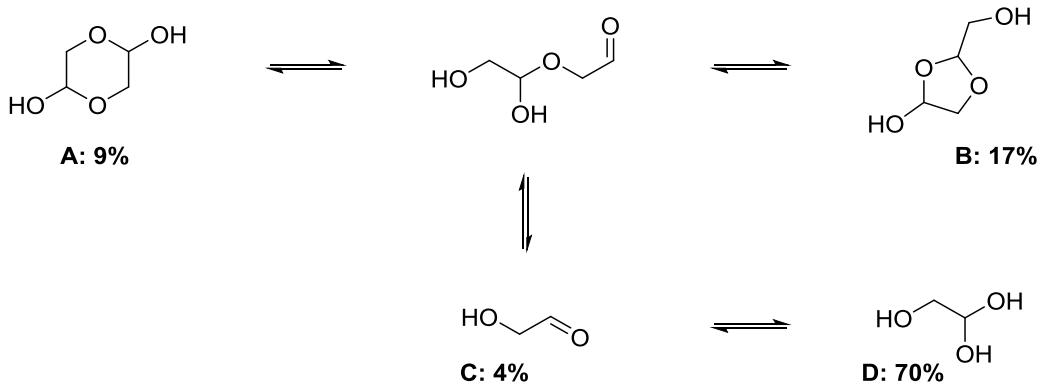

Scheme 3.6: GAD dissolved in water: glycolaldehyde dimer (A), 2-(hydroxymethyl)-1,3-dioxolan-4-ol (B), glycolaldehyde (C) and hydrated glycolaldehyde (D).[202,203]

3.1.3.3 Other Catalysts for Oxidation of Alcohols and Aldehydes

In general, gold-based catalysts are considered the most active catalysts for oxidation of alcohols and aldehydes due to wide substrate scope and high stability under oxidative atmosphere. Aside from gold-based catalysts, Pd- and Pt-based catalysts are among the most widely used heterogeneous catalysts for oxidation of alcohols and aldehydes, followed by Ru, V, Co, Rh, Ag, Cu, Fe and combinations thereof.[34]

Supported gold catalysts appear advantages in selective oxidation at mild conditions affording high selectivity and relatively low activation temperature. High activity of Pt-group based supported catalysts for oxidations have been reported, however, outcompeted by the superior selectivity by supported gold catalysts.[21,77,204] Combinations of gold and Pt-group nanoparticulate supported catalysts has been reported to afford high yields and selectivities at mild conditions.[13,52,62,71,77,78,147,153,176,205–207]

3.2 Experimental Detail

3.2.1 Materials

All reagents were of reagent grade and were used without further purification: glycolaldehyde dimer (≥98%, Sigma-Aldrich), glycolic acid (99%, Sigma-Aldrich), glyoxal trimer dehydrate (≥97%, Sigma-Aldrich), glyoxylic acid (98%, Sigma-Aldrich), oxalic acid (≥99%, Sigma-Aldrich), titania-supported gold nanoparticles (1 wt% ∓0.1%, average gold nanoparticle size of 2-3 nm, Sigma-Aldrich), sodium hydroxide (≥98%, Sigma-Aldrich), potassium carbonate (≥99%, Sigma-Aldrich), pressurized air (99.5%, Air Liquide Denmark), dioxygen (99.5%, Air Liquide Denmark), millipore water.

3.2.2 General Procedure for Oxidation

The oxidations were carried out in a mechanically stirred high-pressure Parr reactor equipped with internal thermocontrol (T316 steel, Teflon™ beaker insert, 100 mL). The Teflon™ beaker was charged with the glycolaldehyde (150 mg, 2.5 mmol), Au/TiO_2 (0-377 mg, 0-0.766 mol% Au) and millipore water (10 g). The Parr reactor was flushed and pressurized with molecular oxygen (1-30 bar), heated to the desired temperature (23-150 ^oC) while constantly stirring at 600 rpm for 1-48 h. After the reaction, the reactor was rapidly cooled to room temperature (23 ^oC), the gas phase was analyzed for CO and CO_2 using a BINOS as describe in Section 0 and the liquid-phase for various oxidation products by HPLC (Agilent Technologies 1200 series, Aminex HPX-87H column from Bio-Rad, 300 mm x 7.8 mm x 9 µm, solvent: 5 mM H_2SO_4, applying a method at 24 ^oC with a flow rate of 0.3 mL/min).

3.3 Results and Discussion

Preliminary screening of catalysts for the aerobic oxidation of GAD yielded promising results for Au/TiO_2, Au/CeO_2 and $Pd\text{-}Bi/TiO_2$ (Figure 3.2). Titania supported cobalt afforded low conversion of GAD, however, reasonable selectivity for the desired oxidation product GA. In general, low selectivities for GA was observed. The highest GA selectivity was obtained from commercially available Au/TiO_2 (1 wt% Au), which was selected for optimization of the reaction conditions (first entry, Figure 3.2). Presumably, formation of the over-oxidation product, CO_2, occurred; however, in these initial experiments only the liquid phase was analyzed. Other identified oxidation products included glyoxal (GLO), glyoxylic acid (GLA) and oxalic acid (OA) depicted in Figure 3.3.

Limited studies of the effect of various reaction conditions on the aerobic oxidation was performed due to limitations of the reaction affording a maximum GA yield around 40%. Selected results are presented in the Figures 3.4 and 3.5.

The effect of decreasing temperature, pressure and time was studied, affording decreasing conversions at milder conditions (Figure 3.4). Significant increase in GA selectivity was observed with decreasing temperatures. However, the yield of GA was also decreasing, and the higher GA selectivities were obtained due to lower conversions of GAD. Atmospheric pressure of air yielded decreased conversion and GA selectivity, possibly due to limited availability of oxygen from poor solubility in water at ambient pressure. Decreasing reaction times yielded lower conversions, however, increasing GA selectivity until reaching a maximum after 3 h of reaction was observed. From these results it appears, that the GA yield is comparable from 3-18 h of reaction, however, shorter reaction times affords lower GA yield.

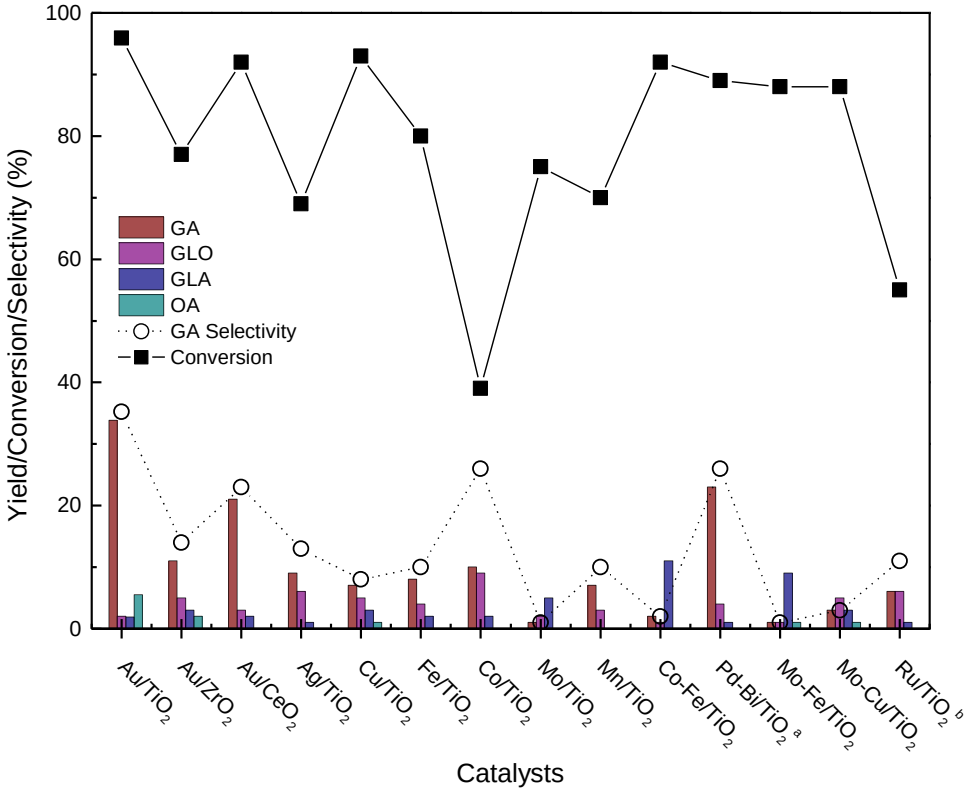

Figure 3.2: Preliminary catalyst screening. Reaction conditions: 2.5 mmol GAD, 1 wt% of the active metal of the catalyst i.e. Au, Pd, Co etc., 10 g H_2O, 80 °C, 6 bar air, 18 h. All catalyst were prepared with 1 wt% of active metal unless otherwise noted. Only the liquid phase was analyzed in these initial experiments. [a] 5 wt%, [b] 2.5 wt%.

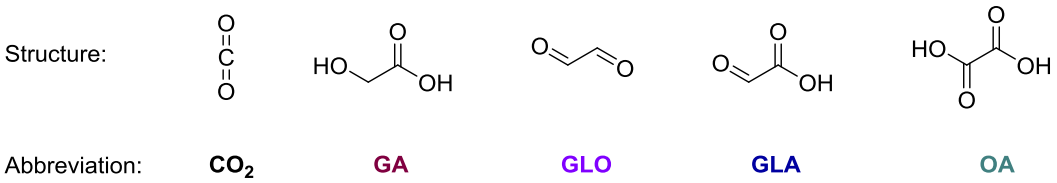

Figure 3.3: Identified oxidation products.

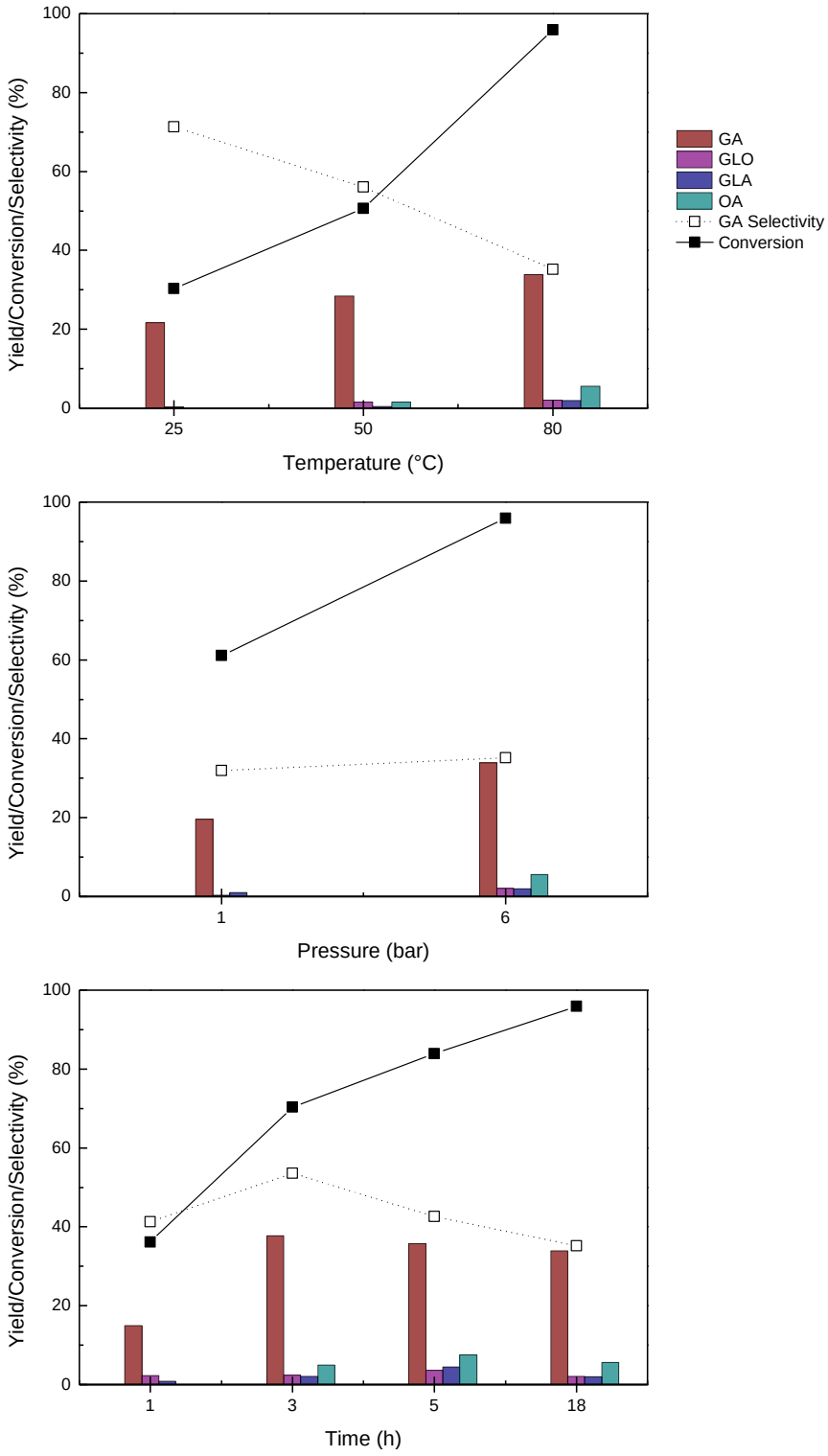

Figure 3.4: The effect of temperature (top), pressure of air (middle) and time (bottom) on the oxidation of GAD. Reaction conditions unless otherwise noted: 2.5 mmol GAD, 1 wt% Au (0.305 mol% Au), 10 g H_2O, 80 °C, 6 bar air, 18 h. Only the liquid phase was analyzed in these initial experiments.

Finally, the effect of Au:GAD ratio was examined, affording increased GA yield using the halved (0.153 mol%) and fourth (0.076 mol%) amount Au (Figure 3.5). Catalyst-deficient oxidation resulted in 44% conversion of GAD, however, poor selectivity for GA. In the absence of gold NP, 73% conversion was obtained with pure titania, affording low GA selectivity, accentuating the importance of gold NP for control of selectivity for the oxidation.

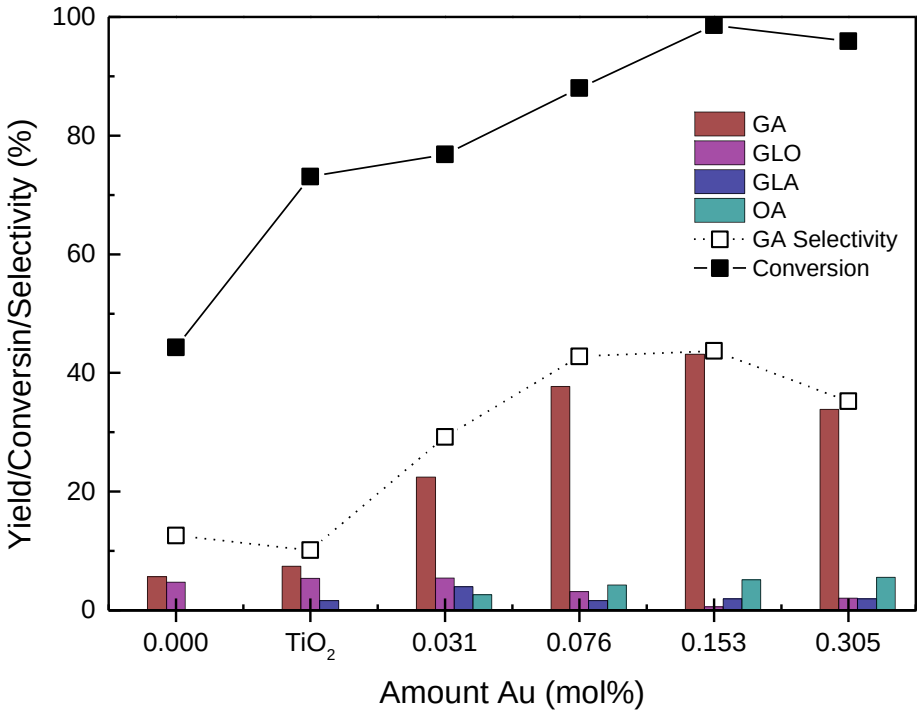

Figure 3.5: The effect of Au:GAD ratio. Reaction conditions unless otherwise noted: 2.5 mmol GAD, 0-1 wt% Au (0-0.305 mol% Au), 10 g H_2O, 80 °C, 6 bar air, 18 h. Only the liquid phase was analyzed in these initial experiments.

Following these results, molecular oxygen was studied as oxidant for the selective oxidation of GAD, using 0.076 mol% Au at 80 °C for 4 h applying 15 bar molecular oxygen. Various temperatures and reaction times were examined, and the results are presented in Figure 3.6. Low temperatures were found to decrease the conversions in addition to decrease the CO_2 yields by averting over-oxidation. Increasing formation of CO_2 was observed with increasing temperatures. Moreover, the GA yield increased with the temperature reaching the highest yield at 80 °C, followed by a rapid decrease in selectivity limited by formation of over-oxidation products. Increasing reaction times afforded increased conversions and a minor decrease of GA yield, implying good product stability over time at the given conditions. Short reaction times was found to yield decreased conversion and GA yield, however, good selectivity for GA was obtained after 1 h of reaction.

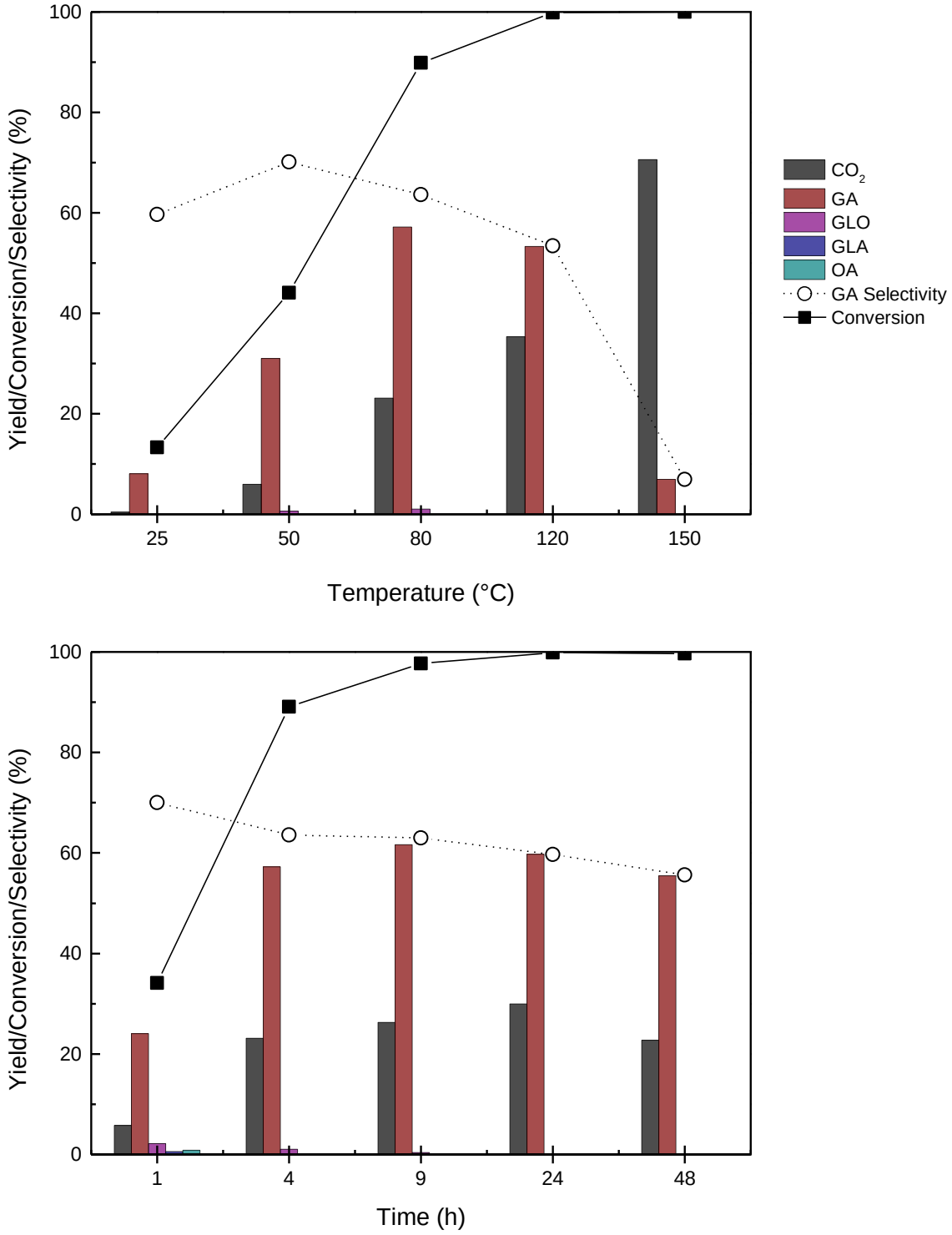

Figure 3.6: The effect of temperature (top) and time (bottom) on the oxidation of GAD. Reaction conditions unless otherwise noted: 2.5 mmol GAD, 0.076 mol% Au, 10 g H_2O, 80 °C, 15 bar O_2, 4 h.

Increasing the pressure oxygen from 6 – 30 bar did not affect the GA yield significantly; however, it was found that ambient pressure of molecular oxygen afforded low conversion and GA yield, presumably due to decreased oxygen-availability (Figure 3.7). A slight increase in GA yield and selectivity was observed from 6 to 15 bar, giving the highest GA yield (57%) applying 15 bar molecular oxygen.

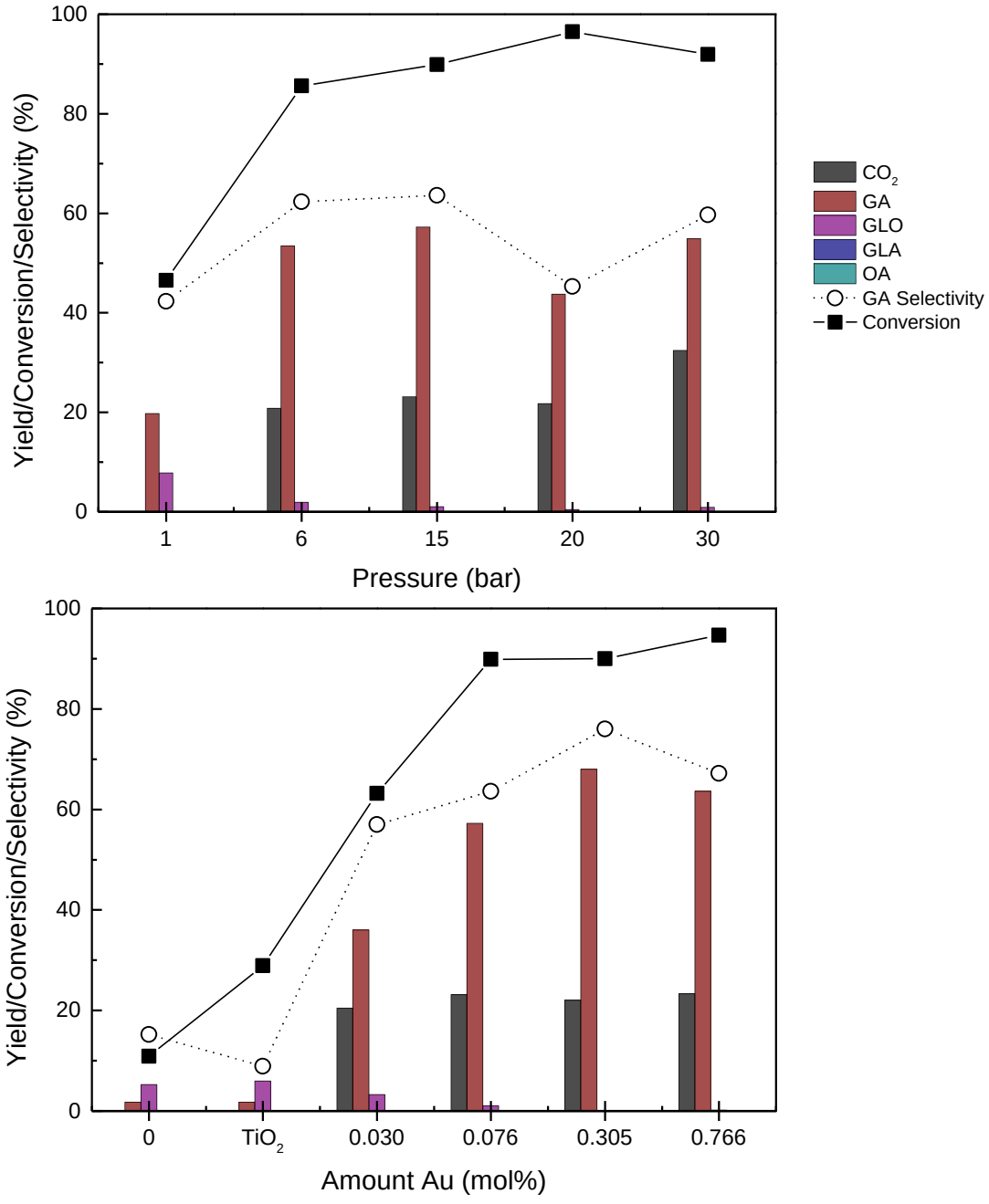

Figure 3.7: The effect of pressure (top) and Au:substrate ratio (bottom) on the oxidation of GAD. Reaction conditions unless otherwise noted: 2.5 mmol GAD, 0.076 mol% Au, 10 g H_2O, 80 °C, 15 bar O_2, 4 h.

Low conversion (11%) and GA selectivity (15%) was found for the catalyst-deficient oxidation of GAD at the given conditions (Figure 3.7). Gold-deprived titania afforded higher conversion (29%), although decreased GA selectivity was found (9%). The conversion and GA selectivity increased with increasing Au:substrate ratio, achieving the highest GA yield of 68% for 0.305 mol% Au. Higher Au:substrate ratio (0.766 mol%) afforded decreased GA yield. Seemingly, 0.305 mol% Au, corresponding to 1 wt% Au relative to GAD, is a quite high catalyst loading considering that the weight of the full catalyst, Au/TiO_2, equals the weight of the added substrate. Following this argument, optimization was continued using 0.076 mol% Au.

As previously mentioned, oxidations with supported gold NP are often performed in the presence of a base for neutralization of the produced carboxylic acids. The effect of base was studied at the optimized conditions (Figure 3.8). The presence of 1 equivalent NaOH accelerated the activity affording full conversions as described in literature, however, the GA selectivity decreased considerably. Formation of various C-4 sugars was detected according to HPLC analysis. Catalytic amount (10 mol%) of NaOH afforded slightly decreased activity, however, the yield of GA was continually limited by the formation of C-4 condensation products. Exchanging the base to the slightly milder base K_2CO_3 afforded lower conversion and no significant increase in GA selectivity was detected. Catalytic amounts of K_2CO_3, 10- and 1 mol%, was studied, yielding full conversion of GAD, however, low yields of GA. Formation of GLA was favored using 10 mol%, indicating over-oxidation of GAD at the given conditions. Decreasing the amount of K_2CO_3 afforded increased GA selectivity, yielding 12% GA and 4% of the over-oxidized product GLA. Notably, little CO_2 formation was observed in the presence of base due to limitations from competing aldol condensations.

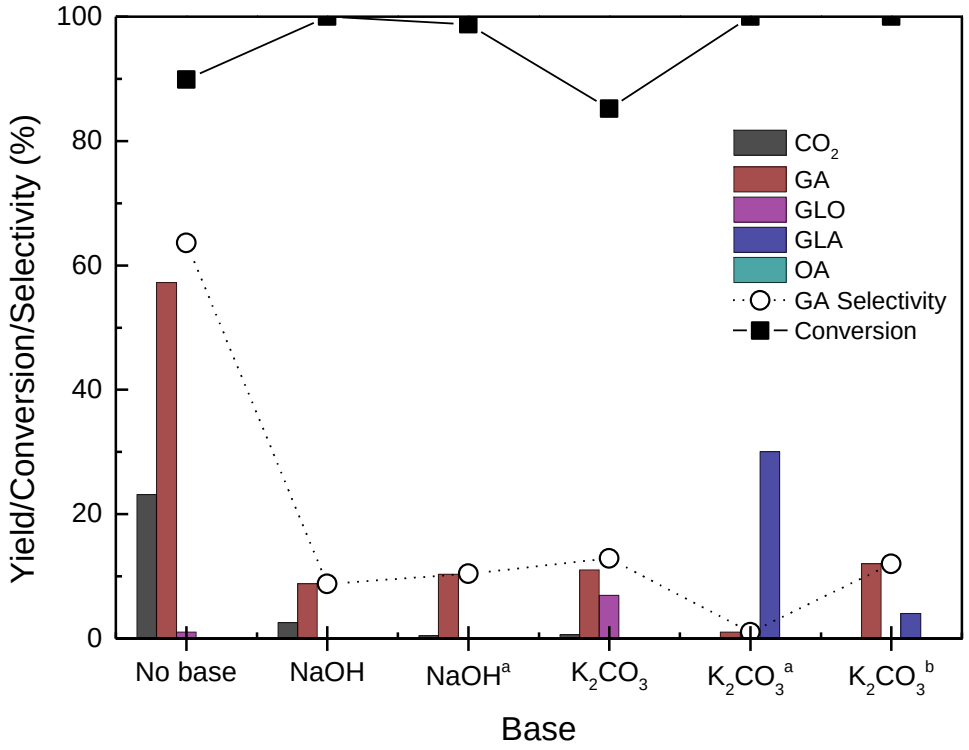

Figure 3.8: The effect of base on the oxidation of GAD. Reaction conditions unless otherwise noted: 2.5 mmol GAD, 0.076 mol% Au, 100 mol% base, 10 g H_2O, 80 °C, 15 bar O_2, 4 h. [a] 10 mol% base, [b] 1 mol% base.

Exchange of atmosphere at the optimized conditions afforded decreased conversions and GA yields for air and argon, demonstrating the importance of oxygen availability (Figure 3.9). Considering the decreased partial pressure of oxygen when applying air as oxygen source, a reasonable GA yield was obtained (48%) under aerobic atmosphere. The oxidation was studied under oxygen-deprived conditions, affording 15% conversion of GAD, hereof 3% GA and 0.5% GLO. Limited availability of oxygen under Ar atmosphere afforded low conversion and little oxidation products, implying that oxygen availability is crucial for the oxidation reaction for re-oxidation of the catalyst. The small amount of oxidation products observed under Ar atmosphere may arise from the oxygen already present in the aqueous phase.

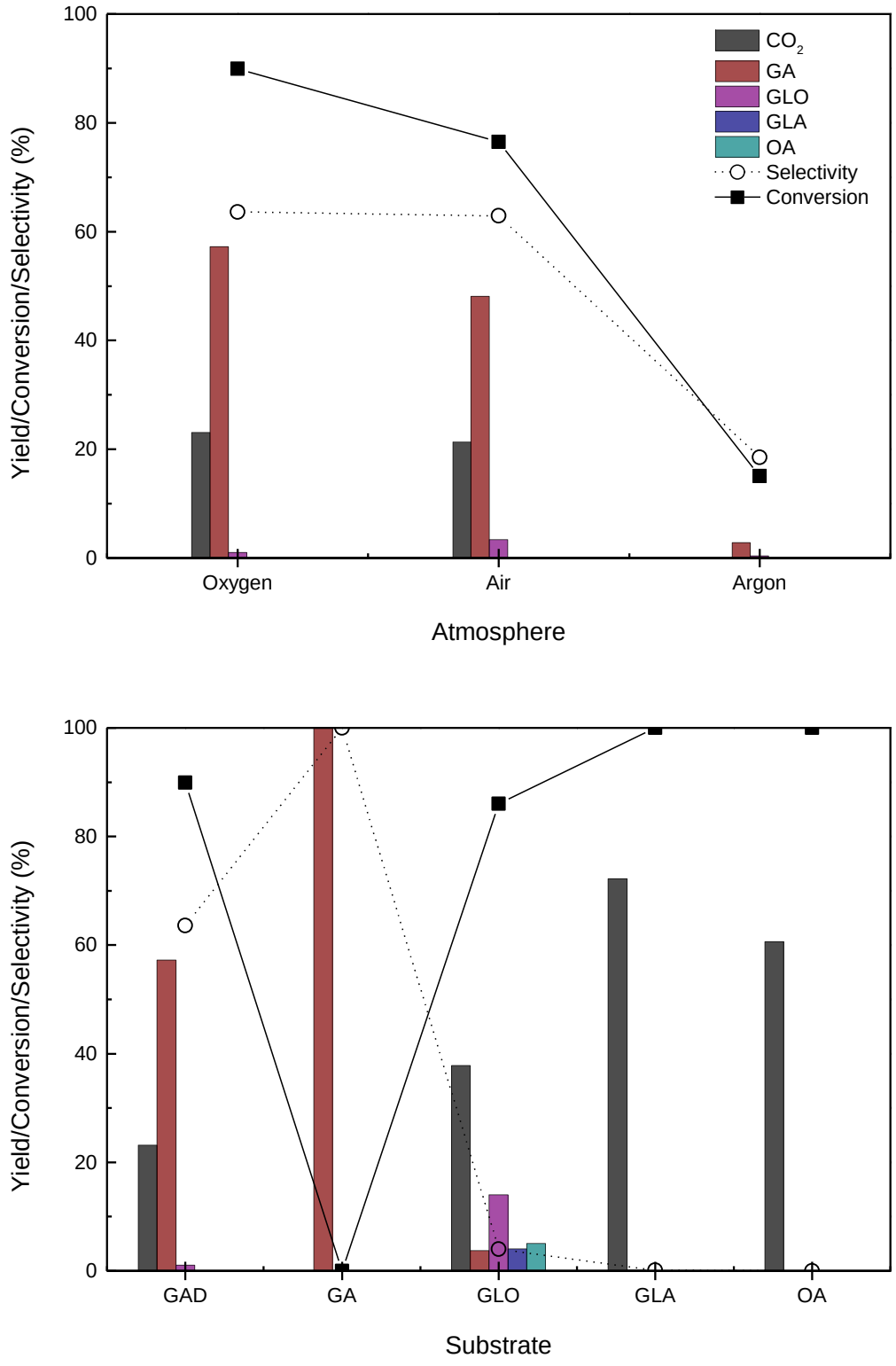

Figure 3.9: The effect of atmosphere on the oxidation of GAD (top), oxidation of various detected oxidation products (bottom). Reaction conditions unless otherwise noted: 2.5 mmol GAD, 0.076 mol% Au, 10 g H_2O, 80 °C, 15 bar O_2, 4 h.

The stability of the oxidation products of GAD was studied at the optimized conditions (Figure 3.9). Surprisingly, no oxidation of GA was detected indicating high stability of GA at the given conditions. Moreover, 4% GA was obtained from GLO, indicating and equilibrium of GAD and GLO and, hence, implying that formation of GLO at mild conditions is not a limiting factor of the selective oxidation. As expected, GLA and OA were fully oxidized into CO_2. No products of the liquid phase was observed according to HPLC analysis with the applied method. The gas phase was analyzed for CO_2 and CO, however, only CO_2 was detected (Figure 3.10).

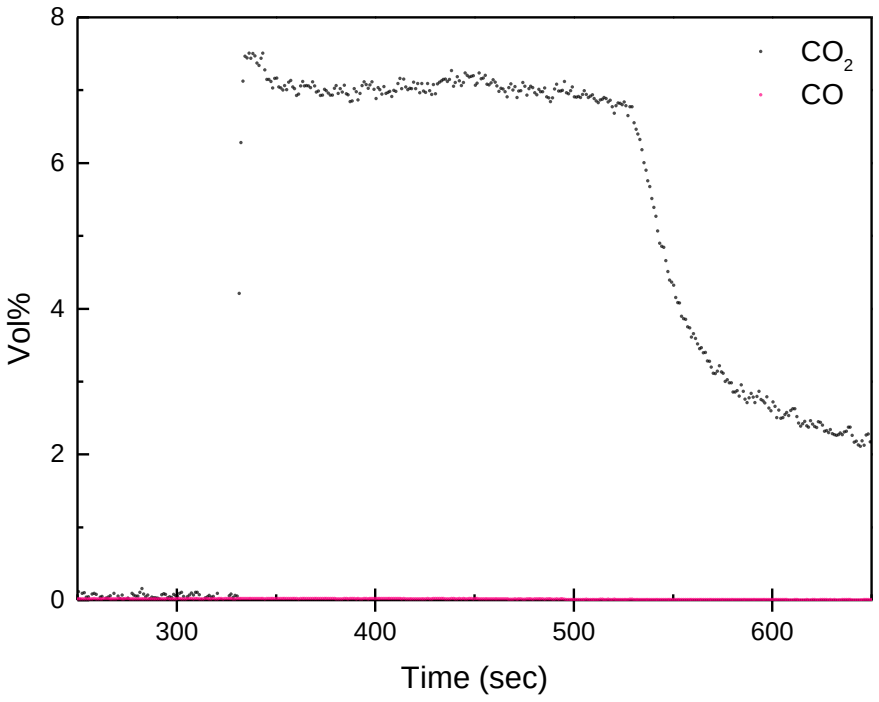

Figure 3.10: Produced CO_2 and CO from oxidation of GLA. Data obtained from analysis by NDIR. Reaction conditions 2.5 mmol GLA, 0.076 mol% Au, 10 g H_2O, 80 °C, 15 bar O_2, 4 h.

The optimized conditions were applied for oxidation of GAD with selected catalysts from the preliminary catalyst screening in Figure 3.2, and the results are presented in Figure 3.11. Au/TiO_2 was found to be the most active catalyst, affording good GA selectivity. In contrast, significantly decreased activity and GA yields were observed for the selected catalysts, indicating that harsher conditions or higher catalyst:GAD ratio are required to obtain higher yields of GA. Interestingly, the Pd-based catalysts favored formation of glyoxal over GA *i.e.* oxidation of the α-hydroxy group to the corresponding aldehyde, indicating faster oxidation of the alcohol over palladium at the given conditions.

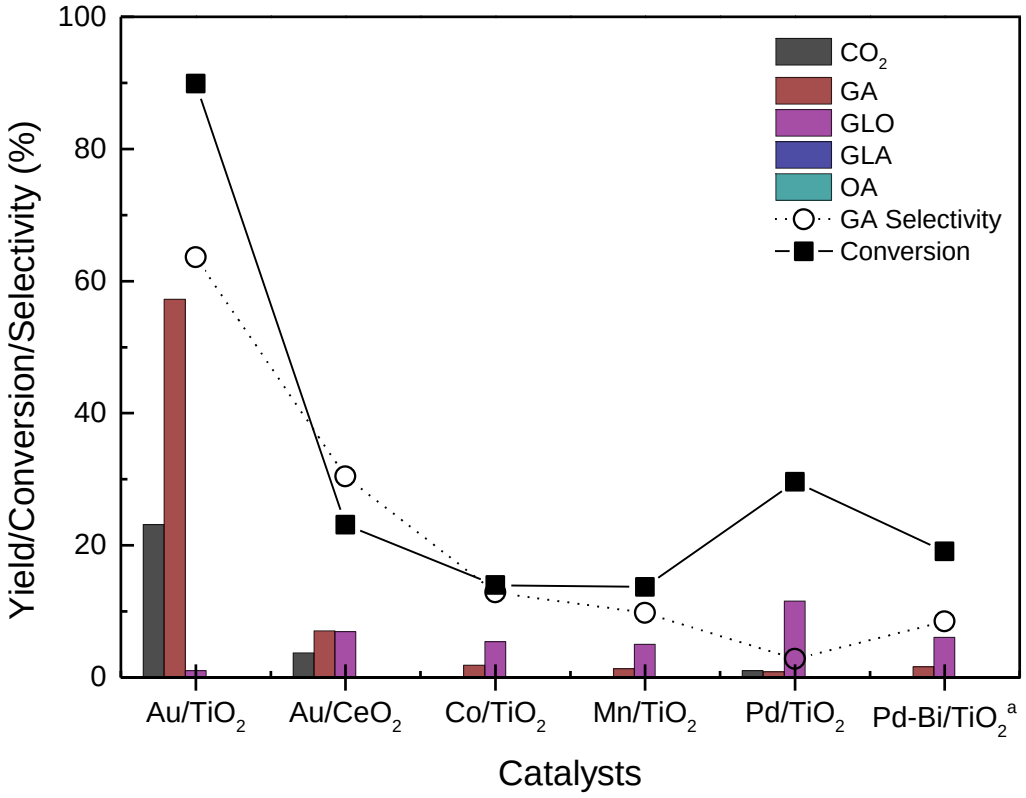

Figure 3.11: Optimized reaction conditions on selected catalysts from the preliminary catalyst screening. Reaction conditions 2.5 mmol GAD, 0.076 mol% metal of 1wt% metal/support,, 10 g H_2O, 80 °C, 15 bar O_2, 4 h. [a] 5 wt%

During the optimization of reaction conditions, a sudden deactivation of the Au/TiO_2 catalyst was observed, affording reduced activities and selectivities of various reactions. Reproduction of early experiments was examined, however, incomparable results were obtained (Figure 3.12). Analysis of the commercial catalyst by TEM revealed an increased particle size of the gold NPs, and a new catalyst was purchased and analyzed by TEM (Figure 3.13). The results presented in this chapter are optimized with the catalyst depicted in Figure 3.13A for the aerobic oxidations, and with the newly purchased catalyst for the oxidations with molecular oxygen in Figure 3.13C. Reduced activity and selectivity was not observed with the newly purchased catalyst (C).

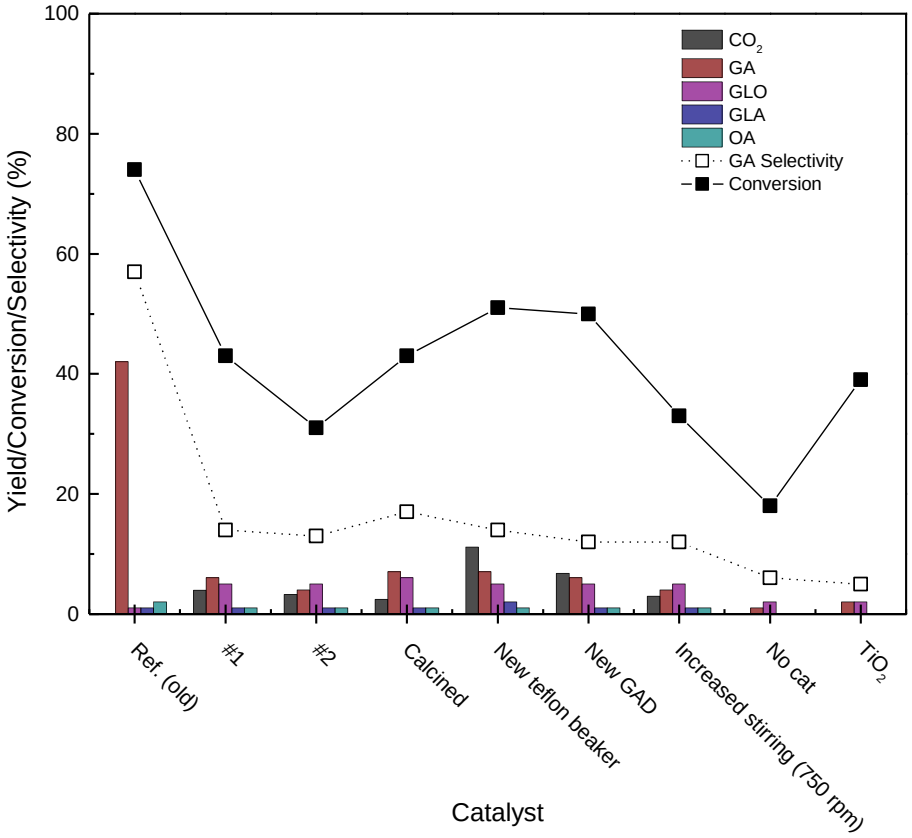

Figure 3.12: Deactivation of Au/TiO_2. Reaction conditions unless otherwise noted: 2.5 mmol GAD, 0.076 mol% Au, 10 g H_2O, 80 °C, 6 bar O_2, 18 h.

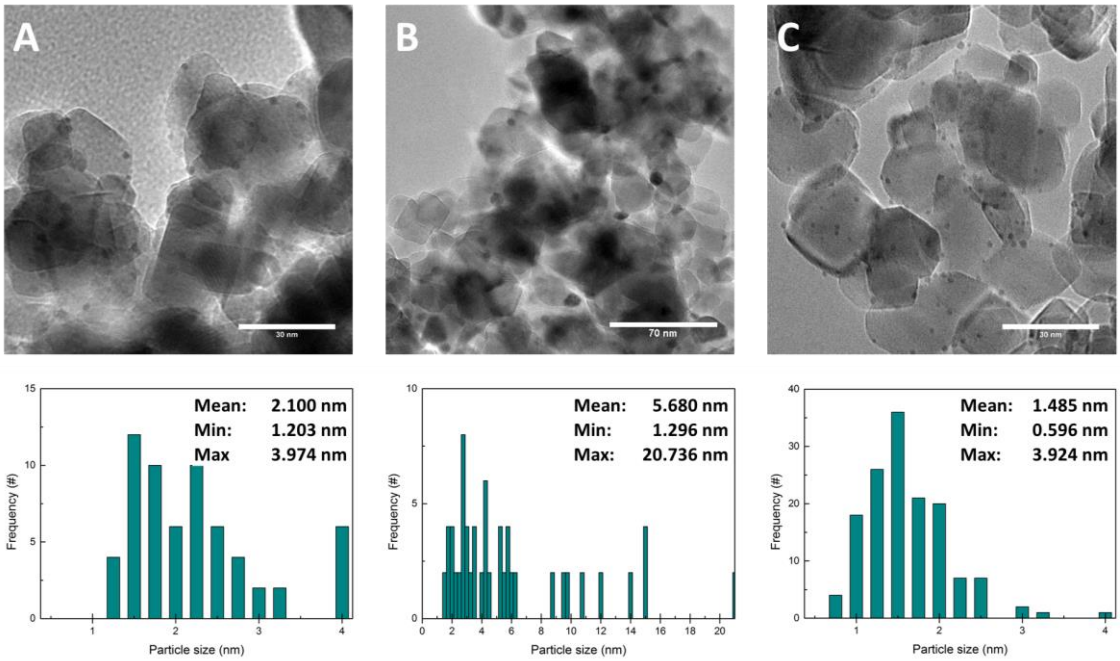

Figure 3.13: TEM images of Au/TiO_2: old (A), deactivated old (B) and newly purchased (C).

From literature, carboxylic acids has been found to deactivate gold NP-based catalysts, especially the oxidation of carbohydrates has been reported to give decreased catalyst activities. To overcome this issue, neutralization of the formed acid has been suggested. However, neutralization with base was not successful in the oxidation of GAD to GA. A few initial experiments were performed in methanol, generating the methyl ester in place of the acid, obtaining neutralization of the formed oxidation products, affording 72% methyl glycolate (MGA) over Au/TIO_2 (Figure 3.14). Various Pd-based catalysts were examined, however, superior selectivity was found over Au/TiO_2.

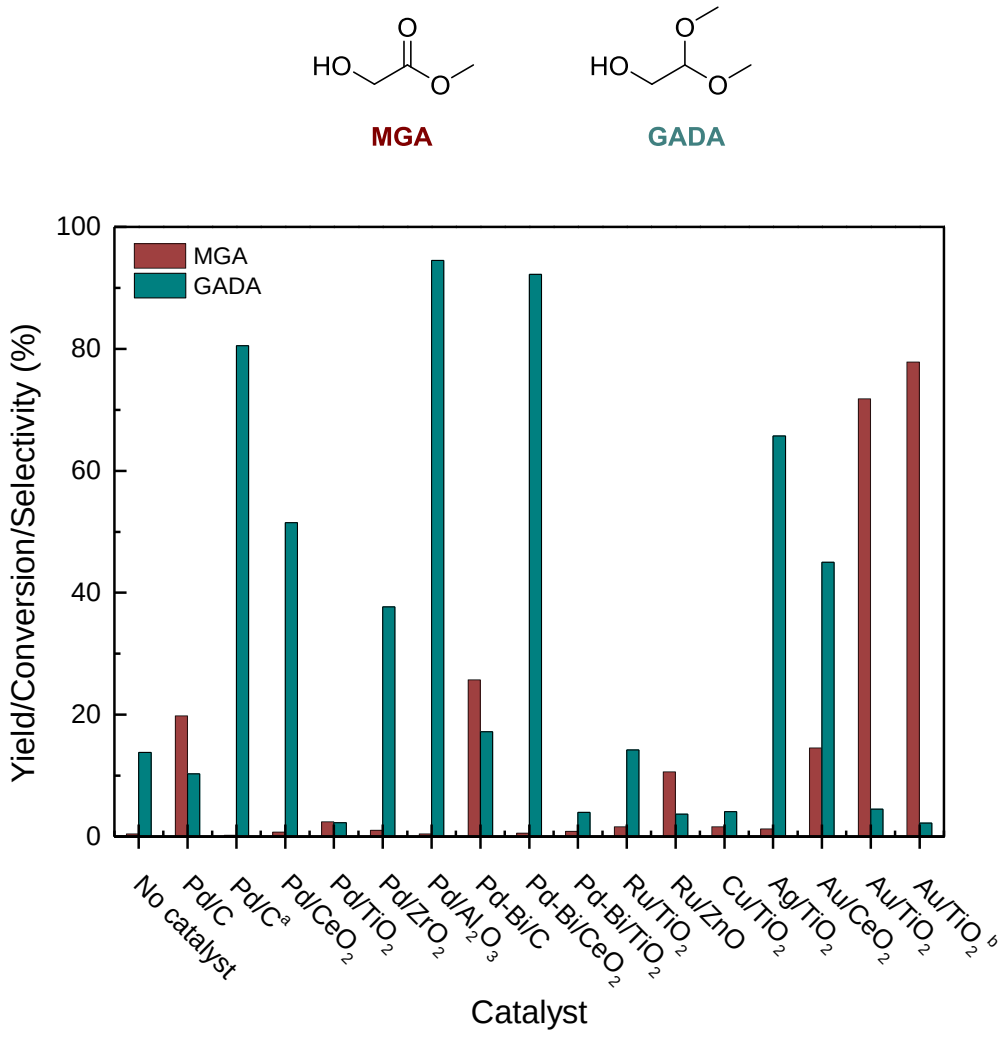

Figure 3.14: Oxidation of GAD in methanol. Reaction conditions: 2.5 mmol GAD, 0.305 mol% Au, 10 g MeOH, 80 °C, 6 bar air, 18 h. Only the liquid phase was analyzed in these experiments. [a] 120 °C, [b] reproduction of results.

Significantly increased selectivity in methanol, indicate an essential limitation of the catalyst by the formed carboxylic acids. However, the aim of this project was to find a method for the selective and base-free oxidation of GAD in water under mild conditions.

3.4 Conclusions

Several catalysts were tested for the selective aerobic oxidation of GAD to GA, obtaining highest GA yield over commercially available titania-supported gold NP. The effect of various reaction conditions of the oxidation over Au/TiO_2 were studied, affording up to 43% GA using 0.153 mol% Au. Decreasing the reaction time and temperature was found to decrease the catalyst activity, however, comparable GA yields were obtained at shorter reaction times. Due to the low GA yields obtained, the atmosphere was exchanged for molecular oxygen, to provide increased availability of oxygen.

The selective oxidation of GAD to GA with molecular oxygen over commercial available titania-supported gold NP was studied, affording up to 68% GA with high catalyst loading (0.305 mol% Au). Higher catalyst loading was found to decrease the GA selectivity, and up to 57% GA was obtained from decreased catalyst loading (0.076 mol% Au) limited by decreased catalyst selectivity.

Substantial effect of the temperature was found, affording increasing activity with increasing temperature as anticipated. GA selectivity was found to increase with increasing temperature, reaching a maximum at 80 ^oC. Hereafter, GA selectivity was found to be limited by formation of the over-oxidation product, CO_2.

Good product stability was observed over time, and was further supported by subjecting GA for oxidation under the optimized conditions, obtaining full recovery of GA. Seemingly, 1h of reaction time was insufficient, affording low conversion and yields, however, good GA selectivity was observed. Close to full conversion was obtained after 9 h, affording slightly increased GA yield, however, at the expense of slightly increased CO_2 formation, yielding a minor decrease of GA selectivity.

Varying pressures of oxygen were found to have little effect on the oxidation from 6 bar and higher. A slight increase in conversion, GA selectivity and GA yield was observed at 15 bar. Atmospheric pressure of oxygen effected product selectivity and conversion, affording decreased yields, possibly due to limited oxygen availability from poorer solubility of oxygen in the aqueous phase.

Decreased conversions and GA yields were observed from exchange of the atmosphere, due to decreased- and deprived oxygen availability applying air and argon, respectively. Addition of base was found to accelerate the catalyst activity, affording full- or close to full conversion of GAD, however, poor GA selectivity was obtained from 1-100 mol% base. Various catalysts were examined for the oxidation of GAD under the optimized conditions, all affording low conversions and GA selectivities.

As briefly mentioned, deactivation of the gold-based catalyst was observed during the optimization, due to agglomeration of gold NP on the titania support. The results presented in this chapter for the oxidation of GAD with molecular oxygen are reproduced experiments catalyzed by a newly purchased gold catalyst, and the gold NP size was examined before use. Decreased activity and selectivity was not observed during the last optimization, presented in this chapter.

A moderate yield of GA was successfully obtained from selective oxidation of GAD over titania-supported gold NPs. The limitation from product inhibition of the gold-based catalyst was overcome by changing the solvent to methanol, neutralizing the formed acidic products producing methyl esters. However, the aim of this project was to find a method for the *aqueous* oxidation of GAD to GA under mild, base-free conditions. A method was developed, affording up to 68% GA at high catalyst loading. At more convenient catalyst loading, 57% GA was obtained, yielding CO_2 as the major by-product followed by minor formation of GLO.

Chapter 4. Oxidations Over Ceria-Supported Ruthenium Hydroxide

In this chapter, oxidations with the heterogeneous ruthenium hydroxide catalyst are presented. A short description of the catalysts and the properties hereof, followed by discussion of results and proposed mechanisms are presented.

4.1 Introduction

Renewable resources, such as biomass, has received considerable attention for production of fuel and chemicals. The demand for mild, efficient and sustainable processes for conversion of biomass-derived compounds into fine and bulk chemicals has increased over the past years, including the demand for liquid-phase oxidation of alcohols and aldehydes.

4.1.1 Current Synthesis of Formic Acid and Acetic Acid

A desired product of liquid-phase oxidations of smaller alcohols is formic acid (FA). FA is widely used in various industries including leather, agricultural, pharmaceutical, chemical, textile, rubber and catalysis.[70,208,209] More recently, FA was found feasible for hydrogen storage due to the selective release of H_2 and CO_2 under mild conditions.[67,210] In 2013, the global capacity of FA was approximately 621 x 10^3 t/a. Approximately 80% of the produced FA is synthesized produced by a two-step process involving generation of methyl formate from methanol and CO followed by hydrolysis of methyl formate, affording FA and methanol which is recycled (Figure 4.1).[208] This process is applied at large companies such as BASF and Kemira. Liquid-phase oxidation of various carbohydrates and other forms of biomass has been reported to yield formic acid as the major product.[70,100,211] The most efficient catalyst reported to this day is the vanadium substituted heteropoly acid (see Chapter 5).[61,67,100,102]

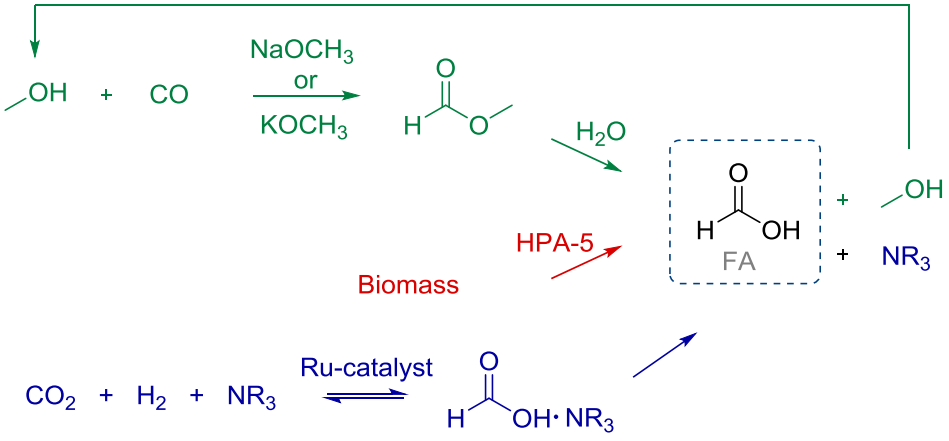

Figure 4.1: Processes for production of formic acid.[61,67,100,102,208]

An additional desired product is acetic acid (AA). AA is mainly used for fabrication of vinyl acetate, acetic anhydride and as solvent in the terephthalic acid production, the principle precursor for polyester.[212,213] In 2010, more than 12x10^6 ton of AA was produced.[212] The most widely used large-scale production is by carbonylation of methanol,[214,215] followed by liquid-phase oxidation of acetaldehyde, butane, naphtha or acetaldehyde.[213] Currently, 0.8 t/a of AA is being produced from biomass-derived compounds, mainly by bio-catalytic upgrading of the low-value bio-ethanol.[116,216]

AA has been produced from methanol under inert atmosphere with a homogeneous ruthenium catalyst.[217] More recently, AA was synthesized from oxidation of ethanol with heterogeneous RuO_x/CeO_2 and $Ru(OH)_x/CeO_2$ catalysts.[63,81]

4.1.2 Ruthenium Catalysis

Various applications for the precious transition metal, ruthenium, have been reported over the years. Several applications within catalysis include homogeneous catalyzed hydrogenations,[218–220] oxidations,[41,43,217,221–227] addition to CC bonds,[228,229] CC bond formation and C-O bond cleavage.[230,231] More recently, heterogeneous ruthenium catalysts have been investigated for various applications, *e.g.* oxidations,[232–239] hydrogenations[240–243] amination,[240] CC bond formation,[244,245] etc. Furthermore, supported ruthenium catalysts have proven feasible for catalytic upgrading of biomass and biomass derivatives.[63,70,81,98,211,245–249] Oxidation of various substrates including ammonia, HCl, hydrocarbons, alcohols, aldehydes and biomass-derived compounds, have been reported utilizing a supported ruthenium oxide catalysts.[63,81,98,205,232,233,235–239,246–263] The various applications of ruthenium in catalysis has rendered ruthenium a very well-studied metal in both homo- and heterogeneous reactions.[223,264–274]

4.1.2.1 Supported Ruthenium Hydroxide

Supported ruthenium hydroxide catalysts ($Ru(OH)_x$/support) was developed by Mizuno and Yamaguchi.[275] It is prepared by deposition-precipitation and dried at low temperature without further activation of the catalyst by calcination or reduction, leaving the hydroxide species intact on the ruthenium center.[276–279] High activity is observed for the $Ru(OH)_x$/support, possibly due to highly dispersed ruthenium hydroxide species on the supports complimented by the coexisting of Lewis acid- and Brønsted basic sites (Ru center and OH^-, respectively) of the catalyst.[275] $Ru(OH)_x$/support has proven active for amine oxidation,[280] liquid-phase oxidation[277,281,282] and reduction of alcohols and carbonyl compounds,[279,283] functional group transformations[276] including oxidative dehydrogenation of alcohols and amines, hydrogen-transfer reactions,[284,285] hydration of nitriles, oxygenation of primary amines to give amides,[278] direct oxidative synthesis of nitriles from primary alcohols and ammonia, and N-alkylation of ammonia with alcohols to produce symmetrical substituted tertiary or secondary amines, see Figure 4.2.[256,276–282,284–288]

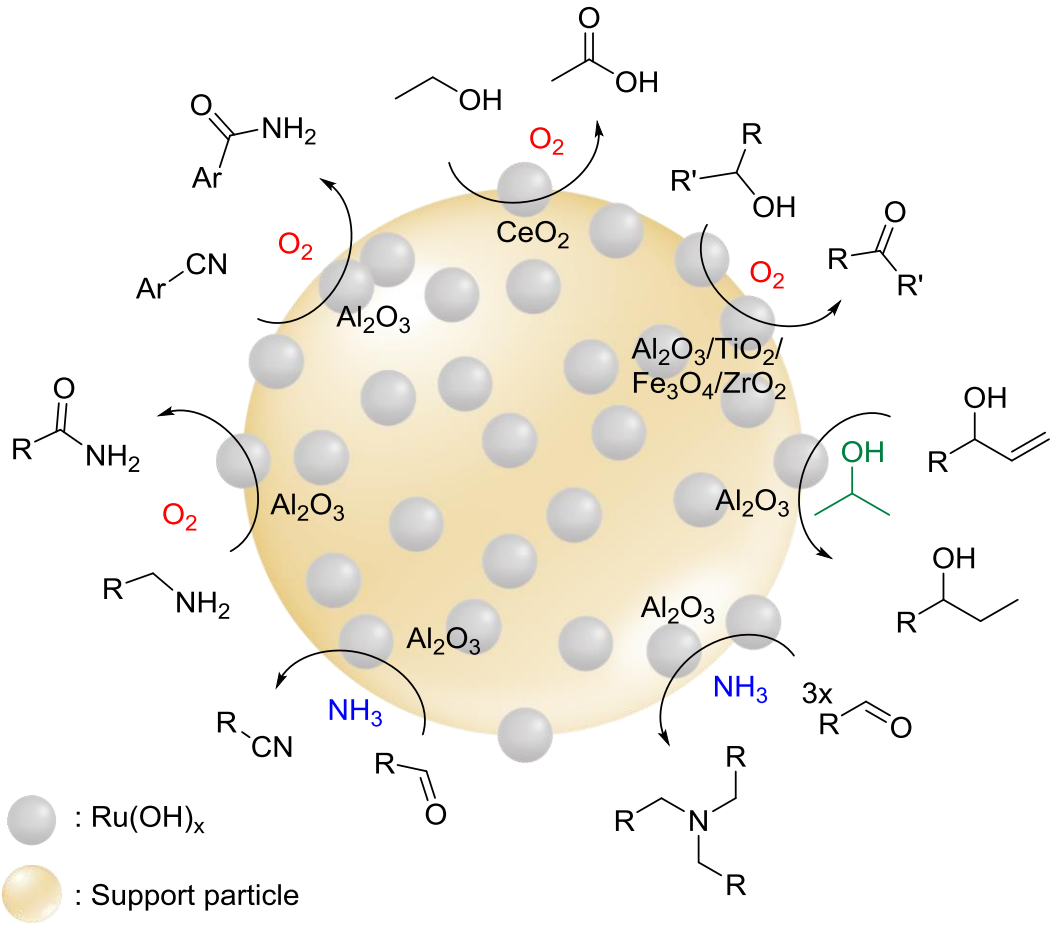

Figure 4.2: Catalytic transformations over supported $Ru(OH)_x$.[256,276–282,284–288]

The work presented in this chapter focus on the supported ruthenium hydroxide catalyzed oxidation of alcohols and aldehydes into formic acid and acetic acid. A mechanism for oxidation of alcohols with molecular oxygen was proposed by Yamaguchi and Mizuno, starting with a ligand exchange of the ruthenium hydroxide (ruthenium specie I) with the substrate alcohol affording a ruthenium alkoxide specie (ruthenium specie II), depicted in Scheme 4.1.[263] Ruthenium specie II then undergo β-hydride elimination affording the ruthenium hydride specie III and release of the oxidized alcohol. The Ruthenium catalyst is re-oxidized by molecular oxygen through peroxo-ruthenium specie IV, to regenerate the ruthenium hydroxide specie I. Monitoring the formation of water and the uptake of molecular oxygen, afforded the stoichiometries presented in Scheme 4.1 (1:1 of H_2O:product and 1:2 of O_2:product). The observed stoichiometries support the oxidative dehydrogenation mechanism proposed by Yamaguchi and Mizuno above the simple dehydrogenation of alcohols (Scheme 4.2 (B) and (A), respectively).[263,282]

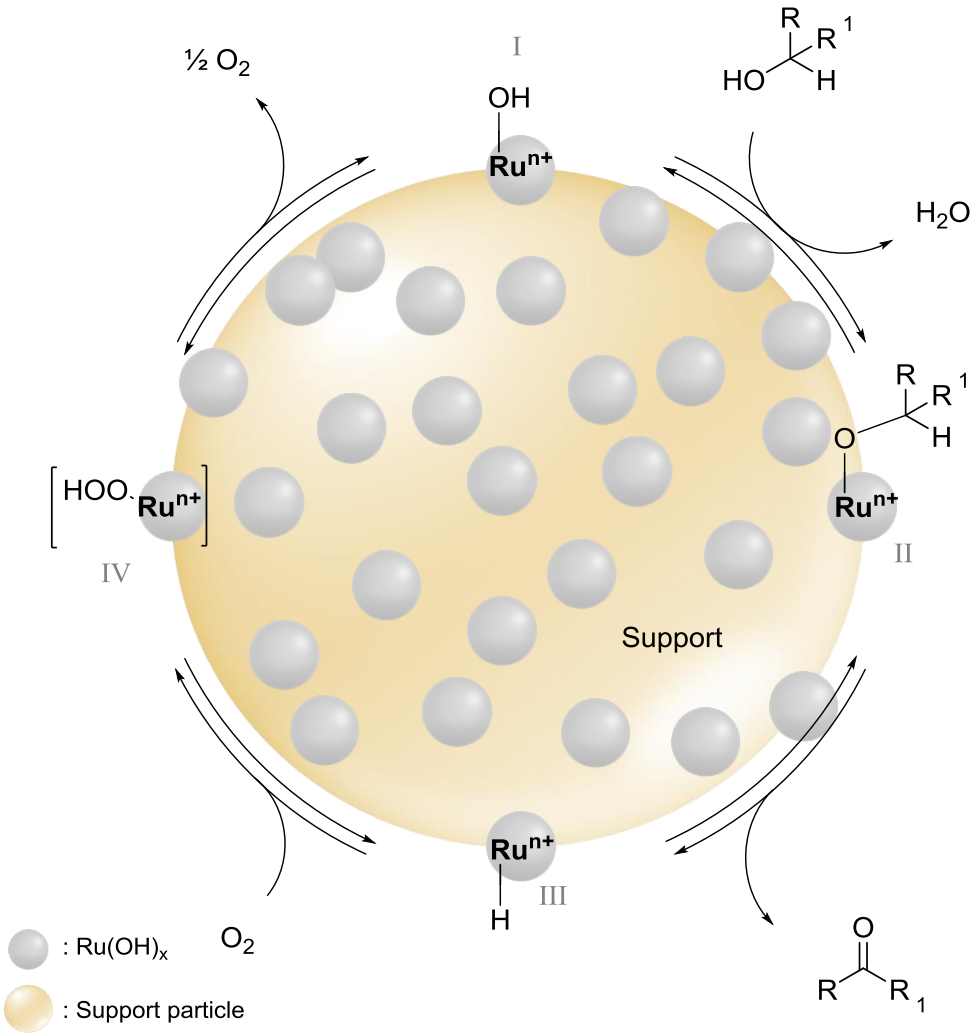

Scheme 4.1: Mechanism of supported $Ru(OH)_x$ catalyzed oxidation of alcohols proposed by Yamaguchi and Mizuno.[263]

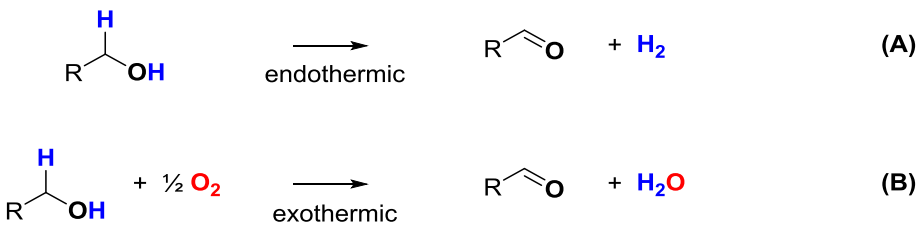

Scheme 4.2: Overview of the catalytic dehydrogenation (A) and catalytic oxidative dehydrogenation (B). Scheme adapted from publication by Brazier *et al.*[282]

The thermodynamic driving force of the oxidative dehydrogenation is the addition of the green oxidant, molecular oxygen, affording the corresponding ketones and aldehydes of the substrate-alcohols at lower pressures, and the corresponding acids of primary alcohols at elevated pressures. The only observed by-product is water, which is considered a green chemical.[282]

Oxidative dehydrogenation of alcohols is currently being used for industrial production of formaldehyde, acetaldehyde and C_5-C_{14} aldehydes.[289] More recently, supported $Ru(OH)_x$ has been reported to catalyze oxidation of biomass-derived compounds such as glycerol, ethanol and HMF.[63,70,94]

4.2 Experimental Detail

4.2.1 Materials

All reagents were of reagent grade and were used without further purification: ruthenium(III) chloride (purum, ~41% Ru, Sigma-Aldrich), cerium(IV) oxide (99.5%, Alfa Aesar), cerium(IV) oxide (nanopowder, ≥99.9%, Sigma-Aldrich), cerium(IV) oxide high surface area nanoparticulate (≥99.9%, Sigma-Aldrich), acetic acid (99.8%, Riedel-de Haën AG), sodium hydroxide (≥98%, Sigma-Aldrich), formic acid (≥98%, Sigma-Aldrich), propanal (≥97%, Sigma-Aldrich), propionic acid (≥99.5%, Sigma-Aldrich), 1,3-propanediol (98%, Sigma-Aldrich), 2,3-butanediol (≥99-99.7%, Fluka); oxygen (99.5%, Air Liquide Denmark), millipore water.

4.2.2 Procedure for Preparation of 1.2 wt% $Ru(OH)_x/CeO_2$

$RuCl_3$ (1.2 mmol, 246.8 mg) was dissolved in millipore water (143 mL) affording a ruthenium concentration of 8.3 mM. CeO_2 (9.76 g) was added, and the reaction solution was stirred for 15 min. 1M NaOH (28 mL) was added and the reaction was left stirring for 18 h. The catalyst was filtered off and washed thoroughly with millipore water until pH neutral filtrate was obtained. Hereafter, the catalyst was dried at 140 ^oC for 40 h. The BET surface area, XRF, SEM-EDS, TEM and XRPD were obtained according to described procedures in Section 2.1.

4.2.3 General Procedure for Oxidations

The oxidations were carried out in 18.4 mL pressure vessels (see section 2.2.1). The mini high-pressure vessels (MVs) were charged with the substrate (5.9 mmol), $Ru(OH)_x/CeO_2$ (114.8 mg, corresponding to 0.23 mol% Ru) and millipore water (4.62 g). The MVs were flushed and pressurized with molecular oxygen (1-30 bar), heated to the desired temperature (23-150 ^oC) while constantly stirring at 500 rpm for 1-70 h. After the reaction, the MVs were rapidly cooled to room temperature (23 ^oC), the gas-phase was analyzed for CO_2 using a Quantek NDIR detector (see Appendix C for example of calculation) and the liquid-phase for various oxidation products by HPLC, Agilent Technologies 1200 series, Aminex HPX-87H column from Bio-Rad, 300 mm x 7.8 mm x 9 µm, solvent: 5 mM H_2SO_4 (see Appendix C for example of calibration curve calculations). The liquid-phase was analyzed using two methods, a low-temperature method at 24 ^oC and an elevated-temperature method at 60 ^oC, with a flow rate of 0.3 and 0.5 mL/min, respectively, to ensure complete separation of all products and substrate.

A reference experiment was performed in a mechanically stirred Parr autoclave equipped with internal thermocontrol (T316 steel, Teflon™ beaker insert, 100 mL), following identical procedure to that of the MVs.

4.3 Results and Discussion

4.3.1 Catalyst Characterization

Catalysts with varying BET surface areas were prepared, see Table 4.1. The ruthenium content was determined from XRF and EDS. TEM of the catalysts were conducted to preclude the formation of accumulated RuO_2 nanoparticles (Figure 4.4).

Table 4.1: Overview of synthesized $Ru(OH)_x/CeO_2$ catalysts and catalyst characterization.

Catalyst	BET Surface Area (m^2/g)		Ru Content (wt%)[a]	
	Catalyst	CeO_2	XRF	EDS
Ru-1	39	42	1.4 (0.56)	1.3 (0.39)
Ru-2	8	4	1.0 (0.062)	0.8 (0.47)
Ru-3	3	3	1.0 (0.011)	1.1 (0.31)
Ru-4	148	42	1.2 (0.0066)	1.4 (0.72)

[a] Standard deviation in parentheses

The Ru-1 and Ru-4 catalysts were prepared with ceria support with particles less than 50 nm, however, the Ru-2 and Ru-3 catalysts were prepared with larger ceria particles (less than 5 µm) resulting in a lower BET surface area. The Ru-2 catalyst was prepared from and old microparticulate ceria, while the Ru-3 catalyst was prepared from newly acquired microparticulate ceria. Previous work has shown, that higher efficiency of the $Ru(OH)_x/CeO_2$ was achieved using a catalyst with a BET surface area of 8 m^2/g in the oxidative dehydrogenation of ethanol.[63,290]

The ruthenium content was determined from XRF and EDS analysis. Two different samples of each catalyst were subjected to XRF and the average of the measured ruthenium loadings is presented in Table 4.1. A slightly higher ruthenium content was detected for the Ru-1 and Ru-4 catalysts, however, the value was within reasonable deviations due to uncertainties of measurements. For the Ru-2 and Ru-3 catalysts, a ruthenium loading of 1.0 wt% was measured, also within reasonable values of deviations from the theoretical value of 1.2 wt%.

The catalysts were imaged by SEM and analyzed using EDS to determine the elemental composition. The SEM pictures are presented in Figure 4.3. From EDS analysis of the Ru-1 to Ru-3 catalysts, varying ruthenium loadings were found (Table 4.1). The ruthenium loadings were deduced from the average of four to six different EDS measurements. Although the detected ruthenium contents are comparable with the loadings found by XRF, the accuracy of the EDS analysis was low due to charging of the samples resulting in movement during the analysis.

A difference in ceria particle size was observed during SEM analysis. As expected, smaller particles was observed for the Ru-1 catalyst (Figure 4.3, a and b) based on nanoparticulate ceria, and larger particles was observed for the Ru-2 and Ru-3 catalysts, prepared from microparticulate ceria.

According to Yamaguchi and Mizuno, no formation of ruthenium nanoparticles are observed in the TEM pictures of the supported, highly dispersed $Ru(OH)_x$ catalysts.[263] The recorded TEM pictures are presented in Figure 4.4. Ruthenium nanoparticles were not observed in the prepared catalysts, however, the detection of ruthenium by XRF and EDS confirmed the presence of ruthenium in the prepared catalysts, indicating formation of highly dispersed $Ru(OH)_x$ species on ceria.

Formation of a veil-substance was observed on the TEM images of the ceria NPs. Similar formations was observed on the ceria microparticles, however, on the microparticles it was possible to isolate agglomerations of the veil-substance on a single ceria particle, Figure 4.4i. Zooming in on the veil-substance of the NPs revealed a combination of veil-substance and small ceria particles (b and c). Possibly, the veil-substance is the highly dispersed ruthenium-hydroxide species. Notably, the agglomerations of the veil-substance was only observed on the microparticle indicating increased dispersion of the ruthenium-hydroxide on ceria NPs.

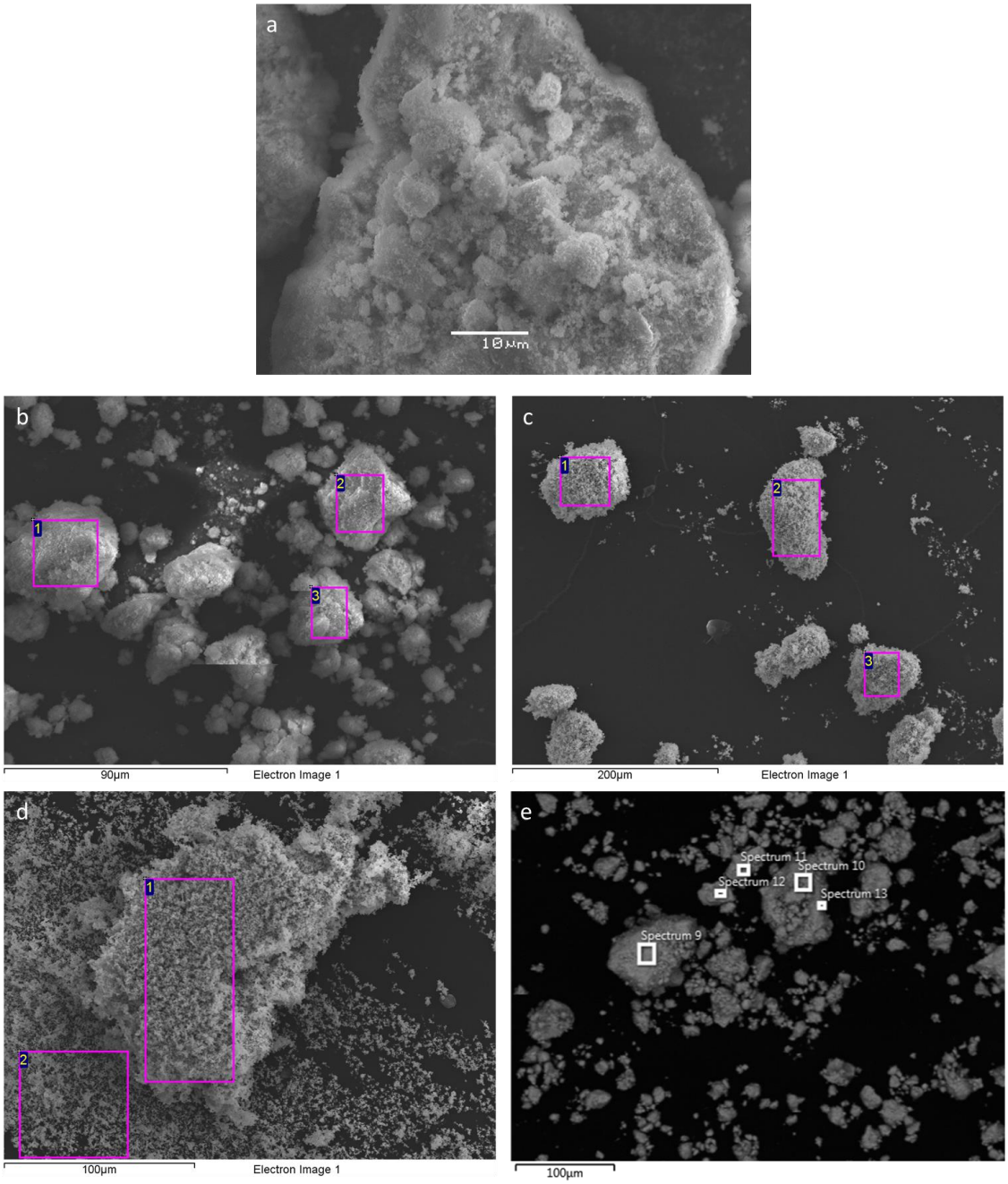

Figure 4.3: SEM-EDS images of a) Ru-1 magnified, b) Ru-1, c) Ru-2, d) Ru-3 and e) Ru-4 catalysts.

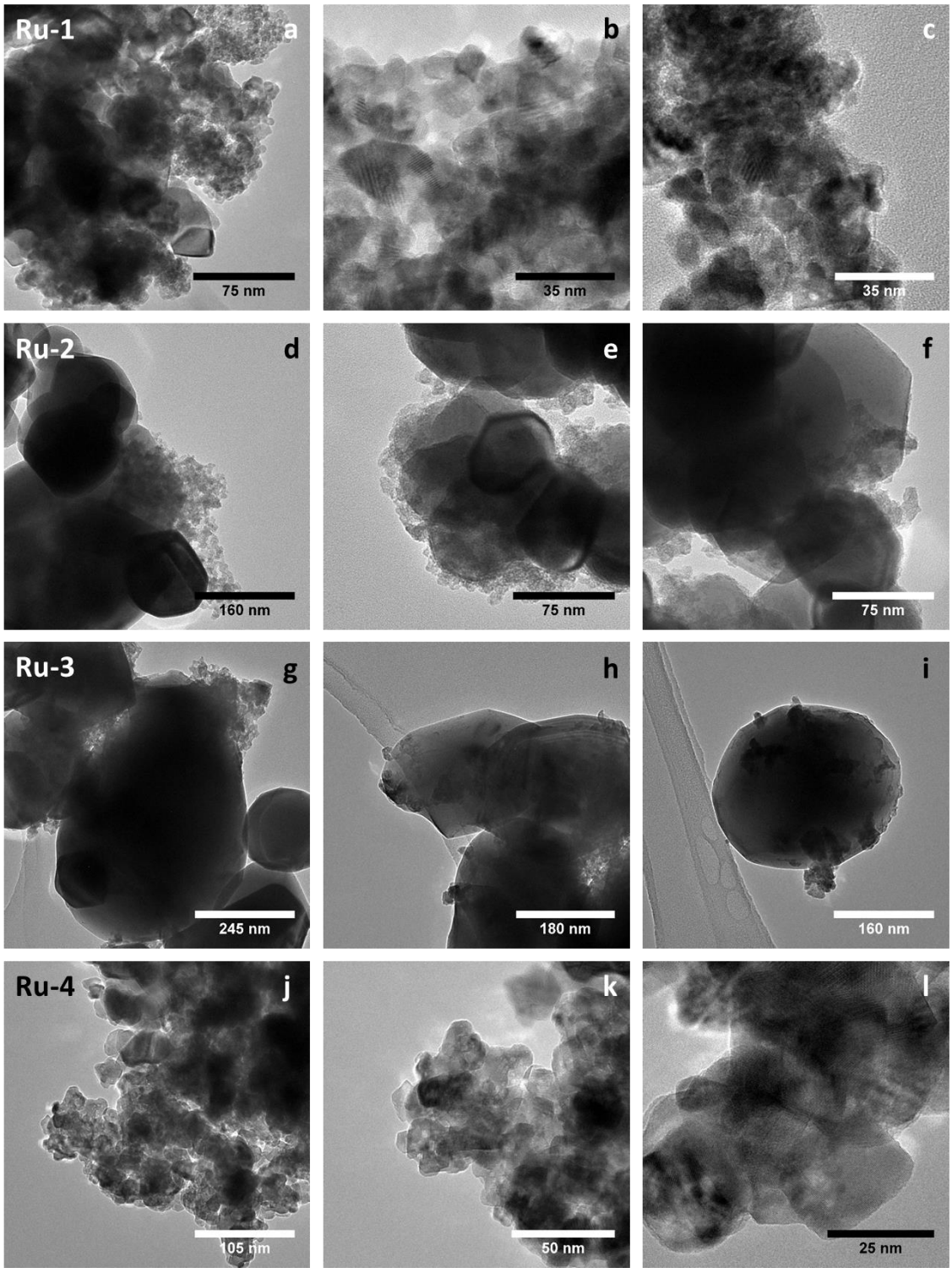

Figure 4.4: TEM images of prepared catalysts; a-c: Ru-1, d-f: Ru-2, g-i: Ru-3 and j-l: Ru-4.

XRPD was recorded for the prepared catalysts, the obtained diffractogram are presented in Figure 4.5. The diffractrograms for the microparticulate ceria (Ru-2 and Ru-3) are comparable to that of untainted ceria, possibly due to the low ruthenium loading (1.2 wt%).[291–293] According the Scherrer equation (Section 2.1.3), the narrow sharp peaks observed for the Ru-2 and Ru-3 catalysts indicate larger particles than observed for the nanoparticulate ceria-supported catalysts (Ru-1 and Ru-4), where broader peaks are observed for ceria. Furthermore, Mizuno and Yamaguchi reported that ruthenium metal clusters and ruthenium oxide were not observed in the XRD pattern of titania- and alumina-supported ruthenium hydroxide, which were identical to that of the parent support, due to formation of the highly dispersed ruthenium hydroxide specie.[284,29463] Various additional peaks were observed in the area 3-28º for the nanoparticulate ceria-supported catalysts, indicating an altered morphology. However, the additional peaks were not comparable with peaks for ruthenium clusters or ruthenium oxide, indicating successful formation of ruthenium hydroxide.[295–297]

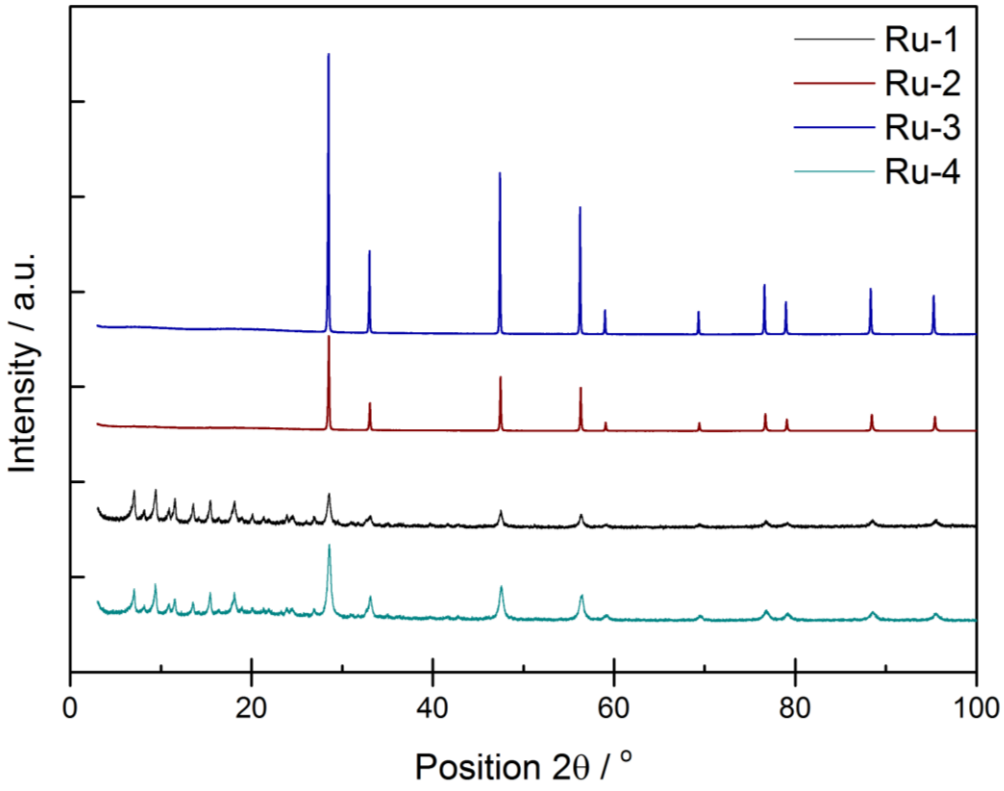

Figure 4.5: XRPD diffractrograms of the prepared catalysts: Ru-1 (black), Ru-2 (red), Ru-3 (blue) and Ru-4 (green).

4.3.2 Oxidation of Glycolaldehyde

Glycolaldehyde (GAD, see Chapter 1) was tested in the $Ru(OH)_x/CeO_2$-catalyzed oxidative dehydrogenation. Unexpectedly, the major product observed after some optimization on the reaction conditions was not glycolic acid (GA), but formic acid (FA) (Scheme 4.3).

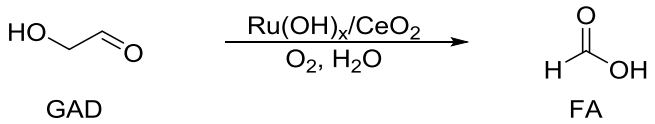

GAD FA

Scheme 4.3: Oxidation of glycolaldehyde to formic acid over $Ru(OH)_x/CeO_2$.

The prepared catalysts were tested for the oxidative dehydrogenation of GAD, and the results are presented in Table 4.2 below. Full conversion of GAD was achieved with all catalysts, however, the major product observed was CO_2, indicating over-oxidation of GAD at the applied conditions. Other identified products include minor quantities of oxalic acid (OA), glycolic acid (GA) and formic acid (FA), depicted in Figure 4.6. Moreover, 6-11% yield of acetic acid (AA) was observed, constituting the second of major products of the oxidation.

Table 4.2: Oxidation of glycolaldehyde with the prepared catalysts.

Entry	Catalyst	Conversion (%)	Yield (%)						
			CO_2	OA	GLO	GLA	GA	AA	FA
1	Ru-1	100	52.5	0.0	0.0	0.0	0.5	6.2	0.0
2	Ru-2	100	50.2	0.2	0.0	0.0	0.7	10.7	0.5
3	Ru-3	100	50.2	0.0	0.0	0.0	0.7	7.4	0.4
4	Ru-4	100	36.6	0.1	0.0	0.0	0.3	9.2	0.2

Reaction conditions: GAD (356.1 mg, 5.9 mmol), $Ru(OH)_x/CeO_2$ (114.8 mg, 0.23 mol% Ru from 1.2 wt% $Ru(OH)_x/CeO_2$), H_2O (4.6 mL), molecular O_2 (30 bar), 150 °C, 16h at 500 rpm.

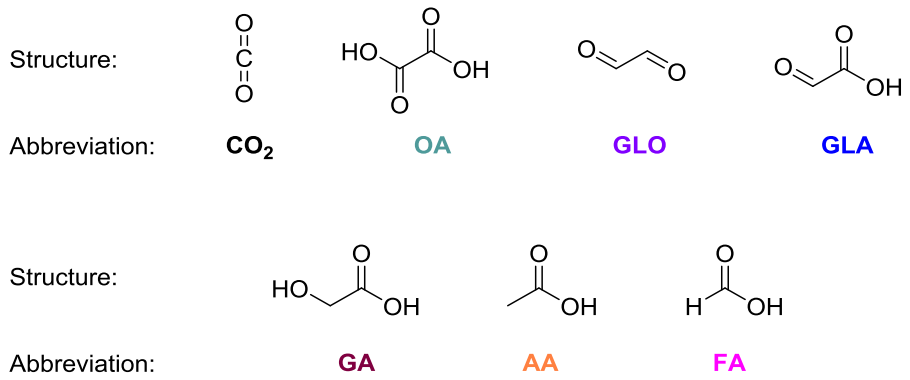

Figure 4.6: Products observed during the ruthenium-catalyzed oxidations of GAD.

Catalyst Ru-1 and Ru-3, medium- and low surface areas, were subjected to oxidations of GAD under various conditions, to optimize the reaction conditions for the selective oxidation of GAD to FA. The results presented in Table 4.2 indicate, that milder conditions are necessary to prevent over-oxidation of GAD. First, the effect of the reaction temperature on the oxidation was studied (Figure 4.7).

Full- or close to full conversion of GAD was observed from 90-150 ^{o}C with both catalysts (black line). At decreased temperatures, full conversion was not achieved within the 16 h of reaction. The selectivity for FA) increased with increasing temperature until reaching a maximum at 80 ^{o}C using the Ru-1 and 90 ^{o}C using the Ru-3 catalyst (dotted line). Subsequent decrease of FA yield (pink bars) was observed at higher temperatures, limited by decomposition into CO_2 and various syrup-like unidentified by-products. At milder temperatures (50 and 70 ^{o}C) a significant difference in catalyst activity and FA yield was observed for Ru-1 and Ru-3, revealing a higher activity of the higher surface area catalyst, Ru-1. However, at elevated temperatures (110 and 120 ^{o}C), the yield of FA decreased severely using Ru-1 compared to Ru-3, indicating a higher activity for Ru-1 resulting in decomposition of FA into CO_2. The lower activity of Ru-3 affords higher stability of FA at elevated temperatures, however, at lower temperatures, higher yields of FA is obtained from oxidations with Ru-1.

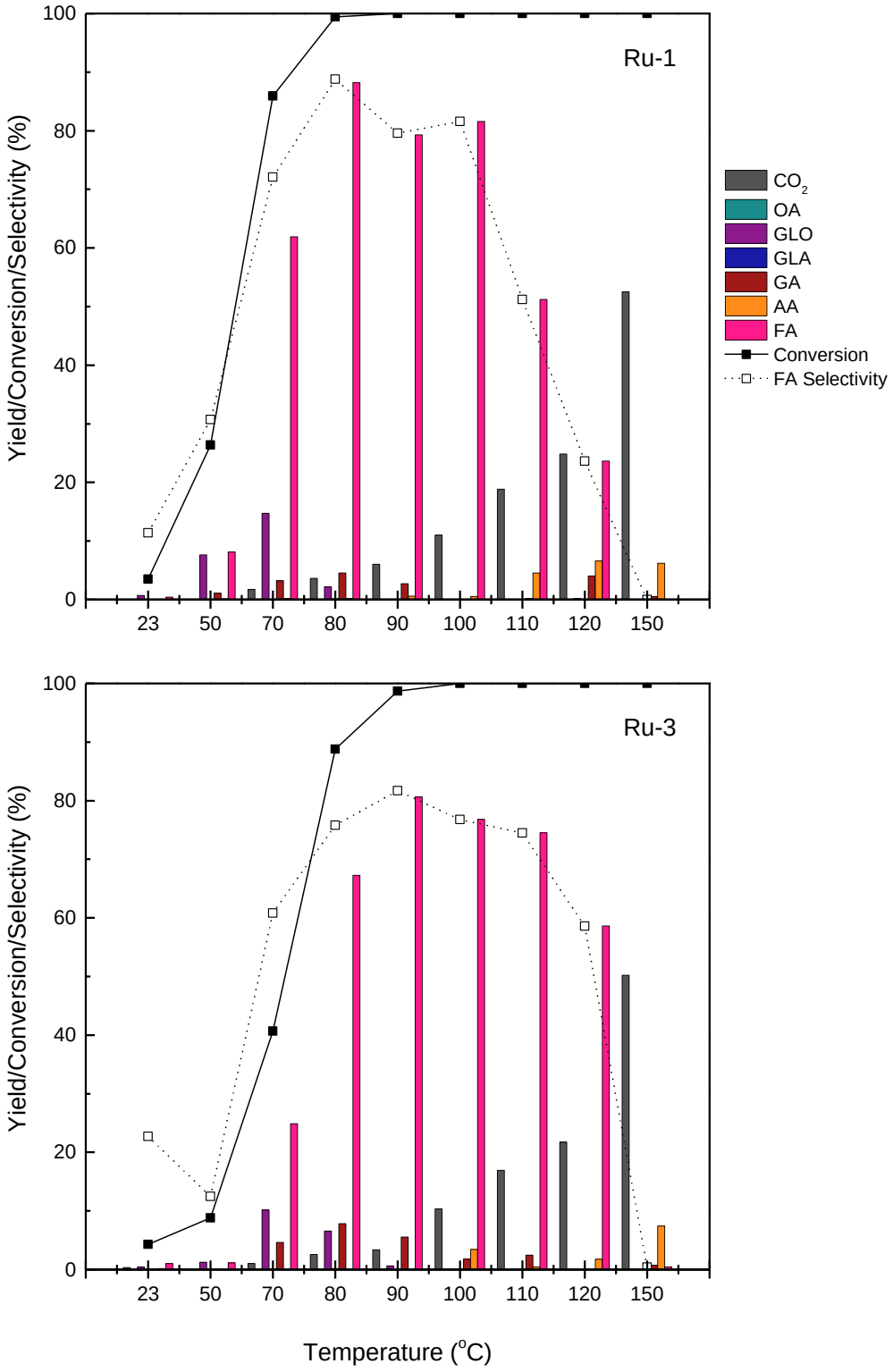

Figure 4.7: Temperature dependence of the $Ru(OH)_x/CeO_2$ Ru-1 (top) and Ru-3 (bottom) catalyzed oxidation of GAD. Reaction conditions: GAD (356.1 mg, 5.9 mmol), $Ru(OH)_x/CeO_2$ (114.8 mg, 0.23 mol% Ru from 1.2 wt% $Ru(OH)_x/CeO_2$), H_2O (4.6 mL), molecular O_2 (30 bar), 23-150 °C, 16h at 500 rpm.

The yield of CO_2 increased with increasing temperature, indication over-oxidation of GAD at elevated temperatures (grey bars). Only small amounts (<10%) of GA was observed, reaching a maximum at 80 ^oC (wine red bars). Small amounts of other by-products was observed at all the investigated temperatures, however, the nature of the identified by-products changed with increasing temperature. GLO and small amounts GA was observed at decreased temperatures. At increased temperatures, the by-products included GA and AA.

To achieve optimized conditions applicable for both catalysts, the following experiments were conducted at 90 ^oC, although the highest yield of FA was achieved at 80 ^oC for the Ru-1-catalyzed oxidation, however, the FA yield for the Ru-3-catalyzed oxidation did not reach a maximum before 90 ^oC.

Second, the effect of applied pressure (1-30 bar) was studied on the Ru-1 and Ru-3 catalysts (Figure 4.8). Full or close to full conversion was achieved from 5 bar O_2 and higher pressures, however, the highest selectivity for FA was observed at 10 bar O_2. Increasing the pressure to 30 bar did not increase the yield of FA. High conversion of GAD using the Ru-1 catalyst at 1 bar molecular oxygen was achieved, however, low selectivity for FA was observed. Instead, formation of several brown by-products was observed at 1 bar O_2. Possibly, the brown by-products were formed due to insufficient oxygen-availability, affording incomplete re-oxidation of the catalyst *i.e.* catalyst deactivation, leading to alternative transformations, such as aldol condensations of GAD affording C4, C5 and C6 sugars, followed by heat treatment, generating syrup-like by-products. Similar trends were observed using the Ru-3 catalyst with 1 bar molecular oxygen. The difference in catalyst activity was prominent using 5 bar molecular oxygen. 10% higher FA yield was obtained using the Ru-1 catalyst compared to that of the Ru-3 catalyst. At higher pressure (30 bar), no significant difference was observed between the two catalysts.

Aerobic oxidations has received considerable attention due to ease of availability and reduced risk of flammability. Air consist mainly of nitrogen (79%), however, almost 21% of air is molecular oxygen, which render air feasible as oxidant. Air was tested as oxidant for the oxidative dehydrogenation of GAD over $Ru(OH)_x/CeO_2$ at the optimized conditions (Table 4.3).

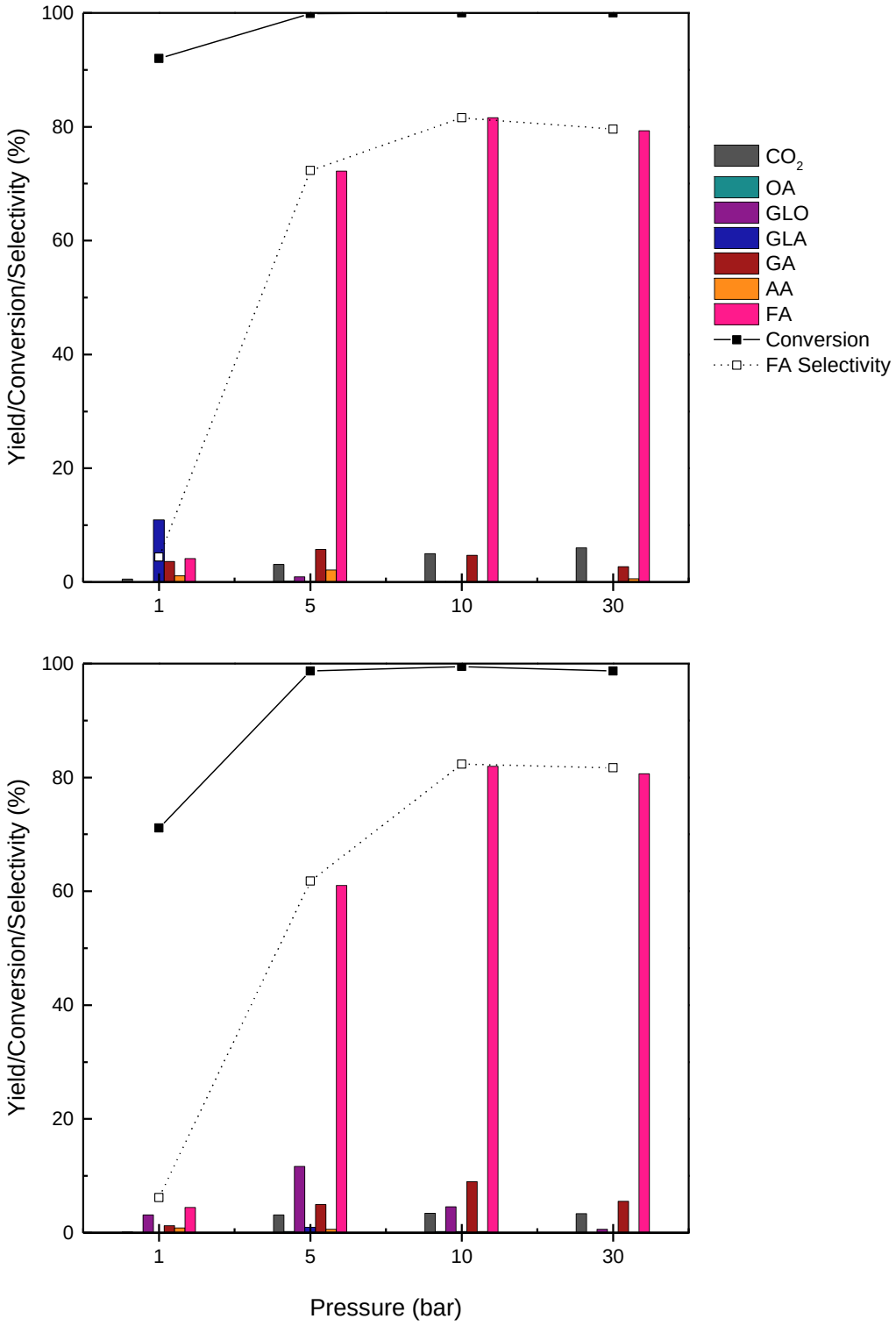

Figure 4.8: Pressure dependence of the $Ru(OH)_x/CeO_2$ (Ru-1 and Ru-3) catalyzed oxidation of GAD. Reaction conditions: GAD (356.1 mg, 5.9 mmol), $Ru(OH)_x/CeO_2$ (114.8 mg, 0.23 mol% Ru from 1.2 wt% $Ru(OH)_x/CeO_2$), H_2O (4.6 mL), molecular O_2 (1-30 bar), 90 °C, 16h at 500 rpm.

Slightly decreased activity was observed for the Ru-1 catalyst, however, a notably decrease in activity was observed for the Ru-3 catalyst. Furthermore, applying air significantly decreased the FA selectivity for both catalysts (Entry 2 and 4). In general, decreased amounts of oxidation- and over-oxidation products was observed, indicating occurrence of competing reactions. Similar to the reactions with 1 bar of molecular oxygen, brown by-products was formed, suggesting insufficient supply of oxygen in the liquid-phase for re-oxidation of the catalyst.

Table 4.3: Oxidation of GAD over $Ru(OH)_x/CeO_2$ with molecular oxygen and air.

Entry	Oxidant	Conversion (%)	Yield (%)							Selectivity FA (%)
			CO_2	OA	GLO	GLA	GA	AA	FA	
Ru-1										
1	O_2	100	5.0	0.1	01.	0.1	4.7	0.1	81.6	81.6
2	Air	98.6	2.8	0.0	0.8	2.7	5.2	0.1	15.6	15.8
Ru-3										
3	O_2	99.5	3.4	0.2	4.5	0.2	8.9	0.2	81.9	82.3
4	Air	79.9	0.9	0.0	1.7	0.0	2.1	3.0	14.9	18.6

Reaction conditions: GAD (356.1 mg, 5.9 mmol), $Ru(OH)_x/CeO_2$ (114.8 mg, 0.23 mol% Ru from 1.2 wt% $Ru(OH)_x/CeO_2$), H_2O (4.6 mL), oxidant (10 bar), 90 °C, 16 h at 500 rpm.

To achieve comparable results in the aerobic oxidation of GAD to FA, higher pressure of air is necessary. For ideal gas mixtures, the mole fraction of a gas component in a gas mixture equals the partial pressure divided by the total pressure, resulting in a partial pressure of 2.1 bar when applying 10 bar air. A partial oxygen pressure of 10 bar would require a total pressure of 47.6 bar. Aerobic oxidation at increased pressure was not tested due to limitations of the equipment capable of handling pressures up to 50 bar.

The effect of various reaction times was studied as shown by Figure 4.9, reaching close to full conversion (99.7 %) after 8 h for the Ru-1-catalyzed oxidation of GAD. The FA yield increased with time reaching a plateau after 8 h. After 70 h of reaction, the yield of FA decreased marginally, indicating high stability of FA over time at the applied conditions. Applying the Ru-3 catalyst decreased the activity, complementing the results obtained from the temperature and pressure studies, reaching close to full conversion after 16 h. At longer reaction times, decreasing yield of FA was limited by formation of small amounts of brown by-products. At short reaction times (1-4 h), formation of GLO was observed for both catalyst. Lower activity of Ru-3 resulted in lower yields of GLO and FA at short reaction

times. Fast conversion and oxidation was achieved using the Ru-1 catalyst, together with high stability of the desired product over time. Using the Ru-3 catalyst, decreased activity and stability affected the oxidation over time.

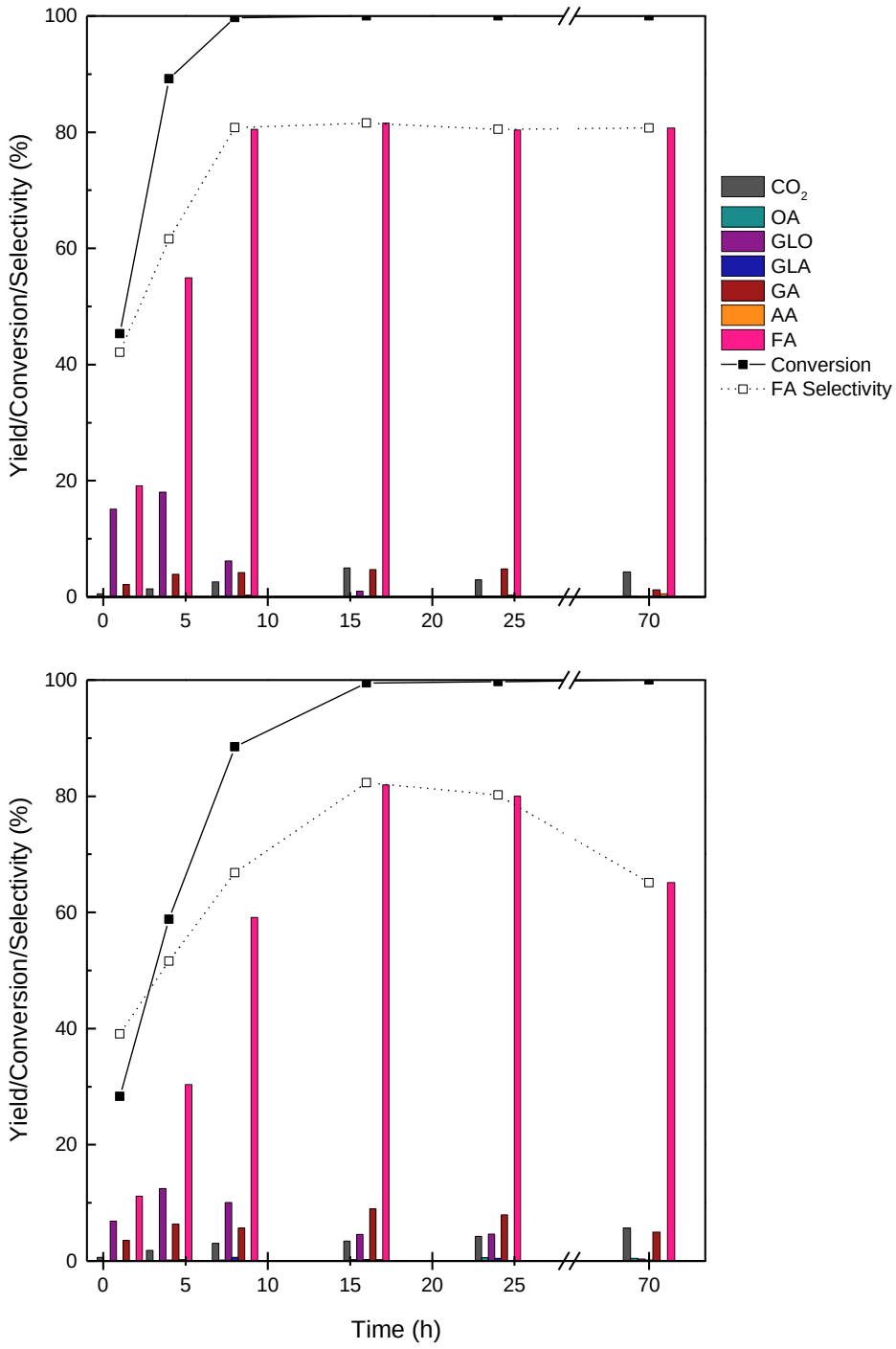

Figure 4.9: Oxidation of GAD over $Ru(OH)_x/CeO_2$ at various reaction times. Reaction conditions: GAD (356.1 mg, 5.9 mmol), $Ru(OH)_x/CeO_2$ (114.8 mg, 0.23 mol% Ru from 1.2 wt% $Ru(OH)_x/CeO_2$), H_2O (4.6 mL), molecular O_2 (10 bar), 90°C, 1-70 h at 500 rpm.

The catalyst-deficient oxidation was found to be almost completely inactive and less than 4% conversion of GAD was observed (Entry 1, Table 4.4). In the absence of Ru, a slightly increased activity was observed for the CeO_2 support-catalyzed oxidation (Entry 2), affording 7% conversion of GAD, supporting the proposed mechanism by Yamaguchi and Mizuno that the ruthenium-containing specie is the active phase of the oxidation, whilst CeO_2 acts as a support (Scheme 4.1). Small amounts of GLO, GLA, GA, AA and FA was observed.

Table 4.4: Oxidation of GAD without catalyst and reuse of Ru-1.

Entry	Catalyst	Run #	Conversion (%)	Yield (%)						
				CO_2	OA	GLO	GLA	GA	AA	FA
1	No cat.	1	3.6	0.0	0.0	0.5	0.0	0.0	0.0	1.4
2	CeO_2	1	7.2	0.0	0.0	1.5	0.1	0.2	0.1	0.7

Reaction conditions: GAD (5.9 mmol), $Ru(OH)_x/CeO_2$ (114.8 mg, 0.23 mol% Ru from 1.2 wt% $Ru(OH)_x/CeO_2$), H_2O (4.6 mL), molecular O_2 (10 bar), 90 °C, 8 h at 500 rpm.

Catalyst Ru-1 proved the most active, and the reuse of Ru-1 was tested on the oxidation of GAD (Figure 4.10). The used catalyst wash thoroughly washed with water and dried 18 h at 140 °C before reuse. The activity was found to slightly decrease with every run, affording 95% conversion after the fourth run. Loss of catalyst activity and selectivity was not observed in the first three runs, affording a FA selectivity around 80%. However, a decrease in FA selectivity was observed after the fourth run, affording 62% FA selectivity and 59% FA yield.

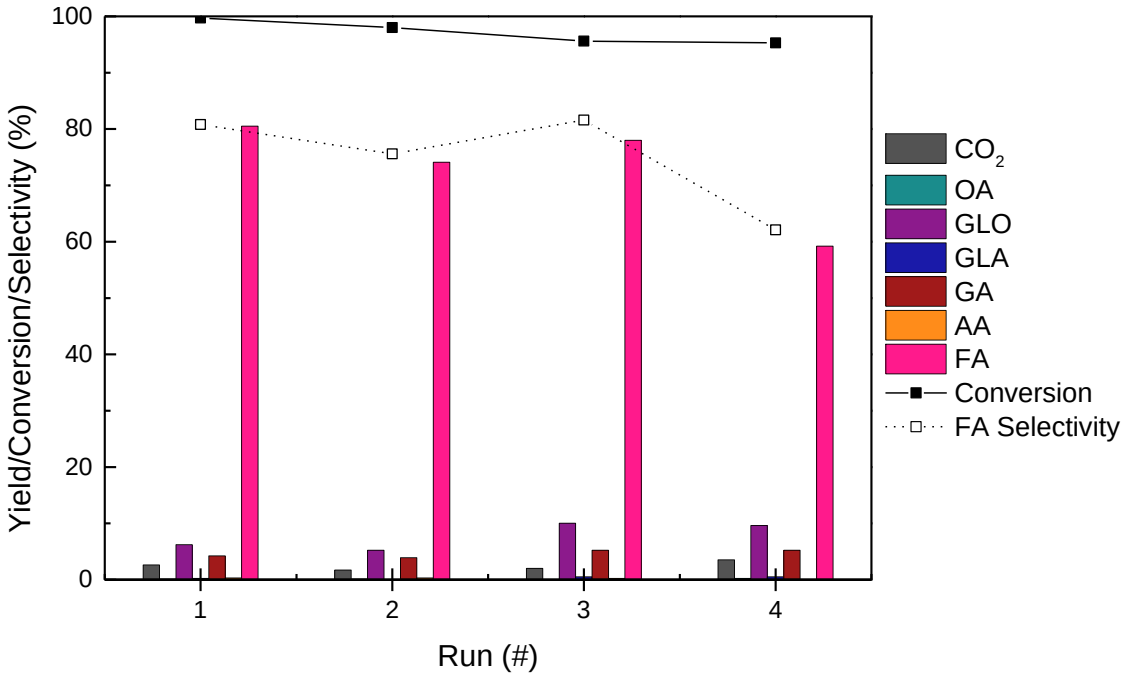

Figure 4.10: Oxidation of GAD over $Ru(OH)_x/CeO_2$, reuse of catalyst Ru-1. Reaction conditions: GAD (356.1 mg, 5.9 mmol), $Ru(OH)_x/CeO_2$ (114.8 mg, 0.23 mol% Ru from 1.2 wt% $Ru(OH)_x/CeO_2$), H_2O (4.6 mL), molecular O_2 (10 bar), 90°C, 8 h at 500 rpm.

The optimized conditions were applied for oxidation of larger sugars (C5 and C6) obtainable from biomass (Table 4.5), yielding 4.5 % of FA from xylose. However, low conversions of the sugars indicated the necessity for harsher conditions for the oxidation of the tested C5 and C6 sugars into FA. Assuming that oxidation of larger sugar molecules follow a similar trend to that of GAD, increased temperatures would afford higher conversion, however, at the expense of FA selectivity. Furthermore, according to the time studies on the oxidation of GAD, higher conversions should achievable from longer reactions time without affecting the yield of FA. Increased reaction time was tested on the oxidation of xylose affording 21% FA yield and 61% conversion after 48h, indicating promising results for the oxidative conversion of sugars with the $Ru(OH)_x/CeO_2$. However, further optimization of reaction conditions for larger sugars is required for obtaining high yields of FA.

Table 4.5: Oxidation of higher sugars.

Entry	Substrate	Conversion (%)	Selectivity						
			CO_2	GLO	GAD	GA	AA	FA	FA (%)
1	GAD	99.7	2.6	6.2	(0.3)	4.2	0.3	80.5	80.8
2	Glucose	23.1	0.0	0.0	0.4	0.2	0.0	1.2	5.2
3	Fructose	27.0	0.1	0.0	0.7	0.6	0.2	1.6	5.8
4	Xylose	25.5	0.3	0.0	0.2	0.2	0.0	4.5	17.7
5	Xylose[a]	60.7	10.3	0.0	0.1	2.0	2.4	20.7	34.0

Reaction conditions: GAD/glucose/fructose/xylose (5.9 mmol), Ru-1 (114.8 mg, 0.23 mol% Ru from 1.2 wt% $Ru(OH)_x/CeO_2$), H_2O (4.6 mL), molecular O_2 (10 bar), 90 °C, 8 h at 500 rpm. [a] reaction time 48 h.

4.3.2.1 Mechanism of Oxidation

The mechanism proposed by Yamaguchi and Mizuno (Scheme 4.1), elucidate the oxidation of GAD to GLO, GA and OA (Scheme 4.4). However, the formation of AA and FA is not clarified by this mechanism. Furthermore, oxidation of GAD to FA include a C-C bond cleavage.

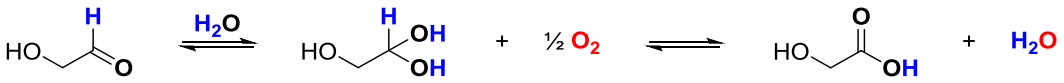

Scheme 4.4: Oxidative dehydrogenation of GAD to GA

Formation of AA and FA from GAD was obtained by Kishida *et al*. by hydrothermal treatment of GAD under basic conditions.[298,299] By investigating reaction products at short reaction times, several intermediates were identified and three reaction pathways were proposed (Scheme 4.5). These included several condensation products of GAD. As previously mentioned, both Lewis acidic- and Brønsted basic sites are present on $Ru(OH)_x/CeO_2$, and hence, possibly formation of base catalyzed condensation products of GAD take place at elevated temperatures. Several of the identified intermediate condensation products described by Kishida were examined for in the obtained products

solutions, including glyceraldehyde, dihydroxyacetone, formaldehyde, lactic acid, D-threose, L-erythrulose, D-erythrose and acrylic acid, however, these were not detected from the analysis of the liquid phase, indicating an aldol condensation-free reaction mechanism. Furthermore, the α-hydrogen of GAD is of lower acidity due to the inductive effect of the oxygen of the α-hydroxy group, rendering aldol condensation of GAD more challenging compared to aldehydes without an α-hydroxy group.[298] The reactions were performed under base-free conditions, leaving only the Brønsted basic sites on the catalyst to catalyze the aldol condensations and oxidation of formaldehyde to FA *via* the Cannizzaro reaction (Scheme 4.5). Neutral pH was measured for the catalyst in water, and moreover, since none of the intermediates observed by Kishida *et al.* was observed, the reaction mechanism proposed in Scheme 4.5 appears dubious.

Supported ruthenium-catalyzed oxidative cleavage of vicinal diols was reported by Takezawa *et al.*, affording various aldehydes.[300] The observed by-products included other oxidation products such as CO_2, GLO and GA. At mild conditions, one of the major products observed was GLO, indicating that GLO is an intermediate on the oxidation of GAD to FA. Possibly, FA was formed from oxidative C-C cleavage of GLO as depicted in Scheme 4.6.[300,301] Hydrated GLO is formed from oxidative dehydrogenation of the α-hydroxy group, following the mechanism proposed by Yamaguchi and Mizuno.[263] Spontaneous formation of the geminal diol by hydration of the formed aldehyde affords ethane-1,1,2,2-tetrol (Scheme 4.6, (A)). Formation of ruthenium-alkoxide specie II with the vicinal diols position the hydrated GLO for oxidative C-C cleavage, releasing two molecules of FA (B). A hydrogen from water is then captured by the deposited electrons of ruthenium and the formed hydroxide specie is transferred to the partially positively charged ruthenium specie (ruthenium specie III), regenerating one Ru-OH (ruthenium specie IV). The formed ruthenium hydride is oxidized through a mechanism similar to that proposed by Yamaguchi and Mizuno (ruthenium specie IV and V), regenerating the ruthenium specie I.

These are just speculations based on literature given that no mechanistic studies were performed during this project.

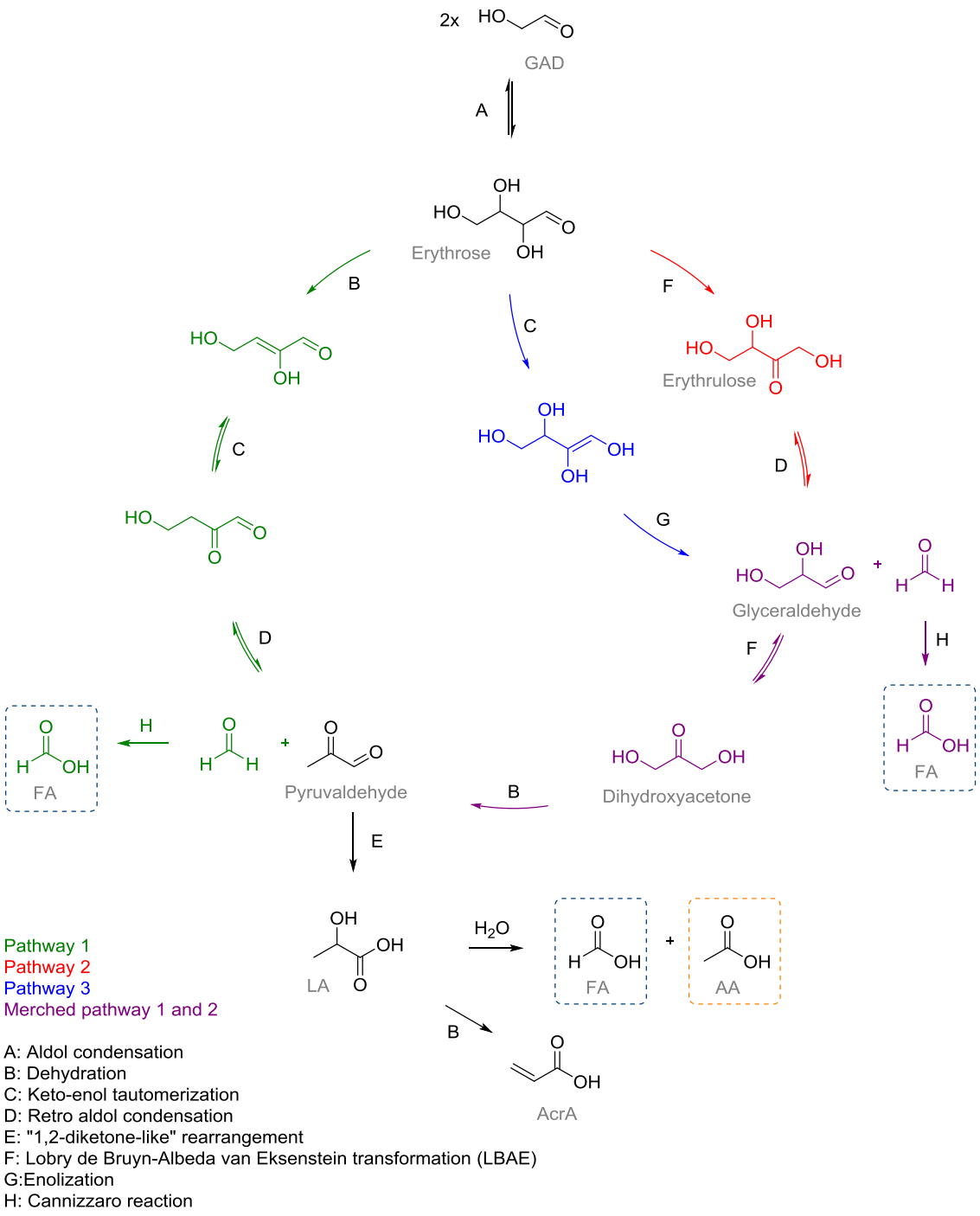

Scheme 4.5: Formation of formic- and acetic acid by hydrothermal treatment of glycolaldehyde. Scheme adapted from Kishida *et al.*[298]

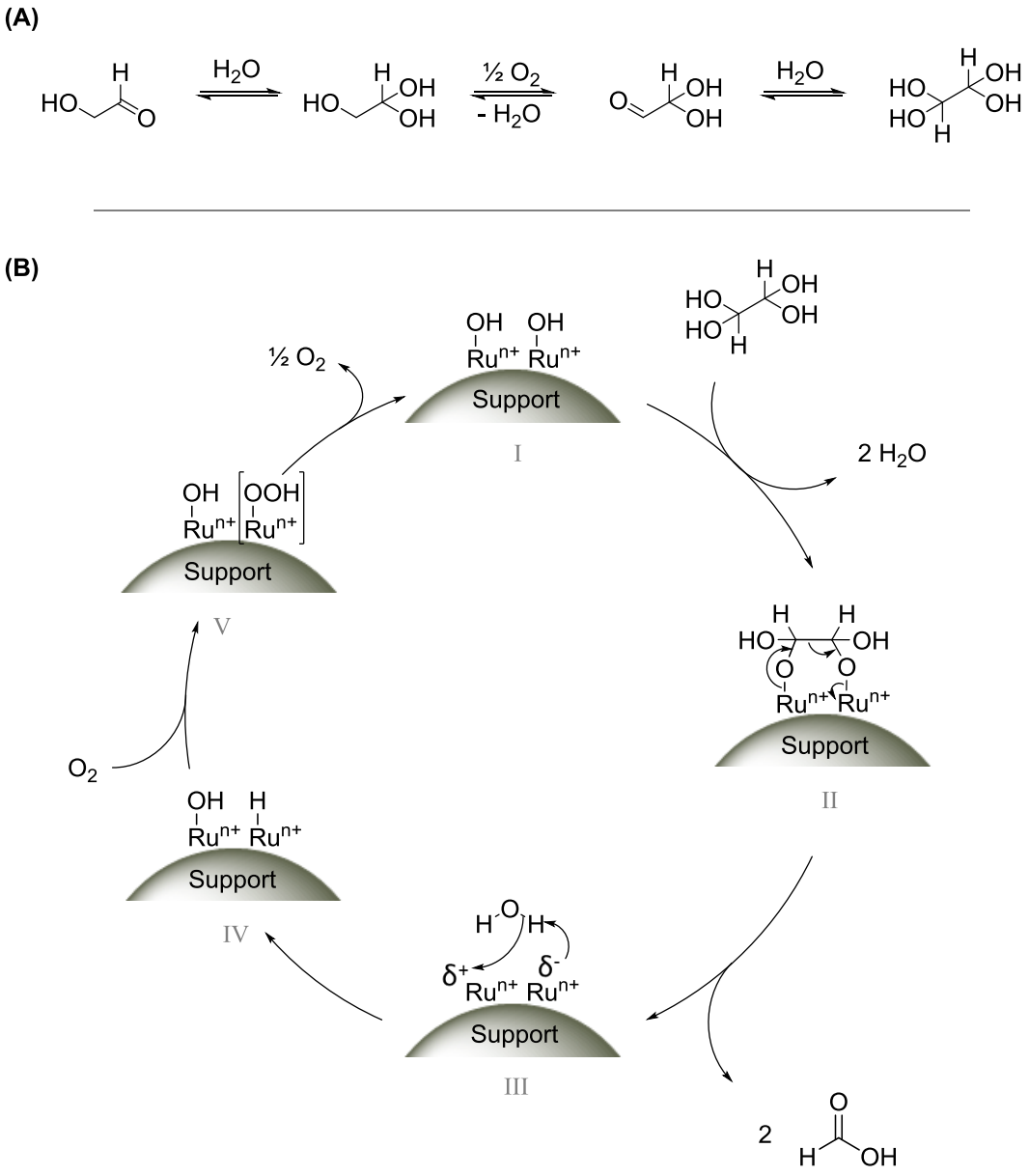

Scheme 4.6: Proposed mechanism for oxidative C-C cleavage of GAD, a) oxidative dehydrogenation of GAD to GLO followed by hydration of the formed aldehyde, b) oxidative cleavage of hydrated GLO forming two molecules of FA.

4.3.3 Oxidation of Alcohols to Acetic Acid

One of the key transformations of organic chemistry is the oxidation of alcohols to carboxylic compounds various industries including polymer and food. The selective oxidation of alcohols and polyols are of great interest in the context of adding value to biomass-derived compounds.[145] As mentioned in section 4.1.1, AA is a highly important organic bulk chemical, and the interest in formation of bio-AA is increasing.

To demonstrate the diversity of the ceria-supported $Ru(OH)_x$ catalyst, various substrates, including 1-propanol (POH), 1-propanal (PAL), propionic acid (PA), 1,3-propanediol and 2,3-butanediol, were subjected to the oxidation over $Ru(OH)_x/CeO_2$ (Scheme 4.7), at conditions previously optimized by Dr. Yuri Gorbanev, presented in Table 4.6.[290]

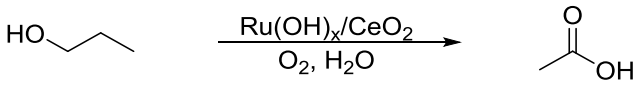

Scheme 4.7: Oxidation of 1-propanol to acetic acid over $Ru(OH)_x/CeO_2$.

Table 4.6: Preliminary test performed for reproduction of previous work in our group by Gorbanev *et al.*[290]

Entry	Substrate	Conversion (%)	Yield (%)					Selectivity AA (%)
			CO_2	PAL	PA	AA	FA	
1	1-propanol	56.4	0.2	7.4	26.5	6.2	2.2	5.5
2	1-propanal	99.3	0.1	(0.7)	65.9	11.4	0.0	5.7
3	Propionic acid	13.3	0.2	0.0	(86.7)	13.6	0.0	51.1
4	1,3-propanediol	39.1	0.1	0.3	0.0	4.1	1.4	5.3
5	2,3-butanediol	34.2	0.1	0.0	0.0	34.2	0.1	99.4

Reaction conditions: 10.16 mL of 1.17 M aqueous solution of the substrate, 0.23 mol% ruthenium from the Ru-4 catalyst, 10 bar molecular oxygen, 150 ^oC, 16h at 500 rpm.

Several products of the liquid-phase were identified according to HPLC analysis including PAL, PA, AA and FA (Scheme 4.8). The gas-phase was analyzed for CO_2, generated from oxidative C-C cleavage of C3 substrates or from over-oxidation of AA.

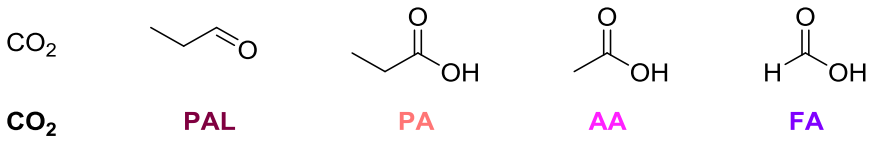

Scheme 4.8: Identified products of the supported $Ru(OH)_x$-catalyzed oxidation of alcohols.

The yields and conversions were not comparable with the results obtained by Dr. Gorbanev.[290] However, the oxidations performed by Dr. Gorbanev were conducted in a 100 mL Parr reactor and the results presented in Table 4.6 in 18.4 mL high pressure reactors. Decreased headspace of the reactors may cause decreased activity and selectivity due to decreased O_2:substrate ratio. A series of down scaled reactions were performed to elucidate the proper O_2:substrate ratio for the mini reactors using 1-propanol as a model substrate (Figure 4.11). Increased conversions were found on smaller scales, however, no general trend of the degree of down-scale was observed at 10 bar (Figure 4.11, top graph). The yield of AA was limited by the formation of PA, affording AA selectivities between 11 and 38%. A reference reaction was conducted in a 100 mL Parr reactor, yielding 52% PA, however, full conversion was not reached at the applied conditions. At increased pressure of molecular oxygen (Figure 4.11, bottom graph), the selectivity of reaction products changed, favoring AA over PA, possibly due to increased concentration of oxygen at increased pressure. Decreasing the scale afforded decreased conversions and yields of PA and AA, however, continuously favoring formation of AA over PA.

Product selectivity was altered by increasing the pressure of molecular oxygen. The O_2:substrate ratio was studied at 10 and 30 bar oxygen, achieving stable product selectivity ratios for each pressure respectively at decreased scales (0.14-0.5 down-scale), however, favoring different product formations. The highest yield was observed at 0.5 scale, applying 5.08 mL of 1.17 M aqueous solution of the substrate, leaving a headspace of 13.32 mL.

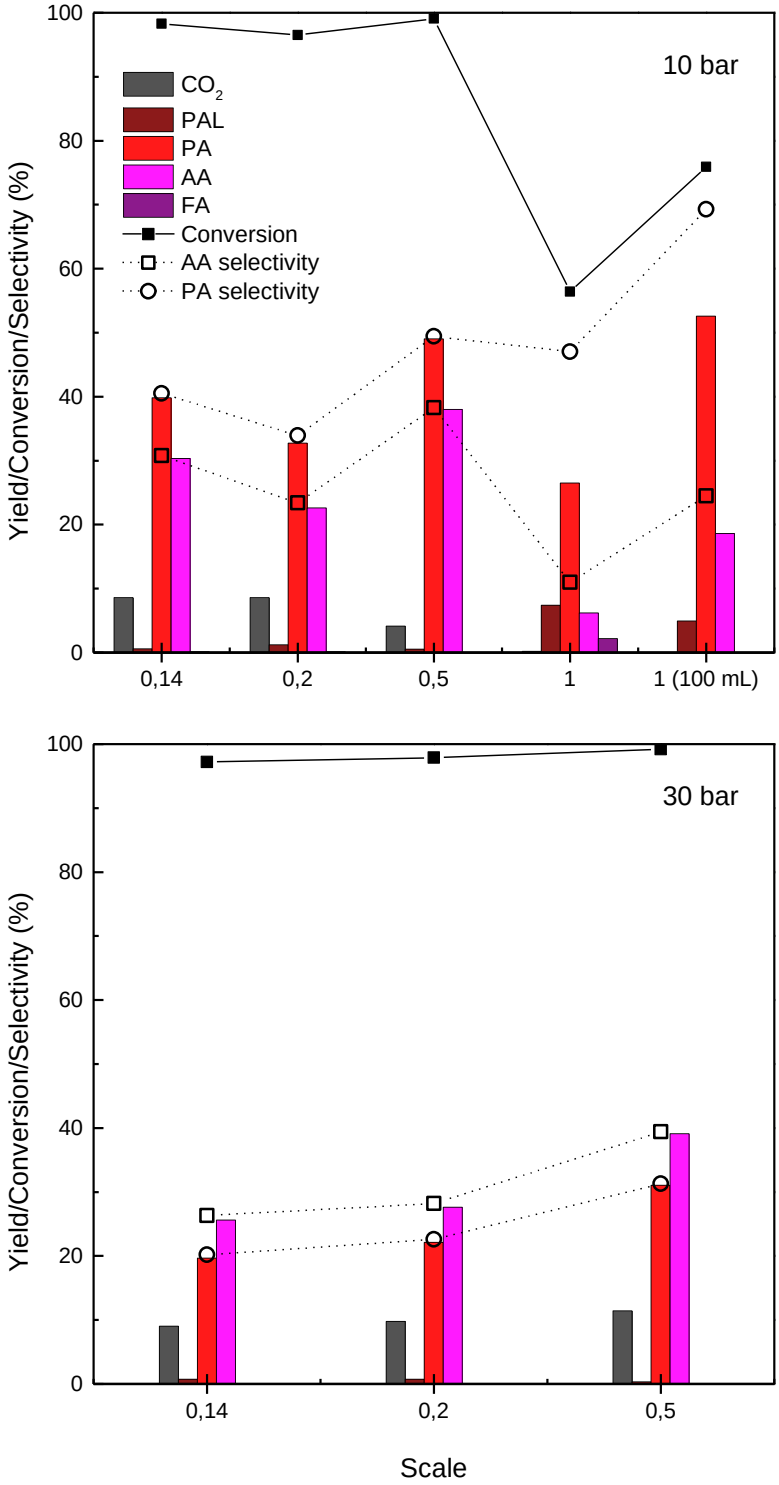

Figure 4.11: Optimization O_2:substrate ratio using Ru-4 and 1-propanol as model substrate. Molecular oxygen pressure: 10 bar (top) and 30 bar (bottom). Reaction conditions: 1.44 (0.14 scale), 2.03 (0.2 scale), 5.08 (0.5 scale) and 10.16 (full scale, 1) mL of 1.17 M aqueous solution of the substrate, 0.23 mol% ruthenium from the Ru-4 catalyst, 10 or 30 bar molecular oxygen, 150 ºC, 16h at 500 rpm.

The effect of varying BET surface area was studied at 10 and 30 bar molecular oxygen on a 0.5 scale, as shown in Figure 4.12. Lower surface area catalysts did not appear to improve the conversion of 1-propanol at 10 bar (Ru-1, Ru-2 and Ru-3, top graph). Notably, the selectivity for AA exceeded the PA selectivity when applying the Ru-1 and Ru-2 catalysts with medium- and low surface areas, respectively. However, the oxidations with Ru-1 and Ru-2 catalysts yielded additional unidentified by-products. Surprisingly, the low surface area Ru-3 catalyst afforded higher selectivity for PA than AA, similar to the high surface area Ru-4 catalyst. Close to full conversion was observed at 30 bar oxygen for all the tested catalysts. For the high- and medium surface area catalysts (Ru-4 and Ru-1), the selectivity for AA was favored over PA. The difference in AA and PA selectivity decreased using Ru-2 and for the low surface area catalyst, Ru-3, the selectivity for PA surpassed that of AA.

At milder conditions (10 bar), the conversion of POH decreased with decreasing surface area, however, indicating no trends in selectivity based on surface area. Increased pressure was observed to improve the product yields and conversions for the Ru-1, Ru-2 and Ru-3 catalysts. Unexpectedly, the selectivity for PA was higher than that of AA using Ru-3 at 30 bar. Furthermore, increased CO_2 formation was detected at 30 bar, suggesting over-oxidation of AA and PA. Notably, AA is a C2 molecule, and C-C cleavage of 1-propanol is necessary to obtain AA, producing equal amounts of C1 molecules such as CO, CO_2, FAD or FA. The liquid-phase was analyzed for FAD and FA, yielding small amounts of FA (purple bars) and no FAD was detected.

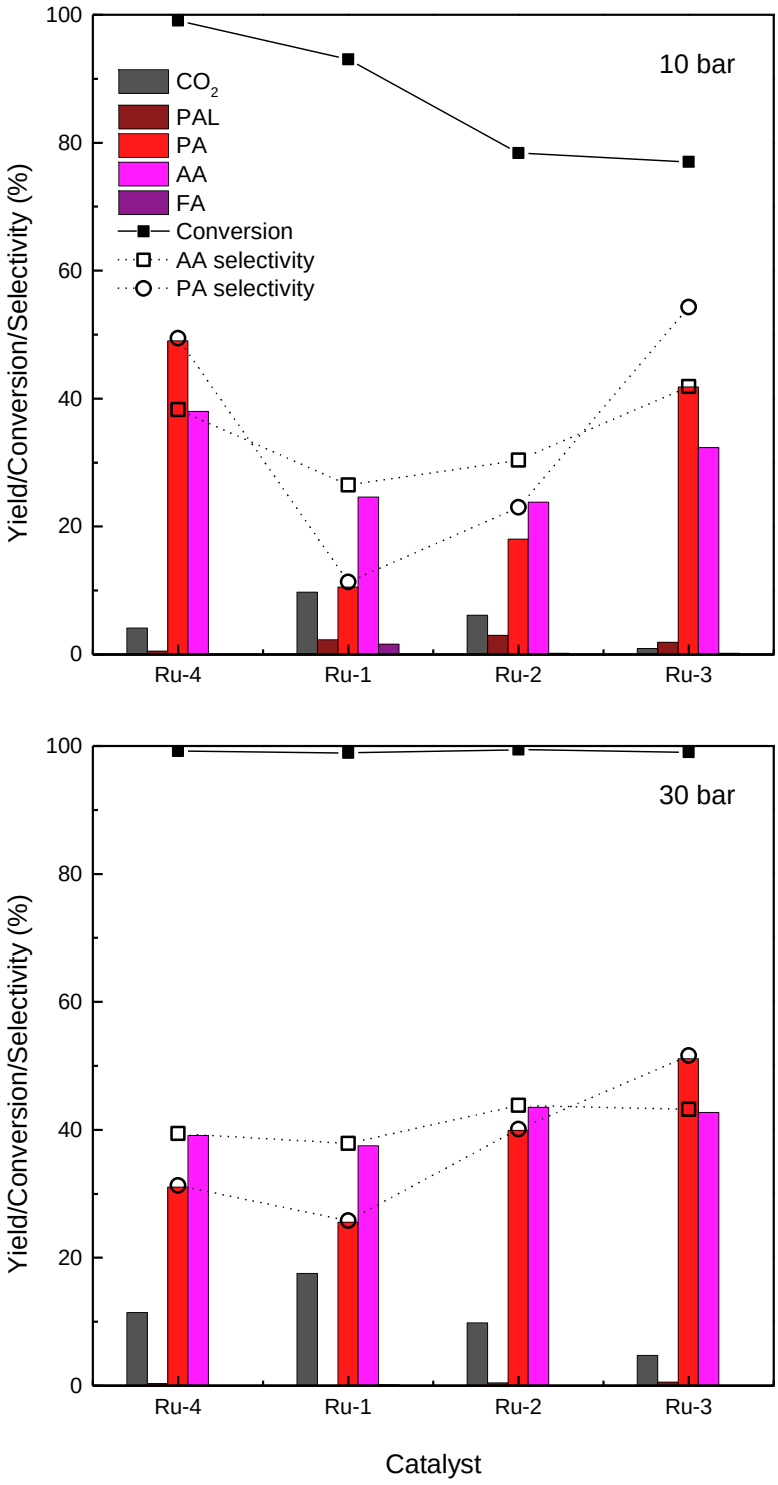

Figure 4.12: Oxidation of 1-propanol applying catalysts with varying BET surface areas at 0.5 scale. Molecular oxygen pressure: 10 bar (top) and 30 bar (bottom). Reaction conditions 0.5 scale: POH (356,1 mg, 5.9 mmol), $Ru(OH)_x/CeO_2$ (114.8 mg, 0.23 mol% Ru from 1.2 wt% $Ru(OH)_x/CeO_2$), H_2O (4.6 mL), molecular O_2 (10 or 30 bar), 150°C, 16 h at 500 rpm.

The effect of the BET surface area was studied on a 0.2 scale with 30 bar molecular oxygen, affording comparable results to that of 0.5 scale, however, decreased yields was observed for all the applied catalysts (Figure 4.13).

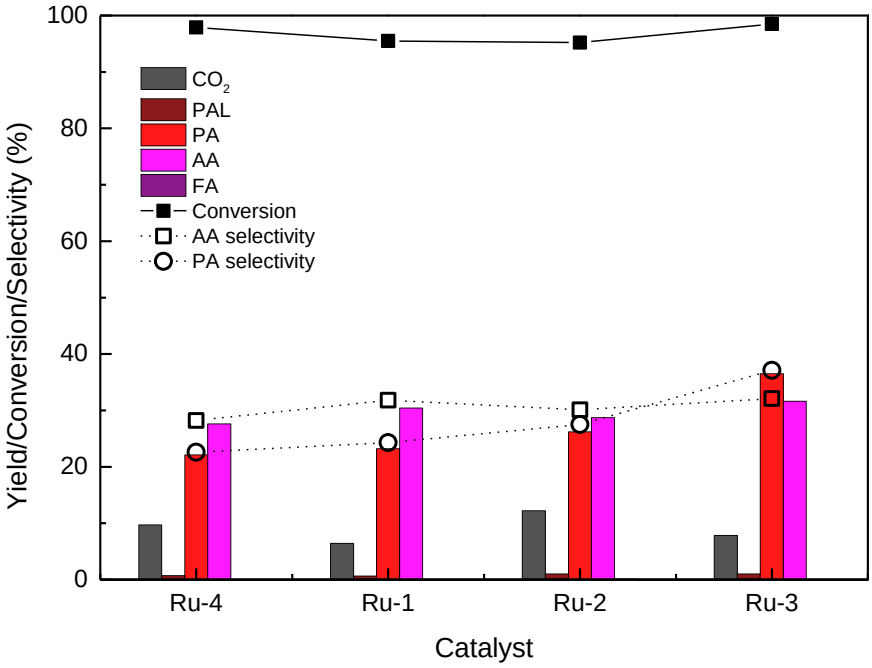

Figure 4.13: Oxidation of 1-propanol applying catalysts with varying BET surface areas at 0.2 scale. Reaction conditions: POH (142.5 mg, 2.4 mmol), $Ru(OH)_x/CeO_2$ (45.9 mg, 0.23 mol% Ru from 1.2 wt% $Ru(OH)_x/CeO_2$), H_2O (1.8 mL), molecular O_2 (30 bar), 150°C, 16 h at 500 rpm.

Due to inadequate obtained AA selectivities, no further optimization was performed on the oxidation of various alcohols over ceria-supported $Ru(OH)_x$. Promising selectivity was for the 2,3-butanediol, however, at low conversion, indicating that harsher conditions are required for successful conversion into AA in high yields.

4.3.3.1 Mechanism of Oxidation

Alcohols are readily oxidized into the corresponding aldehyde in the presence of supported $Ru(OH)_x$ and oxygen at low pressures below 100 °C, indicating fast oxidation of 1-propanol into propanal.[279,302,303] At elevated temperature and

pressure, further oxidation into the carboxylic acid has been reported,[63,81,94] suggesting initial formation of PA at the applied conditions (150 °C, 30 bar, depicted in Scheme 4.9 A). To obtain AA, C-C cleavage is required, generating a C1 and a C2 molecule. Among the observed by-products was CO_2, suggesting decarboxylation of the formed PA (Scheme 4.9 B).[304–307] Oxidative decarboxylation of PA, affording a C2 alkoxide-ruthenium specie (IV), followed by subsequent oxidative dehydrogenation would afford AA as end-product, Scheme 4.9 (B) and (C).

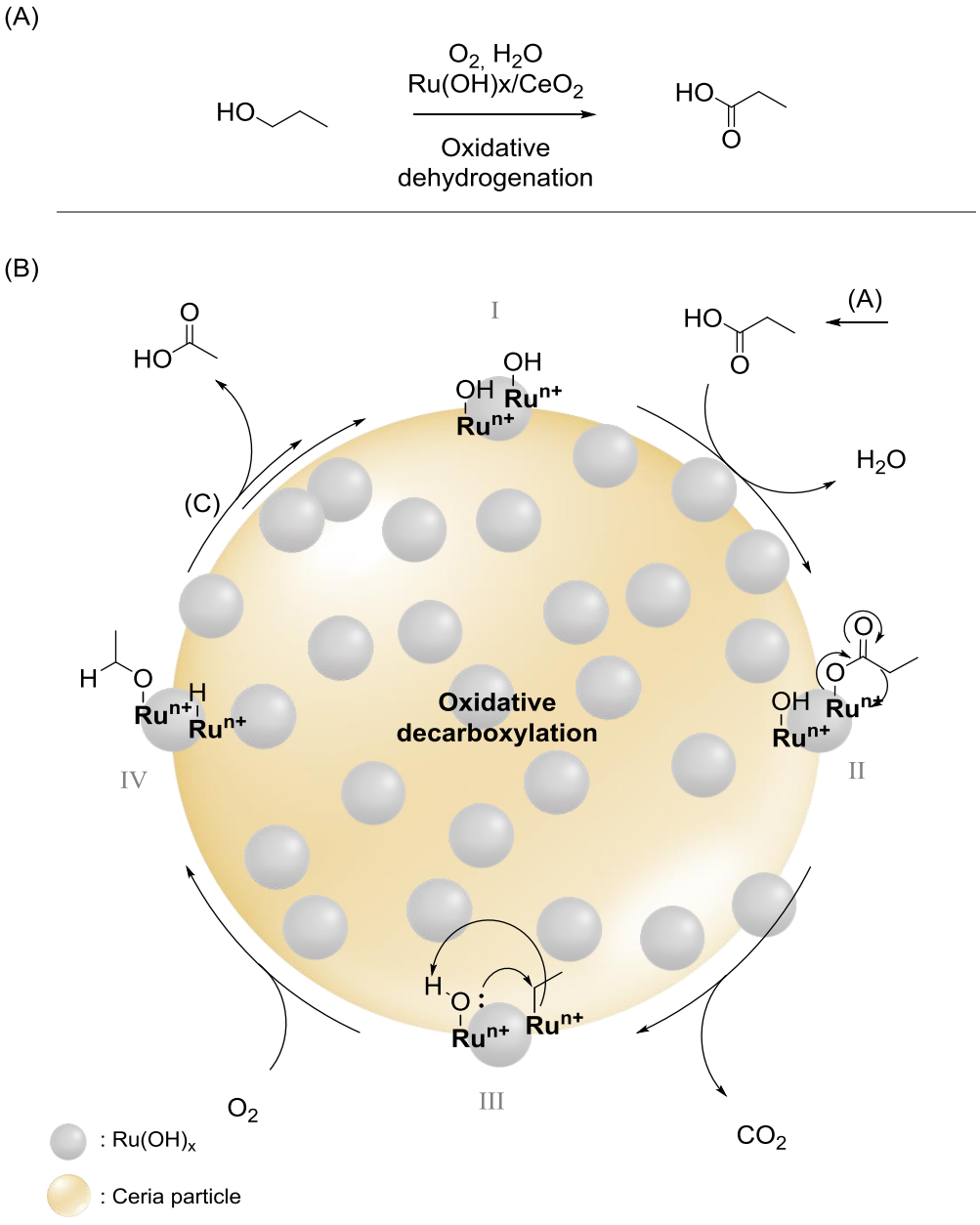

Scheme 4.9: Proposed mechanism for oxidative dehydrogenation of 1-propanol, followed by oxidative cleavage of PA and oxidative dehydrogenation of the formed ethanol.

The yield of CO_2 was calculated from the prospect that each 1-propanol molecule can produce three molecules of CO_2. Assuming the above-described mechanism of decarboxylation applies for this oxidation, CO_2 would be produced in a 1:1 ratio as shown by Scheme 4.10. Alternatively, the reported yield of CO_2 should be multiplied by three, resulting in comparable yields of AA and CO_2, supporting the proposed mechanism of decarboxylation.

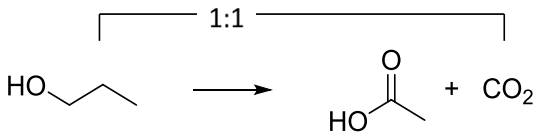

Scheme 4.10: Overview of oxidation of 1-propanol to AA and CO_2.

Other routes for obtaining AA include decomposition of intermediates such as lactic acid. Zhang *et al.* reported on formation of AA and FA from supported platinum-catalyzed oxidation of glyceraldehyde in the presence of a base.[308] Zhang *et al.* proposed a reaction pathway affording lactic acid followed be C-C cleavage into FA and AA. Hydrothermal treatment of GAD was described in section 0 (Scheme 4.5). Considering the higher temperature applied and the presence of Brønsted basic sites on the $Ru(OH)_x/CeO_2$, possible condensation products of the formed aldehyde-intermediate could provide a means of reaction pathway for synthesis of AA and FA. However, little or no FA was observed in the analysis of the liquid phase.

4.4 Conclusions

Preliminary oxidations converting the biomass platform molecule, GAD, into FA, followed by expansion of the scope to include C6 and C5 sugars were successfully performed. In general, the activity of the Ru-1 catalyst exceeded that of the Ru-3 catalyst. Selectivities were found to be improved by optimization of reaction conditions, affording highest yields of FA at mild conditions.

The temperature was found to have a significant effect on the product outcome, affording low conversions at decreased temperatures and decomposition of GAD into CO_2 at elevated temperatures. A fine balance between conversion and FA

yield was found at 80 and 90 °C for the Ru-1 and Ru-3 catalysts yielding 88 and 81% of FA, respectively. Decreasing the pressure to 10 bar did not change the product distribution considerably, however, decreasing conversions and product yields was observed at lower pressures of oxygen, indicating limitations of the oxidation due to oxygen availability. Studying the effect of reaction time showed high activity and FA yield after 8 h using the Ru-1 catalyst. For the Ru-3 catalyst, the highest FA yield was observed after 16 h of reaction, suggesting lower activity of Ru-3 compared to Ru-1. High product stability was found over time for the Ru-1 catalyst at the applied conditions. In contrast, decreasing FA yield was observed at reaction times longer than 16 h for the Ru-3 catalyzed oxidation.

Expansion of the scope was tested with the optimized conditions on glucose, fructose and xylose, affording 1.2, 1.6 and 4.5% FA yield, respectively. Decreased substrate conversions and low yields of FA was observed. Prolonged reaction time of the oxidation of xylose increased the FA yield, affording 21% FA after 48 h. In general, good FA selectivity was found for the larger sugars rendering the Ru-1 catalyst a promising catalyst for the conversion of sugars into FA. However, optimization of the reaction conditions for an expanded scope of sugars is required for obtaining high yields of FA.

In general, the ceria-supported $Ru(OH)_x$ catalysts were found to afford high yields of FA at the optimized conditions with minor effect of the ceria particle size. A slightly decreased activity was observed for the microparticulate ceria-supported catalyst, Ru-3, however, at the optimized conditions the difference in AA yield and selectivity was insignificant. At long reaction times, decreasing AA yield was observed for the Ru-3 catalyst, however, the nanoparticulate ceria-supported catalyst, Ru-1, was found to afford high product stability after 70 h of reaction. Possibly, the general higher activity of the Ru-1 catalyst could also be assigned to the slightly higher ruthenium loading (1.4 wt% from XRF) compared to the Ru-3 catalyst (1.0 wt% from XRF).

Ceria-supported $Ru(OH)_x$ was studied for the oxidation of alcohols to AA. Downscaling of the liquid phase afforded higher activity of the catalyst, possibly due to limited oxygen supply from the smaller headspace of the reactors. Increasing the pressure of molecular oxygen altered the favored selectivity from PA to AA, although the detected AA yield remained unchanged, hence, decreased PA yields were observed at 30 bar. The highest yield of AA was found to be 39%, achieved from oxidation with the Ru-4 catalyst at 30 bar. Given the moderate AA yields at relatively harsh conditions, no further optimization of the oxidation of 1-propanol to AA was attempted.

Chapter 5. Oxidation of Biomass-derived compounds with Wells-Dawson Polyoxometalates

---

The results presented in this chapter was performed at Friedrich-Alexander University (FAU) in Erlangen, Germany in the group of Prof. Dr. Wasserschied in collaboration with Dr. Ing. Jakob Albert and Ph.D.-student Dorothea Voss. The collaboration was continued after returning to the Technical University of Denmark (DTU).

Synthesis and application of Wells-Dawson heteropolyoxometalates were studied and the results are presented in this Chapter.

5.1 Introduction

Polyoxometalates (POMs) constitute a vast field of inorganic chemistry. POMs are inorganic polyatomic ions, which consist of highly symmetrically ordered metal-oxide clusters. The discrete ionic structure provide properties unlike other metal-oxides used in catalysis, e.g. zeolites and metal-oxide support.[309] POMs are multielectron oxidants, strong acids and stable in aqueous solutions up to neutral pH.[309] Since the first report on POMs in 1826, the field of POMs has received considerable attention.[310] Following the structural elucidation of the Keggin POM by X-ray Diffraction in the 1930's, several POM structures has been solved and proven advantageous in many fields.[311] Because of the wide variety of molecular composition, structural diversity, high thermal stability and high solubility in polar solvents, the different POMs have proven useful in various industries including analytical- and clinical chemistry, catalysis, polymer, biochemistry, medicine and molecular electronics.[312–340]

5.1.1 Nomenclature and Historical Perspective

Characteristic for these metal-oxide clusters is the basic well-defined octahedral metal-oxide (MO_x) unit. It should be noted, that it is possible to produce POMs containing other p-block elements in place of oxygen, however, these will not be discussed in this dissertation.[341–347] The metal (M) is termed the addenda atom and by definition, POMs consist of three or more addenda atoms. No defined chemical limitations to M has been reported, however, M is usually found among the group VI (W, Mo, etc.) and group V (V, Nb, Ta, etc.) elements in their high oxidation states.[317,318,348,349] The coordination number of M, $_x$, is typically between four and seven depending on the metal. POMs consisting only of MO_x units are classified as isopolyanions (IPA) and have the general chemical formula $[M_yO_x]^{n-}$. The IPA belongs to one of two major classes of POMs. The other class, heteropolyanions (HPA), satisfy the above mentioned characteristics of POMs, however, additionally, HPAs contain one or more heteroatoms (X) from the p-, d- or f-block. Typically the heteroatom is found in the p-block *i.e.* B, Si, P, As.[317,349] The heteroatom cannot be removed or replaced without altering the structure of the anion. Due to stabilizing effect of the heteroatom on the metal-oxide framework, HPAs have been reported much more thermally stable than IPAs, and consequently the preferred structure for industrial catalytic processes.[350] The general chemical formula for HPAs is $[X_zM_yO_x]^{n-}$ in which the MO_x-octahedra typically are assembled around the central heteroatom. Examples of IPA and HPA are presented in Figure 5.1 below. The HPAs are classified into numerous subgroups according the their y/z ratios.[351] The work presented in this

dissertation focuses on the synthesis of the Wells- Dawson subgroup and the selective substitution of an addenda atoms (Figure 5.1 f).

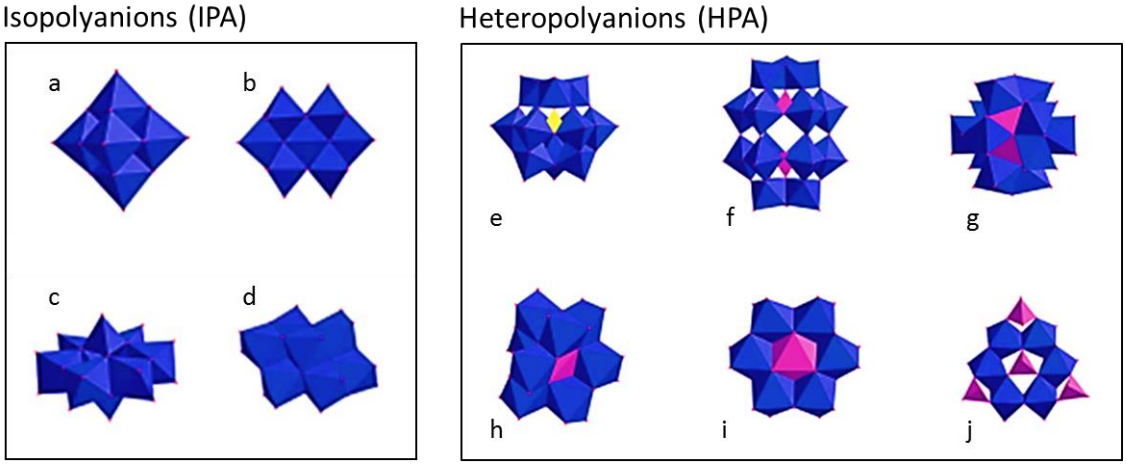

Figure 5.1: Illustrations of POM classes, where the addenda atom octahedra are illustrated in blue and the heteroatom tetrahedra in yellow or pink. (a) Lindqvist, (b) $[X_7O_{24}]^{6-}$, (c) $[\alpha\text{-}X_8O_{26}]^{4-}$, (d) $[\beta\text{-}X_8O_{26}]^{4-}$ (e) Keggin, (f) Wells-Dawson, (g) Silverton, (h) Allman-Waugh, (i) Andersen and (j) Strandberg. Illustrations of IPA and HPA are adapted from Li and Xu.[317]

The first report on HPAs was published by Berzelius in 1826. Herein Berzelius described the formation of a yellow precipitate when adding ammonium molybdate to phosphoric acid.[310] In 1864, Marignac successfully determined the ratio of the addenda- and heteroatom (W/Si) of tungstosilisic acids and their salts.[352] In the late 1800's and early 1900's new theories on coordination chemistry brought the structural elucidation of POMs one step closer. Anticipating the edge- and face-sharing polyhedral theory, Werner proposed structures for IPAs and HPAs (Figure 5.2 c and d).[353,354]

It was not until the late 1920s that the corner-sharing theory of polyhedral was introduced by Linus Pauling (Figure 5.2). Pauling proposed a structure for the Keggin HPA, composed of 12 metal atoms and a heteroatom, based on theoretical principles of coordinated structures in complex crystals. The structure was composed of 12 distorted octahedra (Figure 5.2 a) of the metal-oxide unit

(MO_6), connected to adjacent octahedra in a corner-sharing fashion (see full structure in Figure 5.3).[355]

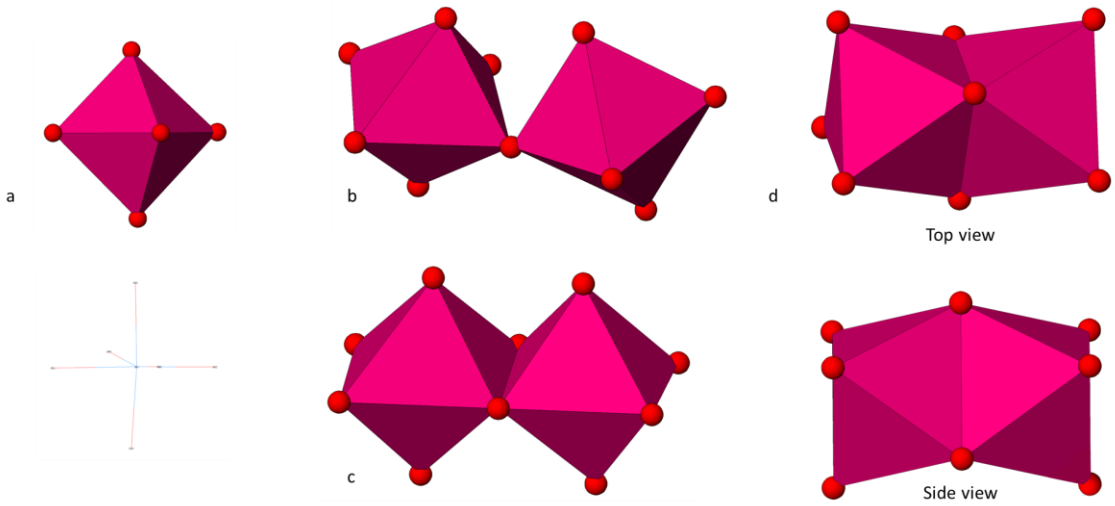

Figure 5.2: Octahedron and octahedra linkages. (a) distorted octahedron, (b) corner-sharing, (c) edge-sharing and (d) face-sharing octahedra. (a), (b) and (c) were modified from recorded single crystal XRD of $P_2W_{18}O_{62}^{6-}$ presented in section 5.4.1. (d) was modified from previous recorded data of epsilon iron nitride.

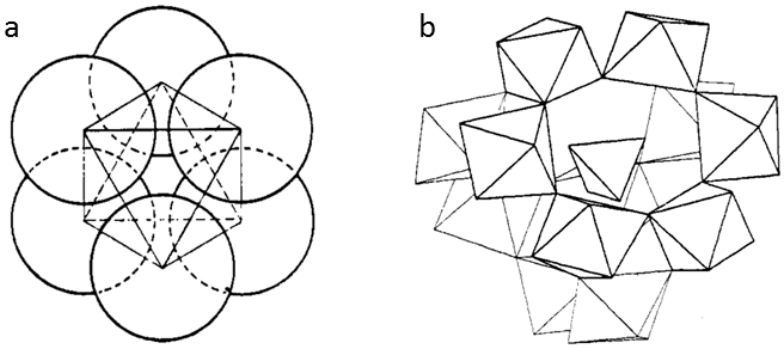

Figure 5.3: Proposed structures by Linus Pauling 1929. (a) distorted octahedron, (b) $[SiO_4W_{12}O_{18}(OH)_{36}]^{4-}$ HPA.[355]

J. F. Keggin was the first to publish the experimentally resolved structure of the $PW_{12}O_{40}^{3-}$ heteropolyanion. In 1933, Keggin reported powder X-ray diffraction data of the $PW_{12}O_{40}^{3-}$ anion, where the distorted WO_6-octahedra were arranged

into four groups (triads), each containing three WO_6 units arranged around a trigonal axis. The WO_6 octahedra of the triads were connected in an edge-sharing linkage (Figure 5.2c), and the triads in turn were connected through the corners to the adjacent triad and to the central PO_4 tetrahedral (Figure 5.2b). This is the structure known today as the Keggin polyoxometalate (Figure 5.4).[311,356]

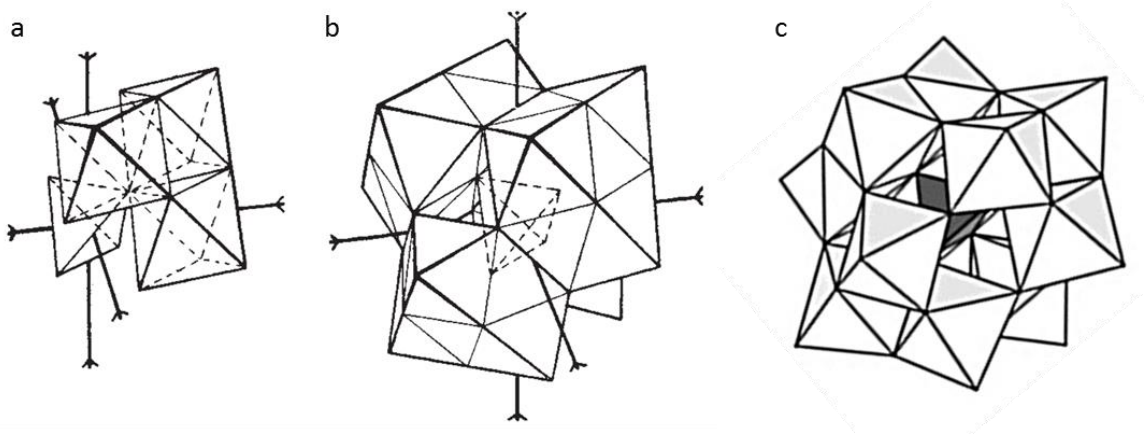

Figure 5.4: (a) Keggin's proposed structure of a triad connected to the central PO_4, (b) Keggin's proposed structure for the complete $PW_{12}O_{40}^{3-}$ HPA[311] and (c) The Keggin structure of the $PW_{12}O_{40}^{3-}$ polyoxoanion published in 2015.[332]

Succeeding development of new and improved analytical tools, several POM structures were elucidated and new classes of POMs were discovered and characterized, and still are today.

5.1.2 Catalysis with Polyoxometalates

From the 1970's and onward, there was a growing interests in POMs applied for catalysis.[46,61,67,309,321,323,328,357–385] The distinctive properties of POMs provide an alternative base for utilization in catalysis. These properties include discrete size, high molecular mass, electron "reservoir", proton storage and transfer ability, the aforementioned thermal stability and super acidity (Brønsted) of the corresponding acids. Furthermore, high solubility in aqueous and some organic

media, depending on the counter cation, provide a promising ground for application within catalysis. The oxygens of each octahedra are polarized towards the positively charged metal in the center, making the oxygens relatively inert and resistant to decomposition.[386] The additional ability to coordinate metals, combined with the above-mentioned properties, provides a wide variety of catalytic possibilities.[340] In homogeneous acid catalysis, heteropoly acids often offer more efficient reactions and reduced waste formation compared to conventional mineral acids.[369,372] Being stronger acids, lower catalyst concentration of heteropoly acids limit side reactions, and render it possible to perform the reaction at milder conditions. Side reactions of the mineral acid, such as sulfonation, chlorination, nitration etc. are omitted and ease of handling of the solid heteropoly acids is preferable compared to conventional liquid acids. Most recently, POMs and their corresponding acids have proven pronounced acid- and oxidation catalysts for the selective conversions of a range of organic compounds, see Figure 5.5..[309,318,323,338–340,358,367,369,372,380,387–392]

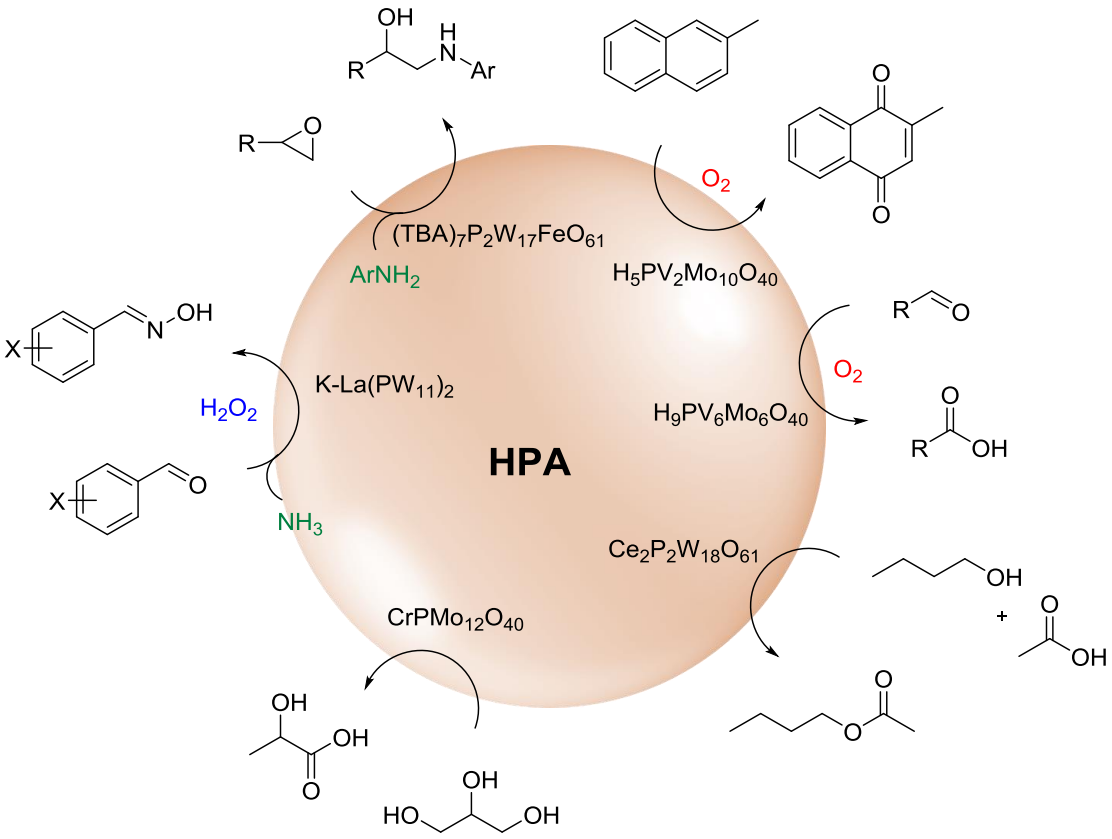

Figure 5.5: Selected HPA-catalyzed transformations.[323,340,390–392]

5.1.2.1 Oxidation Reactions with Polyoxometalates

Various transition metal substituted POMs have proven feasible in liquid-phase oxidation catalysis, with molecular oxygen, hydrogen peroxide or alkylperoxides as oxidant. Multicomponent POMs are generally considered strong oxidation-resistant inorganic metalloporphyrin analogues, functioning as efficient oxidation catalysts with a high turnover frequency (TOF).[372,387,393] The specific redox properties can be tuned by altering the elemental composition of the POM.[340] The fast reversible multi electron redox property of the POM at mild conditions have proven useful in a wide variety of oxidations including production of quinones, oxidation of double bonds, synthesis of methanol from methane, oxidation of alcohols to carboxylic acids, oxidative dehydrogenation of hydrocarbons and numerous other.[339,340,357,367,394–406] In the liquid phase, depending on the pH, different structures of the POM are present. Due to the various possible anions in liquid-phase oxidations, little is known about the exact mechanism of oxidation, however a more general two-step redox mechanism was proposed for oxidation with POM catalysts, depicted in Figure 5.6.[318,340] Proposed exchangeability of the outer oxygens of the POM structure with the environment, based on ^{17}O NMR experiments, indicated that the oxygens of the MO_6 unit actively participate in the oxidation mechanism.[407–409]

Application of POMs for hydrogenations have been reported the last twenty years.[410–414] The POMs have been used either directly as a hydrogenation catalyst[412,413] or as a scaffold for transfer hydrogenation catalysts on benzophenones and alkanals.[410,411]

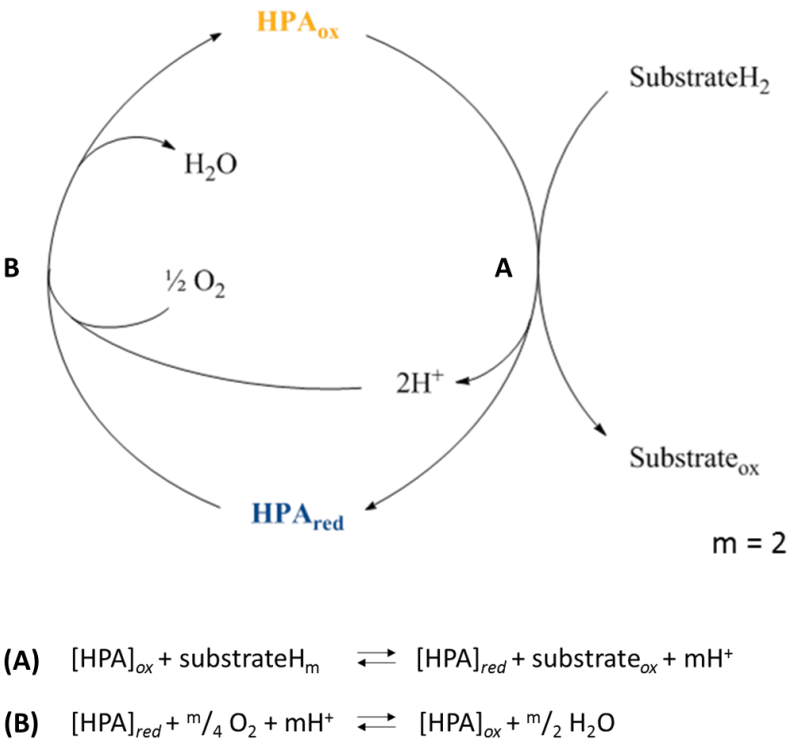

(A) $[HPA]_{ox} + substrateH_m \rightleftharpoons [HPA]_{red} + substrate_{ox} + mH^+$

(B) $[HPA]_{red} + {}^m/_4\, O_2 + mH^+ \rightleftharpoons [HPA]_{ox} + {}^m/_2\, H_2O$

Figure 5.6: Two-step redox mechanism for oxidation over POMs with example of m=2.

5.1.2.2 Industrial Processes

The plethora of POMs are relatively low-priced to produce, however, the more specialized POMs, the higher cost of production. The low-cost production combined with the above-mentioned properties make up a good foundation for using POM catalysts in industrial processes. Especially in acid catalysis, where the POM catalyzed processes often provide the more efficient and cleaner reaction than the conventional mineral acids.[369,372] In 1972, Soda initiated production of propane-2-ol by hydration of propene using an HPA catalyst, thus decreasing the corrosivity and volatility compared to the conventional process with sulfuric acid.[415] Hydration of *iso*butene to *t*-butanol with high concentrations of HPA was first produced in 1984 by Asahi Chemical.[367] Large scale production of polytetramethylene glycol (PTMG) from polymerization of tetrahydrofuran (THF) was published by Aoshima *et al.* in 1990.[366] Other examples include oxidation of methacrolein to methacrylic acid, esterification, acylation of alkylaromatics and oxidation of ethylene to acetaldehyde (Scheme 5.1).[340,367,372,394,399,416]

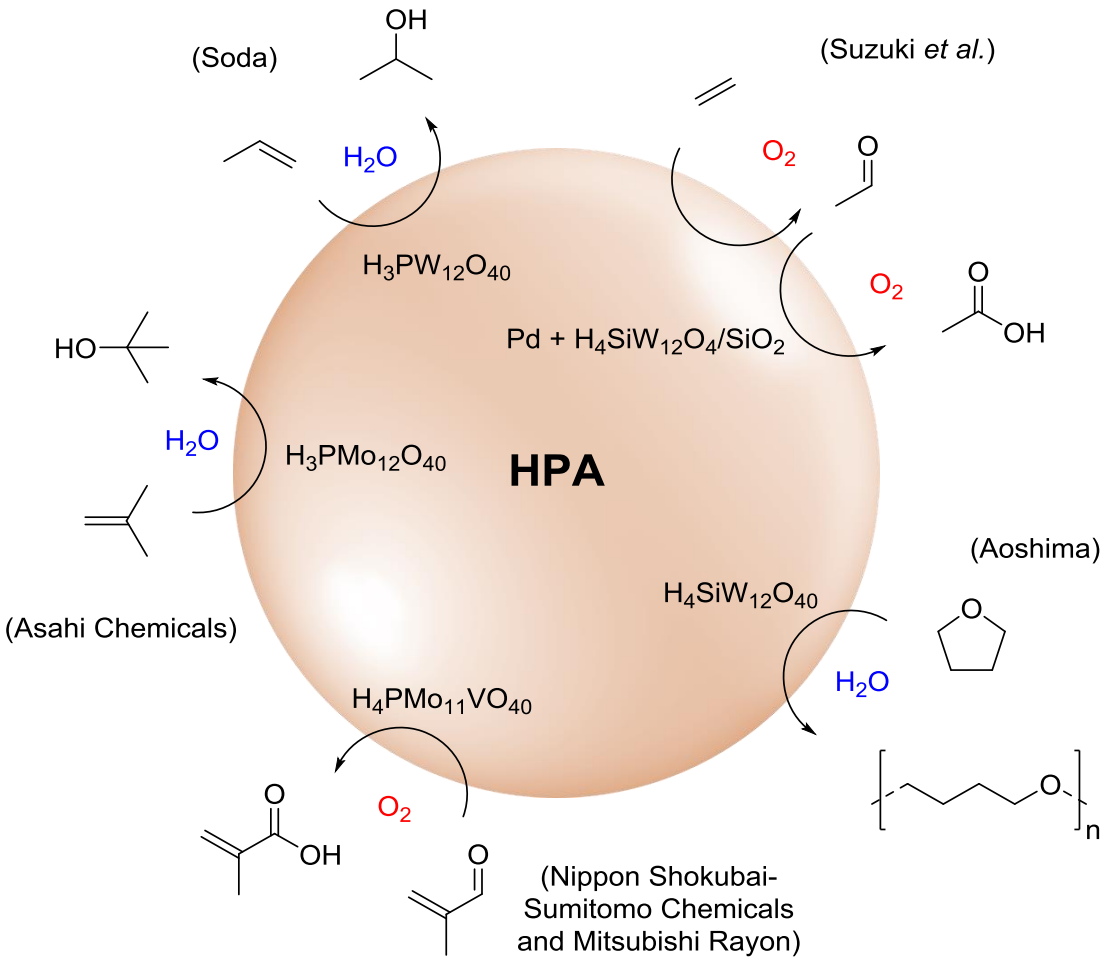

Scheme 5.1: Examples of industrial HPA-catalyzed transformations.[340,366,367,372,394,399,415,416]

5.1.2.3 Catalysis with Biomass

With the increasing demand for energy due to increasing consumption, new or improved methods of production and transportation of energy are of high demand. Renewable resources, such as biomass, wind, hydroelectric, geothermal etc., are of great importance for the future power generation.[46,417] Hydrogen fuel cells have proven useful in energy conversion, thus safe hydrogen storage and easy release of hydrogen is of great importance. Formic acid (FA) has proven a convenient and sustainable material for hydrogen storage and release.[418–421] Several methods of production of FA have been developed, however, one of the most successful approaches is based on conversion of almost any kind of biomass using a Keggin POM as catalyst, the so-called OxFA

process, see Figure 5.7. [61,67,100–102,417,422–429] Substitution of 1-5 addenda atoms with vanadium into the phosphor-molybdo-based Keggin HPA afforded excellent oxidation properties at relatively mild conditions in an aqueous media. Even water-insoluble biomass was converted to FA and CO_2.[100] In 1996, Weinstock *et al.* reported an environmental benign technology for converting wood pulp into paper using POM catalysis.[120] Both lignin- and cellulosic-based biomass have successfully been converted into value-added products, including vanillin and methyl vanillate, FA and acetic acid, respectively.[59,101,382,430]

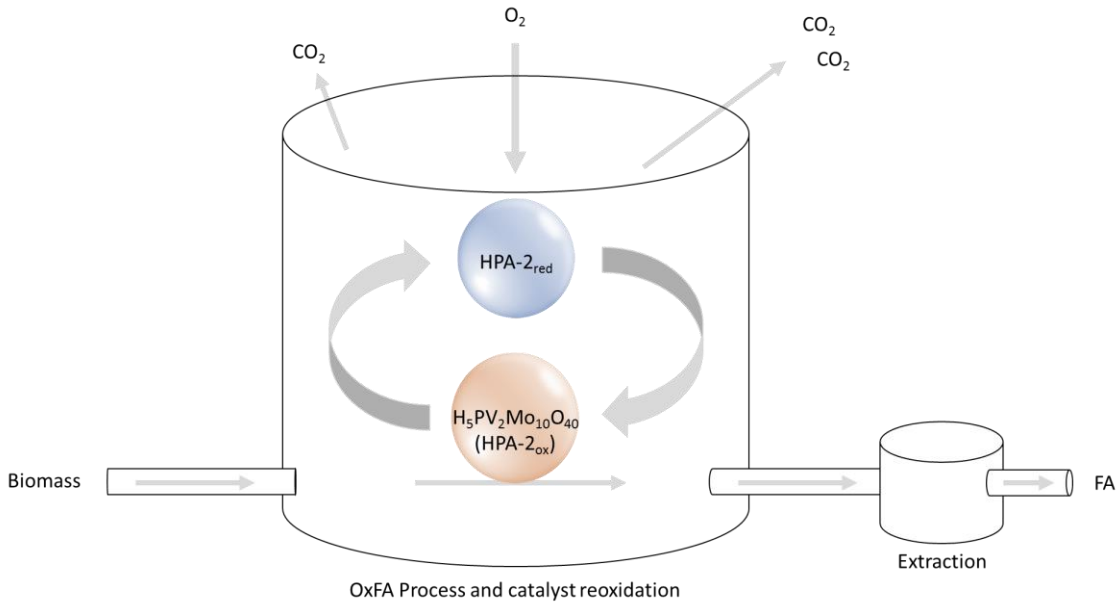

Figure 5.7: OxFA process. Adapted from[432]

5.1.3 Other Applications of Polyoxometalates

The earliest application of POMs exploited the special abilities, such as high molecular weight, electrochemical activity, ability to form colored species when reduced and the many possible variation of elements constructing the framework including the possibility for substitution of one or more of these framework elements.

Determination of P and Si by gravimetric analysis with reduced HPAs was among the earliest and most widely used applications, utilizing the high molecular weight.[433,434] Other applications, including identification of pharmaceuticals, exploit the ability to coagulate proteins and coordinate to organic molecules causing precipitation.[435–439] Highly selective labelling for electron microscopy has been developed using organo-functionalized POMs as imaging agents.[440,441] More recently, antitumor, -viral and –retroviral application of POM-based agents have been proven active.[442–456] The size and shape, electron transfer and coordinating ability and the stability of the POMs make for a wide variety of use in the medicinal industry. The unique electronic properties of POMs have proven useful in electrochromic, ion-selective electrodes and in cation-exchange materials used for radioactive solutions, affording increased stability compared to conventional organic resins. [457–459] The solid acids of POMs are promising solid electrolytes for fuel cells, protonic conductors and even proton-conducting films have been described.[460–465] Many applications have been establish for numerous different POMs and new applications are still being found following the discovery of new variations of POMs.

5.2 Wells-Dawson Polyoxometalate

Following the Keggin structure, the Wells-Dawson (WD) HPA is one of the most well studied POMs, with the general formula $X_2M_{18}^{n-}$ (Figure 5.8). The synthesis of the WD HPA was first reported by Kehrmann in 1892 and was later isolated by Wu in in 1920.[466,467] However, the existence of the X_2M_{18}-POM was not confirmed until 1947 by Wells.[468] The formula was later proved correct by the group of Figgis and Baker and in 1953, Dawson successfully acquired low-resolution X-ray data of the X_2M_{18}-HPA.[351,469–471] Today, this structure is termed Wells-Dawson, recognizing both Wells and Dawson for the elucidation. Strandberg and D'Amour later reported more accurately XRD data of the WD structure, now formulated $[X_2M_{18}O_{62}]^{n-}$.[472,473]

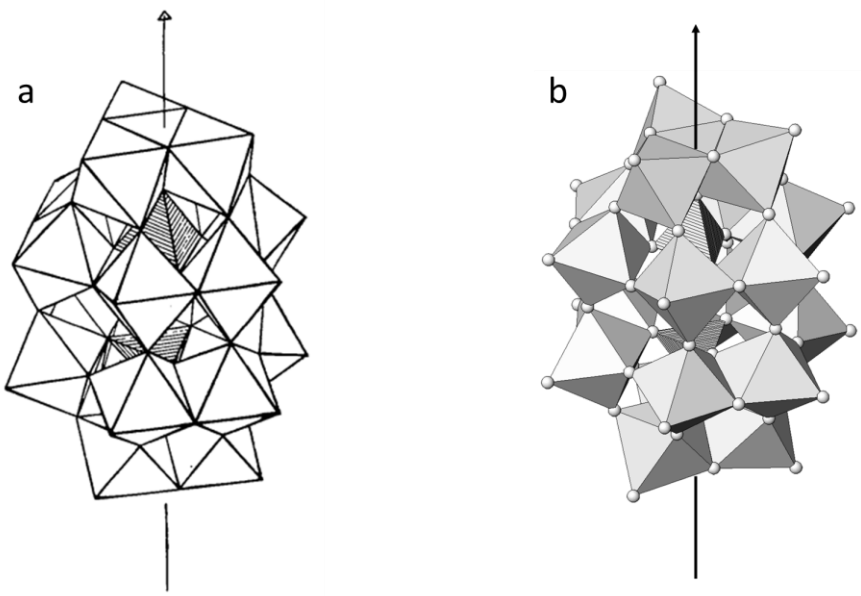

Figure 5.8: Structure of Wells-Dawson HPA. (a) Illustration by Wells in 1975[468] and (b) the recorded single crystal XRD of $P_2W_{18}O_{62}^{6-}$ presented in section 5.4.1.

5.2.1 Structural Details

The WD-POM is assembled from two lacunary Keggin POMs. Lacunary means gap or vacancy, hence, a lacunary Keggin POM is a POM of Keggin structure where one or more of the metal-oxide octahedra are absent, named mono-, di-, trilacunary etc., respectively.

The Keggin structure is one of the most well analyzed POM structures. There are five rotational isomers of the Keggin POM: α, β, γ, δ and ε as suggested by Baker and Figgis in 1970, illustrated in Figure 5.9.[471] The isomer recorded by Keggin was termed alpha, and the four remaining isomers were elucidated from the alpha structure by 60° rotations of the triads. A 60° rotation of one triad does not alter the linkage to the neighboring triads (corner-sharing linkage), however, this isomer is of different symmetry and is termed beta.[474] Disruption of the T_d symmetry slightly decreases the stability. 60° rotation of a second triad affords the gamma isomer where one corner-sharing linkage is replaced by an edge sharing. Three rotated triads yield three edge-sharing linkages in the delta isomer, and the echelon isomer is obtained from rotation of four rotated triads affording six edge-sharing linkages.[349,475] Edge-sharing linkage forces the metal atoms in the two adjacent octahedra closer together and destabilizes the structure by electrostatic repulsion, hence, the more edge-sharing linkages

between the triads, the less stable structure.[475,476] Since both the alpha and beta isomer entail pure corner shared triads, these are the most stable Keggin isomers and often the competing isomers observed during the synthesis of Keggin POMs.[475]

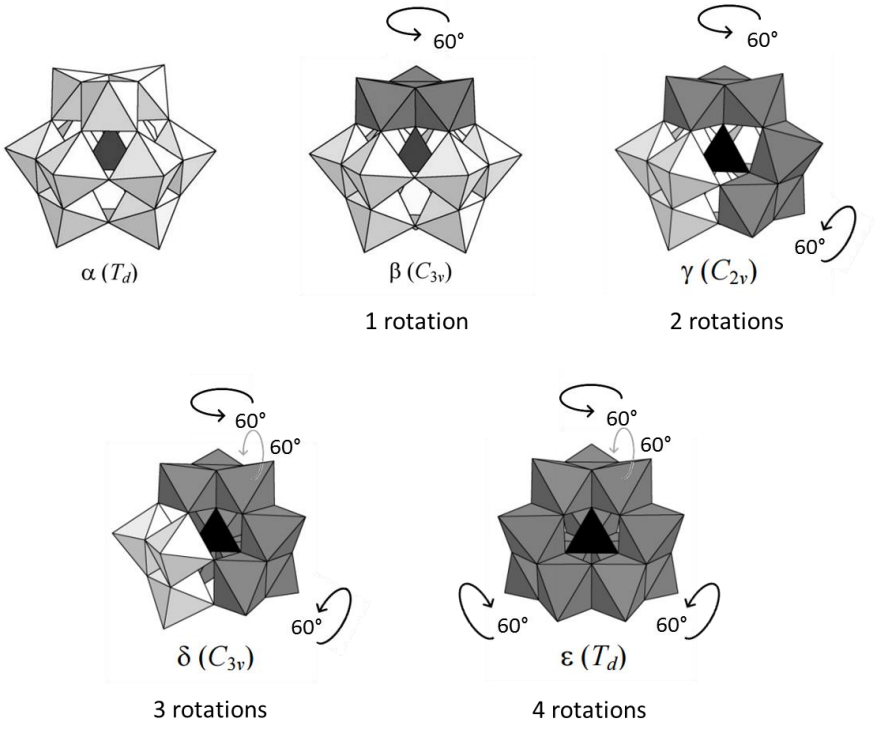

Figure 5.9. Rotational isomers of the Keggin HPA.[477]

In the lacunary Keggin structure composing the WD HPA (XM_9), the three bottom octahedra are absent leaving only one complete triad in the top (Figure 5.10a and b). One octahedra from each of the bottom three triads are vacant, leaving three edge-sharing dyads (to octahedra) linked together in a corner-sharing fashion (Figure 5.10b ring 1). This ring of dyads is termed the belt (ring 1), and the complete triad at the top the cap (ring 2) of the WD HPA. The trilacunary Keggin structure is linked to another trilacunary Keggin unit in a corner-sharing fashion affording the complete WD structure $[X_2M_{18}O_{62}]^{n-}$ (Figure 5.10c). No triads are formed or reformed during this linkage, due to strictly corner-sharing linkage between the two trilacunary Keggin structures.

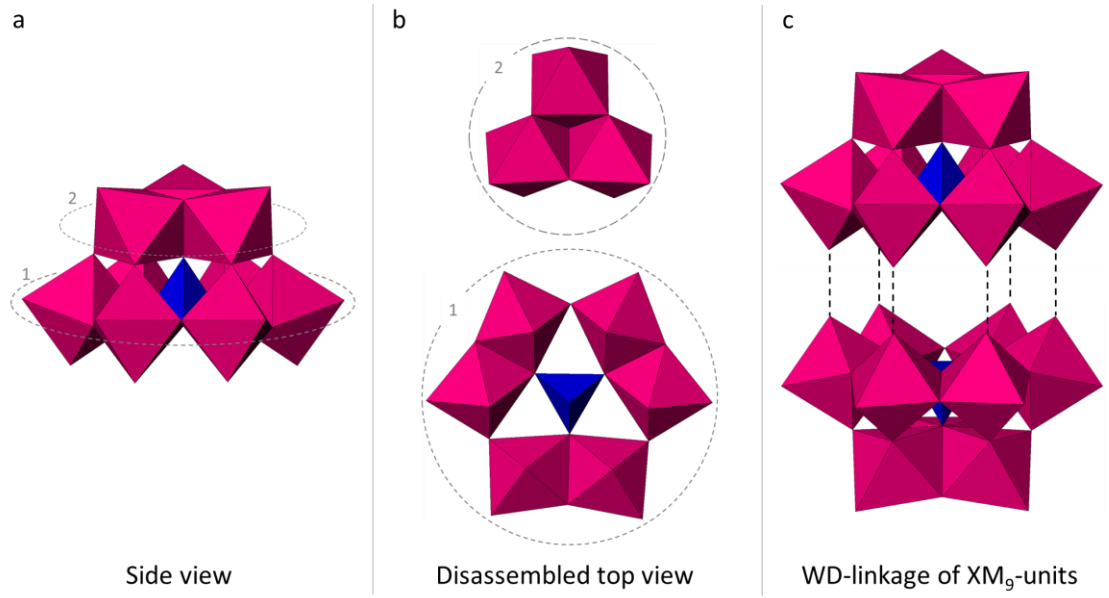

Figure 5.10: (a) XM_9-unit, (b) a top view of the disassembled XM_9-unit and (c) linkage of the two XM_9-units. MO_6 is illustrated in pink, XO_4 in blue. The structures are modified from recorded single crystal XRD of $P_2W_{18}O_{62}^{6-}$ presented in section 5.4.1.

Six rotational isomers of WD HPAs were proposed by Figgis and Baker in 1970, however, only four (α, β, γ, γ*) have been observed experimentally to this day (Table 5.1 and Figure 5.11).[471,478] The nomenclature for these isomers has changed overtime, however, the current formal names are applied in this dissertation.[351,466,471,474,475] The isomers are derived from α and β trilacunary Keggin units, affording three isomers composed of two α-units (α-WD), one α- and one β-unit (β-WD) and two β-units (γ-WD).[479] Three additional isomers are obtained from a 60° rotation of one of the trilacunary units, affording α*-, β*- and γ*-WDs. The rotation of one unit causes the relative belt position to shift, affording two edge-sharing octahedra from one unit to be placed on top of two corner-sharing octahedra from the second, altering the symmetry. Due to the above-mentioned symmetry arguments, α-WD was found to be the most stable isomer followed by β-WD.[351] These are often the competing isomers in the synthesis of WD HPAs.

The work presented in this dissertation focuses on the synthesis of the α-WD HPA, however, competing formation of the β-isomer was observed during the experiments (see section 5.3).

Table 5.1: Rotational isomers of the WD HPAs

Rotational isomers	Trilacunary unit 1	Trilacunary unit 2	Rotation of unit 2, relative to α-WD (°)
α	α	α	0
β	α	β	0
γ	β	β	0
α*	α	α	60
β*	α	β	60
γ*	β	β	60

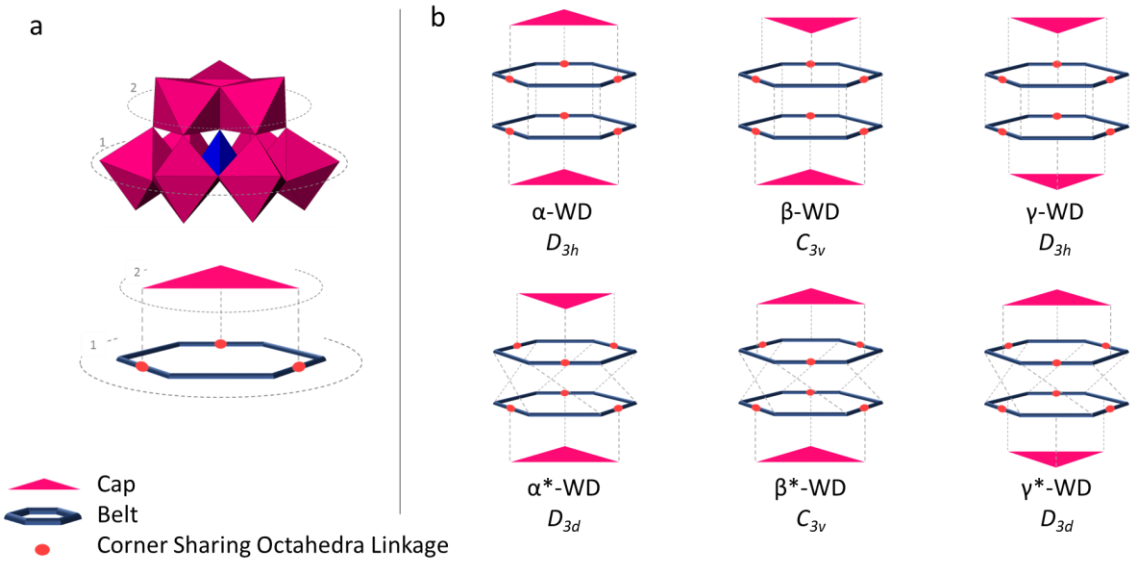

Figure 5.11: Illustrations of the rotational isomers of the WD POM. (a) Schematic representation and (b) schematic illustrations of the rotational isomer.[480]

Lacunary WD HPAs are obtained by increasing the pH of a solution of the WD HPA. Up to six addenda atoms can be removed from the WD HPA, generating a hexalacunary structure. The number of addenda atoms removed is controlled by the pH which differs slightly depending on the elements constructing the HPA.[481,482] The free oxygens of the lacunary specie can coordinate other

elements, such as transition metals, affording mixed addenda- or substituted WD HPAs. The lacunary- and substituted species are labelled according to the location of the lacuna or substituent, *e.g.* ring 1 (belt): $\alpha_1/\beta_1/\gamma_1$ and ring 2 (cap): $\alpha_2/\beta_2/\gamma_2$, respectively (Figure 5.12).[483,484] Substitution in both position 1 and 2 are described in literature,[485–498] however, more catalytic applications have been reported for the 2-lacunary structures, possibly due to the higher stability of the 2-lacunary specie.[481,490] In catalysis, lacunary HPAs have been suggested to act as π-acceptor ligands in the presence of 4d or 5d transition metal ions.[488,499]

With the numerous possible combinations of addenda- and heteroatoms, selective addenda atom substitution with various elements, dimeric linkage between metal-substituted species and bridged connections with organic linkers, a wide variety of different WD POMs have been reported, and novel structures are still being discovered. [315,316,350,464,500–504]

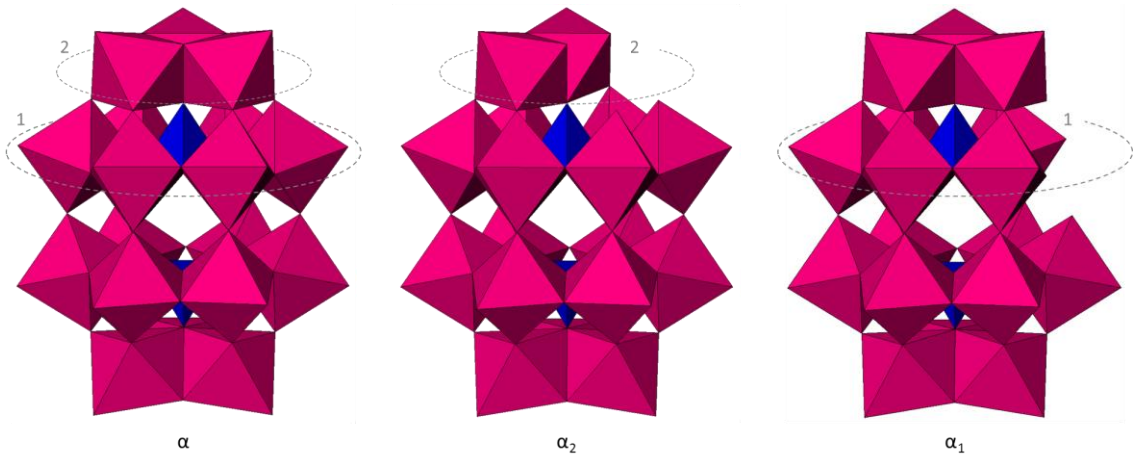

Figure 5.12: Illustration of α-, α_1- and α_2-WD. MO_6 is illustrated in pink, XO_4 in blue. The structures are modified from recorded single crystal XRD of $P_2W_{18}O_{62}^{6-}$ presented in section 5.4.1.

5.2.2 Considerations during Synthesis of Wells-Dawson Heteropoly Anions

The general protocol for synthesis of phosphor-tungstic HPAs entails acidification of an aqueous solution of tungsten- and phosphor precursors in the proper ratio, affording polymerization of WO_x. Depending on the applied conditions such as pH, time and temperature, different HPAs are formed. The synthesis is very pH-sensitive, and several phosphor-tungstic species are present at specific pH values (Table 5.2). The Keggin structure is formed selectively at pH 1, while the Dawson structure is formed around pH 4-6. The strategy for obtaining the isolated WD structure includes formation of a Keggin-like structure at pH 1, refluxing followed by dissolution at neutral pH and precipitation with the desired cation. The earlier WD synthesis, based on Wu's protocol – a two-step synthesis,[505] produced a mixture of the α and β isomers. Two additional steps were added to the synthesis by Droege to obtain isomeric pure α-$K_6P_2W_{18}O_{62}$.[482] In 2004, Nadjo *et al.* reported a two-step synthesis yielding close to isomeric pure α-WD in high yields.[506] The synthesis reported by Nadjo *et al.* was used for preparation of isomeric pure α-$K_6P_2W_{18}O_{62}$.

Lacunary species are synthesized by degradation of the $[P_2W_{18}O_{62}]^{6-}$ anion in a controlled basic media. High pH increase the number of lacuna and small differences in pH determine which lacunary specie is being formed (Table 5.2 and Figure 5.13).[481,482] Notably, the counter cation influences the solubility of the HPA. HPAs are soft ions and will interact strongest with other soft ions, hence, small and hard cations form the most water-soluble HPA salts. [339,507,508]

Table 5.2: Components formed certain pH-values. The table is adapted from Zhu *et al.*[509]

pH	Principal components
1.0	$[PW_{12}O_{40}]^{3-}$
2.2	$[PW_{12}O_{40}]^{3-}$, $[P_2W_{21}O_{71}]^{6-}$, $[PW_{11}O_{39}]^{7-}$
3.5	$[PW_{12}O_{40}]^{3-}$, $[P_2W_{21}O_{71}]^{6-}$, $[PW_{11}O_{39}]^{7-}$, $[P_2W_{19}O_{67}]^{10-}$, $[P_2W_{18}O_{62}]^{6-}$
5.4	$[P_2W_{18}O_{62}]^{6-}$, $[P_2W_{21}O_{71}]^{6-}$, $[PW_{11}O_{39}]^{7-}$
7.3	$[PW_9O_{34}]^{9-}$
8.3	$[PO_4]^{3-}$, $[WO_4]^{2-}$
8.4	$[P_2W_{17}O_{61}]^{10-}$
9.0	$[P_2W_{15}O_{56}]^{12-}$

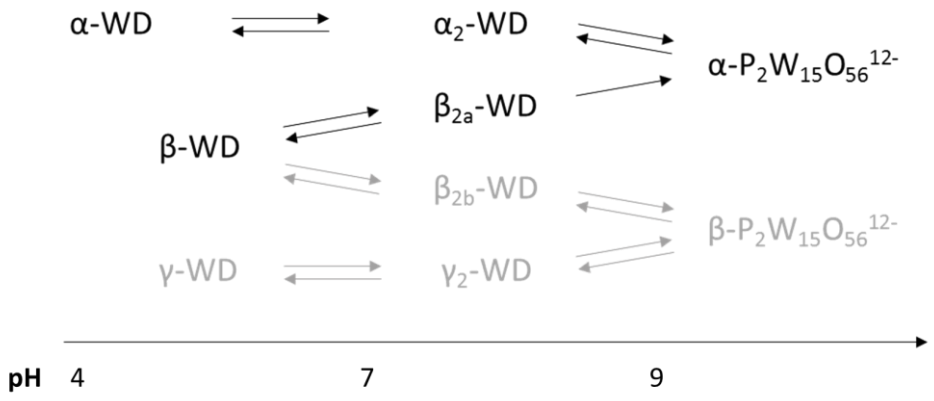

Figure 5.13: Overview of equilibria between the different WD isomers. Adapted from Thouvenot *et al.*.[510]

5.2.3 Catalysis with Wells-Dawson Based Structures

In addition to the aforementioned properties of HPAs, phospho-tungstic WD acids are remarkably stable in both solid-state and aqueous solutions, and even some organic solvents below pH 6.[362,511] WD-based HPAs have been reported to replace conventional acids in deprotection of phenols and methoxymethyl ethers, depyranylation of phenols and alcohols, acylation of *iso*-butylene with methanol and alkylation of *iso*-butane.[362,511–514] The redox properties of especially the phospho-tungstic WD POM has been utilized for oxidation of organic compounds, selected examples are presented in Figure 5.14. Other applications have been reported, including hydrogenation of cyclohexene and Michael addition of alcohols.[362,376–378,511–521]

In the solid state, the phospho-tungstic WD acids possess the same acid- and redox properties as in liquid-phase. This is exploited in gas-phase oxidations, such as oxidative dehydrogenation of *iso*-butane and *iso*-butyraldehyde, selective oxidation of methanol to formaldehyde and oxidation of propane and *iso*-butane to unsaturated carboxylic acids.[371,374,375,377,484,522–524] Conversion of cellulose to methyl levulinate (MLA) was achieved by Sun *et al.* applying the micellar WD-based assembly, $[C_{16}H_{33}N(CH_3)_3]_xH_{6-x}P_2W_{18}O_{62}$, as catalyst. The catalyst showed high activity, which was accredited to the synergistic effect of the strong acidic- and redox properties of the phosphor-tungstic WD POM.[525] Furthermore, clean gasoline from syngas was produced by Wang *et al.* using a phosphor-tungstic WD POM combined with the conventional Fischer-Tropsch catalyst (Co/Al_2O_3).[526]

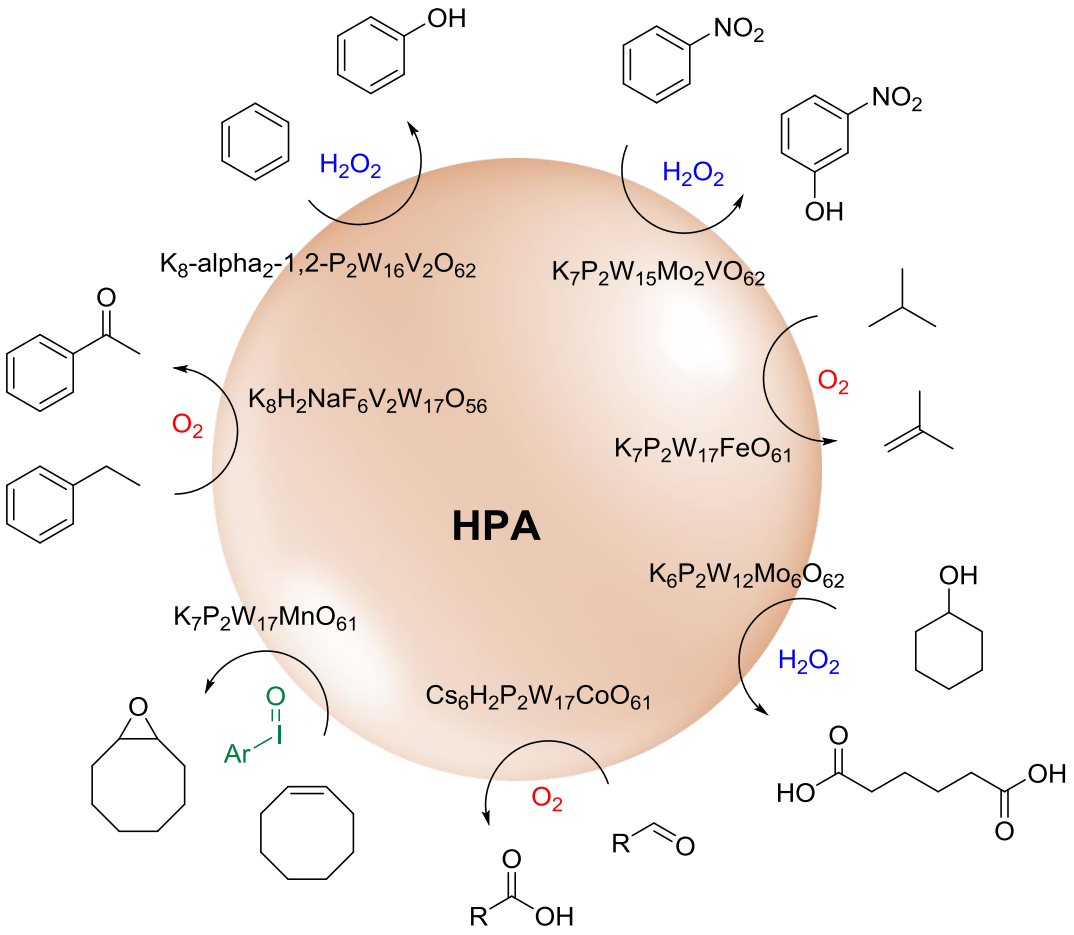

Figure 5.14: Selected oxidations with WD-based catalysts.[378,385,390,515,516,518,519,521]

Tuning of the chemical properties of WD HPA by substitution have been reported, preserving the remarkable redox properties and high thermal stability, affording promising replacements for metalloporphyrins in redox and electrochemical reactions.[379,507,527–529] Applications include olefin epoxidation and oxidation, aliphatic and aromatic hydroxylations, selective peptide hydrolysis and conductive polymers.[376,390,487,530–532]

The synthesis of different metal-substituted α_2-WD POMs is presented in this work.

5.3 Experimental Detail

5.3.1 Materials

All reagents were of reagent grade and were used without further purification: Sodium tungstate dihydrate ($Na_2WO_4 \cdot 2H_2O$, ≥ 99.0 % purity), hydrochloric acid (HCl, 37 wt%), phosphoric acid (H_3PO_4, 85 wt%), potassium chloride (KCl, ≥ 99.0 % purity), potassium hydrogencarbonate ($KHCO_3$, ≥ 99.5 % purity), nickel(II) chloride ($NiCl_2$, 98% purity), copper(II) chloride ($CuCl_2$, 97% purity), cobalt(II) chloride hexahydrate ($CoCl_2 \cdot 6H_2O$, ≥97% purity), zinc(II) chloride ($ZnCl_2$, ≥99% purity), vanadium(IV) oxide sulfate hydrate ($VOSO_4 \cdot xH_2O$, 97% purity), ruthenium(III) chloride hydrate ($RuCl_3 \cdot xH_2O$, 40-49% ruthenium content), tris(2,2'-bipyridyl)dichlororuthenium(II) hexahydrate ($Ru(Bpy)_3Cl_2 \cdot 6H_2O$, 99.95% purity), palladium(II) chloride ($PdCl_2$, 99% purity), iron(III) chloride ($FeCl_3$, ≥99.99% purity), manganese(II) acetate tetrahydrate ($Mn(ac)_3 \cdot 4H_2O$, ≥99% purity), HPA-5 synthesized by previous members of the group of Prof. Wasserscheid, platinum(II) chloride ($PtCl_2$, 98% purity), vanadium(V) oxide ($V2O_5$, ≥98% purity), 1,3-propanediol (99.0 % purity), 1,4-butanediol (99.0 % purity), 1,6-hexanediol (97.0 % purity), sucrose (99.0 % purity) and millipore water.

5.3.2 Synthesis of Metal-substituted Wells-Dawson Polyoxometalate

The substituted WD POMs were synthesized in a three-step procedure, illustrated in Figure 5.15. In the first step, pure α-phospho-tungstic-WD (α-WD) HPA was formed and precipitated with potassium. The monolacunary α_2-phospho-tungstic-WD (α_2-WD) structure was synthesized in the second step and the lacuna was substituted with a hetero addenda metal (M) in the third step (M-WD).

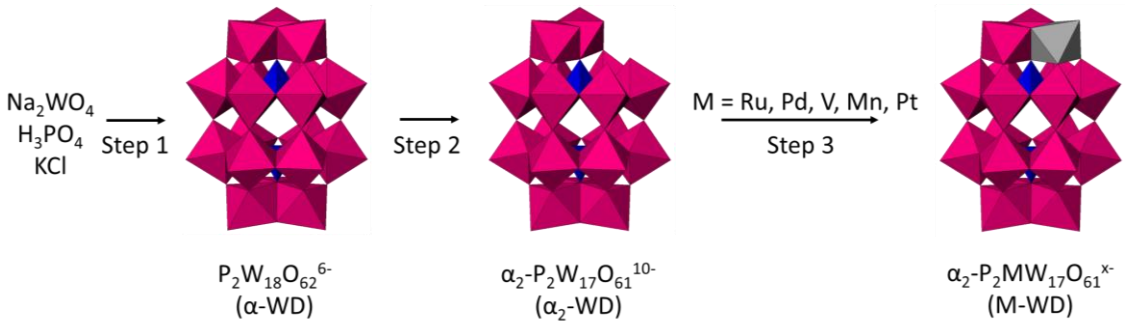

Figure 5.15: Overview of synthesis of substituted Wells-Dawson polyoxometalate. WO_6 is illustrated in pink, PO_4 in blue. The structures are modified from recorded single crystal XRD of $P_2W_{18}O_{62}^{6-}$ presented in section 5.4.1.

5.3.2.1 Synthesis of α-$K_6P_2W_{18}O_{62}$ (Step 1)

Isomeric pure α-phospho-tungsic WD HPA (α-WD) was synthesized according to literature procedure by Nadjo *et al.* and modified by Graham and Finke.[506,533] Deionized water was replaced by millipore water in the described synthesis.

5.3.2.2 Synthesis of α_2-$K_{10}P_2W_{17}O_{61}$ (Step 2)

The isomeric pure α_2-phosphor-tungsic WD HPA (α_2-WD) was synthesized according to literature procedure by Finke *et al.*.[528,534–536] Deionized water was replaced by millipore water in the described synthesis.

5.3.2.3 General Method for Metal Incorporation (Step 3)

The incorporation step was inspired by various published protocols: α_2-$K_{10}P_2W_{17}0_{61}$ (4.5544 g, 1.0 mmol) was dissolved in approx. 15 mL of 90 °C hot water. The metal precursor (1.1 eq., 1.1 mmol) was dissolved in water (20 mL) at room temperature and added dropwise to the dissolved POM under vigorous stirring. The reaction was left 1 h at 90 °C. KCl (3.7274 g, 50.0 mmol) was added and the reaction solution was allowed to cool to room temperature while stirring

for 1h. The precipitate was filtered and wash with cold millipore water followed by recrystallization in boiling water to give α_2-$K_xP_2MW_{17}O_{61}$ (M-WD).[485,488,537–539]

5.3.2.4 General Method for Vanadium Incorporation with $H_9PV_{14}O_{42}$ (Step 3)

Incorporation of vanadium was inspired by vanadium incorporation of the Keggin structure, previously published by Wasserscheid and co-workers[100,540]: V_2O_5 (20.02 g, 110 mmol) was dissolved in 8 °C cold water under stirring. 30% H_2O_2 (150 mL) in water was added dropwise. The temperature did not exceed 9 °C during the addition. The dark red solution was allowed to warm slowly to 30-35 °C causing the release of O_2-gas and a color change to brown-orange (formation of $H_6V_{10}O_{28}$). When the gas release ceased, 25% H_3PO_4 in water (2.95 g, 7.6 mmol in water) was added forming the stable precursor $H_9PV_{14}O_{42}$.[540]

$K_{10}P_2W_{17}O_{61}$ (4.554 g, 1 mmol) was dissolved in 10 mL water and heated to reflux. 2.5 mL of the $H_9PV_{14}O_{42}$ solution was added. The reaction solution was left under reflux for 15 min. The rest of the $H_9PV_{14}O_{42}$ solution (8 mL – the total amount was 10.5 mL) was added slowly to the refluxing reaction solution. The reaction solution was left under reflux overnight. The solution was concentrated and filtrated. The filtrate appeared as a brown and yellow oil-like liquid. KCl (10 g, mmol) was added to form a brown/yellow precipitate. The solution was allowed to precipitate for 3h. The precipitate was filtered off and dried under vacuum for 3h to give the dry α_2-$K_7P_2W_{17}O_{61}V(OH_2)$.[539] The filtrate was collected and concentrated on a rotatory evaporator. The obtained the yellowish-brown solid was recrystallized in boiling water. The precipitate was collected on a glass frit.

5.3.2.5 General Method for Vanadium Incorporation with Na_3VO_4 (Step 3)

The V-WD was synthesized according to literature procedure by Abessi *et al.*.[539] However, sodium-meta-vanadate was replaced by sodium-ortho-vanadate, and millipore water was used in place of deionized water.

5.3.2.6 Catalyst Characterization

The catalysts were characterized by thermogravimetric analysis (TGA) on a Mettler Toledo TGA/DSC 1 with an aluminum sample holder. The measurements were carried out with nitrogen as carrier gas, with a heating rate of 5 K/min up to 240 °C for 1h. ^{31}P-NMR and ^{51}V-NMR (JOEL ECX-400 instrument at FAU and Bruker BioSpin GmbH with a reference of H_3PO_4 at DTU, see Appendix D) was recorded at 162 and 105 MHz, respectively, and ATR-FTIR, powder and single crystal XRD, XRF, ICP and SEM were recorded as described Section in 2.1.

5.3.3 Standard Screening Procedure for Oxidation of Diols

The diol (5.0 g, 50 wt%), metal salt (0.01 eq. towards the diol) and millipore water (5.0 g) was added to a 20 mL high pressure vessel. A magnetic stirring bar was added and the vessel was sealed, flushed with molecular oxygen and pressurized to 20 bar. The reaction was left stirring at 500 rpm for 7 h at 80 °C. The liquid-phase was analyzed by crude ^{1}H- and ^{13}C-NMR (JOEL ECX-400 instrument, at 400 and 100 MHz). The gas-phase was not analyzed in the screenings.

5.3.4 OxBox – Standard Procedure for Oxidation of Sucrose

Sucrose (8.6 – 34.2 g, 25 – 100 mmol), WD-catalyst (1.0 mmol) and water (100.0 g) was added to a 600 mL high pressure vessel. The vessel was sealed in the OxBox system, flushed with molecular oxygen and pressurized to 20 bar. The reaction was left stirring at 1000 rpm for 6 h at 90 – 140 °C. The liquid-phase was analyzed by crude ^{1}H- and ^{13}C-NMR (JOEL ECX-400 instrument, at 400 and 100 MHz) with benzene-inlets containing a mixture benzene:benzene-d_6 of 1:12. These were calibrated with solutions of 1, 3, 5, 10 and 15 wt% of FA in D_2O.The gas-phase was analyzed by GC-TCD (Varian GC 450 with the column Shin-Carbon-ST, 2 m x 0,75 mm inner diameter) according to calibration curves of CO and CO_2. The calibrations and analysis of NMR as well as GC-TCD data, was performed by Ph.D. student Dorothea Voss.

5.4 Results and Discussion

Six different WD catalysts were synthesized and tested for oxidation of 1,3-propanediol, 1,4-butanediol, 1,6-hexanediol and sucrose. An overview of catalysts and the abbreviation used in this dissertation is depicted in Table 5.3. A clear color change was observed after substation of metals into the WD framework (Figure 5.16). The Pt-WD catalysts was synthesized for testing of glycerol hydrogenation (ongoing collaborative project with the group of Prof. Wasserscheid at FAU, Erlangen, Germany). The metals for substitution were selected based on availability and catalytic activity from screening experiments.

Table 5.3: Overview of synthesized catalysts and abbreviations thereof.

Entry	Catalyst	Abbreviation	Oxidation state of M[a]
1	α-$K_6P_2W_{18}O_{62}$	α-WD	-
2	α_2-$K_{10}P_2W_{17}O_{61}$	α_2-WD	-
3	α_2-$K_7P_2W_{17}O_{61}$**Ru**(OH_2)	Ru-WD	+III (p)
4	α_2-$K_8P_2W_{17}O_{61}$**Pd**(OH_2)	Pd-WD	+II (d)
5	α_2-$K_7P_2W_{17}O_{61}$**V**(OH_2)	V-WD	+III (p)
6	α_2-$K_8P_2W_{17}O_{61}$**Mn**(OH_2)	Mn-WD	+II (p)
7	α_2-$K_8P_2W_{17}O_{61}$**Pt**(OH_2)	Pt-WD	+II (d)

[a]Magnetic properties in parentheses, p = paramagnetic, d = diamagnetic

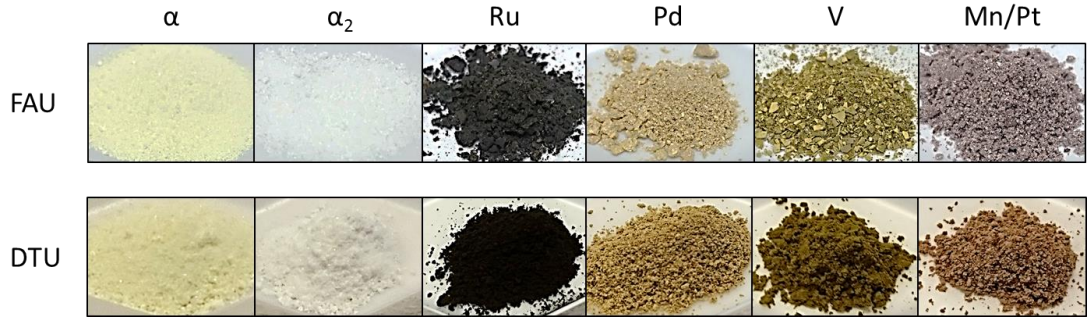

Figure 5.16: Images of the prepared WD catalysts.

5.4.1 Catalyst Characterization

An overview of the prepared catalysts together with the water content is presented in Table 5.4.

Table 5.4: Overview of HPA-catalysts

Entry	Catalyst	Water content (mol%)[a]	
		FAU	DTU
1	α-WD	9	8
2	α_2-WD	11	16
3	Ru-WD	6	9
4	Pd-WD	7	8
5	V-WD	12	9
6	Mn-WD	9	-
7	Pt-WD	-	11

[a] Determined by TGA measurements

5.4.1.1 ^{31}P-NMR

^{31}P-NMR was recorded for all the synthesized catalysts and compared to data found in literature (**Figure 5.17**, for full spectra see Appendix D). An overview of literature references is presented in Table 5.5. The recorded spectra for the α- and α_2-WD were comparable with data found in literature (Table 5.5, Entries 1 and 4). Notably, formation of β-isomer was observed in the α-WD prepared at DTU, and four recrystallizations were required to obtain an adequate α/β ratio (Figure 5.18). In contrast, isomeric pure α-WD was obtained following the procedure described in Section 5.3.2 at FAU. The synthesis of α-WD is very pH sensitive and minor changes of pH can cause isomerization of α- to β-isomer. It is crucial to keep the pH below 2 after addition of HCl during the synthesis. However, the pH was kept below 2 during each experiment, indicating that isomerization was not due to changes in pH. Secondly, each chemical used for the synthesis was exchanged one at the time, with newly acquired chemicals in order to evaluate if this effected the synthesis. However, formation of the β-isomer was also observed with the newly acquired chemicals. Alternatively, three extra recrystallizations were performed (Figure 5.18). It is known from literature, that isomerization of α-WD to β-WD can take place at elevated temperatures.[482] The followed procedure includes refluxing, however, identical procedures were

followed at both universities implying that the refluxing did not cause the isomerization.

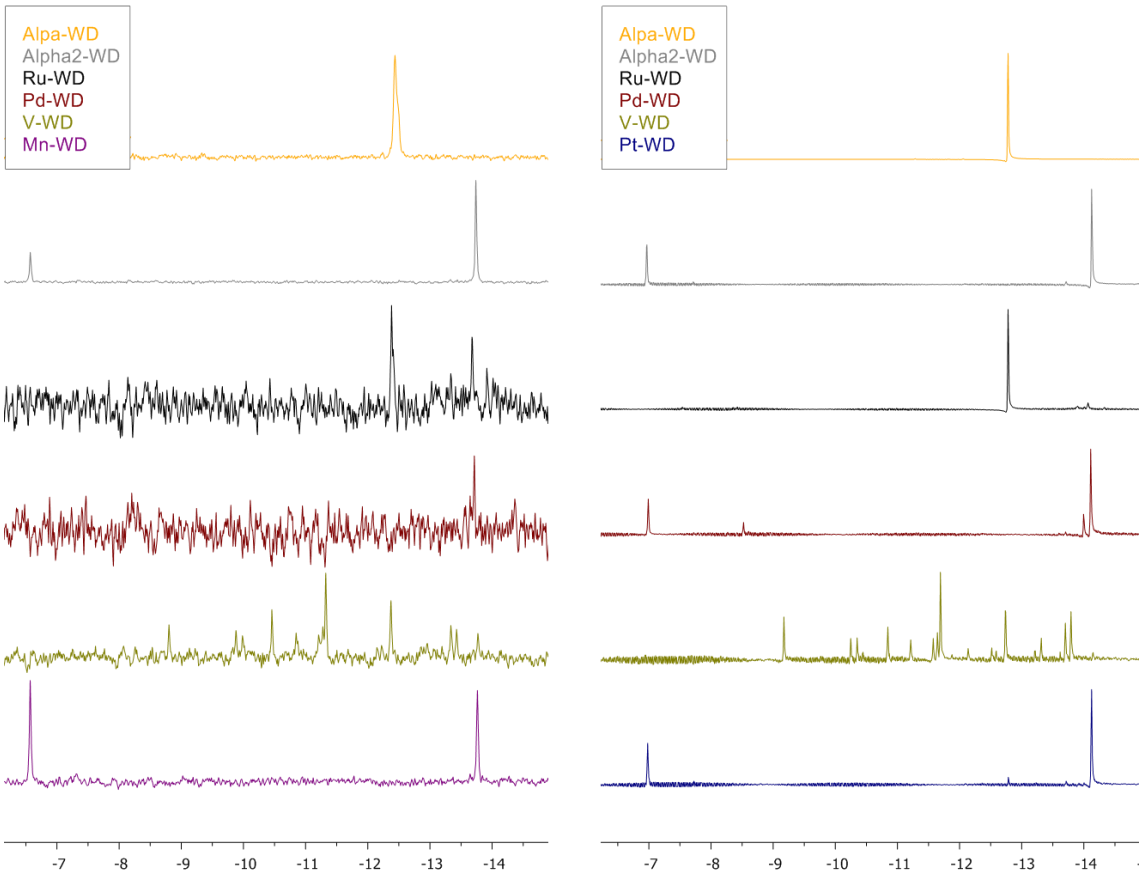

Figure 5.17: ^{31}P-NMR of the synthesized WD catalysts, FAU (left) and DTU (right).

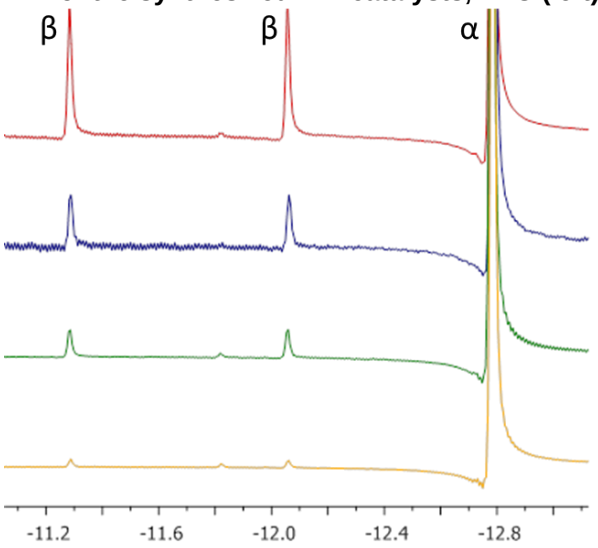

Figure 5.18: Decreasing β-isomer, followed by ^{31}P-NMR (-11.15 and -12.07 ppm).

Table 5.5: Overview of ^{31}P-NMR reported in literature.

Entry	Compound	^{31}P NMR		Reference
		P(1)	P(2)	
1	α-WD	-12.4	-	a
2	β-WD	-11.0	-11.7	b
3	γ-WD	-10.8	-	c
4	α_2-WD	-6.8	-13.6	a
5	α_1-WD	-8.5	-12.8	a
6	$P_2W_{15}O_{56}^{12-}$	+0.1	-13.3	b
7	Ru-WD	-	-12.1	f
8	Pd-WD	-	-11.9	f
9	[*syn*-$Pd_2(\alpha_2$-$P_2W_{17}O_{61}H_3)_2]^{10-}$	-8.2	-13.7	g
10	[*anti*-$Pd_2(\alpha_2$-$P_2W_{17}O_{61}H_{0.5})_2]^{15-}$	-8.1	-13.6	g
11	α_2-V-WD	-10.8	-12.9	a
12	α_2-V-WD	-11.4	-13.5	d
13	α_1-V-WD	-11.8	-12.9	a
14	α_1-V-WD	-12.3	-13.4	d
15	$PV_{14}O_{42}^{9-}$	+1	-	d
16	1,2-$P_2V_2W_{16}O_{62}^{8-}$	-8.8	-13.4	e
17	1,2-$P_2V_2W_{16}O_{62}^{8-}$	-9.3	-13.9	f
18	Mn-WD	+564	-12.3	h

References: (a) Contant *et al.* 2004[541] (b) Contant *et al.* 1990[535] (c) Fedotov *et al.*[407] (d) Harmalker *et al.*[542] (e) Abessi *et al.*[539] (f) Liu *et al.*[537] and (g) Izarova *et al.*[543] (h) Lyon *et al.* [528]

Small impurities in the spectrum for α_2-WD synthesized at DTU was observed, possibly due to the above-mentioned β-isomer impurity (-7.72 and -13.71 ppm). Similar to the peaks for α_2-WD, a difference in peak intensity was observed for the impurity, indicating formation of an asymmetric WD-specie. The poor stability of the α_1-WD (α_1-$K_{10}P_2W_{17}O_{61}$) under the applied conditions render the formation of α_1-WD unlikely, and moreover, the peaks are not comparable with the literature (Table 5.5, Entry 5). The trilacunary anion, $P_2W_{15}O_{56}^{12-}$, is formed at increased pH, however, the data was not comparable with literature (Table 5.2 and Table 5.5, Entry 6). In early synthesis procedures, the fast isomerization of β-isomer to

the monolacunary α_2-isomer under slightly alkaline conditions, was exploited to obtain isomeric pure α-WD, hence, formation of a lacunary β-isomer under the applied conditions is questionable.[482,533,544] The impurity did not decrease significantly with recrystallization from boiling water and was thus used as substrate for synthesis of the metal-substituted WD catalysts at DTU.

One major peak was observed for the Ru-substituted WD HPAs in accordance with literature (Table 5.5, Entry 7). Two additional peaks were observed for the Ru-WD synthesized at FAU (-4.91 and -13.68 ppm). The symmetry and intensity of the additional peaks indicate formation of an asymmetrical α_2-specie, however, the peaks did not compare with literature references. Notably, reformation of α-WD can occur at decreased pH (below 2), which was detected following addition of the acidic $RuCl_3$ solution.

Ru(III) is paramagnetic which can cause shift and broadening of the NMR peaks. Jorris *et al.* argue that the paramagnetic effect of the incorporated ruthenium broaden the P(1) peak into the background and only the peak furthest from Ru, P(2), is observable.[536] Furthermore, the nuclear quadrupole moments of ^{99}Ru and ^{101}Ru provide a mechanism for fast relaxation of P(1), resulting in one sharp peak for P(2) at -12.1 ppm.[537] In general, WDs containing paramagnetic metal ions with nondegenerate ground states afford broadened peaks of P(1).[536] However, incorporation of the diamagnetic Ru(II) affords two inequivalent peaks, similar to the pattern observed for α_2-WD, however, slightly shifted, similar to the two additional peaks observed for the FAU synthesized POM.[488]

Pd(II) is diamagnetic and incorporation in α_2-WD was expected to afford two inequivalent peaks. However, Liu *et al.* argue that the nuclear quadrupole moment of ^{105}Pd cause fast relaxation of the phosphor closest to Pd resulting in a broadened peak for P(1) and a sharp peak for P(2) at -11.9 ppm (Table 5.5, Entry 8).[537,545] Two sets of peaks were observed in the spectra for the DTU-synthesized Pd-WD. The major peaks are comparable with the α_2-WD, however the minor peaks at -8.52 and -14.00 ppm are comparable with peaks reported by Izarova *et al*. for dimeric species of Pd-WD, [*syn*-$Pd_2(\alpha_2\text{-}P_2W_{17}O_{61}H_3)_2]^{10-}$ and [*anti*-$Pd_2(\alpha_2\text{-}P_2W_{17}O_{61}H_{0.5})_2]^{15-}$, illustrated in Figure 5.19. The chemical shifts for the *anti*- and *syn* isomers are displaced by 0.1 ppm which complicate the distinction between these based on ^{31}PNMR (Entries 9 and 10). One peak was observed in the spectrum recorded at FAU in the region of the major α_2 peak, however, due to insufficient resolution the minor peak may not be observable.

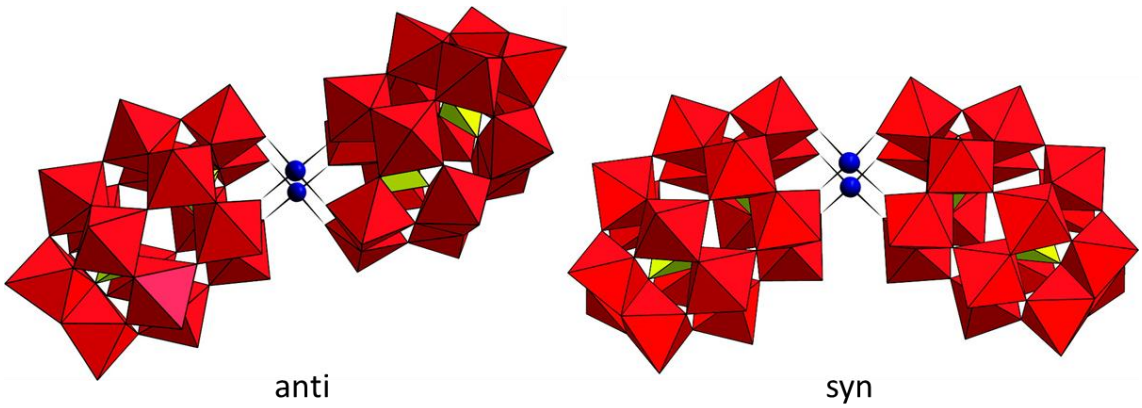

Figure 5.19: Dimeric Pd-WD POMs adapted from Izarova *et al.*[543]

Disregarding the difference in resolution, the spectra for the FAU- and DTU-synthesized V-WD POMs were found to be close to identical. The precursor, $H_9PV_{14}O_{42}$, was recognized as a peak at +1.0 and +1.85 ppm on the DTU and FAU spectra, repectively.[407,546] The prepared V-WD were of greenish brown color suggesting incorporation of a V(III) specie. V(III) is paramagnetic and taking the above-mentioned arguments into account, only the peak for P(2) was expected to be observable. However, data found in literature report observations of two peaks (Entries 11-17). The various observed peaks were all in the WD-HPA region, and the peaks comparable with literature are marked in Figure 5.20.

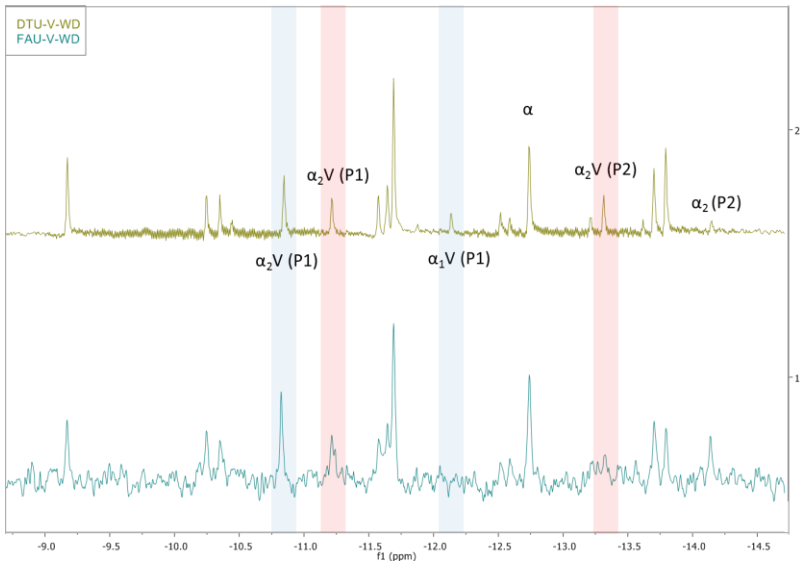

Figure 5.20: V-WD ^{31}P-NMR spectra. The boxes mark chemical shifts reported by Harmalker *et al*. (red)[542] and by Abessi *et al.* (blue)[539]

^{51}V-NMR spectra recorded for the V-WD POMs, however, various peaks were observed and a few were comparable with literature (See Appendix D).

Preparation of the V-WD, in a way similar to the procedure described in Section 0, was found to afford good selectivity for vanadium incorporation according to published literature (Figure 5.21 and Table 5.5, Entry 11-12). The incorporated vanadium originated from Na_3VO_4.[539]

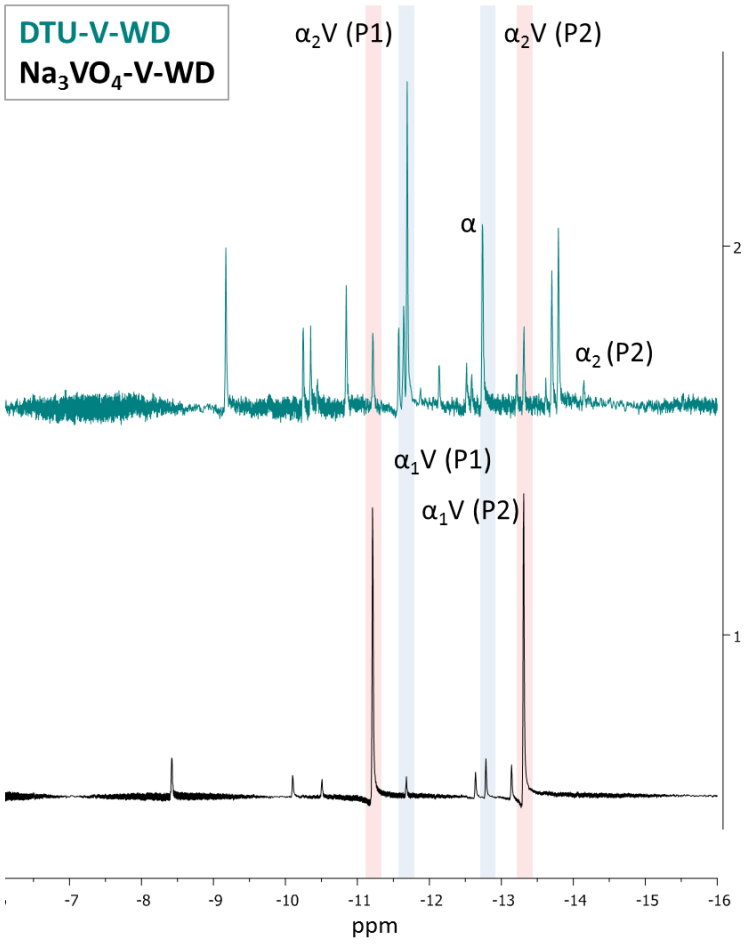

Figure 5.21: Comparison of V-WD prepared from $H_9PV_{14}O_{42}$ (blue) and Na_3VO_4 (black). α_2-V-WD is marked in red boxes, α_1-V-WD in blue boxes.

Mn(III) is paramagnetic and a radical downfield shift of the phosphor peak closest to the incorporated Mn (P1) is observable according to literature (Entry 18). The P2 phosphor-peak appears at -12.3 or -12.5 ppm which is within the region of the recorded spectrum, hence, only the P2 resonance was in the observable region.[528,536] However, peaks around the α_2-WD areas were observed (-6.57 and -13.76 ppm), insinuating unsuccessful incorporation of Mn.

Pt(II) is diamagnetic, and similar to the above-mentioned paramagnetic species, one peak for P2 was expected to be observed around -12 ppm. When zooming in on the -12 ppm area two small peaks appear at -12.1 and -12.4 ppm. One of these peaks could be assigned to the Pt-WD, however, the peaks are of very low intensity and no data of Pt-WD has been published for comparison. Based on ^{31}P-NMR, sufficient evidence of Pt incorporation was not observed.

5.4.1.2 Infrared Spectroscopy

For comparison of the P-O and W-O vibrational stretches, the synthesized WD-POMs were analyzed by ATR-FTIR (Figure 5.22). The P-O stretches are presented in the grey area and the W-O and W-O-W stretches in the yellow area. Bands in the characteristic WD regions were observed for all the substituted WD-catalysts. The spectra were comparable with the spectrum for α_2-WD, considering that small displacement of the bands due to substitution may occur.

The spectra recorded for α-WD and α_2-WD are similar to the data found in literature.[506,510,522,539,547] α-WD is characterized by a sharp band at 1087 cm^{-1}, a weak band at 1021 cm^{-1} and a shoulder at 996 cm^{-1} in the P-O region. In the W-O area, the terminal W-O band appear at 953 cm^{-1}, the “inter” (bridge between corner-sharing octahedra)- and the intra (bridge between edge-sharing octahedra) W-O-W stretches at 901 and 733 cm^{-1}, respectively. Three distinct bands appear in the P-O region for α_2-WD: 1079, 1047 and 1013 cm^{-1}. By removal of a tungsten from the framework, the symmetry is disrupted and alterations of the IR-bands are observed. Similarly in the W-O region, small displacements of the bands place the terminal W-O stretch at 933 cm^{-1}, the “inter” W-O-W at 875 cm^{-1} and the “intra” W-O-W at 714 cm^{-1}. It is known from literature, that substitution into the lacuna with a heteroatom may cause small displacements of these bands.[548,549]

In the spectra for the Ru- and Pd-WDs, comparable bands were observed in both regions, suggesting a preserved α_2-structure with alterations. The relative

intensities of the three distinct bands for α_2-WD in the P-O region (grey box) were increased for the Ru-WD. Comparison of ^{31}PNMR and IR data for the Ru-WD suggest, that the recorded IR spectrum is a combination of two WD-structures, an α- and an α_2-WD specie, both present in the sample. This clarifies the increased relative intensity between the large band (observed in both α and α_2) and the two smaller bands (only α_2) of the P-O region (grey box, Figure 5.22).

In the IR spectra of the vanadium and manganese substituted POMs, an extra shoulder on the sharp P-O band (1103 cm^{-1}) was observed, which suggest possible degradation of the framework or isomerization to α_1-WD. The shoulder-band is characteristic for the multilacunary WD-structures $P_2W_{15}O_{56}^{12-}$ and $P_2W_{12}O_{48}^{12-}$, however, the bands appear at higher frequencies compared to the observed shoulder (Table 5.6). The observed shoulder-band was comparable with literature reported for the α_1-WD, which is plausible due to potential isomerization of α_2 to α_1-WD at elevated temperatures (90 ^oC) and in the presence of a metallic anion, which affects the pH.[485,536]

The IR spectrum for the Pt-WD is nearly identical to the spectra for the α_2-WD. Possibly, Pt has not been substituted into the lacuna and is either coordinated to the structure similar to the potassium cations or did not interact with the WD-structure.

Table 5.6: ATR-FTIR data for α_1-WD, $P_2W_{15}O_{56}^{12-}$ and $P_2W_{12}O_{48}^{12-}$.

POM	P-O (Cm^{-1})	P-O (Cm^{-1})	P-O (Cm^{-1})
α_1-WD	1121	1084	1012
$P_2W_{15}O_{56}^{12-}$	1130	1075	1008
$P_2W_{12}O_{48}^{12-}$	1130	1075	1012

Reported by Contant *et al.*[535]

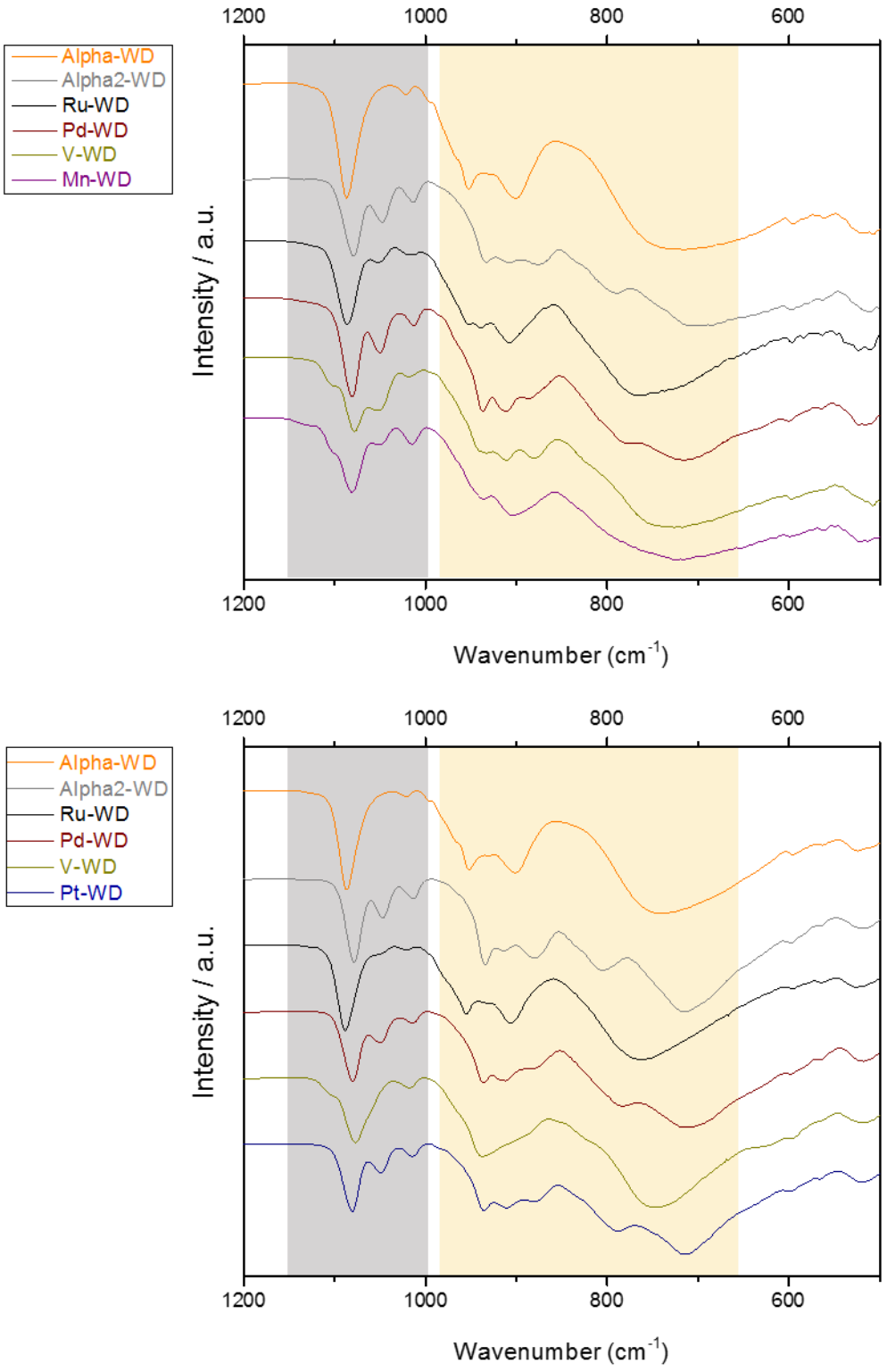

Figure 5.22: FTIR of WD-POMs, FAU (top) and DTU (bottom).

5.4.1.3 Single Crystal- and Powder X-Ray Diffraction

Single crystal XRD was obtained for the α-WD synthesized at FAU (Figure 5.23). Crystals in sufficient size were not obtainable of the α_2- and M-WD POMs. Alternatively, XRPD was recorded for these structures synthesized at DTU (Figure 5.24).

The single crystal data of the α-WD showed that the synthesized α-WD was of triclinic space group, comparable with published data (Table 5.7) and support the data obtained from ^{31}P-NMR and FTIR in the formation of the α-WD HPA.[351,550] A slightly decreased length of the c axis of the unit cell was observed compared to the standardized and data obtained by Dawson. Furthermore, variations in the angles of the unit cell were observed, however, the structure calculated from refinement of the single crystal XRD data revealed an α-isomer of the WD catalyst.

Table 5.7: Overview of single crystal XRD data

Crystal data	α-WD	α-WD (Dawson)[a]	Standardized structure[b]
Chemical formula	$K_6O_{72}P_2W_{18}$	$K_6O_{72}P_2W_{18}$	$K_6O_{72}P_2W_{18}$
Space group	Triclinic, *P*-1	Triclinic, *P*-1	Triclinic, *P*-1
a (Å)	12.7997 (3)	12.86 (12)	12.8600
b (Å)	14.8086 (3)	14.83 (15)	14.8300
c (Å)	18.6220 (5)	22.34 (22)	20.1187
α (°)	101.208 (2)	94.40 (33)	68.815
β (°)	96.832 (2)	116.87 (33)	82.106
γ (°)	115.140 (2)	115.60 (33)	64.400
V (Å^3)	3052.62 (15)	3225.59	3225.60

Standard deviations are presented in parentheses. [a] Dawson 1953[351], [b] ICSD – Inorganic Crystal Structure Database[551]

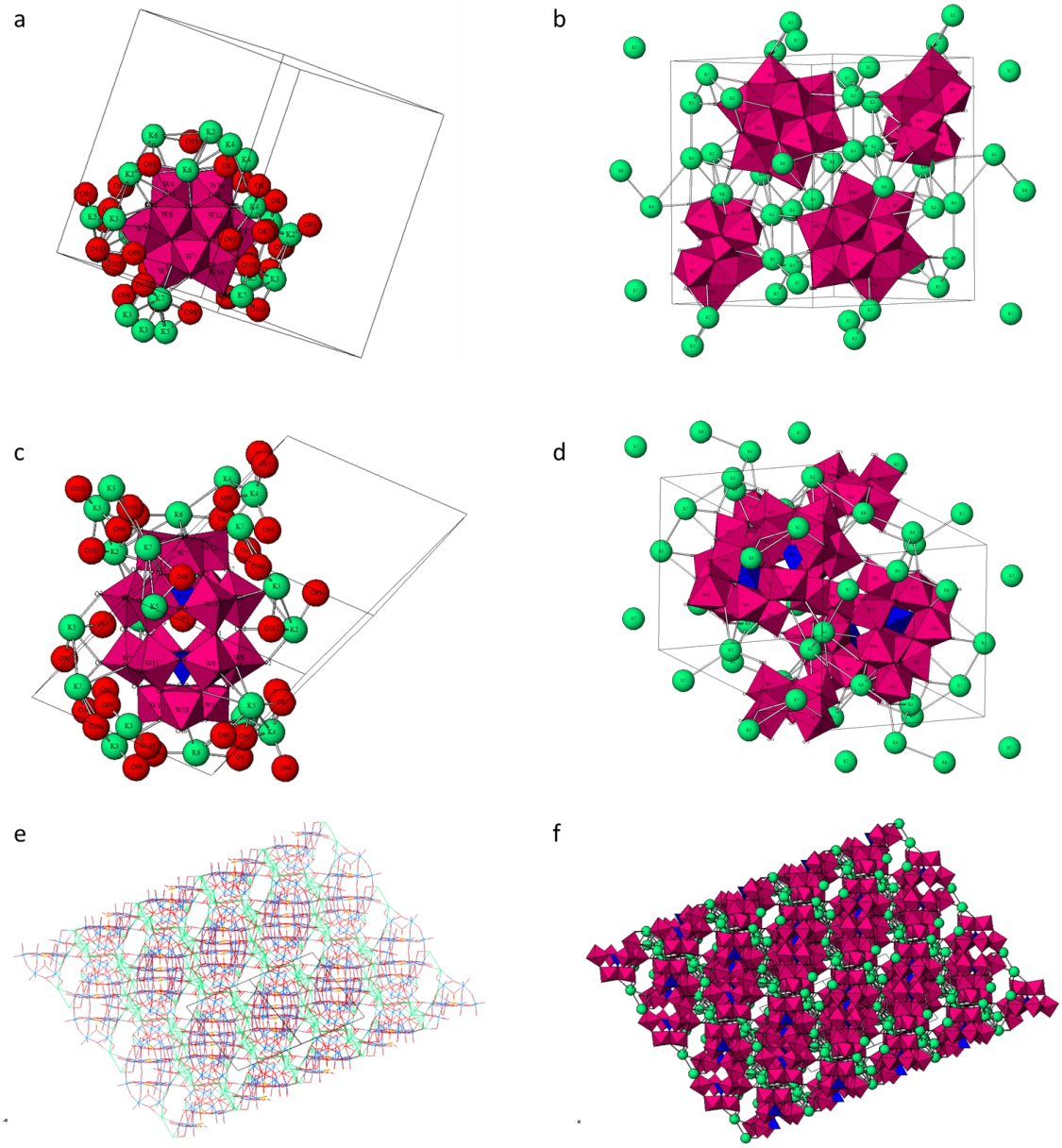

Figure 5.23: Single Crystal X-ray Diffraction of α-WD. (a) top view, (b) top view of full unit cell, (c) side view, (d) top view of full unit cell, (e) skeleton representation of crystal structure and (f) polyhedral representation of crystal structure. Oxygen (red), potassium (green), WO_6 octahedra (pink) and PO_4 tetrahedra (blue).

From the obtained diffractograms presented in Figure 5.24 below, it was found, that peaks in the α- and α_2-regions were observed in the substituted catalysts. The diffractogram of α-WD was comparable with data found in literature.[522,552]

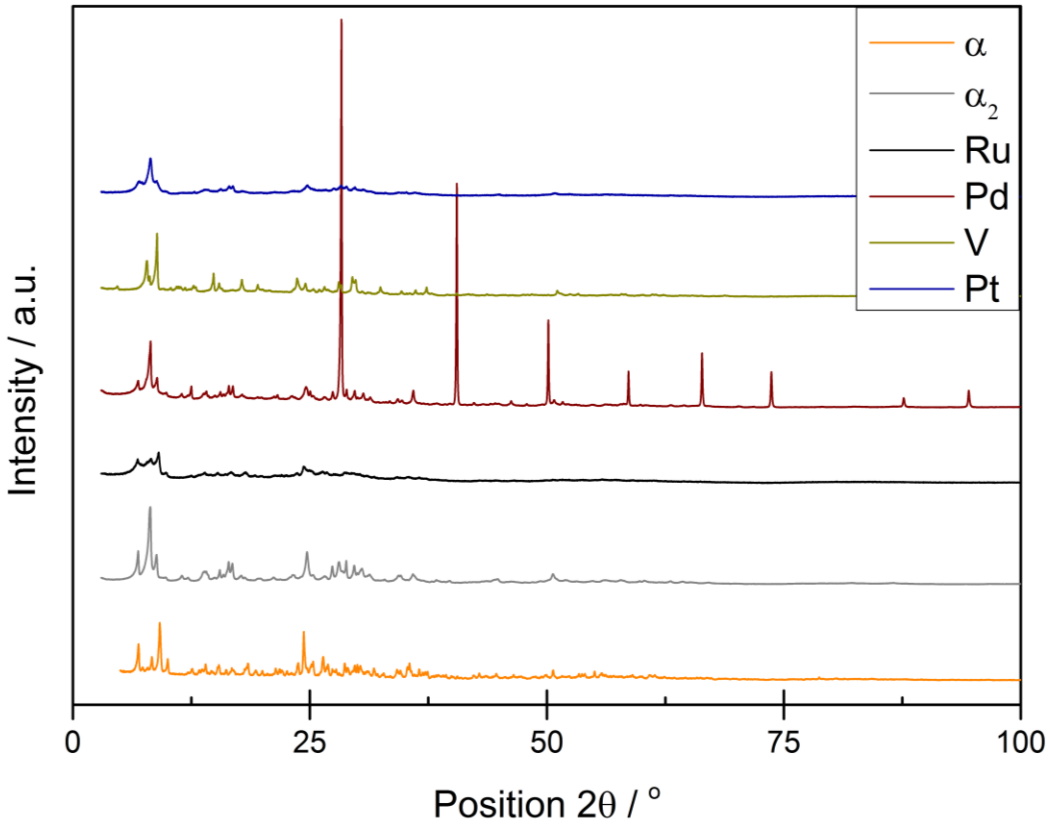

Figure 5.24: X-ray powder diffractograms of synthesized WD POMs (DTU).

Large amounts of potassium chloride was detected in the diffractogram of the Pd-WD (see reference diffractogram for KCl in Appendix D). The peak pattern for the Pd- and Pt-substituted WD was found to be comparable with that of α_2, indication preservation of an α_2-specie. However, due to low resolution, comparison of the specific peak patterns was challenging. The pattern observed for the Ru-WD resembled that of α-WD, indicating unsuccessful incorporation of Ru. Similarities of both α- and α_2-WD was observed in the diffractogram of the vanadium substituted catalyst, indicating preservation of a basic WD-POM structure. However, the differences in the peak patterns for α-, α_2- and V-WD indicate, that pure α and α_2-WD POMs were not present. Peaks comparable with

literature-data was observed, together with additional peaks, possibly arising from the vanadium precursor $H_9PV_{14}O_{42}$ observed in ^{31}P-NMR analysis.[484] Due to limited availability of the FAU-synthesized catalysts, XRPD was recorded only for the DTU-synthesized catalysts.

5.4.1.4 X-Ray Fluorescence

The acquired XRF data for the DTU-synthesized catalysts is presented in Table 5.8. Due to limited availability of the FAU-synthesized catalysts, XRF was recorded only for the DTU-synthesized catalysts. The obtained raw data was converted into molar concentrations relative to phosphor based on calibration obtained from XRF data on the α and α_2-WD POMs (see Appendix D, Table D4). The molar ratio was multiplied by two to facilitate comparison with the catalysts formulas presented in Table 5.3 containing two phosphorous.

Table 5.8: X-ray fluorescence data of the synthesized WD catalysts (DTU).

Entry	WD	W/P		K/P		W/K		Cl/P	M/P
		XRF	Theo.	XRF	Theo.	XRF	Theo.	XRF[a]	XRF[a]
1	α	18.2	(18.0)	5.9	(6.0)	3.0	(3.0)	0.07	-
2	α_2	16.8	(17.0)	10.1	(10.0)	1.6	(1.7)	0.07	-
3	α_2[b]	16.3	(17.0)	10.0	(10.0)	1.6	(1.7)	0.04	-
4	Ru[c]	22.6	(17.0)	24.6	(7.0)	0.9	(2.4)	17.7	0.7
5	Ru[d]	17.2	(17.0)	8.3	(7.0)	2.0	(2.4)	1.4	4.2
6	Pd	30.8	(17.0)	40.2	(8.0)	0.7	(2.1)	51.3	0.3
7	Pd[b]	18.4	(17.0)	12.3	(8.0)	1.5	(2.1)	3.7	0.1
8	Pd[c]	18.3	(17.0)	10.4	(8.0)	1.7	(2.1)	0.9	1.3
9	V[c]	20.3	(17.0)	13.7	(7.0)	1.5	(2.4)	6.6	4.7
10	V[d]	16.9	(17.0)	10.4	(7.0)	1.6	(2.4)	1.5	3.2
11	Pt	20.9	(17.0)	13.7	(8.0)	1.5	(2.1)	2.3	2.5
12	Pt[d]	19.9	(17.0)	10.5	(8.0)	1.9	(2.1)	1.1	2.2
13	Pt[e]	19.1	(17.0)	13.2	(8.0)	1.4	(2.1)	2.8	2.6

The theoretical (Theo.) concentrations are presented in parentheses. [a] Ratio of XRF counts (raw data), [b] Washed with methanol, [c] Recrystallized from MeOH, [d] Recrystallized from boiling water twice, [e] Soxhlet with methanol for 5h

Negligible impurities of chloride was observed for α- and α_2-WD (Table 5.8, Entries 1-3). However, significant amounts of chloride was observed for the metal-substituted POMs (Entries 4 and 6). The amount of chloride was reduced by washing or recrystallizing from methanol or water (Entries 4-13). In general, increased W/P ratios compared to the theoretical ratios, were observed for the metal substituted POMs. The recorded W/P ratio decreased with decreasing chloride content. Notably, the presence of the substituted metals was detected for the metal-substituted POMs.

5.4.1.5 Inductively Coupled Plasma Atomic Emission Spectroscopy

All ICP-AES samples were recorded at FAU. The results are presented in Table 5.9 below (for calculations, see Appendix D, Table D5).

Table 5.9: ICP concentrations converted to ratios relative to the phosphor concentration. The theoretical ratios are presented in parentheses.

Entry	WD	P	W/P		M/P		K/P	
		Theo.	ICP	Theo.	ICP	Theo.	ICP	Theo.
	FAU							
1	α	(2.0)	14.4	(18.0)	0.0	(0.0)	5.4	(6.0)
2	α_2	(2.0)	14.2	(17.0)	0.0	(0.0)	9.4	(10.0)
3	Ru	(2.0)	12.4	(17.0)	1.2	(1.0)	31.6	(7.0)
4	Pd	(2.0)	17.9	(17.0)	0.9	(1.0)	42.6	(8.0)
5	V	(2.0)	17.2	(17.0)	1.4	(1.0)	9.6	(7.0)
6	Mn	(2.0)	14.0	(17.0)	0.7	(1.0)	37.5	(8.0)
	DTU							
7	α	(2.0)	17.6	(18.0)	0.0	(0.0)	4.6	(6.0)
8	α_2	(2.0)	16.2	(17.0)	0.0	(0.0)	8.7	(10.0)
9	Ru	(2.0)	16.1	(17.0)	1.4	(1.0)	10.4	(7.0)
10	Pd	(2.0)	16.2	(17.0)	0.8	(1.0)	7.8	(8.0)
11	V	(2.0)	16.5	(17.0)	1.6	(1.0)	39.2	(7.0)
12	Pt	(2.0)	16.6	(17.0)	0.5	(1.0)	16.1	(8.0)

Decreased concentration of tungsten relative to phosphor was observed for the α-, α_2-, Ru- and Mn-WD catalysts, possibly due to precipitation observed during ICP analysis (Entries 1-3 and 6). W/P ratios comparable with the theoretical ratios were observed for the remaining catalysts. The presence of the incorporated metals was detected for all the metal-substituted catalysts in comparable ratios to the theoretical, indicating the presence of approximately one metal per α_2-WD. However, incorporation into the structure cannot be confirmed based on ICP analysis, only the presence of the metal and the concentration thereof. K/P ratios close to the theoretical ratios of the α- and α_2-WDs were detected. For the metal-substituted WD POMs, an excess of potassium was generally observed, comparable with the results obtained from XRF (Entries 3-6 and 9-12).

5.4.2 Application of Catalysts

The FAU-synthesized WD catalysts were tested for catalytic activity on model substrates of simple biomass derived compounds and the more complex structured sugar, sucrose. The applied conditions were inspired by previous work on POM-catalyzed conversion of sugars into formic acid by Wasserscheid and co-workers.[61,67,100,102]

5.4.2.1 Oxidation of Diols

Initially the prepared WD catalysts were tested in the oxidation of terminal diols into their corresponding acids, see Scheme 5.2. The three diols, 1,3-propanediol, 1,4-butanediol and 1,6-hexanediol, were chosen as model substrates of more complex biomass derived sugars.

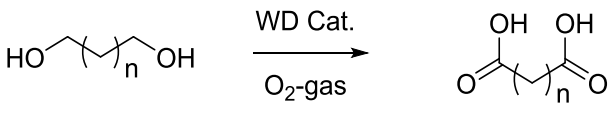

Scheme 5.2: Oxidation of terminal diols, n = 1, 2 and 4.

Malonic- and succinic acid (n = 1 and 2) are among the top 30 of value added chemicals from biomass published by the Office of Scientific and Technical Information in 2004.[553] Malonic acid is used in various manufacturing processes, including electronics, flavors, fragrances, solvents, polymer crosslinking and pharmaceutical.[554–557] Polymers and solvents are some of the products obtained from succinic acid on industrial scale. Furthermore, succinic acid is used as dietary supplement.[558–560] These renewable building blocks are of great technical feasibility and commercial potential. The catalysts were tested on the longer C6-diol (n=4), for conversion into adipic acid, which is used in large amounts for production of nylon.[561–566]

5.4.2.1.1 Screening for Active Metals

A screening for active metals of the oxidation of the selected diols was performed concurrently with the synthesis of the WD catalysts using various metal compounds. Selected screening results are presented in Table 5.10 below (see crude NMR spectra for $PdCl_2$-catalyzed reactions in Appendix D). Various reaction conditions were tested including temperatures ranging from 25-140 ^oC, reaction times of 7-18 h, pressure of 1-40 bar, different oxidants, substrate- and catalyst concentrations (1.46-13.14 M and 1-5 mol%) and different reaction media (water, methanol, ethanol, acetone). The metals were chosen based on catalytic oxidation activity known from literature (vanadium, manganese, cobalt, iron, copper, palladium and ruthenium) and availability.[274] The highly active oxidation catalyst HPA-5 (a vanadium-substituted Keggin based POM) was tested for the oxidation of the selected diols at identical conditions (Entry 11).[61,67,100,102] Increased oxidation activity was not observed testing the above-mentioned conditions, including change of reaction media.

Table 5.10: Selected results from the screening for active metals of the oxidation of 1,3-propanediol.

Entry	Metal compound	Oxidant[a]		
		O_2-gas	H_2O_2	
		80 °C	80 °C	140 °C[c]
1	$NiCl_2$	N.A.	-	-
2	$CuCl_2$	N.A.	-	-
3	$CoCl_2$	N.A.	-	-
4	$ZnCl_2$	N.A.	-	-
5	$VOSO_4$	Trace	A	3 C=O, gem.
6	$RuCl_3$	Trace	A[b]	gem.
7	$Ru(Bpy)_3Cl_2$	Trace	A	-
8	$PdCl_2$	gem.	gem.	3 C=O, 2 gem.
9	$FeCl_3$	N.A.	-	-
10	$Mn(ac)_2$	-	N.A.	N.A.
11	HPA-5	Trace	A	3 C=O, gem.

Reaction conditions: substrate concentration of 13.14 M (50 wt%) in water, 1 mol% catalyst, 20 bar molecular oxygen or 10 bar nitrogen and 10 mol% hydrogen peroxide unless otherwise noted. [a]Observations based on 1H- and 13C-NMR, no catalytic activity (N.A.), catalytic activity outside of the C=O region (A), peaks in carbonyl regions of 13C-NMR (C=O) and geminal diol formation (gem.), [b]2.5 mol% catalyst and c 5.63 M substrate concentration.

Very little or no activity was observed for most of the metal compounds under molecular oxygen pressure at 80 °C. The highest activity was observed for Pd(II) under the above-mentioned conditions (Entry 8). Substituting molecular oxygen with the more water soluble oxidant, hydrogen peroxide, afforded increased formation and intensity of peaks observed in the geminal diol and carbonyl areas (Entries 5-8, 11). At increased temperature (140 °C), a further increase of the carbonyl and geminal diol intensities was observed. Geminal diols are formed from hydration of aldehydes, indicating partial oxidation of the alcohol moiety. Various peaks in the carboxylic acid- and ester area (200-160 ppm in ^{13}C-NMR) was observed for vanadium, palladium and HPA-5, indicating catalytic oxidation activity of these metals. Similar results were observed for oxidation of 1,4-butanediol and 1,6-hexanediol (data not shown). The most active metals were found to be palladium and vanadium.

5.4.2.1.2 Oxidation of 1,3-propanediol with Synthesized M-substituted Wells-Dawson Catalysts

The FAU-synthesized WD catalysts were tested in the screening setup for oxidation of 1,3-propanediol. The products were analyzed according to ^{1}H-NMR and ^{13}C-NMR, presented in Table 5.11 (see NMR spectra in Appendix D). No conversion of 1,3-propanediol was observed under oxidant-deprived conditions and without a catalyst (Entry 1). Addition of 1 eq. H_2O_2 in the absence of catalyst afforded observed oxidative activity, and various peaks were observed in the aliphatic and C-O regions of the ^{13}C-NMR spectrum, in addition to the trace amounts of carbonyl products observed in the carbonyl region of both NMR spectra (*i.e.* aldehyde and carboxylic acid protons in ^{1}H-NMR) (Entry 2). In the presence of WD catalysts, increased activity was observed affording increased peak formation in the carbonyl and geminal diol regions together with increased intensity of the carbonyl peaks observed in the absence of WD catalysts. However, this was not observed in the presence of Ru- and Mn-WD catalyst (Entries 5 and 8), where little or no conversion was detected. Zooming in on the carbonyl region of the ^{1}H-NMR, various peaks were observed, agreeing with observations from ^{13}C-NMR. However, the relative low intensities observed in ^{1}H- and ^{13}C-NMR implied formation of trace amounts of the carbonylic species.

Table 5.11: Overview of results from FAU-WD catalyzed oxidation of 1,3-propanediol.

Entry	Catalyst	Observations in	
		^{1}H NMR	^{13}C NMR
1[a]	No cat.	N.A.	N.A.
2	No cat.	~9.3, ~8.1, various around 4.0, ~2.5 and ~2.0	Various C=O, gem. and C-O
3	α-WD	~9.4, ~8.1, various between 6.75-6.0 and around 4.0, ~2.5 and ~2.0	Various C=O, gem. and C-O
4	α_2-WD	~9.7, ~9.4, ~9.3, ~8.3, ~7.2, various between 6.75-6.0 and around 4.0, ~2.5 and ~2.0	Various C=O, gem. and C-O
5	Ru-WD	N.A.	Trace of C-O
6	Pd-WD	~9.7, ~9.5, ~9.3 ~8.2, various between 6.75-6.0 and around 4.0, ~2.5 and ~2.0	Various C=O, gem. and C-O
7	V-WD	~9.6, ~9.4, ~9.2, ~8.2, various between 6.75-6.0 and around 4.0, ~2.5 and ~2.0	Various C=O, gem. and C-O
8	Mn-WD	N.A.	Trace, no C=O

Reaction conditions: all reactions were performed with a substrate concentration of 5.66 M in water, 1 mol% catalyst, 1 eq. H2O2, under 10 bar nitrogen, at 140 oC for 7 h, unless otherwise noted. No catalytic activity (N.A.), peaks in carbonyl regions of 13C-NMR (C=O), geminal diol formation (gem.) and peaks in C-O region of 13C-NMR (C-O). aNo oxidant.

5.4.2.2 Oxidation of Sucrose

The catalytic activity of the FAU-synthesized WD catalysts was studied on the oxidation of sucrose in a larger setup with continuous oxygen feed (the OxBox). Sucrose, table sugar, is a common and available sugar and was used as model substrate for oxidation of biomass-derived sugars. The results are presented in Table 5.12. The gas-phase of the reactions was analyzed for CO and CO_2, and the liquid-phase for FA and sucrose both measured according to calibrated inlets of benzene in ^{1}H-NMR (see experimental section 5.3.4).

Table 5.12: Overview of results from FAU-WD catalyzed oxidation of sucrose.

Entry	Catalyst	Conversion (%)	CO_2 (mol%)	CO (mol%)	FA (mol%)	FA selectivity (%)
1	α-WD	N.A.	-	-	-	-
2	α_2-WD	98.7	98.1	-	0.5	0.5
3	Ru-WD	1.3	0.4	-	0.9	69.2
4	Pd-WD	1.8	1.8	-	-	-
5	V-WD	N.A.	-	-	-	-
6	Mn-WD	N.A.	-	-	-	-
7[a]	α-WD	0.1	-	-	-	-
8[a,b]	α-WD	37.1	16.2	1.2	19.7	53.1

Reaction conditions: Sucrose (25 mmol), the WD catalyst (4 mol%, 1mmol) and millipore water (100 g) was added to the high-pressure vessel. The vessel was sealed and flushed with molecular oxygen. The reaction was left 6h at 90 ^oC under 20 bar molecular oxygen at a stirring rate of 1000 rpm unless otherwise noted . [a]100 mmol sucrose and 1 mol% catalyst, [b]140 ^oC.

Generally, little or no conversion of sucrose was observed over the WD catalysts, however, high activity was obtained from oxidation over the monolacunary α_2-WD (Table 5.12, Entry 2). Unfortunately, the α_2-WD afforded low FA selectivity resulting in over-oxidation and formation of 98% CO_2. Surprisingly, good FA selectivity was obtained from oxidation over the Ru-WD catalyst, however, low conversion was obtained in accordance with the inactivity observed in the oxidations of diols (Entry 3). Increased substrate concentration was found to have no effect on the reaction activity (Entry 7). Increasing the temperature afforded increased conversion over the α-WD catalyst, resulting in formation of 20% FA (Entry 8), implying that harsher conditions are required for achieving increased catalyst activity. However, the oxidation was limited by the formation of CO_2, affording 53% FA selectivity.

The FAU-synthesized WD catalyst were found to afford low catalytic activities or low FA selectivities in the oxidation of sucrose at the applied conditions. Alternative application of the DTU-synthesized WD catalysts is currently being studied at FAU, affording promising results in the catalytic hydrogenation of glycerol.

5.5 Conclusions

Metal-substituted phospho-tungstic based Wells-Dawson polyoxometalates were synthesized and characterized according to literature. Differences and similarities between literature and obtained characterization data was observed, however, incongruence within literature reported characterization afforded challenging comparisons. The characterization of the precursors, α- and α_2-WD, was in agreement with reported data, and these were applied as references in the characterization of the metal-substituted Wells-Dawson catalysts. Elemental analysis (XRF and ICP) of the substituted catalysts afforded elemental concentrations comparable with the expected concentrations, notably, an excess of potassium chloride was detected and decreased by washing (XRF). The crystal structure of α-WD was obtained from single crystal XRD, implying successful preparation of the α-WD. Indication of peaks and bands in the phosphor-tungstic regions were observed for the substituted Wells-Dawson catalysts in XRD diffractograms and ATR-FTIR spectra implying the presence of Wells-Dawson-structured species. From ^{31}P-NMR, indication of successful ruthenium incorporation was found. For palladium, manganese and platinum-incorporation, peaks comparable with the α_2-Wells-Dawson structure was observed, indicating unsuccessful incorporation of the metals. Notably, the impurity observed in the NMR spectrum for the DTU-synthesized Pd-Wells-Dawson catalyst was found comparable with literature on the dimeric palladium Wells-Dawson specie, $(PdP_2W_{17}O_{61})_2$.

The catalytic activity of the FAU-synthesized catalysts was studied for the oxidation of 1,3-propanediol and sucrose. Low conversions were observed in the oxidation of 1,3-propanediol, however, trace amounts of carbonylic products was observed according to ^{1}H- and ^{13}C-NMR, implying low catalytic activity for conversion of 1,3-propanediol at the applied conditions. Under catalyst-deprived conditions, decreased conversion was observed, implying decreased catalytic activity in the absence of catalyst.

In general, little or no activity was observed in the oxidation of sucrose over the prepared catalysts. However, high activity and selectivity for CO_2 was observed in the oxidation over α_2-Wells-Dawson catalyst, indicating that milder conditions are required for successful formation of formic acid. At increased temperature (140 ^{o}C), 20% formic acid was obtained from glucose, catalyzed by the α-Wells-Dawson catalyst, indicating catalytic activity for the prepared α-catalyst, however, at increased temperatures compared to known catalysts.

The catalysts were prepared with the aim of obtaining highly active and selective catalysts for the oxidative conversion of biomass-derived compounds. However,

the metal-substituted Wells-Dawson catalysts did not improve the activity or selectivity in the oxidation of diols and sucrose. Possibly, the inactivity of the prepared catalyst was due to impurities of the catalyst or unsuccessful incorporation of the metals. Current ongoing work in collaboration with Dr. Ing. Jakob Albert at FAU, show promising application of the prepared WD catalysts for the hydrogenation of glycerol.

Chapter 6. Concluding Remarks

The work presented in this dissertation was based on the requisite for new sustainable methods of obtaining commodity chemicals from a renewable feedstock, due to continuing depletion of fossil sources, which is the preferred feedstock in the majority of current industrial processes. Biomass has proven a promising renewable feedstock for production of bulk and fine chemicals. In this dissertation, oxidative catalytic transformations of biomass-derived compounds have been investigated with the motivation of developing industrial applicable and sustainable methods for the catalytic upgrading of biomass–derived compounds for future production of bio-renewable chemicals.

Catalysis is of great interest in the contemporary chemical industry due to increased efficiency and reduced production of waste chemicals. Oxidative catalytic upgrading of chemicals was examined in this work, with primary focus on heterogeneous catalysis, which is advantageous over homogeneous catalysis due to easier separation and regeneration of the catalyst. However, the generally higher product selectivity of homogeneous catalysis is beneficial in industrial processes, and investigation of in homogeneous catalyst was examined for the oxidative catalytic transformation of biomass-derived compounds. The oxidations were explored in an environmentally benign aqueous media using an abundant and inexhaustible green oxidant (air or molecular oxygen).

A protocol for selective oxidation of glycolaldehyde into glycolic acid over commercial available supported gold nanoparticles was presented in Chapter 3. Up to 68% glycolic acid was obtained at high catalysts loading, limited by CO_2 formation *i.e.* over-oxidation. At more representable catalyst loading for industrial application, 57% glycolic acid was obtained. However, due to often impure reaction mixtures of various biomass-derived compounds together with glycolaldehyde from industrial processes, higher activity and selectivity is

necessary for sufficient conversion of glycolaldehyde into glycolic acid. Additionally, catalyst instability was observed, and the search for a more robust catalyst was initiated. The effect of supported ruthenium hydroxide was studied on the oxidation of glycolaldehyde and was found to yield formic acid as end product at the applied conditions. High yields of formic acid was obtained from oxidation over ceria-supported ruthenium hydroxide. Little effect was found from changing of the support surface area of the catalyst at the optimized conditions, affording 81 and 88% formic acid at low and increased BET surface areas, respectively. However, degradation of FA was observed for the low-surface area catalyst over time, whereas the higher-surface area catalyst was found to yield high substrate stability over time.

Generally observed for oxidations of glycolaldehyde was the effect of high temperatures affording over-oxidation products. However, reduced conversions was observed from decreased temperatures. The optimal temperature range was found to be 80-90 ^{o}C for aqueous, base-free oxidations of glycolaldehyde. Minor effect was observed at high pressures of oxidant, however, at decreased pressures, low oxygen-availability was limiting the catalyst activity and decreased conversions was observed.

The ceria-supported ruthenium hydroxide catalyst was further examined for the oxidation alcohols to acetic acid, however, low yields of acetic acid (39%) was obtained from oxidation of the model substrate, 1-propanol, at 150 ^{o}C applying a pressure of 30 bar molecular oxygen.

Homogeneous catalyzed conversion of biomass-derived compounds was examined over the synthesized Wells-Dawson-based heteropolyoxometalates in collaborative work with the group of Prof. Wasserscheid, FAU, Erlangen. However, insufficient characterization of metal incorporation lead to speculations of whether the metal was incorporated into the structure or present as a separate salt. Due to time-limitations, the catalysts were only tested in oxidations of simple alcohols and sucrose without further characterization. However, little or no oxidation products was observed in the oxidation of alcohols. Studying the catalysts in the oxidation of sucrose afforded 20% formic acid at 140 ^{o}C using the Wells-Dawson precursor, indicating oxidative catalytic activity of the Wells-Dawson structure.

The contents of this dissertation have demonstrated the initial stages of the development of protocols for oxidation of biomass-derived glycolaldehyde. Oxidation of alcohols was less successful, however, activity was observed in the conversion of 1-propanol to acetic acid and sucrose into formic acid. Investigation of sustainable protocols for selective catalytic oxidative upgrading of biomass-derived compounds is an essential process in the development for application of biomass as a renewable feedstock on industrial scale.

Bibliography

1. C. Baskar, S. Baskar, and R. S. Dhillon, in *Biomass Conversion: the Interface of Biotechnology, Chemistry and Materials Science*, Springer-Verlag Berlin Heidelberg, 2012, p. 6.

2. J. R. H. Ross, in *Heterogeneous Catalysis*, Elsevier, 2012, pp. 47–64.

3. J. Hagen, in *Industrial Catalysis*, Wiley-VCH Verlag GmbH & Co. KGaA, 2015, pp. 1–16.

4. I. Chorkendorff and J. W. Niemantsverdriet, in *Concepts of Modern Catalysis and Kinetics*, Wiley-VCH Verlag GmbH & Co. KGaA, 2003, p. 1.

5. B. M. Trost, *Acc. Chem. Res.*, 2002, **35**, 695–705.

6. B. Trost, *Science.*, 1991, **254**, 1471–1477.

7. B. H. Davis, *Handb. Heterog. Catal.*, 2008, 16–37.

8. H. Knözinger and K. Kochloefl, *Ullmann's Encycl. Ind. Chem.*, 2000, **1**, 2–5, 14–20, 36–39.

9. G. Rothenberg, in *Catalysis: Concepts and Green Applications*, Wiley-VCH Verlag GmbH & Co. KGaA, 2008, pp. 39–75.

10. J. Hagen, in *Industrial Catalysis*, Wiley-VCH Verlag GmbH & Co. KGaA, 2015, p. 47.

11. G. Rothenberg, in *Catalysis: Concepts and Green Applications*, Wiley-VCH Verlag GmbH & Co. KGaA, 2008, pp. 127–187.

12. S. H. Overbury, P. A. Bertrand, and G. A. Somorjai, *Chem. Rev.*, 1975, **75**, 547–560.

13. B. . Hvolbæk, T. V. W. . Janssens, B. S. . Clausen, H. . Falsig, C. H. . Christensen, and J. K. . Nørskov, *Nano Today*, 2007, **2**, 14–18.

14. N. Lopez, T. V. W. Janssens, B. S. Clausen, Y. Xu, M. Mavrikakis, T. Bligaard, and J. K. Nørskov, *J. Catal.*, 2004, **223**, 232–235.

15. P. T. Anastas, *Chem. Rev.*, 2007, **107**, 2167–2168.

16. P. Anastas and N. Eghbali, *Chem. Soc. Rev.*, 2010, **39**, 301–312.

17. R. A. Sheldon, *J. Mol. Catal. A Chem.*, 1996, **107**, 75–83.

18. C. H. Christensen, J. Rass-Hansen, C. C. Marsden, E. Taarning, and K. Egeblad, *ChemSusChem*, 2008, **1**, 283–289.

19. B. Voss, S. I. Andersen, E. Taarning, and C. H. Christensen, *ChemSusChem*, 2009, **2**, 1152–1162.

20. R. A. Sheldon, *Green Chem.*, 2007, **9**, 1273.

21. T. Ishida and M. Haruta, *Angew. Chemie - Int. Ed.*, 2007, **46**, 7154–7156.

22. A. Corma, S. Iborra, and A. Velty, *Chem. Rev.*, 2007, **107**, 2411–502.

23. O. a. Simakova, R. J. Davis, and D. Y. Murzin, in *SpringerBriefs in Molecular Science*, Springer International Publishing, 2013, vol. 8, pp. 1–28.

24. T. Splettstoesser, *http://www.scistyle.com*, 2011.

25. R. Vinu and L. J. Broadbelt, *Energy Environ. Sci.*, 2012, **5**, 9808–9826.

26. M. Sasaki, K. Goto, K. Tajima, T. Adschiri, and K. Arai, *Green Chem.*, 2002, **4**, 285–287.

27. D. Mohan, Pittman Charles U., and P. H. Steele, *Energy & Fuels*, 2006, **20**, 848–889.

28. W. Magerlein, J.-P. Melder, J. Pastre, J. Eberhardt, T. Krug, and M. Kreitschmann, 2012, US 20120271068 A1.

29. S. Van De Vyver and Y. Roman-Leshkov, *Angew. Chemie - Int. Ed.*, 2015, **54**, 12554–12561.

30. S. Tolborg, S. Meier, S. Saravanamurugan, P. Fristrup, E. Taarning, and I. Sádaba, *ChemSusChem*, 2016, **9**, 3054–3061.

31. H. Kishida, F. Jin, X. Yan, T. Moriya, and H. Enomoto, *Carbohydr. Res.*, 2006, **341**, 2619–2623.

32. X. Yan, F. Jin, K. Tohji, A. Kishita, and H. Enomoto, *AIChE J.*, 2010, **56**, 2727–2733.

33. L. C. Costa, 1982, US4321414.

34. M. Shibata and N. Furuya, *Electrochim. Acta*, 1994, **39**, 1877–1880.

35. P. K. Sen, A. B. Bilkis, and K. K. Sen Gupta, *Int. J. Chem. Kinet.*, 1998, **30**, 613–619.

36. N. I. Butkovskaya, N. Pouvesle, A. Kukui, and G. Le Bras, *J. Phys. Chem. A*, 2006, **110**, 13492–13499.

37. S. Yamaguchi, T. Matsuo, K. Motokura, Y. Sakamoto, A. Miyaji, and T. Baba, *ChemSusChem*, 2015, **8**, 853–860.

38. S. Yamaguchi, T. Matsuo, K. Motokura, A. Miyaji, and T. Baba, *ChemCatChem*, 2016, **8**, 1386–1391.

39. A. N. Simonov, O. P. Pestunova, L. G. Matvienko, V. N. Snytnikov, O. A. Snytnikova, Y. P. Tsentalovich, and V. N. Parmon, *Adv. Sp. Res.*, 2007, **40**, 1634–1640.

40. M. S. Holm, Y. J. Pagan-Torres, S. Saravanamurugan, A. Riisager, J. A. Dumesic, and E. Taarning, *Green Chem.*, 2012, **14**, 702–706.

41. C. Parmeggiani and F. Cardona, *Green Chem.*, 2012, **14**, 547.

42. C.-H. C. Zhou, J. N. Beltramini, Y.-X. Fan, and G. Q. M. Lu, *Chem. Soc. Rev.*, 2008, **37**, 527–49.

43. T. F. Blackburn and J. Schwartz, *J. Chem. Soc. Commun.*, 1977, **5**, 157–158.

44. C. P. Vinod, K. Wilson, and A. F. Lee, *J. Chem. Technol. Biotechnol.*, 2011, **86**, 161–171.

45. P. Gallezot, *Chem. Soc. Rev.*, 2012, **41**, 1538–58.

46. G. W. Huber, S. Iborra, and A. Corma, *Chem. Rev.*, 2006, **106**, 4044–4098.

47. H. Li, Z. Fang, R. L. Smith, and S. Yang, *Prog. Energy Combust. Sci.*, 2016, **55**, 98–194.

48. T. Thananatthanachon and T. B. Rauchfuss, *Angew. Chemie Int. Ed.*, 2010, **49**, 6616–6618.

49. O. C. Navarro, A. C. Canós, and S. I. Chornet, *Top. Catal.*, 2009, **52**, 304–314.

50. A. Kelloway and P. Daoutidis, *Ind. Eng. Chem. Res.*, 2014, **53**, 5261–5273.

51. A. a. Rosatella, S. P. Simeonov, R. F. M. Frade, and C. a. M. Afonso, *Green Chem.*, 2011, **13**, 754–793.

52. M. J. Climent, A. Corma, and S. Iborra, *Green Chem.*, 2011, **13**, 520–540.

53. P. Gallezot, *Green Chem.*, 2007, **9**, 295–302.

54. P. Mäki- Arvela, B. Holmbom, T. Salmi, and D. Y. Murzin, *Catal. Rev.*, 2007, **49**, 197–340.

55. J. Haber, in *Handbook of Heterogeneous Catalysis*, Wiley-VCH Verlag GmbH & Co. KGaA, 2008, pp. 3359–3384.

56. T. Mallat and A. Baiker, *Chem. Rev.*, 2004, **104**, 3037–3058.

57. V. I. Sobolev, K. Y. Koltunov, O. A. Simakova, A.-R. Leino, and D. Y. Murzin, *Appl. Catal. A Gen.*, 2012, **433–434**, 88–95.

58. M. López, O. A. Simakova, E. V. Murzina, S. M. Willför, I. Prosvirin, A. Simakov, and D. Y. Murzin, *Appl. Catal. A Gen.*, 2015, **504**, 248–255.

59. J. Chen, S. Wang, J. Huang, L. Chen, L. Ma, and X. Huang, *ChemSusChem*, 2013, **6**, 1545–1555.

60. S. E. Davis, B. N. Zope, and R. J. Davis, *Green Chem.*, 2012, **14**, 143–147.

61. R. Wolfel, N. Taccardi, A. Bosmann, and P. Wasserscheid, *Green Chem.*, 2011, **13**, 2759–2763.

62. S. Demirel, K. Lehnert, M. Lucas, and P. Claus, *Appl. Catal. B Environ.*, 2007, **70**, 637–643.

63. Y. Gorbanev, S. Kegnæs, C. W. Hanning, T. W. Hansen, and A. Riisager, *A C S Catal.*, 2012, **2**, 604–612.

64. P. Qi, S. Chen, J. Chen, J. Zheng, X. Zheng, and Y. Yuan, *ACS Catal.*, 2015, **5**, 2659–2670.

65. A. Villa, C. Campione, and L. Prati, *Catal. Letters*, 2007, **115**, 133–136.

66. B. Jørgensen, S. E. Christiansen, M. L. D. Thomsen, and C. H. Christensen, *J. Catal.*, 2007, **251**, 332–337.

67. J. Reichert, B. Brunner, A. Jess, and J. Albert, *Energy Environ. Sci.*, 2015, **8**, 2985–2990.

68. C. H. Christensen, B. Jørgensen, J. Rass-Hansen, K. Egeblad, R. Madsen, S. K. Klitgaard, S. M. Hansen, M. R. Hansen, H. C. Andersen, and A. Riisager, *Angew. Chemie Int. Ed.*, 2006, **45**, 4648–4651.

69. F. F. Bamoharram, *Synth. React. Inorganic, Met. Nano-Metal Chem.*, 2011, **41**, 893–922.

70. J. Xu, Y. Zhao, H. Xu, H. Zhang, B. Yu, L. Hao, and Z. Liu, *Appl. Catal. B Environ.*, 2014, **154**–**155**, 267–273.

71. C. L. Bianchi, P. Canton, N. Dimitratos, F. Porta, and L. Prati, *Catal. Today*, 2005, **102**–**103**, 203–212.

72. A. T. Bell, *Science*, 2003, **299**, 1688–1691.

73. R. Schlögl and S. B. Abd Hamid, *Angew. Chemie Int. Ed.*, 2004, **43**, 1628–1637.

74. D. Astruc, F. Lu, and J. R. Aranzaes, *Angew. Chemie Int. Ed.*, 2005, **44**, 7852–7872.

75. V. Polshettiwar and R. S. Varma, *Green Chem.*, 2010, **12**, 743–754.

76. M. Besson, F. Lahmer, P. Gallezot, P. Fuertes, and G. Fleche, *J. Catal.*, 1995, **152**, 116–121.

77. T. Takei, T. Akita, I. Nakamura, T. Fujitani, M. Okumura, K. Okazaki, J. Huang, T. Ishida, and M. Haruta, in *Advances in Catalysis*, eds. B. Gates and F. Jentoft, Academic Press, 2012, vol. 55, pp. 1–126.

78. S. E. Davis, M. S. Ide, and R. J. Davis, *Green Chem.*, 2013, **15**, 17–45.

79. M. Nagai and R. D. Gonzalez, *Ind. Eng. Chem. Prod. Res. Dev.*, 1985, **24**, 525–531.

80. J. Muzart, *Tetrahedron*, 2003, **59**, 5789–5816.

81. A. B. Laursen, Y. Y. Gorbanev, F. Cavalca, P. Malacrida, A. Kleiman-Schwarsctein, S. Kegnæs, A. Riisager, I. Chorkendorff, and S. Dahl, *Appl. Catal. A Gen.*, 2012, **443**–**434**, 243–250.

82. X. Li and E. Iglesia, *Chem. - A Eur. J.*, 2007, **13**, 9324–9330.

83. M. Comotti, C. Della Pina, R. Matarrese, M. Rossi, and A. Siani, *Appl. Catal. A Gen.*, 2005, **291**, 204–209.

84. Y. Önal, S. Schimpf, and P. Claus, *J. Catal.*, 2004, **223**, 122–133.

85. S. Biella, L. Prati, and M. Rossi, *J. Catal.*, 2002, **206**, 242–247.

86. Y. Cao, X. Liu, S. Iqbal, P. J. Miedziak, J. K. Edwards, R. D. Armstrong, D. J. Morgan, J. Wang, and G. J. Hutchings, *Catal. Sci. Technol.*, 2016, **6**, 107–117.

87. Y. Onal, S. Schimpf, and P. Claus, *J. Catal.*, 2004, **223**, 122–133.

88. M. Comotti, C. Della Pina, and M. Rossi, *J. Mol. Catal. A Chem.*, 2006, **251**, 89–92.

89. A. Mirescu and U. Prüße, *Appl. Catal. B Environ.*, 2007, **70**, 644–652.

90. H. D. Berndt, B. A. D. Haji, J. D. Kowalczyk, I. D. Pitsch, and U. D. Prüße, 2009, DE10319917B4.

91. Y. Zhang, X. Cui, F. Shi, and Y. Deng, *Chem. Rev.*, 2012, **112**, 2467–2505.

92. H. Ait Rass, N. Essayem, and M. Besson, *ChemSusChem*, 2015, **8**, 1206–1217.

93. O. Casanova, S. Iborra, and A. Corma, *J. Catal.*, 2009, **265**, 109–116.

94. Y. Y. Gorbanev, S. Kegnæs, and A. Riisager, *Catal. Letters*, 2011, **141**, 1752–1760.

95. E. de Jong, M. A. Dam, L. Sipos, and G.-J. M. Gruter, in *Biobased Monomers, Polymers, and Materials*, American Chemical Society, 2012, vol. 1105, pp. 1–13.

96. P. Gallezot and A. Kiennemann, in *Handbook of Heterogeneous Catalysis*, Wiley-VCH Verlag GmbH & Co. KGaA, 2008, pp. 2447–2459.

97. Z. Miao, T. Wu, J. Li, T. Yi, Y. Zhang, and X. Yang, *RSC Adv.*, 2015, **5**, 19823–19829.

98. A. S. Nagpure, A. K. Venugopal, N. Lucas, M. Manikandan, R. Thirumalaiswamy, and S. Chilukuri, *Catal. Sci. Technol.*, 2015, **5**, 1463–1472.

99. S. E. Davis, L. R. Houk, E. C. Tamargo, A. K. Datye, and R. J. Davis, *Catal. Today*, 2011, **160**, 55–60.

100. J. Albert and P. Wasserscheid, *Green Chem.*, 2015, **17**, 5164–5171.

101. J. Zhang, M. Sun, X. Liu, and Y. Han, *Catal. Today*, 2014, **233**, 77–82.

102. J. Albert, R. Wolfel, A. Bosmann, and P. Wasserscheid, *Energy Environ. Sci.*, 2012, **5**, 7956–7962.

103. P. Atkins and J. De Paula, in *Atkins' physical chemistry*, Oxford University Press, 8th edn., 2006, pp. 909–958.

104. J. M. Hollas, in *Modern spectroscopy*, Wiley-VCH Verlag GmbH & Co. KGaA, 4th edn., 2004, pp. 479–501.

105. P. J. Potts, in *A Handbook of Silicate Rock Analysis*, Springer Netherlands, Dordrecht, 1987, pp. 286–325.

106. R. Schneider, in *Surface and Thin Film Analysis*, Wiley-VCH Verlag GmbH & Co. KGaA, 2011, pp. 293–310.

107. D. C. Harris, in *Quantitative chemical analysis*, W. H. Freeman and Co., 2010, pp. 486–495.

108. J. C. Yang, M. W. Small, R. V Grieshaber, and R. G. Nuzzo, *Chem. Soc. Rev.*, 2012, **41**, 8179–8194.

109. J. Liu, *Microsc. Microanal.*, 2004, **10**, 55–76.

110. G. Will, in *Powder Diffraction: The Rietveld Method and the Two-Stage Method*, 2006, pp. 11–15.

111. A. L. Patterson, *Phys. Rev.*, 1939, **56**, 978–982.

112. D. W. H. Rankin, N. W. Mitzel, and C. A. Morrison, in *Structural Methods in Molecular Inorganic Chemistry*, Wiley, 1 st., 2013, pp. 329–333, 368.

113. S. Brunauer, P. H. Emmett, and E. Teller, *J. Am. Chem. Soc.*, 1938, **60**, 309–319.

114. H. T. Sun and P. C. Hsi, 2002, US6469303.

115. N. Abudukelimu, H. Xi, Z. Gao, Y. Zhang, Y. Ma, X. Mamat, and W. Eli, *Mater. Sci. Eng. with Adv. Res.*, 2015, **1**, 31–37.

116. J. Rass-Hansen, H. Falsig, B. Jørgensen, and C. H. Christensen, *J. Chem. Technol. Biotechnol.*, 2007, **82**, 329–333.

117. M. P. Checiński, A. Brückner, J. Radnik, and A. Köckritz, *Appl. Catal. A Gen.*, 2009, **366**, 212–219.

118. J. E. Bäckvall, Ed., in *Modern Oxidation Methods*, 2nd edn., 2005, pp. 147, 169–170.

119. Z. Guo, B. Liu, Q. Zhang, W. Deng, Y. Wang, and Y. Yang, *Chem. Soc. Rev.*, 2014, **43**, 3480–3524.

120. K. Miltenberger, in *Ullmann's Encyclopedia of Industrial Chemistry*, Wiley-VCH Verlag GmbH & Co. KGaA, 2000, pp. 486–487.

121. F. T. Mariño, J. Torres, M. Hamdan, C. R. Rodríguez, and E. L. Cabarcos, *J. Biomed. Mater. Res. Part B Appl. Biomater.*, 2007, **83B**, 571–579.

122. L. Moy, H. Murad, and R. Moy, *J. Dermatol. Surg. Oncol.*, 1993, **19**, 243–246.

123. C. M. Ditre, *Dermatol. Ther.*, 2000, **13**, 165–172.

124. Y. Takenaka, N. Hayashi, M. Takeda, S. Ashikaga, and M. Kawashima, *J. Dermatol.*, 2012, **39**, 350–354.

125. J. T. Hong, E. J. Kim, K. S. Ahn, K. M. Jung, Y. P. Yun, Y. K. Park, and S. H. Lee, *Mol. Carcinog.*, 2001, **31**, 152–160.

126. L. D. John, 1936, US2152852.

127. S. Suzuki, 1975, US3911003 A.

128. H. Klug, 1979, DE2810906 A1.

129. M. Vaygouny, 1917, US1227706 A.

130. O. Liebknecht, 1906, US837083 A.

131. Y. Kuroda and H. Watanabe, 2003, US7164040 B2.

132. E. Leupold and H. Arpe, 1979, DE2741505 A1.

133. Z. She, J. Zhu, and H. Na, 2016, CN104355982 B.

134. S. D. Barnicki, R. T. Hembre, and S. N. Falling, 2013, US20130261329A1.

135. G. C. Bond and P. A. Sermon, *Gold Bull.*, 1973, **6**, 102–105.

136. P. A. Sermon, *Gold Bull.*, 1976, **9**, 129–131.

137. M. Haruta, T. Kobayashi, H. Sano, and N. Yamada, *Chem. Lett.*, 1987, **16**, 405–408.

138. M. Haruta, N. Yamada, T. Kobayashi, and S. Lijima, *J. Catal.*, 1989, **115**, 301–309.

139. M. Besson and P. Gallezot, *Catal. Today*, 2000, **57**, 127–141.

140. A. Corma and M. E. Domine, *Chem. Commun.*, 2005, 4042–4044.

141. S. A. Shahzad, M. A. Sajid, Z. A. Khan, and D. Canseco-Gonzalez, *Synth. Commun.*, 2017, **47**, 735–755.

142. A. S. K. Hashmi, *Chem. Rev.*, 2007, **107**, 3180–3211.

143. R. Coquet, K. L. Howard, and D. J. Willock, *Chem. Soc. Rev.*, 2008, **37**, 2046–2076.

144. B. K. Min and C. M. Friend, *Chem. Rev.*, 2007, **107**, 2709–2724.

145. A. Corma and H. Garcia, *Chem. Soc. Rev.*, 2008, **37**, 2096–2126.

146. D. J. Gorin, B. D. Sherry, and F. D. Toste, *Chem. Rev.*, 2008, **108**, 3351–3378.

147. M. Stratakis and H. Garcia, *Chem. Rev.*, 2012, **112**, 4469–4506.

148. A. S. K. Hashmi and G. J. Hutchings, *Angew. Chemie - Int. Ed.*, 2006, **45**, 7896–7936.

149. C. W. Corti, R. J. Holliday, and D. T. Thompson, *Appl. Catal. A Gen.*, 2005, **291**, 253–261.

150. D. J. Gorin and F. D. Toste, *Nature*, 2007, **446**, 395–403.

151. M. Haruta and M. Daté, *Appl. Catal. A Gen.*, 2001, **222**, 427–437.

152. G. J. Hutchings and M. Haruta, *Appl. Catal. A Gen.*, 2005, **291**, 2–5.

153. J. Gong and C. B. Mullins, *Acc. Chem. Res.*, 2009, **42**, 1063–1073.

154. B. Nkosi, N. J. Coville, and G. J. Hutchings, *J. Chem. Soc. Chem. Commun.*, 1988, 71–72.

155. M. Haruta, *Catal. Today*, 1997, **36**, 153–166.

156. R. Meyer, C. Lemire, S. K. Shaikhutdinov, and H.-J. Freund, *Gold Bull.*, 2004, **37**, 72–124.

157. G. J. Hutchings, *Catal. Today*, 2005, **100**, 55–61.

158. W. C. Ketchie, Y. L. Fang, M. S. Wong, M. Murayama, and R. J. Davis, *J. Catal.*, 2007, **250**, 94–101.

159. S. Demirel-Gülen, M. Lucas, and P. Claus, *Catal. Today*, 2005, **102**–**103**, 166–172.

160. G. C. Bond and D. T. Thompson, *Catal. Rev. Sci. Eng.*, 1999, **41**, 319–388.

161. M. Haruta, *Gold Bull.*, 2004, **37**, 27–36.

162. G. J. Hutchings, *Gold Bull.*, 1996, **29**, 123–130.

163. A. Abad, P. Concepción, A. Corma, and H. García, *Angew. Chemie Int. Ed.*, 2005, **44**, 4066–4069.

164. A. Villa, D. Wang, G. M. Veith, F. Vindigni, and L. Prati, *Catal. Sci. Technol.*, 2013, **3**, 3036–3041.

165. F. M. Menger and C. Lee, *Tetrahedron Lett.*, 1981, **22**, 1655–1656.

166. E. G. Rodrigues, M. F. R. Pereira, and J. J. M. Órfão, *Appl. Catal. B Environ.*, 2012, **115**–**116**, 1–6.

167. H. Wang, W. Fan, Y. He, J. Wang, J. N. Kondo, and T. Tatsumi, *J. Catal.*, 2013, **299**, 10–19.

168. J. Zhu, J. L. Figueiredo, and J. L. Faria, *Catal. Commun.*, 2008, **9**, 2395–2397.

169. M. Turner, V. B. Golovko, O. P. H. Vaughan, P. Abdulkin, A. Berenguer-Murcia, M. S. Tikhov, B. F. G. Johnson, and R. M. Lambert, *Nature*, 2008, **454**, 981–983.

170. S. Biella and M. Rossi, *Chem. Commun.*, 2003, 378–379.

171. S. Carrettin, P. McMorn, P. Johnston, K. Griffin, and G. J. Hutchings, *Chem.*

Commun., 2002, 696–697.

172. L. Zhou, M. Chen, Y. Wang, Y. Su, X. Yang, C. Chen, and J. Xu, *Appl. Catal. A Gen.*, 2014, **475**, 347–354.

173. L.-C. Wang, L. He, Q. Liu, Y.-M. Liu, M. Chen, Y. Cao, H.-Y. He, and K.-N. Fan, *Appl. Catal. A Gen.*, 2008, **344**, 150–157.

174. C. Bianchi, F. Porta, L. Prati, and M. Rossi, *Top. Catal.*, 2000, **13**, 231–236.

175. B. Zope and R. Davis, *Top. Catal.*, 2009, **52**, 269–277.

176. M. H. Ab Rahim, M. M. Forde, R. L. Jenkins, C. Hammond, Q. He, N. Dimitratos, J. A. Lopez-Sanchez, A. F. Carley, S. H. Taylor, D. J. Willock, D. M. Murphy, C. J. Kiely, and G. J. Hutchings, *Angew. Chemie - Int. Ed.*, 2013, **52**, 1280–1284.

177. M. J. Climent, A. Corma, J. C. Hernández, A. B. Hungría, S. Iborra, and S. Martínez-Silvestre, *J. Catal.*, 2012, **292**, 118–129.

178. L. Prati and F. Porta, *Appl. Catal. A Gen.*, 2005, **291**, 199–203.

179. L. Prati and M. Rossi, *Stud. Surf. Sci. Catal.*, 1997, **110**, 509–516.

180. P. Beltrame, M. Comotti, C. Della Pina, and M. Rossi, *Appl. Catal. A-general*, 2006, **297**, 1–7.

181. M. Comotti, C. Della Pina, E. Falletta, and M. Rossi, *Adv. Synth. Catal.*, 2006, **348**, 313–316.

182. N. Dimitratos, J. A. Lopez-Sanchez, D. Lennon, F. Porta, L. Prati, and A. Villa, *Catal. Letters*, 2006, **108**, 147–153.

183. L. Prati and M. Rossi, *J. Catal.*, 1998, **176**, 552–560.

184. S. Biella, L. Prati, and M. Rossi, *Inorganica Chim. Acta*, 2003, **349**, 253–257.

185. S. Carrettin, P. McMorn, P. Johnston, K. Griffin, C. J. Kiely, and G. J. Hutchings, *Phys. Chem. Chem. Phys.*, 2003, **5**, 1329–1336.

186. S. Carrettin, P. McMorn, P. Johnston, K. Griffin, C. J. Kiely, G. A. Attard, and G. J. Hutchings, *Top. Catal.*, 2004, **27**, 131–136.

187. F. Porta and L. Prati, *J. Catal.*, 2004, **224**, 397–403.

188. L. Prati, A. Villa, D. Su, D. Wang, Z. Krpetic, and F. Porta, *Stud. Surf. Sci. Catal.*, 2006, **162**, 553–560.

189. M. Pagliaro, R. Ciriminna, H. Kimura, M. Rossi, and C. Della Pina, *Angew. Chemie - Int. Ed.*, 2007, **46**, 4434–4440.

190. M. Comotti, C. Della Pina, R. Matarrese, and M. Rossi, *Angew. Chemie - Int. Ed.*, 2004, **43**, 5812–5815.

191. N. K. Gupta, S. Nishimura, A. Takagaki, and K. Ebitani, *Green Chem.*, 2011, **13**, 824.

192. M. Comotti, C. Della Pina, E. Falletta, and M. Rossi, *Adv. Synth. Catal.*, 2006, **348**, 313–316.

193. A. Tsuji, K. T. V. Rao, S. Nishimura, A. Takagaki, and K. Ebitani, *ChemSusChem*, 2011, **4**, 542–548.

194. B. N. Zope, D. D. Hibbitts, M. Neurock, and R. J. Davis, *Science*, 2010, **330**, 74–78.

195. A. Abad, A. Corma, and H. García, *Chem. - A Eur. J.*, 2007, **14**, 212–222.

196. B. N. Zope and R. J. Davis, *Green Chem.*, 2011, **13**, 3484–3491.

197. M. Okumura, Y. Kitagawa, M. Haruta, and K. Yamaguchi, *Chem. Phys. Lett.*, 2001, **346**, 163–168.

198. I. X. Green, W. Tang, M. Neurock, and J. T. Yates, *Science*, 2011, **333**, 736–739.

199. F. Boccuzzi, A. Chiorino, S. Tsubota, and M. Haruta, *J. Phys. Chem.*, 1996, **100**, 3625–3631.

200. S. Minicò, S. Scirè, C. Crisafulli, A. M. Visco, and S. Galvagno, *Catal. Letters*, 1997, **47**, 273–276.

201. T. Ishida, M. Nagaoka, T. Akita, and M. Haruta, *Chem. - A Eur. J.*, 2008, **14**, 8456–8460.

202. Y. Kobayashi and H. Takahashi, *Spectrochim. Acta Part A Mol. Spectrosc.*, 1979, **35**, 307–314.

203. G. C. S. Collins and W. O. George, *J. Chem. Soc. B*, 1971, 1352–1355.

204. A. Abad, C. Almela, A. Corma, and H. García, *Tetrahedron*, 2006, **62**, 6666–6672.

205. M. I. Qadir, J. D. Scholten, and J. Dupont, *J. Mol. Catal. A Chem.*, 2014, **383**–**384**, 225–230.

206. W. C. Ketchie, M. Murayama, and R. J. Davis, *J. Catal.*, 2007, **250**, 264–273.

207. S. Albonetti, R. Mazzoni, and F. Cavani, in *Transition Metal Catalysis in Aerobic Alcohol Oxidation*, 2015, pp. 17–24.

208. J. Hietala, A. Vuori, P. Johnsson, I. Pollari, W. Reutemann, and H. Kieczka, in *Ullmann's Encyclopedia of Industrial Chemistry*, Wiley-VCH Verlag GmbH & Co. KGaA, 2000, pp. 1, 5–9.

209. K. Weissermel and H. Arpe, in *Industrial Organic Chemistry*, 4th edn., 2003, pp. 15–57.

210. J. Eppinger and K. Huang, *ACS Energy Lett.*, 2017, **2**, 188–195.

211. G. McGinnis, S. Prince, C. Biermann, and J. Lowrimore, *Carbohydr. Res.*, 1984, **128**, 51–60.

212. C. Le Berre, P. Serp, P. Kalck, and G. P. Torrence, in *Ullmanns Encyclopedia*, Wiley-VCH Verlag GmbH & Co. KGaA, 2013, pp. 1, 4–18.

213. N. Yoneda, S. Kusano, M. Yasui, P. Pujado, and S. Wilcher, *Appl. Catal. A Gen.*, 2001, **221**, 253–265.

214. P. M. Maitlis, A. Haynes, G. J. Sunleyb, and M. J. Howardb, *J. Chem. Soc., Dalt. Trans.*, 1996, 2187–2196.

215. M. J. Howard, M. D. Jones, M. S. Roberts, and S. A. Taylor, *Catal. Today*, 1993, **18**, 325–354.

216. T. W. Simpson, A. N. Sharpley, R. W. Howarth, H. W. Paerl, and K. R. Mankin, *J. Environ. Qual.*, 2008, **37**, 318–324.

217. T. Yamakawa, M. Hiroi, and S. Shinoda, *J. Chem. Soc. Trans.*, 1994, 2265–2269.

218. J. Grosselin, C. Mercier, G. Allmang, and F. Grass, *Organometallics*, 1991, **10**, 2126–2133.

219. T. Ohta, H. Takaya, M. Kitamura, K. Nagai, and R. Noyori, *J. Org. Chem.*, 1987, **52**, 3174–3176.

220. G. Allmang, F. Grass, J. Grosselin, and Mercier, *J. Mol. Catal.*, 1991, **66**.

221. J. Zhang, G. Leitus, Y. Ben-David, and D. Milstein, *J. Am. Chem. Soc.*, 2005, **127**, 10840–10841.

222. A. Dijksman, A. Marino-Gonzalez, A. M. I. Payeras, I. Arends, and R. A. Sheldon, *J. Am. Chem. Soc.*, 2001, **123**, 6826–6833.

223. M. J. Schultz and M. S. Sigman, *Tetrahedron*, 2006, **62**, 8227–8241.

224. C. Chen and S. H. Hong, *Org. Biomol. Chem.*, 2011, **9**, 20–26.

225. S. Murahashi, T. Naota, K. Ito, Y. Maeda, and H. Taki, *J. Org. Chem.*, 1987, **52**, 4319–4327.

226. K. B. Sharpless, K. Akashi, and K. Oshima, *Tetrahedron Lett.*, 1976, **17**, 2503–2506.

227. G. Csjernyik, A. Éll, L. Fadini, B. Pugin, and J. Bäckvall, *J. Org. Chem.*, 2002, **67**, 1657–1662.

228. B. M. Trost, M. Portnoy, and H. Kurihara, *J. Am. Chem. Soc.*, 1997, **119**, 836–837.

229. B. M. Trost, R. E. Brown, and F. D. Toste, *J. Am. Chem. Soc.*, 2000, **122**, 5877–5878.

230. D. B. Grotjahn and H. C. Lo, *Organometallics*, 1996, **15**, 2860–2862.

231. S. Muthusamy, N. Kumarswamyreddy, V. Kesavan, and S. Chandrasekaran, *Tetrahedron Lett.*, 2016, **57**, 5551–5559.

232. F. Gao and D. W. Goodman, *Phys. Chem. Chem. Phys.*, 2012, **14**, 6688–6697.

233. H. Over, O. Balmes, and E. Lundgren, *Catal. Today*, 2009, **145**, 236–242.

234. X. Cui, J. Zhou, Z. Ye, H. Chen, L. Li, M. Ruan, and J. Shi, *J. Catal.*, 2010, **270**, 310–317.

235. A. P. Amrute, C. Mondelli, M. A. G. Hevia, and J. Perez-Ramirez, *J. Phys. Chem. C*, 2011, **115**, 1056–1063.

236. J. Pérez-Ramírez, N. López, and E. V Kondratenko, *J. Phys. Chem. C*, 2010, **114**, 16660–16668.

237. Y. Wang, K. Jacobi, W.-D. Schöne, and G. Ertl, *J. Phys. Chem. B*, 2005, **109**, 7883–7893.

238. S. Heylen, N. Delcour, C. E. A. Kirschhock, and J. A. Martens, *ChemCatChem*, 2012, **4**, 1162–1166.

239. H. Liu and E. Iglesia, *J. Phys. Chem. B*, 2005, **109**, 2155–2163.

240. V. Srivastava, *Catal. Letters*, 2016, **146**, 2630–2640.

241. J. Pritchard, G. A. Filonenko, R. Van Putten, E. J. M. Hensen Ab, and E. A. Pidko, *Chem. Soc. Rev.*, 2015, 3808–3833.

242. H. Liu, R. Fang, Z. Li, and Y. Li, *Chem. Eng. Sci.*, 2015, **122**, 350–359.

243. X. Cui, A.-E. Surkus, K. Junge, C. Topf, J. Radnik, C. Kreyenschulte, and M. Beller, *Nat. Commun.*, 2016, **7**, 11326.

244. B. Dong, X. Guo, B. Zhang, X. Chen, J. Guan, Y. Qi, S. Han, and X. Mu, *Catalysts*, 2015, **5**, 2258–2270.

245. V. Ritleng, C. Sirlin, and M. Pfeffer, *Chem. Rev.*, 2002, **102**, 1731–1770.

246. X. Guo, J. Guan, B. Li, X. Wang, X. Mu, and H. Liu, *Sci. Rep.*, 2015, **5**, 16451.

247. X. Ying, W. Tiejun, M. Longlong, and C. Guanyi, *Energy Convers. Manag.*, 2012, **55**, 172–177.

248. M. Gatti, B. Lombardi, D. Gazzoli, G. Santori, F. Pompeo, and N. Nichio, *Catalysts*, 2016, **7**, 1–13.

249. M. Melián-Rodríguez, S. Saravanamurugan, S. Kegnæs, and A. Riisager, *Top. Catal.*, 2015, **58**, 1036–1042.

250. H. Ji, T. Mizugaki, K. Ebitani, and K. Kaneda, *Tetrahedron Lett.*, 2002, **43**, 7179–7183.

251. K. Motokura, D. Nishimura, K. Mori, T. Mizugaki, K. Ebitani, and K. Kaneda, *J. Am. Chem. Soc.*, 2004, **126**, 5662–5663.

252. K. Yamaguchi and N. Mizuno, *Angew. Chemie Int. Ed.*, 2003, **42**, 1480–1483.

253. D. G. Lahr and B. H. Shanks, *J. Catal.*, 2005, **232**, 386–394.

254. Y. N. Tchenar and A. Choukchou-braham, 2012, **35**, 673–681.

255. Y. Kim and S. Hwang, *Ind. Eng. Chem. Res.*, 2014, **53**, 12548–12552.

256. K. Yamaguchi and N. Mizuno, *Chem. – A Eur. J.*, 2003, **9**, 4353–4361.

257. P. Panagiotopoulou, D. I. Kondarides, and X. E. Verykios, *J. Phys. Chem. C*, 2011, **115**, 1220–1230.

258. A. Kleiman-Shwarsctein, A. B. Laursen, F. Cavalca, W. Tang, S. S. Dahl, and I. Chorkendorff, *Chem. Commun.*, 2012, **48**, 967–969.

259. X. Yang, X. Wang, and J. Qiu, *Appl. Catal. A Gen.*, 2010, **382**, 131–137.

260. T. L. Gunale and V. V. Mahajani, *J. Chem. Technol. Biotechnol.*, 2008, **83**, 1154–1162.

261. J. Béziat, M. Besson, P. Gallezot, and S. Durécu, *Ind. Eng. Chem. Res.*,

1999, **38**, 1310–1315.

262. V. Balek, T. Mitsuhashi, A. Watanabe, V. Zeleňák, J. Šubrt, P. Bezdička, and J. Boháček, *J. Colloid Interface Sci.*, 2003, **260**, 70–74.

263. K. Yamaguchi and N. Mizuno, *Angew. Chemie Int. Ed.*, 2002, **41**, 4538–4542.

264. C. Pan, K. Pelzer, K. Philippot, B. Chaudret, F. Dassenoy, P. Lecante, and M. Casanove, *J. Am. Chem. Soc.*, 2001, **123**, 7584–7593.

265. Y. Na, S. Park, S. B. Han, H. Han, S. Ko, and S. Chang, *J. Am. Chem. Soc.*, 2004, **126**, 250–258.

266. S. Bontemps, L. Vendier, and S. Sabo-Etienne, *J. Am. Chem. Soc.*, 2014, **136**, 4419–4425.

267. R. Martinez, M.-O. Simon, R. Chevalier, C. Pautigny, J.-P. Genet, and S. Darses, *J. Am. Chem. Soc.*, 2009, **131**, 7887–7895.

268. L. Wu, I. Fleischer, R. Jackstell, and M. Beller, *J. Am. Chem. Soc.*, 2013, **135**, 3989–3996.

269. D. Tanaka, Y. Sato, and M. Mori, *J. Am. Chem. Soc.*, 2007, **129**, 7730–7731.

270. S. H. Hong, A. G. Wenzel, T. T. Salguero, M. W. Day, and R. H. Grubbs, *J. Am. Chem. Soc.*, 2007, **129**, 7961–7968.

271. M. Murakami and S. Hori, *J. Am. Chem. Soc.*, 2003, **125**, 4720–4721.

272. Y. Chen, D. M. Ho, and C. Lee, *J. Am. Chem. Soc.*, 2005, **127**, 12184–12185.

273. M. Pagliaro, S. Campestrini, and R. Ciriminna, *Chem. Soc. Rev.*, 2005, **34**, 837–845.

274. T. Punniyamurthy, S. Velusamy, and J. Iqbal, *Chem. Rev.*, 2005, **105**, 2329–2364.

275. D. Bhattarai, J. Lee, and G. Keum, in *Encyclopedia of Reagents for Organic Synthesis*, John Wiley & Sons, Ltd, 2001, pp. 1–6.

276. K. Yamaguchi and N. Mizuno, *Synlett*, 2010, 2365–2382.

277. N. Mizuno and K. Yamaguchi, *Catal. Today*, 2008, **132**, 18–26.

278. J. W. Kim, K. Yamaguchi, and N. Mizuno, *Angew. Chemie - Int. Ed.*, 2008, **47**, 9249–9251.

279. M. Kotani, T. Koike, K. Yamaguchi, and N. Mizuno, *Green Chem.*, 2006, **8**, 735–741.

280. K. Mori, K. Yamaguchi, T. Mizugaki, K. Ebitani, and K. Kaneda, *Chem. Commun.*, 2001, 461–462.

281. D. S. Mannel, S. S. Stahl, and T. W. Root, *Org. Process Res. Dev.*, 2014, **18**, 1503–1508.

282. J. B. Brazier, K. Hellgardt, and K. K. (Mimi) Hii, *React. Chem. Eng.*, 2017, **2**, 60–67.

283. C. Hao, S. Wang, M. Li, L. Kang, and X. Ma, *Catal. Today*, 2011, **160**, 184–190.

284. J. W. Kim, T. Koike, M. Kotani, K. Yamaguchi, and N. Mizuno, *Chem. - A Eur. J.*, 2008, **14**, 4104–4109.

285. K. Yamaguchi, T. Koike, M. Kotani, M. Matsushita, S. Shinachi, and N. Mizuno, *Chem. – A Eur. J.*, 2005, **11**, 6574–6582.

286. D. V. Bavykin, A. A. Lapkin, S. T. Kolaczkowski, and P. K. Plucinski, *Appl. Catal. A Gen.*, 2005, **288**, 175–184.

287. A. Dijksman, I. W. C. E. Arends, and R. a. Sheldon, *Chem. Commun.*, 1999, **2**, 1591–1592.

288. K. Yamaguchi, K. Mori, T. Mizugaki, K. Ebitani, and K. Kaneda, *J. Am. Chem. Soc.*, 2000, **122**, 7144–7145.

289. C. Kohlpaintner, M. Schulte, J. Falbe, P. Lappe, J. Weber, and G. D. Frey, in *Ullmann's Encyclopedia of Industrial Chemistry*, Wiley-VCH Verlag GmbH & Co. KGaA, 2000, pp. 6–7.

290. Y. Gorbanev, Ph.D. Dissertation - Technical University of Denmark, 2012.

291. S. Akbayrak, Y. without dot]n Tonbul, and S. Ozkar, *Dalt. Trans.*, 2016, **45**, 10969–10978.

292. Y. Kuwahara, W. Kaburagi, and T. Fujitani, *RSC Adv.*, 2014, **4**, 45848–45855.

293. L. Claes, J. Verduyckt, I. Stassen, B. Lagrain, and D. E. De Vos, *Chem. Commun.*, 2015, **51**, 6528–6531.

294. K. Yamaguchi, T. Koike, J. W. Kim, Y. Ogasawara, and N. Mizuno, *Chem. - A Eur. J.*, 2008, **14**, 11480–11487.

295. Q. Dai, S. Bai, Z. Wang, X. Wang, and G. Lu, *Appl. Catal. B Environ.*, 2012, **126**, 64–75.

296. A. R. Derk, G. M. Moore, S. Sharma, E. W. McFarland, and H. Metiu, *Top. Catal.*, 2014, **57**, 118–124.

297. M. Farahmandjou and M. Zarinkamar, *J. Ultrafine Grained Nanostructured Mater.*, 2015, **48**, 5–10.

298. H. Kishida, F. Jin, X. Yan, T. Moriya, and H. Enomoto, *Carbohydr. Res.*, 2006, **341**, 2619–2623.

299. Z. Srokol, A.-G. Bouche, A. van Estrik, R. C. J. Strik, T. Maschmeyer, and J. A. Peters, *Carbohydr. Res.*, 2004, **339**, 1717–1726.

300. E. Takezawa, S. Sakaguchi, and Y. Ishii, *Org. Lett.*, 1999, **1**, 713–5.

301. D. Yang and C. Zhang, *J. Org. Chem.*, 2001, **66**, 4814–4818.

302. K. Yamaguchi, J. W. Kim, J. He, and N. Mizuno, *J. Catal.*, 2009, **268**, 343–349.

303. V. V. Costa, M. J. Jacinto, L. M. Rossi, R. Landers, and E. V. Gusevskaya, *J. Catal.*, 2011, **282**, 209–214.

304. K. S. Kim and M. A. Barteau, *Langmuir*, 1988, **4**, 945–953.

305. J. M. Vohs and M. A. Barteau, *Surf. Sci.*, 1988, **201**, 481–502.

306. P. G. Blake and K. J. Hole, *J. Chem. Soc. B*, 1966, 577–579.

307. V. I. Sobolev and K. Y. Koltunov, *Appl. Catal. A Gen.*, 2013, **466**, 45–50.

308. C. Zhang, T. Wang, X. Liu, and Y. Ding, *Chinese J. Catal.*, 2016, **37**, 502–509.

309. M. Misono, *Catal. Rev.*, 1987, **29**, 269–321.

310. J. J. Berzelius, *Ann. Phys.*, 1826, **82**, 369–392.

311. J. F. Keggin, *Nature*, 1933, **131**, 908–909.

312. C. Ritchie, A. Ferguson, H. Nojiri, H. N. Miras, Y. F. Song, D. L. Long, E. Burkholder, M. Murrie, P. Kögerler, E. K. Brechin, and L. Cronin, *Angew. Chemie - Int. Ed.*, 2008, **47**, 5609–5612.

313. C. Ritchie, A. Ferguson, H. Nojiri, H. N. Miras, Y. Song, D. Long, E. Burkholder, M. Murrie, P. Kögerler, E. K. Brechin, and L. Cronin, *Angew. Chemie*, 2008, **120**, 5691–5694.

314. I. M. Mbomekalle, B. Keita, L. Nadjo, P. Berthet, K. I. Hardcastle, C. L. Hill, and T. M. Anderson, *Inorg. Chem.*, 2003, **42**, 1163–1169.

315. H. N. Miras, J. Yan, D.-L. Long, and L. Cronin, *Chem. Soc. Rev. Chem. Soc. Rev*, 2012, **41**, 7403–7430.

316. X. López, J. J. Carbó, C. Bo, and J. M. Poblet, *Chem. Soc. Rev.*, 2012, **41**, 7537–71.

317. F. Li and L. Xu, *Dalton Trans.*, 2011, **40**, 4024–4034.

318. M. T. Pope and A. Müller, *Angew. Chemie Int. Ed. English*, 1991, **30**, 34–48.

319. C. Li, W. Qi, H. Cao, Y. Qi, S. Zhang, S. Xu, J. Sun, and S. Guo, *Biomed. Pharmacother.*, 2016, **79**, 78–86.

320. H. Stephan, M. Kubeil, F. Emmerling, and C. E. Müller, *Eur. J. Inorg. Chem.*, 2013, 1585–1594.

321. S. Nlate and C. Jahier, *Eur. J. Inorg. Chem.*, 2013, 1606–1619.

322. S. Mandic, M. R. Healey, J. M. Gotthardt, K. G. Alley, R. W. Gable, C. Ritchie, and C. Boskovic, *Eur. J. Inorg. Chem.*, 2013, 1631–1634.

323. S. Zhao, L. Huang, and Y. F. Song, *Eur. J. Inorg. Chem.*, 2013, **40**, 1659–1663.

324. X. F. Wang, J. Cao, K. L. Huang, Y. Q. Xu, Y. N. Chi, and C. W. Hu, *Eur. J. Inorg. Chem.*, 2013, 1788–1792.

325. S. Chakraborty, L. Jin, Y. Li, Y. Liu, T. Dutta, D. M. Zhu, X. Yan, A. Keightley, and Z. Peng, *Eur. J. Inorg. Chem.*, 2013, 1799–1807.

326. A. Chatkon, P. B. Chatterjee, M. A. Sedgwick, K. J. Haller, and D. C. Crans, *Eur. J. Inorg. Chem.*, 2013, 1859–1868.

327. E. Ishikawa and T. Yamase, *Eur. J. Inorg. Chem.*, 2013, **28**, 1917–1925.

328. R. Q. Meng, B. Wang, H. M. Sui, B. Li, W. Song, L. X. Wu, B. Zhao, and L. H. Bi, *Eur. J. Inorg. Chem.*, 2013, 1935–1942.

329. R. Ishimoto, K. Kamata, and N. Mizuno, *Eur. J. Inorg. Chem.*, 2013, 1943–1950.

330. Y. Luo, X. Yu, and H. Zhang, *CrystEngComm*, 2014, **16**, 6664–6669.

331. A. Bijelic and A. Rompel, *Coord. Chem. Rev.*, 2015, **299**, 22–38.

332. A. Lesbani, A. Marpaung, M. Verawaty, H. Rizki Amalia, and R. Mohadi, *J. Pure Appl. Chem. Res.*, 2015, **4**, 5–11.

333. Y. Ren, M. Wang, X. Chen, B. Yue, and H. He, *Materials.*, 2015, **8**, 1545–1567.

334. C. Wang, C. Liu, Y. Hu, X. Bu, T. Zhao, K. Chou, and Q. Li, *J. Mater. Chem. A*, 2015, **3**, 21424–21427.

335. Y.-F. Qiu, H. Liu, J.-X. Liu, C. Zhang, Z. Ma, P.-A. Hu, and G.-G. Gao, *J.*

Mater. Chem. C, 2015, **3**, 6322–6328.

336. T. Yamase, *J. Mater. Chem.*, 2005, **15**, 4773.

337. K. Nomiya, H. Torii, T. Hasegawa, Y. Nemoto, K. Nomura, K. Hashino, M. Uchida, Y. Kato, K. Shimizu, and M. Oda, *J. Inorg. Biochem.*, 2001, **86**, 657–667.

338. A. Corma, *Chem. Rev.*, 1995, **95**, 559–614.

339. R. J. J. Jansen, H. M. van Veldhuizen, M. A. Schwegler, and H. van Bekkum, *Recl. des Trav. Chim. des Pays-Bas*, 1994, **113**, 115–135.

340. I. V Kozhevnikov, *Chem. Rev.*, 1998, **98**, 171–198.

341. T. R. Halbert, T. C. Ho, E. I. Stiefel, R. R. Chianelli, and M. Daage, *J. Catal.*, 1991, **130**, 116–129.

342. E. Cadot, V. Béreau, B. Marg, S. Halut, and F. Sécheresse, *Inorg. Chem.*, 1996, **35**, 3099–3106.

343. E. Cadot, V. Béreau, and F. Sécheresse, *Inorg. Chim. Acta*, 1996, **252**, 101–106.

344. E. Cadot, B. Salignac, and S. Halut, *Angew. Chem. Int. Ed.*, 1998, **37**, 611–613.

345. V. Béreau, E. Cadot, H. Bögge, A. Müller, and F. Sécheresse, *Inorg. Chem.*, 1999, **38**, 5803–5808.

346. R. J. Errington, R. L. Wingad, W. Clegg, and M. R. J. Elsegood, *Angew. Chemie - Int. Ed.*, 2000, **39**, 3884–3886.

347. A. Bino, M. Ardon, D. Lee, B. Spingler, and S. J. Lippard, *J. Am. Chem. Soc.*, 2002, **124**, 4578–4579.

348. P. Gouzerh and M. Che, *Actual. Chim.*, 2006, **298**, 9–22.

349. H. Sartzi, H. N. Miras, L. Vilà- Nadal, D. Long, and L. Cronin, *Angew. Chemie Int. Ed.*, 2015, **54**, 15488–15492.

350. C. M. Granadeiro, B. De Castro, S. S. Balula, and L. Cunha-Silva, *Polyhedron*, 2013, **52**, 10–24.

351. B. Dawson, *Acta Crystallogr.*, 1953, **6**, 113–126.

352. M. C. Marignac, *Ann. Chim. Phys.*, 1864, **4**, 5–76.

353. A. Werner, *Neure Anschauungen auf dem Gebiete der Anorganischen Chemie*, 1920.

354. A. Werner, *Berichte der Dtsch. Chem. Gesellschaft*, 1907, **40**, 15–69.

355. L. Pauling, *J. Am. Chem. Soc.*, 1929, **51**, 2868–2880.

356. J. F. Keggin, *Proc. R. Soc. London A Math. Phys. Eng. Sci.*, 1934, **144**, 75–100.

357. K. Matveev, *Chem. Informationsd.*, 1977, **8**, 2199–2924.

358. I. V. Kozhevnikov and K. I. Matveev, *Appl. Catal.*, 1983, **5**, 135–150.

359. I. V. Kozhevnikov, *Stud. Surf. Sci. Catal.*, 1994, **90**, 21–34.

360. I. V Kozhevnikov, *Russ. Chem. Rev.*, 1987, **56**, 811.

361. J. B. Moffat, *Chem. Eng. Commun.*, 1989, **83**, 9–29.

362. G. M. Maksimov and I. V Kozhevnikov, *React. Kinet. Catal. Lett.*, 1989, **39**, 317–322.

363. K. Y. Lee, N. Mizuno, T. Okuhara, and M. Misono, *Bull. Chem. Soc. Jpn.*, 1989, **62**, 1731–1739.

364. M. Fournier, C. Louis, M. Che, P. Chaquin, and D. Masure, *J. Catal.*, 1989, **119**, 400–414.

365. M. Schwegler, M. Floor, and H. van Bekkum, *Tetrahedron Lett.*, 1988, **29**, 823–826.

366. A. Aoshima, S. Tonomura, and S. Yamamatsu, *Polym. Adv. Technol.*, 1990, **1**, 127–132.

367. M. Misono and N. Nojiri, *Appl. Catal.*, 1990, **64**, 1–30.

368. O. A. Kholdeeva, A. V Golovin, and I. V Kozhevnikov, *React. Kinet. Catal. Lett.*, 1992, **46**, 107–113.

369. I. V. Kozhevnikov, *Catal. Rev.*, 1995, **37**, 311–352.

370. R. Neumann, A. M. Khenkin, and M. Dahan, *Angew. Chemie Int. Ed. English*, 1995, **34**, 1587–1589.

371. S. Shikata, T. Okuhara, and M. Misono, *J. Mol. Catal. A Chem.*, 1995, **100**, 49–59.

372. T. Okuhara, N. Mizuno, and M. Misono, *Adv. Catal.*, 1996, **41**, 113–252.

373. I. V. Kozhevnikov, A. Sinnema, A. J. A. Van Der Weerdt, and H. Van Bekkum, *J. Mol. Catal. A Chem.*, 1997, **120**, 63–70.

374. S. Shikata, S. Nakata, T. Okuhara, and M. Misono, *J. Catal.*, 1997, **166**, 263–271.

375. G. Baronetti, L. Briand, U. Sedran, and H. Thomas, *Appl. Catal. A Gen.*, 1998, **172**, 265–272.

376. R. Ben-Daniel, A. M. Khenkin, and R. Neumann, *Chem. – A Eur. J.*, 2000, **6**, 3722–3728.

377. T. Wijesekera, J. Lyons, and P. Ellis, 2000, WO0009262 A1.

378. A. N. Kharat, P. Pendleton, A. Badalyan, M. Abedini, and M. M. Amini, *J. Mol. Catal. A Chem.*, 2001, **175**, 277–283.

379. L. E. Briand, G. T. Baronetti, and H. J. Thomas, *Appl. Catal. A Gen.*, 2003, **256**, 37–50.

380. N. Mizuno, K. Yamaguchi, and K. Kamata, *Coord. Chem. Rev.*, 2005, **249**, 1944–1956.

381. G. Maayan, B. Ganchegui, W. Leitner, and R. Neumann, *Chem. Commun.*, 2006, 2230–2232.

382. T. Voitl and P. von Rohr, *ChemSusChem*, 2008, **1**, 763–769.

383. L. M. Sanchez, Á. G. Sathicq, G. T. Baronetti, H. J. Thomas, and G. P. Romanelli, *Can. J. Chem.*, 2013, **91**, 137–142.

384. M. N. Sokolov, S. A. Adonin, E. V Peresypkina, P. A. Abramov, A. I. Smolentsev, D. I. Potemkin, P. V Snytnikov, and V. P. Fedin, *Inorganica Chim. Acta*, 2013, **394**, 656–662.

385. M. Moudjahed, L. Dermeche, S. Benadji, T. Mazari, and C. Rabia, *J. Mol. Catal. A Chem.*, 2016, **414**, 72–77.

386. G. Li, Y. Ding, J. Wang, X. Wang, and J. Suo, *J. Mol. Catal. A Chem.*, 2007, **262**, 67–76.

387. C. L. Hill and C. M. Prosser-McCartha, *Coord. Chem. Rev.*, 1995, **143**, 407–455.

388. B. Keita and L. Nadjo, *J. Mol. Catal. A Chem.*, 2007, **262**, 190–215.

389. C. Zhang, P. Ma, H. Chen, J. Wang, and J. Niu, *J. Coord. Chem.*, 2011, **64**, 2178–2185.

390. N. Aramesh, B. Yadollahi, and V. Mirkhani, *Inorg. Chem. Commun.*, 2013, **28**, 37–40.

391. X. Cao, J. Ren, C. Xu, K. Zhang, C. Zhan, and J. Lan, *Chinese J. Chem. Eng.*, 2013, **21**, 500–506.

392. M. Tao, D. Zhang, X. Deng, X. Li, J. Shi, and X. Wang, *Chem. Commun.*, 2016, **52**, 3332–3335.

393. R. Sheldon, *Top. Curr. Chem.*, 1993, **164**, 21–43.

394. K. I. Matveev, E. G. Zhizhina, N. B. Shitova, and L. I. Kuznetsova, *Kinet. i Katal.*, 1977, **18**, 380–386.

395. I. V. Kozhevnikov, *J. Mol. Catal. A Chem.*, 1997, **117**, 151–158.

396. Z. Yang, N. Jia, N. Zhang, X. Zhao, T. Li, Y. Wei, and W. Chen, *Chem.*

Bull., 2014, **77**, 521–526.

397. S. Fujibayashi, K. Nakayama, M. Hamamoto, S. Sakaguchi, Y. Nishiyama, and Y. Ishii, *J. Mol. Catal. A-chemical*, 1996, **110**, 105–117.

398. M. Hamamoto, K. Nakayama, Y. Nishiyama, and Y. Ishii, *J. Org. Chem.*, 1993, **58**, 6421–6425.

399. N. Mizuno and M. Misono, *Chem. Rev.*, 1998, **98**, 199–218.

400. Y. Kim, H. Kim, J. Lee, K. Sim, Y. Han, and H. Paik, *Appl. Catal. A Gen.*, 1997, **155**, 15–26.

401. H. Ogawa, H. Fujinami, K. Taya, and S. Teratani, *Bull. Chem. Soc. Jpn.*, 1984, **57**, 1908–1913.

402. E. Monflier, S. Tilloy, E. Blouet, Y. Barbaux, and A. Mortreux, *J. Mol. Catal. A Chem.*, 1996, **109**, 27–35.

403. K. Nowińska and D. Dudko, *Appl. Catal. A Gen.*, 1997, **159**, 75–87.

404. I. Bar-Nahum, A. M. Khenkin, and R. Neumann, *J. Am. Chem. Soc.*, 2004, **126**, 10236–10237.

405. N. Mizuno, T. Hirose, M. Tateishi, and M. Iwamoto, *J. Mol. Catal.*, 1994, **88**, L125–L131.

406. R. Neumann and M. Lissel, *J. Org. Chem.*, 1989, **54**, 4607–4610.

407. M. A. Fedotov and R. I. Maksimovskaya, *J. Struct. Chem.*, 2006, **47**, 952–978.

408. W. G. Klemperer and K. A. Marek, *Eur. J. Inorg. Chem.*, 2013, **28**, 1762–1771.

409. R. I. Maksimovskaya and K. G. Burtseva, *Polyhedron*, 1985, **4**, 1559–1562.

410. G. Modugno, A. Monney, M. Bonchio, M. Albrecht, and M. Carraro, *Eur. J. Inorg. Chem.*, 2014, **2014**, 2356–2360.

411. F. Lin and Y.-H. (Cathy) Chin, *J. Catal.*, 2016, **341**, 136–148.

412. S. Boujday, J. Blanchard, R. Villanneau, J.-M. Krafft, C. Geantet, C. Louis, M. Breysse, and A. Proust, *ChemPhysChem*, 2007, **8**, 2636–2642.

413. V. Kogan, Z. Aizenshtat, and R. Neumann, *New J. Chem.*, 2002, **26**, 272–274.

414. M. Masteri-Farahani, J. Movassagh, F. Taghavi, P. Eghbali, and F. Salimi, *Chem. Eng. J.*, 2012, **184**, 342–346.

415. Y. Onoue, Y. Mitzutani, S. Akiyama, and Y. Izumi, *Chemtech*, 1978, **8**, 432–435.

416. M. Misono, I. Ono, G. Koyano, and A. Aoshima, *Pure Appl. Chem.*, 2000, **72**, 1305–1311.

417. F. Joó, *ChemSusChem*, 2008, **1**, 805–808.

418. S. Fukuzumi, T. Kobayashi, and T. Suenobu, *ChemSusChem*, 2008, **1**, 827–834.

419. S. Enthaler, *ChemSusChem*, 2008, **1**, 801–804.

420. C. Fellay, P. J. Dyson, and G. Laurenczy, *Angew. Chemie Int. Ed.*, 2008, **47**, 3966–3968.

421. B. Loges, A. Boddien, H. Junge, and M. Beller, *Angew. Chemie Int. Ed.*, 2008, **47**, 3962–3965.

422. R. Sato, H. Choudhary, S. Nishimura, and K. Ebitani, *Org. Process Res. Dev.*, 2015, **19**, 449–453.

423. H. Choudhary, S. Nishimura, and K. Ebitani, *Appl. Catal. B Environ.*, 2015, **162**, 1–10.

424. J. Yun, F. Jin, A. Kishita, K. Tohji, H. Enomoto, and J. Y. and F. J. and A. K. and K. T. and H. Enomoto, *J. Phys. Conf. Ser.*, 2010, **215**, 12126.

425. V. P. Muiuane, M. Ferreira, P. Bignet, A. P. Bettencourt, and P. Parpot, *J. Environ. Chem. Eng.*, 2013, **1**, 1237–1244.

426. F. M. Jin, J. Yun, G. M. Li, A. Kishita, K. Tohji, and H. Enomoto, *Green Chem.*, 2008, **10**, 612–615.

427. J. Yun, G. Yao, F. Jin, H. Zhong, A. Kishita, K. Tohji, H. Enomoto, and L. Wang, *AIChE J.*, 2016, **62**, 3657–3663.

428. F. Jin, J. Yun, G. Li, A. Kishita, H. Enomoto, and K. Tohji, *Abstr. Pap. Am. Chem. Soc.*, 2007, 234.

429. J. Li, D.-J. Ding, L. Deng, Q.-X. Guo, and Y. Fu, *ChemSusChem*, 2012, **5**, 1313–1318.

430. M. Liu, W. Deng, Q. Zhang, Y. Wang, and Y. Wang, *Chem. Commun.*, 2011, **47**, 9717–9719.

431. I. A. Weinstock, R. H. Atalla, R. S. Reiner, M. A. Moen, K. E. Hammel, C. J. Houtman, C. L. Hill, and M. K. Harrup, *J. Mol. Catal. A Chem.*, 1997, **116**, 59–84.

432. D. W. Jbach, J. Tenbrink, M. Schmidt, and D. F. Kohler, *http://www.oxfa.eu/en/process/*.

433. D. B. Dubovik, T. I. Tikhomirova, A. V Ivanov, P. N. Nesterenko, and O. A. Shpigun, *J. Anal. Chem.*, 2003, **58**, 802–819.

434. E. Dorokhova and I. Alimarin, *Russ. Chem. Rev.*, 1965, **34**, 574–594.

435. G. Legler, C. M. Müller-Platz, M. Mentges-Hettkamp, G. Pflieger, and E. Jülich, *Anal. Biochem.*, 1985, **150**, 278–287.

436. M. L. Matheke, G. Kessler, and K. M. Chan, *Clin. Chem.*, 1987, **33**, 2109–2110.

437. G. Russell Warnick, C. Mayfield, J. Benderson, J.-S. Chen, and J. J. Albers, *Am. J. Clin. Pathol.*, 1982, **78**, 718–723.

438. S. . Bareyt, S. . Piligkos, B. . Hasenknopf, P. . Gouzerh, E. . Lacôte, S. . Thorimbert, and M. . Malacria, *Angew. Chemie - Int. Ed.*, 2003, **42**, 3404–3406.

439. E. N. Semenovskaya, *J. Anal. Chem. USSR*, 1987, **41**, 1339–1346.

440. J. F. W. Keana, M. D. Ogan, Y. Lu, M. Beer, and J. Varkey, *J. Am. Chem. Soc.*, 1985, **107**, 6714–6715.

441. J. F. W. Keana, Y. Wu, and G. Wu, *J. Org. Chem.*, 1987, **52**, 2571–2576.

442. L. Wang, B. B. Zhou, and J. R. Liu, *Prog. Chem.*, 2013, **25**, 1131–1141.

443. V. Goovaerts, K. Stroobants, G. Absillis, and T. N. Parac-vogt, *Inorganics*, 2015, **3**, 230–245.

444. G. Chottard, M. Michelon, M. Hervé, and G. Hervé, *Biochim. Biophys. Acta - Protein Struct. Mol. Enzymol.*, 1987, **916**, 402–410.

445. R. H. Kimberlin and C. A. Walker, *Arch. Virol.*, 1983, **78**, 9–18.

446. T. Yamase, H. Fujita, and K. Fukushima, *Inorganica Chim. Acta*, 1988, **151**, 15–18.

447. R. H. Glew, M. S. Czuczman, W. F. Diven, R. L. Berens, M. T. Pope, and D. E. Katsoulis, *Comp. Biochem. Physiol. Part B Comp. Biochem.*, 1982, **72**, 581–590.

448. D. Dormont, B. Spire, F. Barré-Sinoussi, L. Montagnier, and J. C. Chermann, *Ann. l'Institut Pasteur / Virol.*, 1985, **136**, 75–83.

449. F. Bussereau, M. Picard, J. Blancou, and P. Sureau, *Acta Virol.*, 1988, **32**, 33–49.

450. J. T. Rhule, C. L. Hill, D. a. Judd, and R. F. Schinazi, *Chem. Rev.*, 1998, **98**, 327–358.

451. K. Narasimhan, S. Pillay, N. R. Bin Ahmad, Z. Bikadi, E. Hazai, L. Yan, P. R. Kolatkar, K. Pervushin, and R. Jauch, *ACS Chem. Biol.*, 2011, **6**, 573–581.

452. J. Wang, X. Qu, Y. Qi, J. Li, X. Song, L. Li, D. Yin, K. Xu, and J. Li, *PLoS One*, 2014, **9**, e98292.

453. E. Bae, J. Won, B. Hee, J. Yeo, J. Yoon, H. Joon, and W. Choi, *Chemosphere*, 2008, **72**, 174–181.

454. D.-D. Zhang, P.-F. Guo, L.-L. Hu, X.-W. Chen, and J.-H. Wang, *J. Mater. Chem. B*, 2017, **5**, 750–756.

455. Z. Dong, R. Tan, J. Cao, Y. Yang, C. Kong, J. Du, S. Zhu, Y. Zhang, J. Lu, B. Huang, and S. Liu, *Eur. J. Med. Chem.*, 2011, **46**, 2477–2484.

456. S. M. Hosseini, E. Amini, M. T. Kheiri, and P. Mehrbod, *Int J Mo1 Cell Med Winter*, 2012, **1**, 21–29.

457. T. Shimidzu, A. Ohtani, M. Aiba, and K. Honda, *J. Chem. Soc. Faraday Trans. 1*, 1988, **84**, 3941–3949.

458. J. Smit, *Nature*, 1958, **181**, 1530–1531.

459. Y. Vlasov, M. Miloshova, P. Antonov, A. Efa, and E. Bychkov, *Sov. Electrochem.*, 1983, **19**, 1054–1059.

460. M. Tatsumisago and T. Minami, *J. Am. Ceram. Soc.*, 1989, **72**, 484–486.

461. O. Nakamura and I. Ogino, *Mater. Res. Bull.*, 1982, **17**, 231–234.

462. O. Nakamura, I. Ogino, and T. Kodama, *Solid State Ionics*, 1981, **3**, 347–351.

463. O. Nakamura, I. Ogino, R. N. Castellano, and J. B. Goodenough, *Solid State Ionics*, 1982, **6**, 337–339.

464. M. Kourasi, R. G. A. Wills, A. A. Shah, and F. C. Walsh, *Electrochim. Acta*, 2014, **127**, 454–466.

465. A. Hardwick, P. G. Dickens, and R. C. T. Slade, *Solid State Ionics*, 1984, **13**, 345–350.

466. H. Wu, *J. Biol. Chem.*, 1920, **43**, 189.

467. F. Kehrmann, *Zeitschrift für Anorg. Chemie*, 1892, **1**, 423–441.

468. A. F. Wells, *Structural Inorganic Chemistry*, Oxfor University Press, Oxford, 1st edn., 1947.

469. G. A. Tsigdinos, Bachelor's Thesis - Boston University, 1952.

470. G. A. Tsigdinos, Boston University, 1961.

471. L. C. W. Baker and J. S. Figgis, *J. Am. Chem. Soc.*, 1970, **92**, 3794 – 3797.

472. R. Strandberg, *Acta Chem. Scand.*, 1975, 29a, 350–358.

473. H. d'Amour, *Acta Crystallogr. Sect. B Struct. Crystallogr. Cryst. Chem.*, 1976, **32**, 729–740.

474. K. Yamamura and Y. Sasaki, *J. Chem. Soc. Chem. Commun.*, 1973, 648–649.

475. M. T. Pope, *Inorg. Chem.*, 1976, **15**, 2008–2010.

476. M. T. Pope, *Inorg. Chem.*, 1972, **11**, 1973–1974.

477. X. L. Fernández, Ph. D. Dissertation - Unicersity of Rovira I Virgili, 2003.

478. J. Zhang, A. M. Bond, P. J. S. Richardt, and A. G. Wedd, *Inorg. Chem.*, 2004, **43**, 8263–8271.

479. S. Matsunaga, E. Miyamae, I. Yusuke, and K. Nomiya, *Inorganics*, 2016, **4**, 1–10.

480. F. Q. Zhang, W. Guan, L. K. Yan, Y. T. Zhang, M. T. Xu, E. Hayfron-Benjamin, and Z. M. Su, *Inorg. Chem.*, 2011, **50**, 4967–4977.

481. R. Massart, R. Contant, J. M. Fruchart, J. P. Ciabrini, and M. Fournier, *Inorg. Chem.*, 1977, **16**, 2916–2921.

482. R. G. Finke, M. W. Droege, P. J. Domaillezb, and P. J. Domaille, *Inorg. Chem.*, 1987, **26**, 3886–3896.

483. S. Sheshmani, M. A. Fashapoyeh, M. Mirzaei, B. A. Rad, S. N. Ghortolmesh, and M. Yousefi, *Indian J. Chem. - Sect. A Inorganic, Phys. Theor. Anal. Chem.*, 2011, **50**, 1725–1729.

484. L. E. Briand, H. J. Thomas, and G. T. Baronetti, *Appl. Catal. A Gen.*, 2000, **201**, 191–202.

485. R. Contant, M. Abbessi, and J. Canny, *Inorg. Chem.*, 1997, **36**, 4961–4967.

486. J. H. Choi, T. H. Kang, Y. Bang, J. K. Lee, J. C. Song, and I. K. Song, *Catal. Commun.*, 2015, **65**, 66–71.

487. D. R. Park, H. Kim, J. C. Jung, S. H. Lee, and I. K. Song, *Res. Chem. Intermed.*, 2008, **34**, 845–851.

488. Y. Sakai, A. Shinohara, K. Hayashi, and K. Nomiya, *Eur. J. Inorg. Chem.*, 2006, **2006**, 163–171.

489. H.-S. Liu, J. Peng, and L.-X. Wang, *Zeitschrift für Anorg. und Allg. Chemie*, 2009, **635**, 2688–2691.

490. J. Bartis, Y. Kunina, M. Blumenstein, and L. C. Francesconi, *Inorg. Chem.*, 1996, **35**, 1497–1501.

491. X. Wu, H. Cai, Q. Wu, and W. Yan, *Mater. Lett.*, 2016, **181**, 1–3.

492. L. Sanchez, A. Sathicq, G. Baronetti, and H. Thomas, *Curr. Catal.*, 2014, **3**, 147–154.

493. N. S. Antonova, J. J. Carbó, U. Kortz, O. A. Kholdeeva, and J. M. Poblet, *J. Am. Chem. Soc.*, 2010, **132**, 7488–7497.

494. D. R. Park, S. Park, Y. Bang, and I. K. Song, *Appl. Catal. A Gen.*, 2010, **373**, 201–207.

495. H. Yasuda, L.-N. He, T. Sakakura, and C. Hu, *J. Catal.*, 2005, **233**, 119–122.

496. D. Jabbour, B. Keita, I. M. Mbomekalle, L. Nadjo, and U. Kortz, *Eur. J. Inorg. Chem.*, 2004, **4**, 2036–2044.

497. N. J. Crano, R. C. Chambers, V. M. Lynch, and M. A. Fox, *J. Mol. Catal. A Chem.*, 1996, **114**, 65–75.

498. D. E. Katsoulis and M. T. Pope, *J. Chem. Soc.{,} Dalt. Trans.*, 1989, 1483–1489.

499. E. Arendt, S. Zehri, P. Eloy, and E. M. Gaigneaux, *Eur. J. Inorg. Chem.*, 2012, **2012**, 2792–2801.

500. U. Kortz, S. S. Hamzeh, and N. A. Nasser, *Chem. - A Eur. J.*, 2003, **9**, 2945–2952.

501. O. A. Kholdeeva, *Eur. J. Inorg. Chem.*, 2013, 1595–1605.

502. M. Ammam, *J. Mater. Chem. A*, 2013, **1**, 6291–6312.

503. S. G. Mitchell, C. Streb, H. N. Miras, T. Boyd, D.-L. Long, and L. Cronin, *Nat. Chem.*, 2010, **2**, 308–312.

504. F. Zhang, H. Wu, D. Cao, and X. Zhang, *J. Mol. Struct. THEOCHEM*, 2005, **755**, 119–126.

505. H. Wu, *J. Biol. Chem.*, 1920, **43**, 189–220.

506. I.-M. Mbomekalle, Y. W. Lu, B. Keita, and L. Nadjo, *Inorg. Chem. Commun.*, 2004, **7**, 86–90.

507. C. L. Hill and R. B. Brown, *J. Am. Chem. Soc.*, 1986, **108**, 536–538.

508. F. Corigliano and S. Di Pasquale, *Inorganica Chim. Acta*, 1975, **12**, 99–101.

509. Z. Zhu, R. Tain, and C. Rhodes, *Can. J. Chem.*, 2003, **81**, 1044–1050.

510. R. Contant and R. Thouvenot, *Inorganica Chim. Acta*, 1993, **212**, 41–50.

511. G. Romanelli, J. C. Autino, G. Baronetti, and H. Thomas, *Molecules*, 2001, **6**, 1006–1011.

512. G. Baronetti, H. Thomas, and C. A. Querini, *Appl. Catal. A Gen.*, 2001, **217**, 131–141.

513. D. K. Lyon and R. G. Finke, *Inorg. Chem.*, 1990, **29**, 1787–1789.

514. Y. Lin and R. G. Finke, *Inorg. Chem.*, 1994, **33**, 4891–4910.

515. D. Mansuy, J. F. Bartoli, P. Battioni, D. K. Lyon, and R. G. Finke, *J. Am. Chem. Soc.*, 1991, **113**, 7222–7226.

516. A. M. Khenkin and R. Neumann, *Inorg. Chem.*, 2000, **39**, 3455–3462.

517. J. Hu and R. C. Burns, *J. Mol. Catal. A Chem.*, 2002, **184**, 451–464.

518. K. Nomiya, Y. Nemoto, T. Hasegawa, and S. Matsuoka, *J. Mol. Catal. A Chem.*, 2000, **152**, 55–68.

519. K. Nomiya, K. Hashino, Y. Nemoto, and M. Watanabe, *J. Mol. Catal. A Chem.*, 2001, **176**, 79–86.

520. G. P. Romanelli, G. Baronetti, H. J. Thomas, and J. C. Autino, *Tetrahedron Lett.*, 2002, **43**, 7589–7591.

521. F. Cavani, R. Mezzogori, and A. Trovarelli, *J. Mol. Catal. A -chemical*, 2003, **204**, 599–607.

522. C. Comuzzi, G. Dolcetti, A. Trovarelli, F. Cavani, F. Trifirò, J. Llorca, and R. G. Finke, *Catal. Letters*, 1996, **36**, 75–79.

523. J. Hu and R. C. Burns, *J. Mol. Catal. A Chem.*, 2007, **152**, 141–155.

524. J. O. F. Catal, F. Cavani, C. Comuzzi, G. Dolcetti, E. Etienne, R. G. Finke, G. Selleri, F. Trifirò, and A. Trovarelli, *J. Catal.*, 1996, **160**, 317–321.

525. Z. Sun, X. Zhang, S. Wang, X. Li, X. Wang, and J. Shi, *RSC Adv.*, 2015, **5**, 94155–94163.

526. C. Wang, X. Bu, J. Ma, C. Liu, K. Chou, X. Wang, and Q. Li, *Catal. Today*, 2016, **274**, 82–87.

527. X. Wei, R. E. Bachman, and M. T. Pope, *J. Am. Chem. Soc.*, 1998, **120**, 10248–10253.

528. D. K. Lyon, W. K. Miller, T. Novet, P. J. Domaille, E. Evitt, D. C. Johnson, and R. G. Finke, *J. Am. Chem. Soc.*, 1991, **113**, 7209–7221.

529. S. Ellis and I. V Kozhevnikov, *J. Mol. Catal. A Chem.*, 2002, **187**, 227–235.

530. S. Herrmann, C. Ritchie, and C. Streb, *Dalt. Trans.*, 2015, **44**, 7092–7104.

531. E. Arendt, S. Ghislain, and E. M. Gaigneaux, *Catal. Today*, 2010, **155**, 227–240.

532. S. Vanhaecht, G. Absillis, and T. N. Parac-Vogt, *Dalt. Trans.*, 2013, **42**, 15437–15446.

533. C. R. Graham and R. G. Finke, *Inorg. Chem.*, 2008, **47**, 3679–3686.

534. W. J. Randall, D. K. Lyon, P. J. Domaille, R. G. Finke, A. M. Khenkin, and

A. C. Hill, *Inorg. Synth.*, 1998, 242–268.

535. R. Contant, W. G. Klemperer, and O. Yaghi, *Inorg. Synth.*, 1990, **27**, 104–111.

536. T. L. Jorris, M. Kozik, N. Casan-Pastor, P. J. Domaille, R. G. Finke, W. K. Miller, and L. C. W. Baker, *J. Am. Chem. Soc.*, 1987, **109**, 7402–7408.

537. H. Liu, B. Yue, W. Sun, Z. Chen, S. Jin, J. Deng, and G. Xie, *Transit. Met. Chem.*, 1997, **22**, 321–325.

538. S. Vanhaecht, G. Absillis, and T. N. Parac-Vogt, *Dalt. Trans.*, 2012, **41**, 10028.

539. M. Abbessi, R. Contant, R. Thouvenot, and G. Hervé, *Inorg. Chem.*, 1991, **30**, 1695–1702.

540. V. F. Odyakov and E. G. Zhizhina, *React. Kinet. Catal. Lett.*, 2008, **95**, 21–28.

541. R. Contant, M. Abbessi, R. Thouvenot, and G. Hervé, *Inorg. Chem.*, 2004, **43**, 3597–3604.

542. S. P. Harmalker, M. A. Leparulo, and M. T. Pope, *J. Am. Chem. Soc.*, 1983, **105**, 4286–4292.

543. N. V Izarova, A. Banerjee, and U. Kortz, *Inorg. Chem.*, 2011, **50**, 10379–10386.

544. D. J. Edlund, R. J. Saxton, D. K. Lyon, and R. G. Finke, *Organometallics*, 1988, **7**, 1692–1704.

545. A. J. Stapleton, M. E. Sloan, N. J. Napper, and R. C. Burns, *Dalt. Trans.*, 2009, 9603–9615.

546. A. T. Harrison and O. W. Howarth, *J. Chem. Soc. Dalt. Trans.*, 1985, 1953–1957.

547. T. Ueda, Y. Nishimoto, R. Saito, M. Ohnishi, and J. Nambu, *Inorganics*, 2015, **3**, 355.

548. C. Rocchiccioli-deltcheff and R. Thouvenot, *Spectrosc. Lett.*, 1979, **12**, 127–138.

549. O. Bechiri, M. Abbessi, R. Belghiche, and L. Ouahab, *Comptes Rendus Chim.*, 2014, **17**, 135–140.

550. K. Y. Matsumoto and Y. Sasaki, *J. Chem. Soc. Chem. Commun.*, 1975, 691–692.

551. D. H. Müller, .

552. X. Han, L. Xu, F. Li, and N. Jiang, *Eur. J. Inorg. Chem.*, 2011, 4564–4570.

553. T. Werpy and G. Petersen, *Off. Sci. Tech. Inf.*, 2004, **1**, 21–61.

554. M. E. M. Chbihi, A. Cherqaoui, D. Takky, F. Hahn, H. Huser, and J. L. C. Lamy, *J. Chim. Phys.*, 1999, **96**, 522–534.

555. M. Ştefănescu, O. Ştefănescu, M. Stoia, and C. Lazau, *J. Therm. Anal. Calorim.*, 2007, **88**, 27–32.

556. M. S. Ide and R. J. Davis, *J. Catal.*, 2013, **308**, 50–59.

557. O. Stefanescu and M. Stefanescu, *J. Organomet. Chem.*, 2013, **740**, 50–55.

558. E. K. Kunec and D. J. Robins, *J. Chem. Soc. Perkin Trans. 1*, 1987, 1089–1093.

559. O. Stefanescu, T. Vlase, G. Vlase, N. Doca, and M. Stefanescu, *Thermochim. Acta*, 2011, **519**, 22–27.

560. Y. Ryabenkova, P. J. Miedziak, D. W. Knight, S. H. Taylor, and G. J. Hutchings, *Tetrahedron*, 2014, **70**, 6055–6058.

561. J. Kaulen and H.-J. Schäfer, *Tetrahedron*, 1982, **38**, 3299–3308.

562. H. Tohma, T. Maegawa, S. Takizawa, and Y. Kita, *Adv. Synth. Catal.*, 2002, **344**, 328–337.

563. D. Sloboda-Rozner, P. Witte, P. L. Alsters, and R. Neumann, *Adv. Synth. Catal.*, 2004, **346**, 339–345.

564. Y. Kiyotaka, Y. Atsushi, and W. Nobuhiro, 2014, JP2015203010A.

565. J. Tuteja, S. Nishimura, H. Choudhary, and K. Ebitani, *ChemSusChem*, 2015, **8**, 1862–1866.

566. J. Tuteja, S. Nishimura, and K. Ebitani, *Catal. Today*, 2016, **265**, 231–239.

567. R. Gupta, W. Huang, L. C. Francesconi, and T. Polenova, *Solid State Nucl. Magn. Reson.*, 2016, **In Press**, doi.org/10.1016/j.ssnmr.2016.12.004.

Appendix A Supporting Information Chapter 2

Schematic drawings of designed MVs.

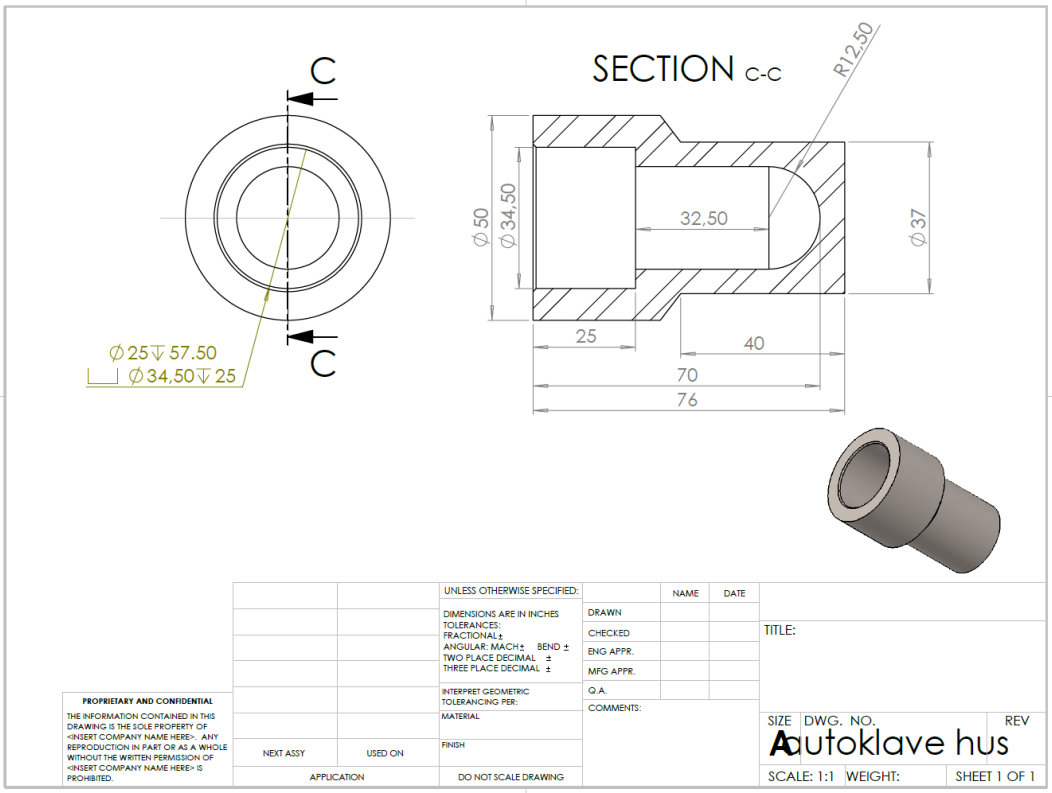

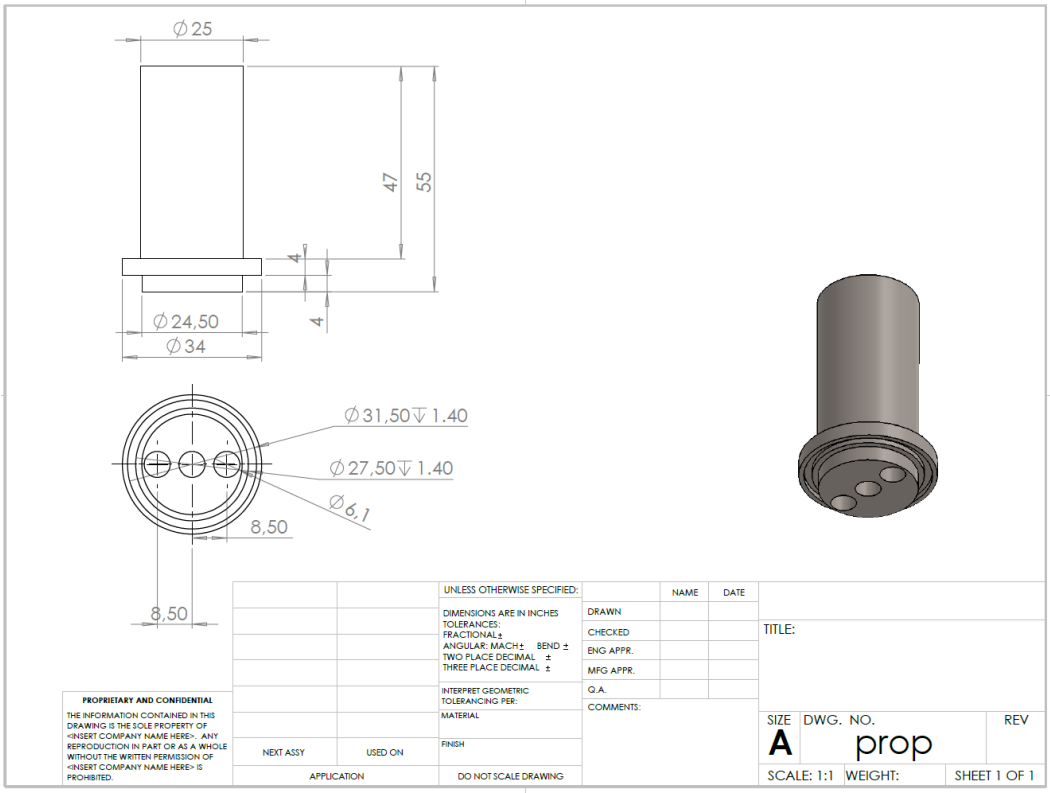
∅25
47
55
4
4
∅24,50
∅34
∅31,50↧1.40
∅27,50↧1.40
∅6,1
8,50
8,50
UNLESS OTHERWISE SPECIFIED:
DIMENSIONS ARE IN INCHES
TOLERANCES:
FRACTIONAL ±
ANGULAR: MACH ± BEND ±
TWO PLACE DECIMAL ±
THREE PLACE DECIMAL ±
INTERPRET GEOMETRIC TOLERANCING PER:
MATERIAL
FINISH
NEXT ASSY
USED ON
APPLICATION
DO NOT SCALE DRAWING
NAME
DATE
DRAWN
CHECKED
ENG APPR.
MFG APPR.
Q.A.
COMMENTS:
TITLE:
SIZE
A
DWG. NO.
prop
REV
SCALE: 1:1
WEIGHT:
SHEET 1 OF 1
PROPRIETARY AND CONFIDENTIAL
THE INFORMATION CONTAINED IN THIS DRAWING IS THE SOLE PROPERTY OF <INSERT COMPANY NAME HERE>. ANY REPRODUCTION IN PART OR AS A WHOLE WITHOUT THE WRITTEN PERMISSION OF <INSERT COMPANY NAME HERE> IS PROHIBITED.

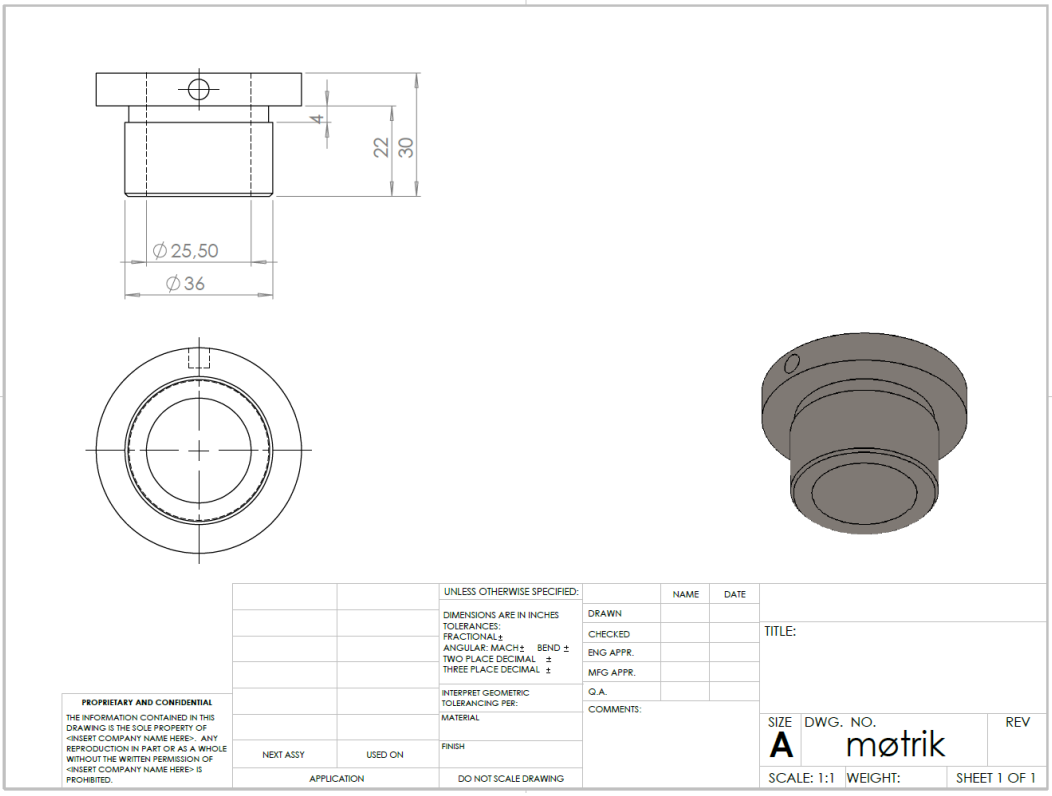
4
22
30
∅25,50
∅36
UNLESS OTHERWISE SPECIFIED:
DIMENSIONS ARE IN INCHES
TOLERANCES:
FRACTIONAL ±
ANGULAR: MACH ± BEND ±
TWO PLACE DECIMAL ±
THREE PLACE DECIMAL ±
INTERPRET GEOMETRIC TOLERANCING PER:
MATERIAL
FINISH
NEXT ASSY
USED ON
APPLICATION
DO NOT SCALE DRAWING
NAME
DATE
DRAWN
CHECKED
ENG APPR.
MFG APPR.
Q.A.
COMMENTS:
TITLE:
SIZE
A
DWG. NO.
møtrik
REV
SCALE: 1:1
WEIGHT:
SHEET 1 OF 1
PROPRIETARY AND CONFIDENTIAL
THE INFORMATION CONTAINED IN THIS DRAWING IS THE SOLE PROPERTY OF <INSERT COMPANY NAME HERE>. ANY REPRODUCTION IN PART OR AS A WHOLE WITHOUT THE WRITTEN PERMISSION OF <INSERT COMPANY NAME HERE> IS PROHIBITED.

Appendix B Supporting Information Chapter 3

XRF Data

Table B1: Recorded XRF data for tested catalysts

Catalyst	Concentration (wt%)		
	Active Metal 1	Active Metal 2	Support Metal
Au/CeO_2	Out of range	-	100.0
Ag/TiO_2	Out of range	-	100.0
Cu/TiO_2	1.2	-	98.8
Fe/TiO_2	1.3	-	98.7
Co/TiO_2	1.5	-	98.5
Mo/TiO_2	Out of range	-	100.0
Mn/TiO_2	2.7	-	97.3
$Co\text{-}Fe/TiO_2$	0.6	0.7	98.6
$Pd\text{-}Bi/TiO_2$[a]	3.8	Out of range	96.2
$Mo\text{-}Fe/TiO_2$	Out of range	0.7	99.3
$Mo\text{-}Cu/TiO_2$	Out of range	0.8	99.2
Ru/TiO_2[b]	3.1	-	96.9
Pd/TiO_2	1.7	-	98.1

[a] 5 wt% and [b] 2.5 wt% theoretical loading.

The recorded spectrum for catalyst containing elements outside of the calibration range is presented below, verifying the presence of metals in the samples.

Au/CeO_2

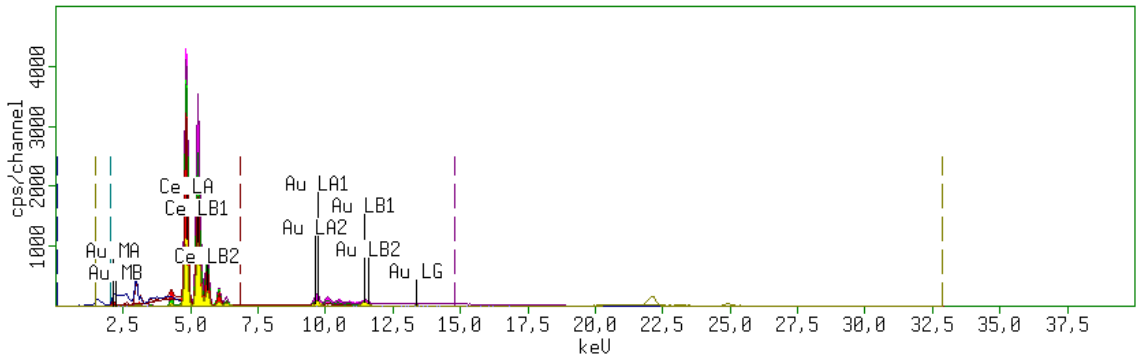

Ag/TiO_2

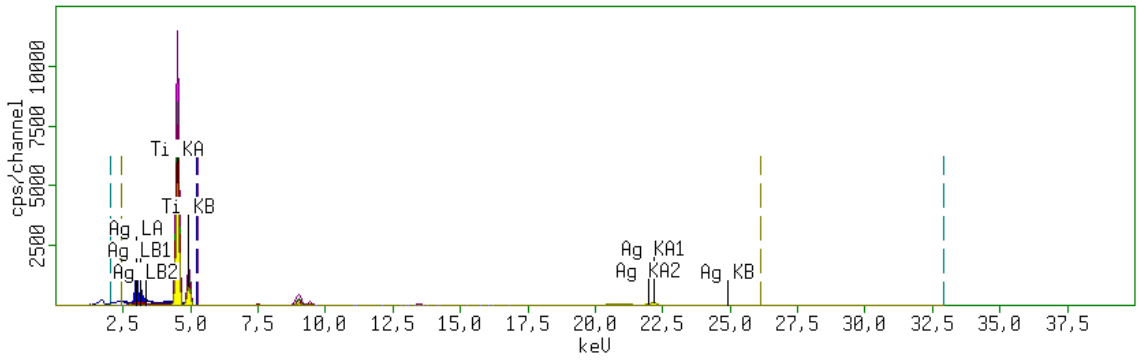

Mo/TiO_2

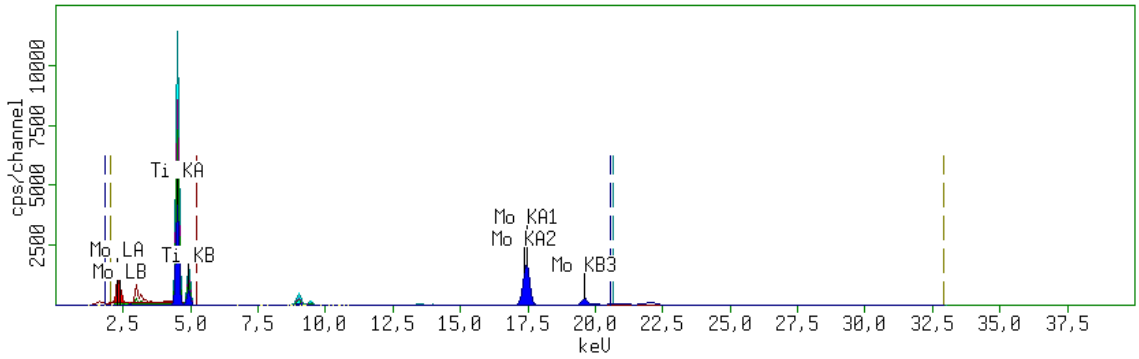

Mo-Fe/TiO_2

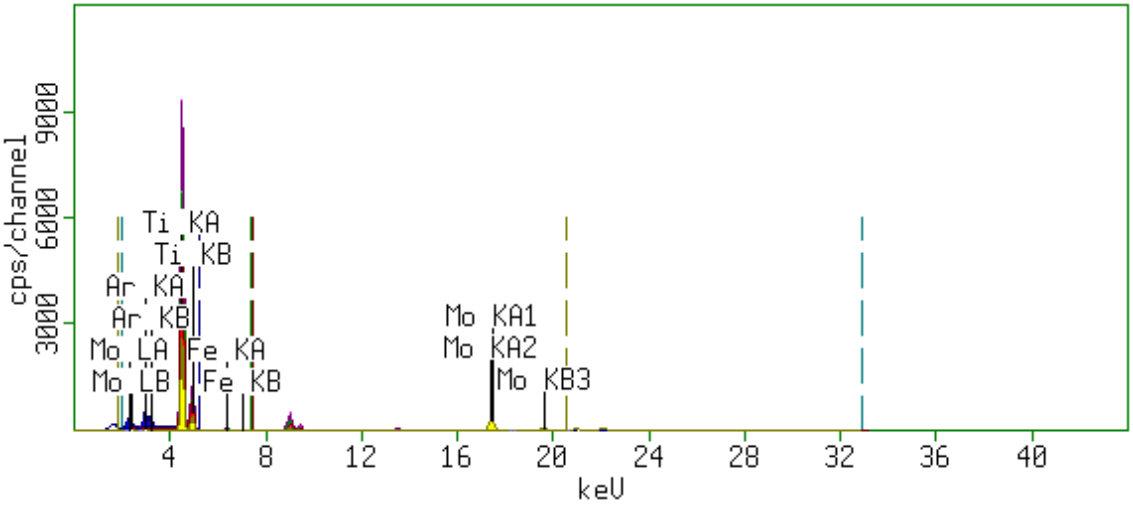

Mo-Cu/TiO_2

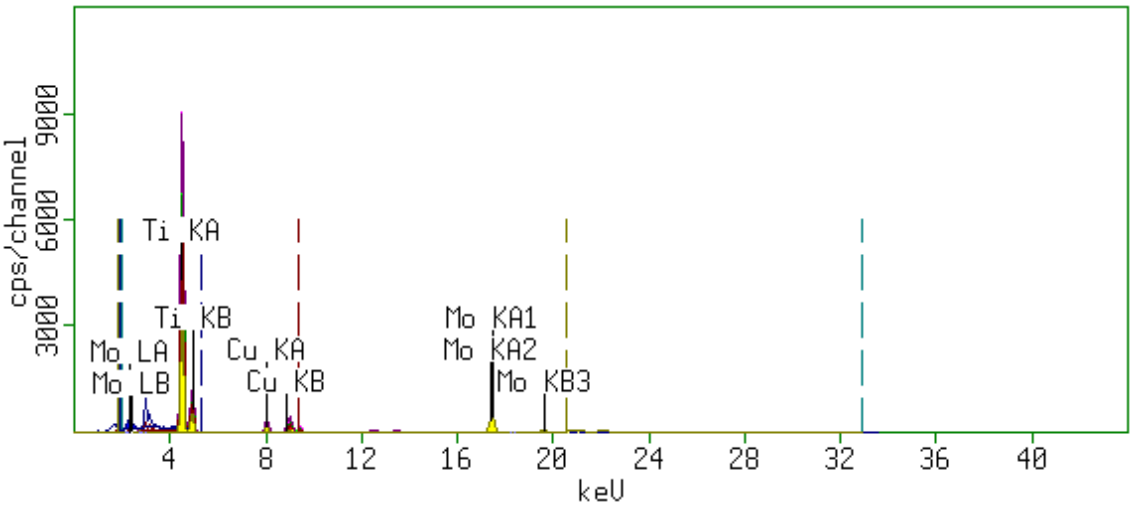

Pd-Bi/TiO_2

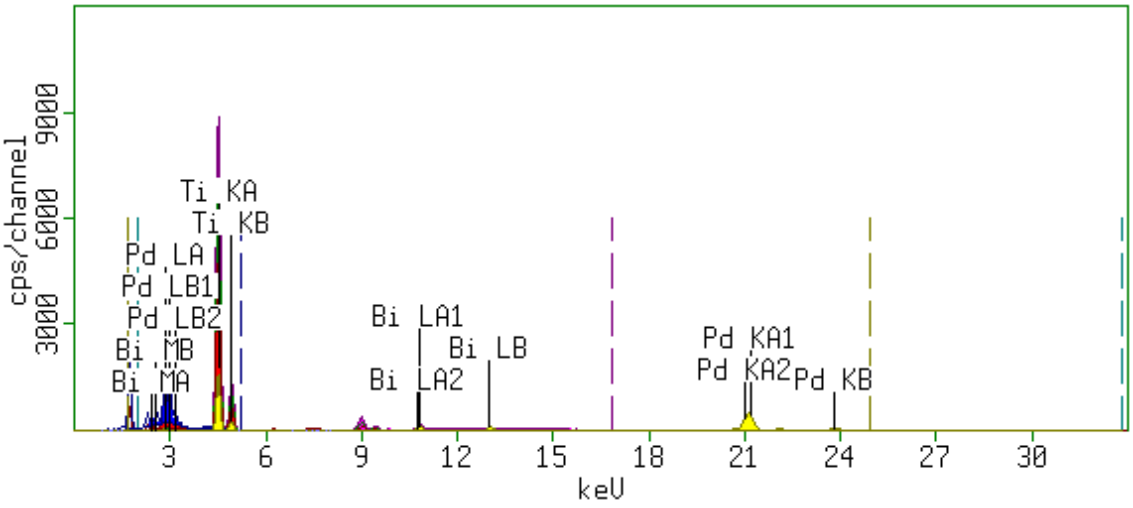
cps/channel
9000
6000
3000
Ti KA
Ti KB
Pd LA
Pd LB1
Pd LB2
Bi MB
Bi MA
Bi LA1
Bi LB
Bi LA2
Pd KA1
Pd KA2
Pd KB
3
6
9
12
15
18
21
24
27
30
keV

HPLC Calibration Curves

Example of calculated calibration curve, Glycolaldehyde (24 ºC). New calibration curves were recorded every three months.

Table B2: HPLC data obtained for solutions A-E

Entry	Conc. (M)	HPLC (AUC)		
		1st run	2nd run	3rd run
A	0,00299	13945,6	13305,9	13276,6
B	0,01295	60134,0	59270,2	58435,8
C	0,02620	120387,8	119379,9	119321,3
D	0,09887	464568,2	466331,2	466449,3
E	0,20038	954644,3	952181,9	948739,8

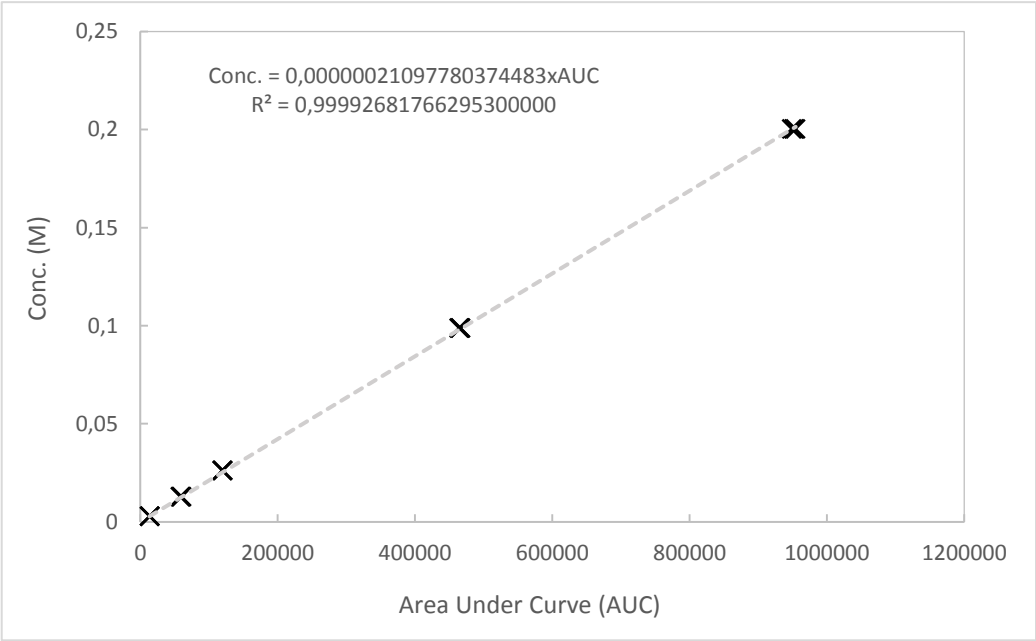

Figure B1: Graphical presentation of calibration curve and obtained equation applied for calculation of glycolaldehyde concentrations in experiments.

BINOS Calibration Curve

A series of concentrations of CO_2 and nitrogen was measures by Leonard Schill, affording the calibration equation:

$$\text{Vol\% } CO_2 = 1{,}3949x(\text{data output})+2{,}2303501$$

The difference between the raw data and the corrected data is presented in Figure B2

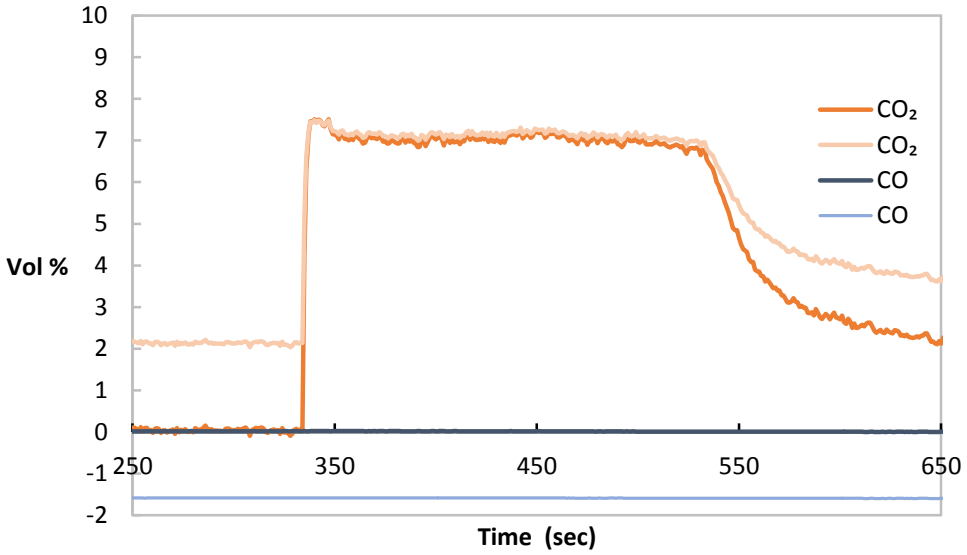

Figure B2: Raw data from BINOS (light blue for CO and light orange for CO_2) and corrected data (dark blue for CO and orange for CO_2).

Name	Value	Unit
m(GAD)	185,4	mg
n(GAD)	2,504220977	mmol
p	18	bar
V(pressure vessel)	79,14	mL
V(reaction)	10,032	mL
V(Head Space)	69,108	mL
Temperature	23,2	C
Temperature	296,35	K
R	0,083144622	L*bar/(mol*K)
Vol% CO_2	7,01672285	%
V(CO_2)	4,849116827	mL
n(CO_2) = pV/(RT)	3,542387438	mmol
mol% CO_2	70,7	%

Table B3: Calculation of developed mol% CO_2. The numbers in bold were specific for this experiment.

Appendix C Supporting Information Chapter 4

HPLC Calibration Curves

Example of calculated calibration curve, formic Acid (24 °C)

Table C1: HPLC data obtained for solutions A-G

Entry	Conc. (M)	HPLC (AUC)		
		1st run	2nd run	3rd run
A	0,0485	69683,6	69319,1	6923,4
B	0,1024	149562,4	149351,2	148661,9
C	0,4967	719318,8	720103,9	718489,2
D	1,0352	1504520	1496301	1481714
E	1,5745	2251573	2221963	2227601
F	1,9774	2772196	2765220	2764179
G	2,6292	3597681	3592480	3608423

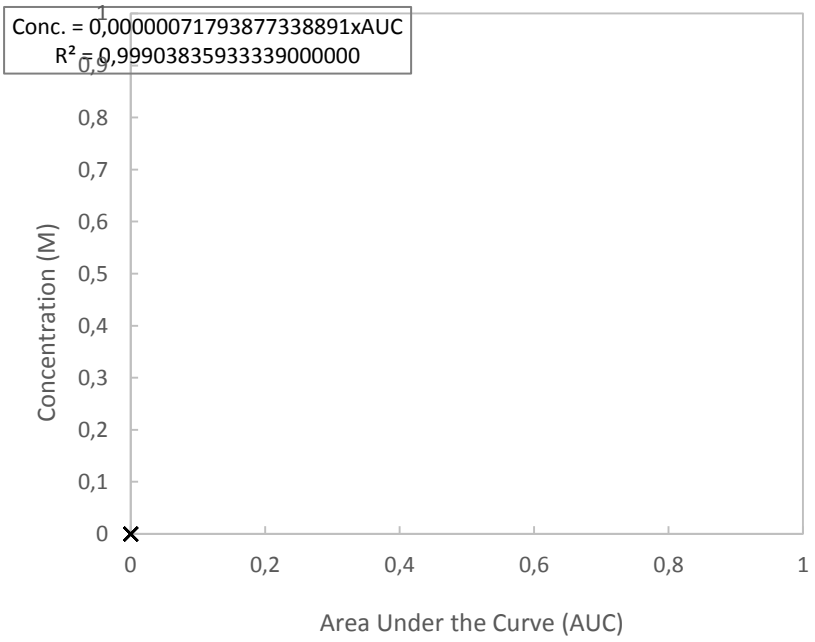

Figure C1: Graphical presentation of calibration curve and obtained equation applied for calculation of formic acid concentrations in experiments.

Calculation of mol% CO_2

Vol%-data was recorded by Quantek Carbon Dioxide Analyzer, plotted in Figure C2. From the average volume concentration, the molar percentage of CO_2 was calculated, see Table C2. The numbers in bold in Table C2 are specific for this example (oxidation of GAD to AA, reaction time of 70 h). The volume percentage of CO_2 was obtained from averaged values, in this example from 96-309 sec.

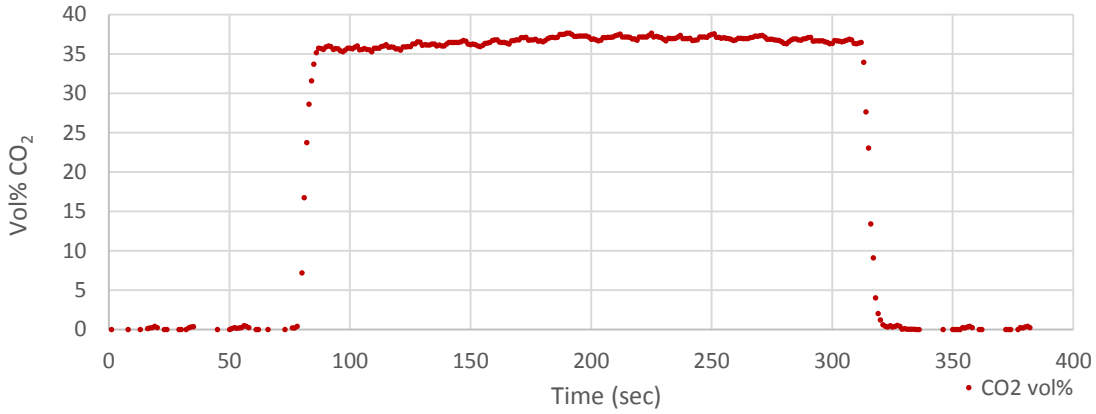

Figure C2: Raw data recovered from Quantek NDIR detected plotted against time.

Name	Value	Unit
m(GAD)	356,3	mg
n(substrate)	5,933191234	mmol
Pressure	24,5	bar
V(MV)	18,4	mL
V(reaction)	4,6381	mL
V(Head Space)	13,7619	mL
Temperature	23,2	°C
Temperature	296,35	K
R	0,083144622	L*bar/(mol*K)
Vol% CO_2	36,67831776	%
V(CO_2)	5,047633411	mL
n(CO_2) = pV/(RT)	5,018972282	mmol
mol% CO_2	42,30	%

Table C2: Calculation of developed mol% CO_2. The numbers in bold were specific for this experiment.

XRF of Ru-1 and Ru-3

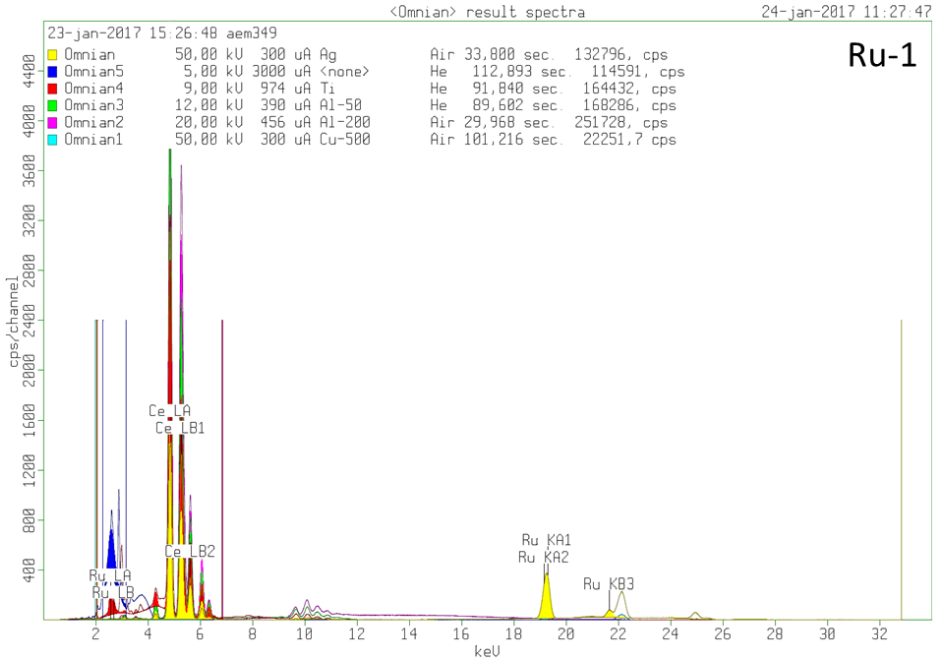

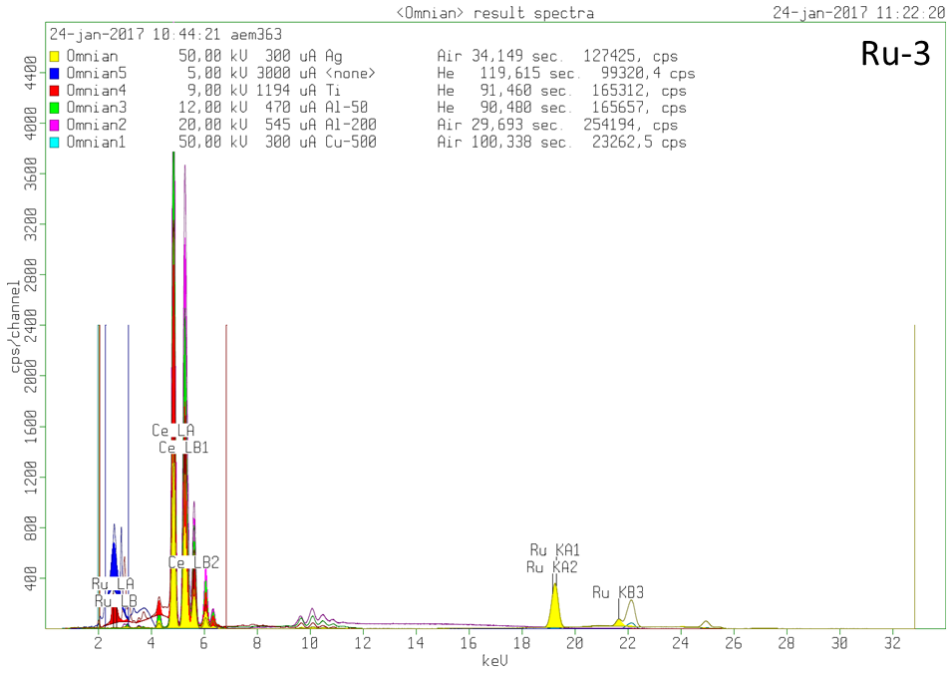

Appendix D Supporting Information for Chapter 5

Technical details of ^{31}P-NMR instruments.

Table D1: Conditions for 31P NMR recordings at FAU and DTU.

University	FAU	DTU
Instrument	JEOL ECX400	Bruker BioSpin GmbH
Solvent	D_2O	D_2O
Temperature	20.6 ^oC	24.9 ^oC
# scans	256	512
Relaxation delay	1 s	2 s
Pulse width	18.5	11.7
Acquisition time	5.0627	0.5112
Frequency	161.81	161.98
Standard	None	85 wt %H_3PO_4

^{31}P-NMR spectra of the synthesized WD cataæysts.

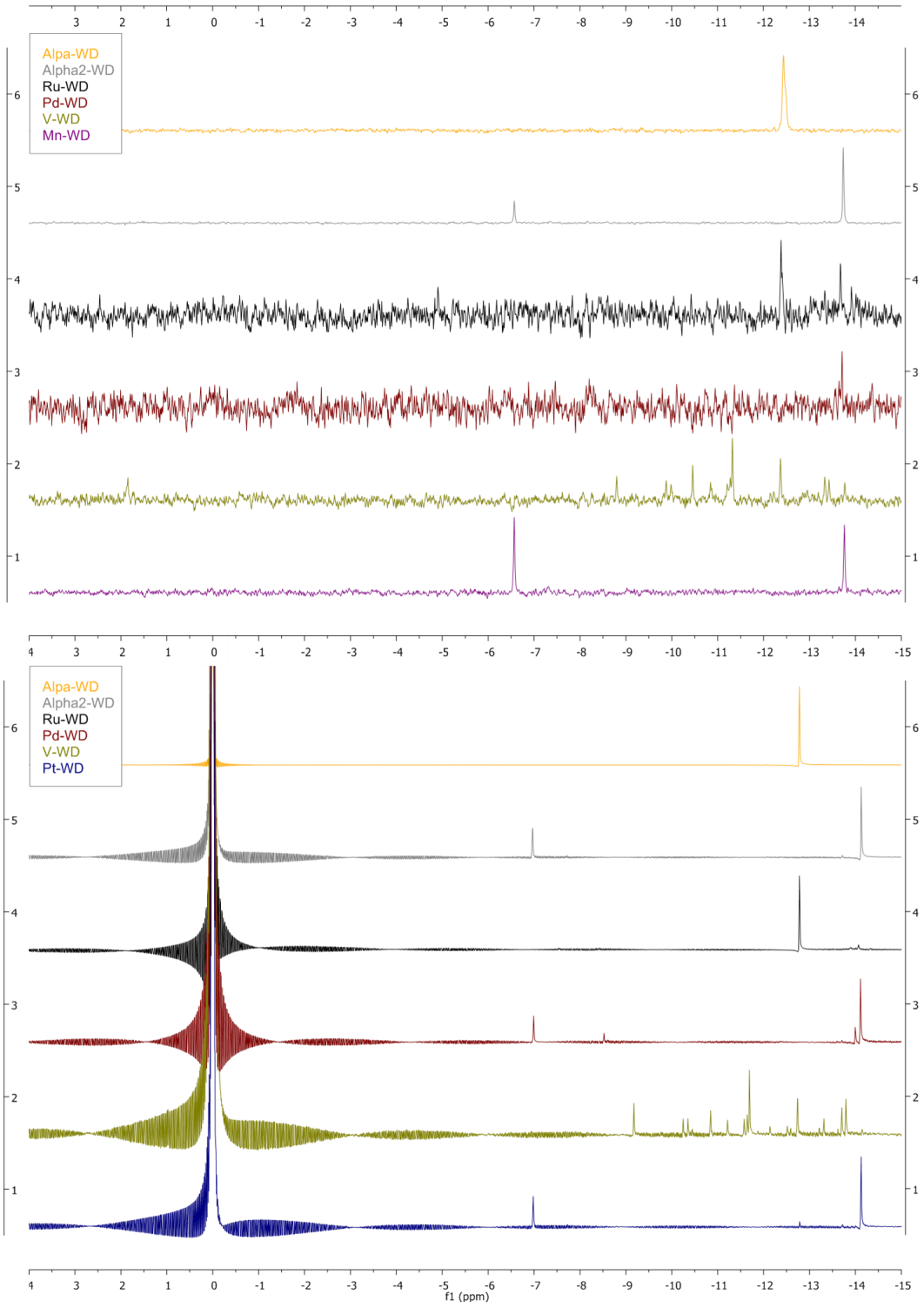

Figure D1: ^{31}PNMR of synthesized WD catalysts including H_3PO_4 reference.

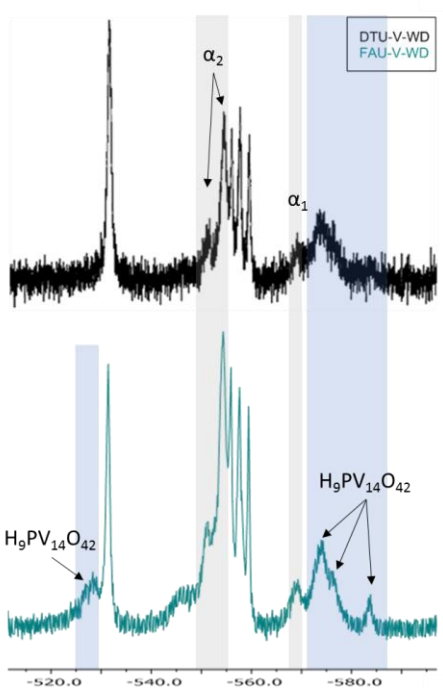

Figure D2: Selected section of the recorded ^{51}V NMR of FAU- and DTU-V-WD catalysts, both recorded at FAU at 105 MHz.

Table D2: Overview of reported ^{51}V NMR shifts

Entry	Compound	δ ^{51}V NMR (ppm)			
		Harmalker *et al.* (24 MHz)[542]	Abessi *et al.* (101 MHz)[539]	Odyakov *et al.* (105 MHz)[540]	Gupta et al. (105 MHz)[567]
1	α2-V-WD	-554.7	-553.8		-551.4
2	α1-V-WD	-570.0			-572.3
3	$H_9PV_{14}O_{42}$	-522, -572, -589		-529.3, -583.5, -590.4	
4	$H_6V_{10}O_{28}$			-421.0, -507.9, -526.8	
5	1,2-$P_2V_2W_{16}O_{62}^{8-}$	-528	-527.5		-527.0

Single Crystal XRD

Table D3: Single Crystal XRD data and structure refinement for α-WD[a]

Crystal data	α-WD
Chemical formula	$K_6O_{72}P_2W_{18}$
M_r	4757.84
Crystal system, space group	Triclinic, *P*1
Temperature (K)	299
a, *b*, *c* (Å)	12.7997 (3), 14.8086 (3), 18.6220 (5)
α, β, γ (°)	101.208 (2), 96.832 (2), 115.140 (2)
V (Å^3)	3052.62 (15)
Z	2
Radiation type	Mo *K*α
D_c (gcm^{-3})	5.176
μ (mm^{-1})	34.35
F(000)	4104
2θ range (°)	3.16 – 29.39
Data collection	
T_{min}, T_{max}	0.287, 1.000
No. of measured, independent and observed [$I > 2\sigma(I)$] reflections	50784, 15022, 12790
R_{int}	0.060
$(\sin \theta/\lambda)_{max}$ (Å^{-1})	0.695

[a] Computer programs: CrysAlis PRO, Agilent Technologies, Version 1.171.37.34 (release 22-05-2014 CrysAlis171 .NET) (compiled May 22 2014, 16:03:01), SHELXS (Sheldrick, 2008), SHELXL (Sheldrick, 2015), Olex2 (Dolomanov et al., 2009).

Refinement	
$R[F^2 > 2\sigma(F^2)]$, $wR(F^2)$, S	0.043, 0.102, 1.12
No. of reflections	15022
No. of parameters	883
$\Delta\rho_{max}$, $\Delta\rho_{min}$ (e Å^{-3})	2.70, −3.67
Limiting indices	-17≤*h*≤15, -19≤*k*≤20, -25≤*l*≤25
Diffractometer	SuperNova, Dual, Cu at zero, Atlas
Absorption correction	Multi-scan *CrysAlis PRO*, Agilent Technologies, Version 1.171.37.34 (release 22-05-2014 CrysAlis171 .NET) (compiled May 22 2014,16:03:01) Empirical absorption correction using spherical harmonics, implemented in SCALE3 ABSPACK scaling algorithm.

X

RPD of KCl

The diffractogram was recorded by Ph.D. student Chiraphat Kumpidet at FAU.

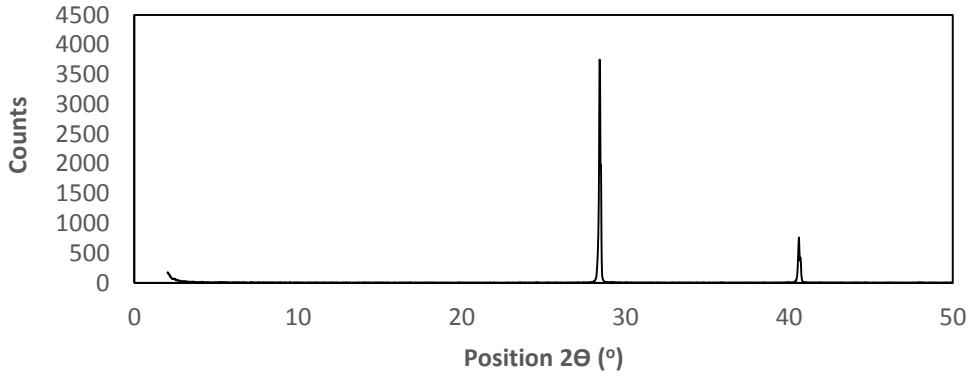

Figure D3: Diffractogram of KCl

XRF calibration

POM	XRF counts			Theoretical molar conc.
	P	W	W/P	
α-WD	1501,690	75969,37	50,589	9,000
α2-WD	1534,458	71447,88	46,562	8,500

Table D4: Raw XRD data acquired (counts) and calculated ratios thereof.

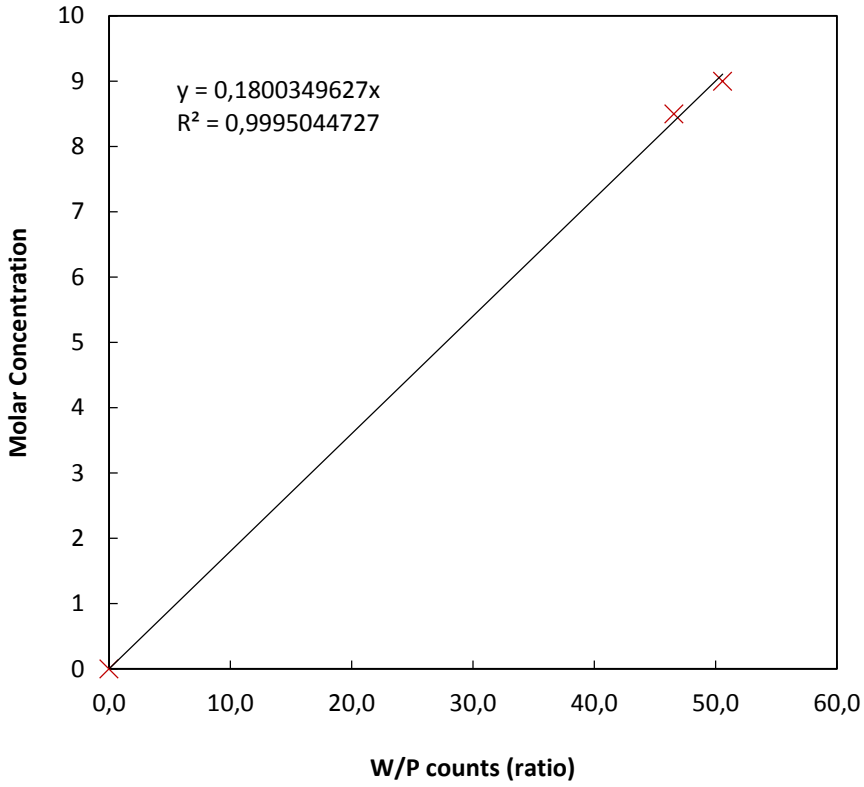

Figure D4: Calibration curve based on data presented in Table D4.

The data obtained from the calibration was multiplied by two due the easier comparison with the presented elemental formula of the catalysts containing two phosphorous.

ICP-AES

The elemental concentration obtained from ICP-AES analysis was converted into molar concentration (mmol) and related to phosphor (ratio) and multiplied by two for easier comparison with the presented elemental formulas. An example of the manganese substituted WD POM is presented in Table D5.

Element	M (g/mol)	C (mg/L)	n (mmol)	Ratio	x2
W	183.8400	53.8841	0.2931	7.0227	14.0454
P	30.9738	1.2927	0.0417	1.0000	2.0000
K	39.0983	30.6348	0.7835	18.7733	37.5466
V	50.9415	0.0000	0.0000	0.0000	0.0000
Ru	101.0700	0.0000	0.0000	0.0000	0.0000
Pd	106.4200	0.0000	0.0000	0.0000	0.0000
Mn	54.9380	0.8214	0.0149	0.3582	0.7165

Table D5: Conversion of ICP concentrations.

Screening results obtained for $PdCl_2$ (example with 1,3-propanediol)

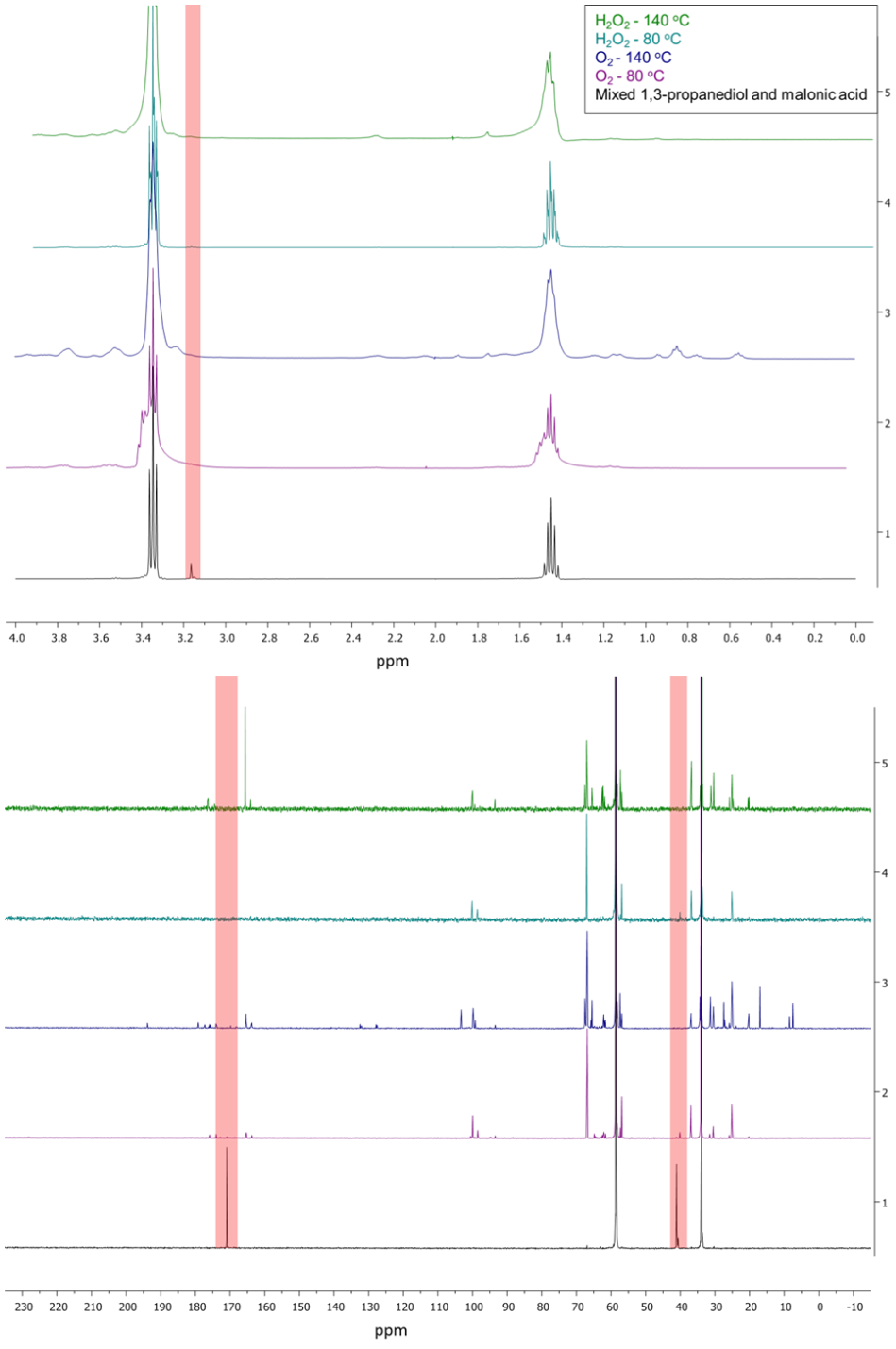

Figure D5: Palladium catalyzed oxidations of 1,3-propanediol. ^{1}HNMR (top) and ^{13}CNMR (bottom). The boxes mark malonic acid (red).

Synthesized WD-catalyzed oxidation of 1,3-propanediol

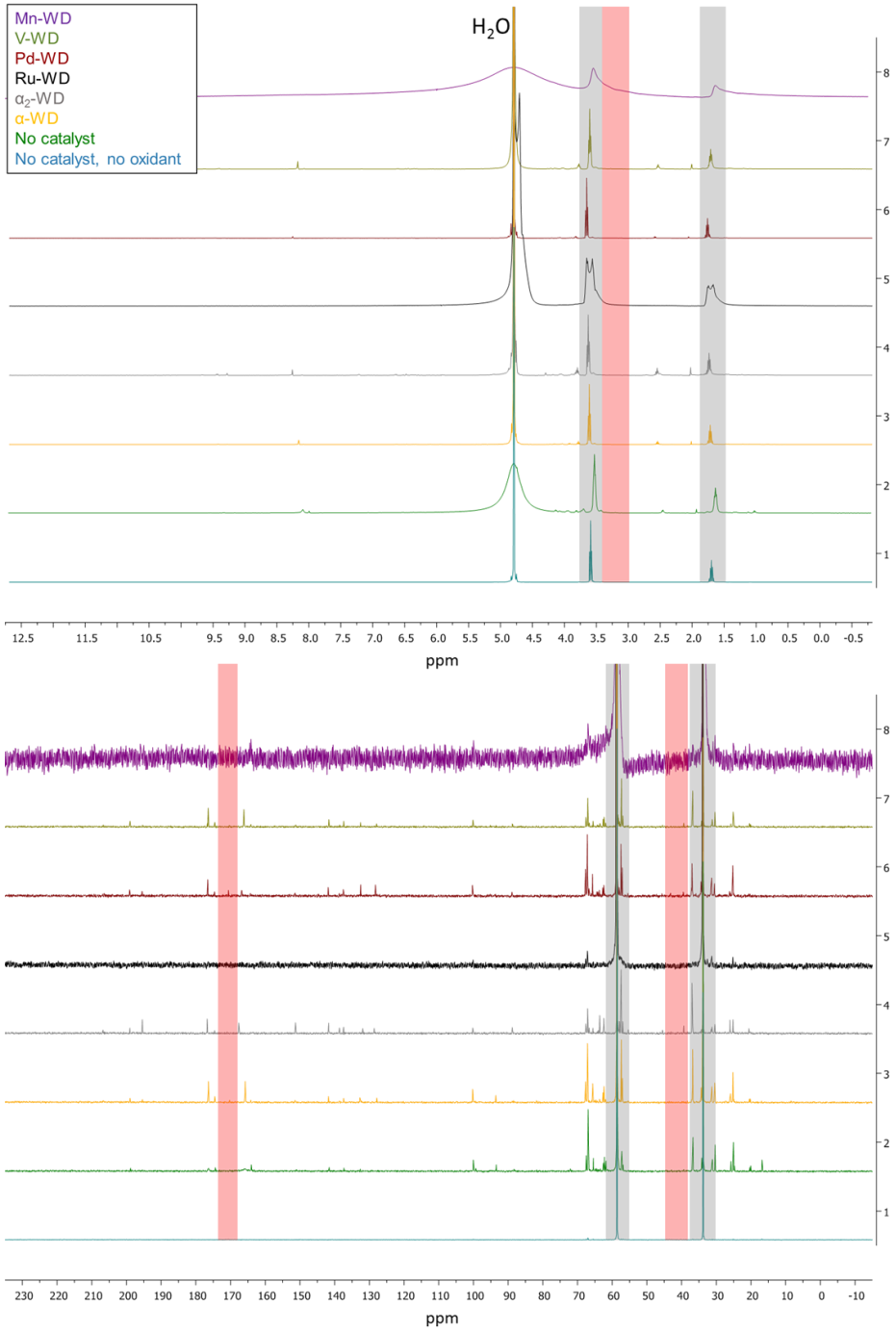

Figure D6: Spectra for oxidation of 1,3-propanediol with synthesized FAU-WDs. ^{1}HNMR (top), ^{13}CNMR (bottom), the boxes mark malonic acid peaks (red), 1,3-propanediol (grey).

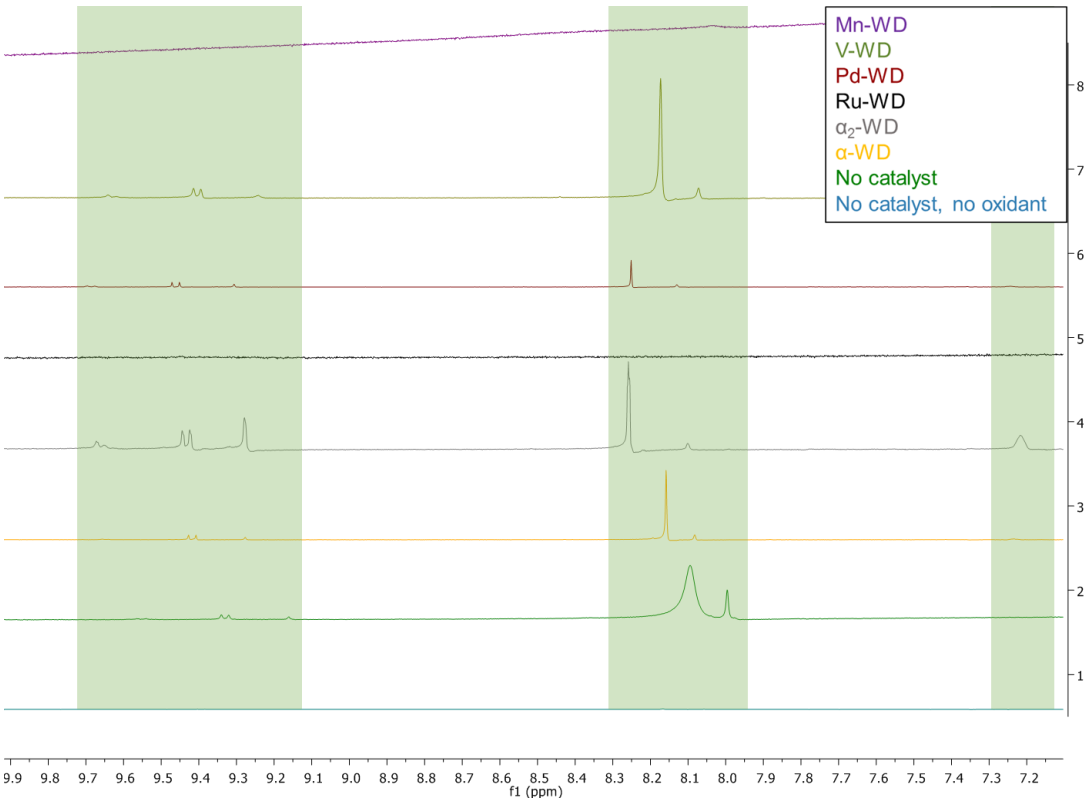

Figure D7: Enlarged ^{1}HNMR spectra of the aldehyde and acid areas of the oxidation of 1,3-propanediol over the synthesized WD catalysts.

Appendix E Disseminations

Publication of the work presented in this dissertation is in preparation. The preparative titles are presented below.

Selective Base-free Oxidation of Glycolaldehyde to Glycolic Acid

A. E. Modvig, S. Shunmugavel, P. Fristrup and A. Riisager

Selective Formation of Formic Acid from Biomass-derived Compounds over Supported Ruthenium Hydroxide Catalyst

A. E. Modvig and A. Riisager

Other disseminations related to the work presented in this dissertation

Oral Presentations

"Selective Oxidation of Glycolaldehyde" - *DTU Chemistry PhD symposium, November 5-6 2015, Frederiksdal, Denmark.*

"Selective oxidation of glycolaldehyde to value added chemicals" - Nordic Symposium on Catalysis, June 2016, Lund, Sweden.

"Selective oxidation of glycolaldehyde to value added chemicals" - *New Year's Symposium with FAU, January 6 2016, Lyngby, Denmark*

Oral Flash Presentations

"Oxidative Catalytic Upgrading of Biomass to Glycolics" - FP1306 COST Action (LIGNOVAL) Second MC Meeting & First Workshop, February 3-5 2015, Belgrade, Serbia.

"Catalytic Upgrading of Carbohydrates and Derivatives from Biomass by Oxidation" - BioValue Annual Assembly, September 14-15 2015, Copenhagen, Denmark.

Poster Presentations

"Oxidative catalytic upgrading of carbohydrates and derivatives from biomass" - *BioValue Annual Assembly, September 3-4, 2014 Thiele, Denmark.*

"Oxidative Catalytic Upgrading of Carbohydrates and Derivatives from Biomass" - *DTU Chemistry PhD symposium, November 20-21 2014, Frederiksdal, Denmark.*

"Selective Oxidative Glycolaldehyde" - *1st IGSS Seminar, June 10 2015, Odense, Denmark.*

"Selective Oxidative Glycolaldehyde" - *Annual Meeting of Danish Chemical Society, June 11 2015, Odense, Denmark.*

"Oxidative Catalytic Upgrading of Biomass-derived Glycolaldehyde to Glycolics" - *Europacat XII, August 30 to September 4th 2015, Kazan,Russia.*

"Selective Oxidation of Glycolaldehyde" - ECAT Summer school June 12-17, 2016, Vogüé, France

"Selective Oxidation of Glycolaldehyde" - *BioValue Annual Assembly, September 16 2016, Copenhagen, Denmark.*

"Selective Oxidation of Glycolaldehyde" - *DTU Chemistry PhD symposium, November 10-11 2016, Frederiksdal, Denmark*